SUPPORTED METAL CATALYSTS FOR FRIEDEL-CRAFTS ALKYLATION

By:

TAPIWA HLATYWAYO

BSc HONS: (CHEMICAL TECHNOLOGY)

MIDLANDS STATE UNIVERSITY -ZIMBABWE

Submitted in fulfillment of the requirements for degree of Magister Scientiae in Chemistry

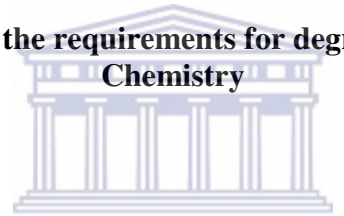

Department of Chemistry
University of the Western Cape

Supervisor: Dr S.J.J. Titinchi

Co-supervisor: Prof. L.F. Petrik

July 2013

KEYWORDS

Friedel-Crafts alkylation

HBEA

MCM-41

Hierarchical Zeolite X

Coal fly ash

Ion exchange

Incipient wetness impregnation,

Benzene

t-Butylbenzene

t-Butylchloride

Catalysis

Physico-chemical properties

DECLARATION

I declare that "***SUPPORTED METAL CATALYSTS FOR FRIEDEL-CRAFTS ALKYLATION"*** is my own work, that it has not been submitted for any degree or examination in any other university, and that all the sources I have used or quoted have been indicated and acknowledged by complete references

TAPIWA HLATYWAYO **July 2013**

Signed……..

ABSTRACT

The research focused on the synthesis, characterisation and activity of zeolite supported metal catalysts for the Friedel-Crafts alkylation of benzene with *t*-butyl chloride. Alkyl benzenes are traditionally produced via systems that employ the use of Lewis acids or strong mineral acids. There have been widespread concerns over these approaches based on their environmental impacts and separation difficulties. Recent approaches have endeavoured the much to use more environmentally eco-friendly systems and zeolites have proved to be versatile support materials. The use of zeolites has also shown to greatly improve product selectivity as well as easing separation constraints. However the adoption of zeolites on large scale Friedel-Crafts alkylation has been hampered by the high cost of zeolite production from commercial sources. On the other hand fly ash has been found to be a viable starting material for zeolite synthesis. Apart from that South Africa is faced with fly disposal challenges and there is continual accumulation of fly ash at the coal fired power stations, which provide about 77 % of the power produced in the country. In this light the use of fly ash will help to reduce the disposal constraints as well as providing a cheap starting material for zeolite synthesis.

In this study the hierarchical Zeolite X has been successfully synthesised from fly ash via a hydrothermal treatment. The zeolite was then loaded with Fe/Mn via two approaches namely liquid phase ion exchange and incipient wetness impregnation. For comparison purposes seasoned commercial support materials namely HBEA and MCM-41 were also loaded with the same metals and characterised with various techniques namely; HRSEM, EDS, HRTEM, XRD, SAED, ICP-OES and N_2 adsorption analysis,

It was found from the characterisation undertaken that the integrity of the respective supports was generally retained upon metal loading. Both the ICP-OES and the EDS proved that the desired metals were successfully introduced onto the zeolitic support materials. The calculated percentage metal loading for the catalysts prepared via incipient wetness impregnation was closely related to the actual values obtained from the ICP-OES analysis for both the monometallic and the bimetallic catalysts (Fe/Mn). It was observed that the amount of metal that can be introduced on a zeolite via liquid phase ion exchange is largely dependent on the cation exchange capacity of the zeolite

and of the catalysts prepared using 0.25 M Fe solution it was found that Zeolite X had the highest Fe wt% loading of 11.4 %, with the lowest loading of 2.2 % obtained with the MCM-41 supported catalyst.

The XRD patterns for the both HBEA and the MCM-41 supported metal catalysts resembled the patterns of the respective prestine support materials except in the case of catalysts with anFe wt % of more than 10, which exhibited peaks due to the Fe_2O_3 crystallites. In the case of the hierarchical Zeolite X, the metal loaded support had a significant reduction in the XRD peak intensities.

The prepared catalysts were tested for the alkylation of benzene with *t*-butyl chloride. The benzene was also used as the solvent. The alkylation reaction was carried out in a round bottomed flask under reflux conditions and stirring at a temperature of 45 ^{o}C over a period of 5 h. A total of 18 catalysts was tested and the highest percentage conversion of 100 % was obtained with the 10%FeH after a reaction time of 2 h. The general trend obtained with the majority of the catalysts was characterised with a rapid initial increase and then steady state was achieved. Generally after a reaction time of 3 h almost all the catalysts had reached steady state in terms of the percentage conversion obtained.

The outcomes reflect that the inclusion of Mn does not enhance the conversion but rather decreases it. It was also found that the Mn was not active in the alkylation of benzene as shown by the inactivity of the 10%MnM, where 10% by weight Mn was loaded on MCM-41. However the other monometallic catalysts containing Mn supported on Zeolite X and HBEA were found to be active. The activity is attributed to the presence of Brønsted acid sites in these zeolites which are not present in MCM-41.

The selectivity studies reflect that the inclusion of Mn does slightly improve the selectivity towards the formation of the monoalkylated product (*t*-butyl benzene). The highest selectivity of 91.1 % was obtained with the 10%FeMnM after a reaction time of 4 h. MCM-41 supported catalysts had a relatively higher selectivity compared to the other supports. Considering the Fe monometallic catalysts tested it generally can be said that the yield were in the order HBEA > MCM-41 > Zeolite X. It however should be noted that the percentage yield is calculated from the conversion and selectivity percentages, this implies that the factors affecting these parameters will consequently affect the percentage yield obtained.

The alkylation reaction was found to be characterised by the formation of two intermediate products which could not be identified. These products were formed during the transient start up stages of the reaction and would disappear from the reaction mixture with longer reaction times, and after 3 h in almost all the reactions studied the intermediates were not detected in the reaction mixture. The main products found were the monoalkylated product (desired product) and the para isomer (1,4-t-di-butyl benzene). There were no other dialkylated isomers or trialkylated products detected. The formation of the *para* isomer was usually after a reaction time of 2 h in most reactions.

The research managed to show that the hierarchical Zeolites X can be synthesised from fly ash and ion exchange and incipient wetness impregnation are appropriate approaches that can be used to introduce Fe/Mn onto the support materials studied. The catalysts prepared were active to varying degrees in the Friedel-Crafts alkylation of benzene with *t*-butylchloride, with the exception of the 10%MnM which was found to be inactive.

DEDICATION

You probably could have left a mark in this life

But you only left scars on the hearts of others

And on yours still

I mean you the child soldier

Of course by circumstances beyond your control

If only you were given a chance

But hope is not lost

I refer to you, the child soldier

What was meant to be, shall be

My heart bleeds at your unfortunate predicament

Because it's not of your making

I bewail your asperity, you the child soldier

For you serve not, your desires nor interests

But of the covetous, vainglorious and unrepentant

Whose souls have gone beyond reproach

I bemoan your plight, you the child soldier

(Tapiwa Hlatywayo)

http://www.newtimes.co.rw/new

This work is dedicated to all those who have been deprived of the opportunity to be who they should be, with particular concern for the child soldier.

ACKNOWLEDGEMENTS

Numerous benevolent souls have invested both time and effort in transforming this project into a tangible reality. Had it not been so, then the project would have as well remained a mere dream, confined in the walls of the unknown and the undiscovered. I however need to put special mention to my academic promoter Dr Salam Titinchi for his guidance from the very onset up till the end of this research project. His undivided attention and continual support proved to be a vital cog in motivating this endeavour, and to this end I can pronounce with all humbleness and say, "mission accomplished."

Special mention is also due to my co-promoter Professor Leslie Petrik, for providing a homely and conducive environment within her research group, the Environmental and Nanosciences Group (ENS). The story of the success of this project would be a misrepresentation of reality if her academic input and material support in this research is left unmentioned. Every time I searched for reason, she inspired.

To my colleagues whom I now call family, at the ENS, I say thank you for walking this journey with me. Your presence and the warmth of your companionship have always given me continual solace and were indeed a constant reminder that I am never alone. Your goodness overwhelms my soul so much such that it cannot be reduced to mere words.

I also desire the much to convey my sincere gratitude to the technical support I received from Miranda Waldron (UCT), Subelia Botha (UWC) Tanya Dreyer (UCT), Stephanie Snoek (UCT), Isle Wells (UWC) for HRSEM, HRTEM, XRD, N_2-sorption analysis respectively. I further extend my profound gratitude to NRF for funding my studies and to Eskom Holdings for providing funding to meet the research costs.

Work of such magnitude could not have been attempted without making reference to the works of others. It is in that light that I perceive it more than necessary to extend my gratitude to all the publishers and owners of the sources cited in this document.

Lastly but mostly I thank the Sovereign God the Father of all mercies, provider and giver of all strength and wisdom, for the Divine guidance, wisdom of understanding and the good health that has carried me through the trying times during my research. I owe you my life.

TABLE OF CONTENTS

LIST OF FIGURES

LIST OF TABLES

LIST OF ABBREVIATIONS

ASTM	American Standards of Testing Materials
ATR	Attenuated Total Reflectance
BET	Brunauer – Emmett -Teller
EDS	Energy Dispersive Spectroscopy
FC	Fridel-Crafts
FTIR	Fourier Transformed Infrared Spectroscopy
ICP	Inductive Coupled Plasma
IE	Ion – Exchange
IWI	Incipient Wetness Impregnation
IZA	International Zeolite Association
MCM	Mobil Composition of Matter
SAED	Selected Area Electron Dispersion
SDA	Structure Directing Agent
SEM	Scanning Electron Microscopy
t-BB	*t*-butylbenzene
t-BC	*t*-butylchloride
TGA	Thermo Gravimetric Analysis
TPD	Temperature Programmed Desorption
TPR	Temperature Programmed Reduction
wt %	Weight Percentage
XRD	X-ray Diffraction

CHAPTER 1

1.0 Introduction

This chapter presents an introduction and gives the background of the Friedel-Crafts reactions. It then narrows down to the chemistry of alkyl benzenes together with their applications and synthesis routes. It also presents the broad aim alongside the specific objectives of the study. It goes on to outline the problem statement, research questions, motivation of study and finally the thesis layout.

1.1 Friedel-Crafts Reactions

The Friedel-Crafts (FC) reaction is one of the most useful electrophilic aromatic substitution reactions (McMurry, 2012). The approach is named after Charles Friedel and James Mason Crafts who in 1877 discovered the alkylation of benzene using $AlCl_3$ as the catalyst (Olah, 2003). From the time of its discovery numerous research activities centred on the Friedel-Crafts reaction have been undertaken, and based on the outcomes of these activities it can be established that there are many transformations that can be listed under the FC reaction. In the early 1960's, FC reactions were defined as any organic reaction that involves isomerisation, elimination, cracking, polymerisation or addition, that takes place under the catalytic influence of either a Lewis acid or a Brønsted acid. Lately the generally accepted definition is confined to the specific functionalisation as either acylation or alkylation (Bandini et al, 2009). Friedel-Crafts alkylation involves the introduction of an alkyl group on the aromatic ring. This is traditionally achieved by reacting the alkyl halide with the aromatic compound in the presence of $AlCl_3$ (McMurry, 2012).

The FC reaction can be pronounced as one of the oldest organic transformations that occur under the catalytic influence of alkyl halides. The application of the reaction on both laboratory and industrial scales has been on the rise. The reaction forms an essential synthetic step in various commercial processes. It has been extensively studied and a lot of understanding has been accrued over a period of more than 130 years. The major advances that have been brought forward are mainly in the development of systems that enhance reactivity and selectivity. Attention has also been given to the use of environmentally eco-friendly approaches which do not use catalysts that pose

environmental threats and also to minimise the production of hazardous waste. There has been a marked shift towards the development of greener and economically sustainable options (Bandini et al, 2009).

During the early 1990's much attention was given to challenges around catalysis and stereo-control, with particular interest in developing a sound understanding of specific catalyst-substrate interactions with the intent to develop efficient and sustainable catalyst systems (Bandini et al, 2009).

1.1.1 Alkyl benzenes

Alkyl benzenes are a range of liquid chemicals characterised by a low boiling point. They find many industrial applications either as solvents or chemical process intermediates. In definition they are single ring aromatic hydrocarbons with a variety of aliphatic side chains joined to the ring. Of their most pronounced applications are their uses in the plastic industry and as blending stocks in the increase of octane number in fuels. They are also used as solvents in paints, adhesives and pesticides (Snyder, 1981). One other significant application of alkyl benzenes is in the production of synthetic detergents where they act as intermediates. In this process linear alkyl benzenes (LAB) are generated when straight chain alkyl groups are used. These LABs result in the formation of soft degradable alkylates. In the event that branched alkyl groups are used hard non-degradable alkylates are produced. Long chain benzene alkylates also find use as lubricants (Riegel, 2003).

The general synthesis route for alkyl benzenes is usually via the Friedel-Crafts alkylation method in which Lewis acids or strong mineral acids are used to catalyse the reaction. The alkylation of benzene is based on the electrophilic attack of the aromatic ring by an alkylating agent (Adams, 1946). The treatment of an alkyl halide in the presence of $AlCl_3$ results in the formation of a carbocation electrophile R^+. The $AlCl_3$ complexes with the Cl in the alkyl halide, this action results in the weakening of the C-Cl bond and induces charge separation according to the following reaction scheme.

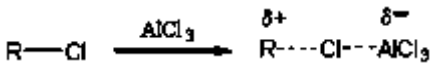

Reaction scheme 1.1: Dissociation of alkyl halide by $AlCl_3$

The π electrons on the benzene ring then attack the carbocation resulting in the formation of a C-C bond. This yields a new intermediate carbocation/arenium ion, with the final step being the loss of a proton giving yield to a neutral alkylated ring (R-Ph) alongside HCl, and the $AlCl_3$ (catalyst) is regenerated (McMurry, 2012 and Fox et al, 2004). The general mechanism is presented in the following scheme.

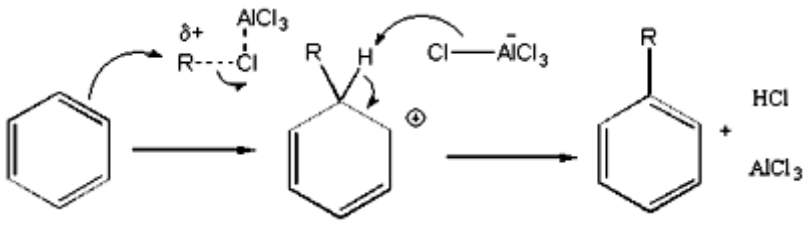

Reaction scheme 1.2: Mechanism of benzene alkylation in the presence of $AlCl_3$

It should however be noted that the reaction is not as straight forward as projected. It is characterised by cationic rearrangement, when primary or secondary alkyl halides are used. In general, all primary alkyl halides undergo rearrangement when treated with $AlCl_3$. This is due to the formation of an appreciable positive charge on the primary carbon atom. In terms of stability the order is such that; tertiary > secondary > primary, so in essence primary carbocations are not stable (Fox et al, 2004). A typical outcome can be depicted by the reaction of benzene with 1-chlorobutane in presence of $AlCl_3$.

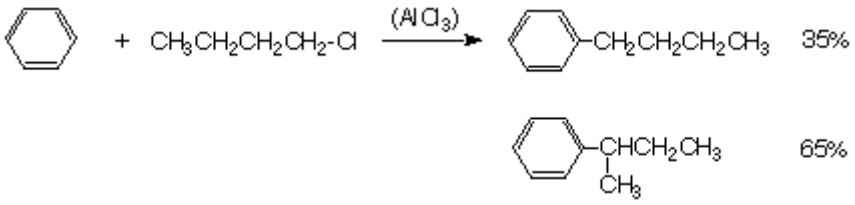

Scheme 1.3: Alkylation of benzene with 1-chlorobutane

One of the major problems associated with the Friedel-Crafts alkylation of benzene with alkyl halides is the formation of more than one product. However the use of supported acid catalysts can greatly improve both selectivity and the yield. The use of traditional catalysts such as mineral acids is usually accompanied with separation complications (Harmer et al, 2001). The use of excess benzene favours the formation of monoalkylated products (Bidart et al, 2006). There are a variety of alkylating agents that

can be employed in the Friedel –Crafts alkylation reactions but the most commonly used are alkyl halides, alcohols, alkenes, olefins, ethers, highly strained cyclo-paraffins and esters (Adams, 1946).

There are a number of established catalysts that are used for alkylation of aromatic compounds with the commonly applied ones being $AlCl_3$, $FeCl_3$, $SbCl_5$, BF_3, $ZnCl_2$, $TiCl_4$, HF, H_2SO_4, H_3PO_4 and P_2O_5 (Adams, 1946). Super acids such as $HF{\bullet}SbF_5$ and $HSO_3F{\bullet}SbF_5$ have also been applied as catalysts for the alkylation of aromatic compounds (Rueping and Nachtsheim, 2010). The use of these catalysts presents a number of complications namely handling, storage, massive waste and production of polyalkylated products (Chiu et al., 2004; Rueping and Nachtsheim, 2010). The use of zeolites has received much attention recently. Bidart et al., (2006) reported that it is achievable to have a selectivity of 98% with a 96% conversion when iron loaded zeolite Y was used. There has been a trend to move towards green chemistry, which advocates for the use of environmentally eco-friendly catalysts such as zeolites for the alkylation process.

1.2 Problem Statement

The use of Lewis acids and strong mineral acids in the industrial production of alkyl benzenes have a number of constrains. Lewis acids do not require the use of stoichiometric quantities and upon reaction completion none of the catalyst is recovered. These acids are also characterised by separation problems which usually result in the liberation of HCl and large quantities of aqueous and salt waste (Clark, 1998). On the other hand strong mineral acids present handling problems as well as corrosion to industrial equipment. Separation of catalyst from product is also a great challenge (Harmer, 2001).

Faced with these challenges there is a need to create new, efficient and sustainable catalysts, which are environmentally eco-friendly and easily separable from the reaction matrix. Acid zeolites have proved to be a possible alternative as Friedel-Crafts alkylation catalysts, but their use should be economically viable for industry to adopt the approach. Commercial zeolites are a bit expensive (Georgiev, 2009). However numerous research activities have proved that various zeolites can be easily produced from fly ash (Ojha et al., 2004, Querol et al., 2002, Sutarno et al., 2007).

South Africa is largely dependent on coal combustion for power generation, and in the combustion of coal, vast amounts of fly ash are generated and accumulate year in and year out. This poses disposal constraints at the power stations, so converting the fly ash into a usable material such as zeolite catalyst solves two problems; reducing disposal challenges surrounding the accumulation of fly ash, as well as creating a suitable environmentally eco-friendly catalyst for application in the alkylation of benzene. The background of fly ash will be presented in detail in Chapter 2.

If the problems addressed herein are solved this would bring relief to both the environment as well as industry since a sustainable and cheap catalyst would have been made available for use in the Friedel-Crafts alkylation process.

1.3 Broad Aim

The broad aim of the study is to synthesise an active supported metal catalyst for the Friedel-Crafts alkylation of benzene with alkyl halide using green chemistry approaches.

1.4 Specific Objectives

- To synthesise hierarchical Zeolite X from South African Fly ash collected from Hendrina power station.
- To load the fly ash synthesised hierarchical Zeolite X with iron and manganese by ion exchange and incipient wetness impregnation using iron nitrate and manganese acetate as metal precursors.
- To load commercial support materials, namely mesoporous MCM-41 and zeolite HBEA with iron and manganese by ion exchange and incipient wetness impregnation using iron nitrate and manganese acetate as metal precursors.
- To characterise the supported metal catalysts by HRSEM, HRTEM, EDS, ICP-OES, XRD, SAED and N_2-adsorption.
- To compare the catalytic activity of the metal loaded support materials for the alkylation of benzene with *t*-butylchloride, with particular interest on conversion, selectivity, product distribution and percentage yield.
- To determine the effect of doping Fe supported catalysts with Mn on the catalytic activity.

- To determine the effect of the pore system of the support on the catalytic activity of the supported metal catalysts.

1.5 Research Questions

- The present work would address a variety of issues with regard to the possibility of using fly ash synthesised zeolites as possibly metal support materials for the alkylation of benzene using alkyl halides. It is against this background that the following questions were coined and this study presents answers to their feasibility.
- Is South African fly ash usable as a starting material for the synthesis of the hierarchical Zeolite X and how reproducible are the synthesis outcomes?
- Are the substrates under study; MCM-41, HBEA, and the hierarchical Zeolite X, suitable support materials for the Friedel-Crafts alkylation of benzene with *t*-butylchloride.
- Can iron and manganese be easily incorporated on MCM-41, Zeolite HBEA, or the hierarchical Zeolite X via incipient wetness impregnation or ion exchange without regulating the pH and retain the crystallinity of the parent support material upon metal loading?
- Can the use of bimetallic catalysts containing both iron and manganese improve the activity in comparison to monometallic catalysts?
- Does support pore size or acidity have any marked influence in determining the percentage conversion as well as the product selectivity, when applied for the Friedel-Crafts alkylation of benzene?

1.6 Motivation of Study

This study is motivated by a number of hypotheses and the hope to realise the set objectives is based on these hypotheses. The broad intent being to provide an alternative green route in the alkylation of aromatics with alkyl halides, by employing the use of acid zeolites. Zeolites have many applications and based on the possibility that they can be easily synthesised from coal fly ash, the present study focuses on the synthesis of the hierarchical Zeolite X from South African coal fly ash. Different zeolites have been successfully synthesised from coal fly ash and Querol et al, (2002), present a review citing various work in which the zeolites were synthesised by different researchers.

Bidart et al, (2006) reports that Fe loaded zeolites can be used for the FC alkylation of benzene. The present work intents to test the feasibility of using coal fly ash synthesised zeolites as supports for Fe and Mn and compare the resultant catalysts with standard commercial catalysts for the activity in the alkylation of benzene with *t*-butylchloride.

1.7 Research Approach

In order to realise the objectives, various experiments were carried out. The first activity was the synthesis of the hierarchical Zeolite X from South African fly ash collected from Hendrina power station. The synthesis was done via a fusion step followed by hydrothermal treatment and finally crystallisation (Musyoka et al, 2011). Upon synthesis the zeolite was loaded with iron and manganese, using iron nitrate and manganese acetate as the respective metal precursors. Two loading approaches were employed, namely conventional ion exchange and incipient wetness impregnation. The same approaches were applied to prepare the metal loaded commercial supports used as comparatives in the present study, which were MCM-41 (Sigma Aldrich) and HBEA (SUD Chemie).

Both ion exchange and incipient wetness impregnation are seasoned approaches that have been extensively studied. However it is very difficult to create a ratio of 1:1, iron to manganese bimetallic catalyst using ion exchange since the exchange rate of the respective metals is not the same. Iron tends to exchange better than manganese due to its smaller hydration shell (Weitkamp et al, 1999), so if a 50:50 solution of iron and manganese is used the resultant catalyst would have more iron than manganese, and due to this reason only monometallic catalysts were prepared via liquid phase ion exchange. On the contrary it is relatively easy to create a 1:1 iron to manganese ratio via incipient wetness impregnation and the dispersion of the metal is expected to be relatively better in comparison to that obtainable with monometallic catalyst of corresponding metal percentage weight. This is due to the fact that when two metals are simultaneously introduced there is tendency of the metals forming an alloy than large independent metal crystallites. Both monometallic and bimetallic catalysts were prepared via incipient wetness impregnation.

Upon synthesis of the respective metal catalysts the same were subjected to a variety of material characterisation. The morphology was determined via scanning electron

microscopy (SEM) and high resolution transmission electron microscopy (HRTEM) with the aim being to establish whether the integrity of the respective supports was retained upon metal loading. Qualitative elementary composition was carried out with Electron Dispersive Spectrum (EDS) analysis. Quantitative elementary composition was then done via inductively coupled plasma optical emission spectrometry (ICP-OES). Determination of the crystallinity and mineralogical identity of the catalysts was done via X-ray diffraction (XRD) analysis. This would also enable one to determine whether larger metal crystallites were formed on the surface of the support. Numerous reports in literature do attest to the fact that if a metal loading of about 10 wt % is achieved, then peaks due to the metal crystallites can be observed on the XRD patterns (Balle, 2009). Further characterisation was carried out via N_2-adsorption to determine the surface area of the respective catalysts. Selected area electron dispersion (SAED) was performed to evaluate the crystal structure and the degree of polycrystallinity of the loaded supports. The surface area and pore distribution of the prepared catalysts was done by N_2-adsorption.

On completion of the characterisation of the metal loaded supports the catalytic screening of the catalyst was undertaken. To minimise side reactions and enhance selectivity excess benzene was used as both reactant as well as solvent. The Friedel-Crafts alkylation of benzene with *t*-butylchloride was undertaken at a temperature of 45 ^{0}C under reflux and samples were taken at specific time interval within a reaction time of 5 h, and analysed using gas chromatography (GC). From the generated chromatograms calculation of the conversion of *t*-butylchloride, selectivity of *t*-butylbenzene, product distribution and percentage yield of the *t*-butylbenzene were performed. Products were qualitatively determined using mass spectrometry.

1.8 Scope and Delimitation of Study

The present work strives to present a cheap and effective catalyst for the Friedel-Crafts alkylation of benzene with alkyl chlorides. The main focus is to present a comparative study between metal loaded commercial support materials namely, HBEA and MCM-41, with metal loaded coal fly ash synthesised hierarchical Zeolite X. Comparison of the results obtained was also made with other catalysts presented in open literature.

Every zeolitic material has its own optimum preparation conditions that enhance the activity of the catalyst. For instance, when a zeolitic material is metal loaded via conventional ion exchange, a good metal dispersion may be achieved when a particular pH of the metal precursor solution is used (Centi, 2001). However in the present study pH regulation was not done, all the respective supports used herein were loaded at the same operating conditions.

The catalyst screening undertaken was simply meant to identify a promising route for catalyst preparation that can in future be further investigated and optimised. The present study did not undertake optimisation studies. The kinetics, mechanisms and thermodynamics of the benzene alkylation reactions were not investigated in this work. With regards to bimetallic catalysts the effect of the mass ratios of the metals was not investigated either, only a 1:1 ratio of Fe:Mn was used.

1.9 Thesis Outline

This section presents the dissertation's chapter chronology as well as overviews of the main contents of the respective chapters. The intent is to give a brief set out of the content constituting this document. The dissertation is divided into seven chapters.

The first chapter covers a brief introduction to alkyl benzenes as well as the catalysts applied for the process. The chapter goes on to introduce the possibility of the application of zeolites as possible green route and suitable catalyst support materials for the Friedel-Crafts alkylation. The idea of using fly ash as a cheap starting material for zeolite synthesis is also brought forward.

The second chapter gives the study background focusing mainly on the advantages of using fly ash as a starting material for zeolite synthesis as well as a general background of zeolites and their respective synthesis routes. The chapter also gives an insight in the environmental concerns with regard to continual accumulation of fly ash at the power stations. The chapter goes on to review the literature with regard to numerous zeolite synthesis approaches from both pure chemicals as well as waste materials, fly ash inclusive. Particular attention is given to the synthesis of Zeolite X. The various metal loading methods are also presented and the focus is on the methods applied in this research namely ion exchange and incipient wetness impregnation. Details with regard to the various characterisation techniques applicable to uncovering the nature of both

the unloaded and the metal loaded support materials are laid down. In essence characterisation is done via the following techniques; HRSEM, HRTEM, EDS, SAED, XRD, N_2-adsorption, and ICP-OES. The effects of the various parameters during metal loading and post loading treatment and how they can determine the nature and character of the final catalyst are reviewed. Furthermore, the mechanism of the Friedel-Crafts alkylation of benzene is also looked into and how the nature of the support influences both percentage conversion as well as selectivity. Outcomes from related research activities are also highlighted herein.

The third chapter presents the materials and methods, giving the experimental details used with regard to firstly the synthesis of Zeolite X from fly ash. This is followed by the details pertaining to the respective metal loading approaches applied (ion exchange and incipient wetness impregnation). The settings and conditions of the instrumentation used for characterisation then follows and finally the operating conditions applied during the Friedel-Crafts alkylation of benzene are given.

The fourth chapter presents characterisation outcomes of the synthesised zeolites as well as the metal loaded zeolites. The data generated from the respective characterisation activities is presented, together with the appropriate facts and postulations that are deemed responsible for these outcomes. Comparison is also made to the results generated from other related research outcomes and when discrepancies are noted possible attributions are put forward.

The fifth chapter presents the catalytic activity of the catalysts for the Friedel-Crafts alkylation of benzene. Of much interest is the percentage conversion of the *t*-butylchloride, the percentage selectivity towards the formation of the *t*-butylbenzene, the product distribution and the percentage yield of the *t*-butylbenzene. The effect of doping the Fe catalyst with Mn is also presented. The effect of the amount of metal, the pore system and acidity of the support and the reaction time are also discussed.

The sixth chapter gives an overall conclusion of the outcomes obtained both for characterisation of the catalysts as well as the catalytic activities of the respective metal supported catalysts. Based on the conclusion drawn appropriate recommendations are presented. The seventh and final chapter presents the appendix in which tables and other data generated in the research and not presented in the main document are laid out. All references are consolidated in one section at the end of the dissertation.

CHAPTER 2

2.0 Literature review

This chapter gives a general background of the feedstock materials applied herein as well as their environmental considerations together with the advantages of their application in creating a cheap, efficient and sustainable catalyst for the Friedel-Crafts alkylation reaction. Consideration is given to fly ash, highlighting the formation as well as its environmental implications. Zeolites will then be introduced alongside their most conspicuous applications. The different metal loading approaches are also presented with emphasis given to ion exchange and incipient wetness impregnation, since these are the approaches applied in the present study. The final section of this chapter presents the Friedel-Crafts alkylation reaction kinetics, thermodynamics, catalysts and the different alkylating agents used in the reaction.

2.1 Fly ash

Fly ash is the residue that results from the burning of pulverised bituminous coal in power stations. It is also referred to as pulverised fly ash or combustion coal product. However the term fly ash is generally used (Sear, 2001). Fly ash is made up of fine inorganic glassy spherical particles (Eary et al, 1990). The particle size is within the range of 10 – 100 microns and due to their small size, the particles are carried away in the flue gas stream after coal combustion and collected via electrostatic precipitators or filter fabric bag houses (Rafalowski, 2003). The much coarser and heavier particles are usually collected via mechanical cyclones and is termed bottom ash. The chemical and mineralogical properties of the fly ash vary depending on the type of coal burnt, but in general the major components are silica, alumina and iron oxides which constitutes about 75 – 85 % of the bulk material (Sear, 2001). The silicon and the aluminium are usually in the amorphous phase with a smaller percentage being crystalline and in the form of mullite and quartz (Musyoka, 2009), while iron oxides exist as magnetite and haematite (Sear, 2001). In certain instances other crystalline phases such as crystobalite, gypsum, lime, portlandite and periclase may be present (Suarez-Ruiz and Crelling 2008). In total an estimate of about 36.7 million tonnes of fly ash are produced in South African power stations yearly, and with the ever increasing demand for power this volume is expected to rise continually. However of all this quantity only 5.7 % is

converted to usable material while the rest is stacked in ash dams and landfills (Vadapalli et al, 2009).

2.1.1 Chemical composition of coal fly ash

The chemical and mineralogical as well as the physical properties of fly ash are largely dependent on the type of coal burnt. However there are some common elements that constitute the composition of all sources of fly ash as both majors and traces. Apart from the characteristic silica, alumina and iron oxides found in significant quantities in fly ash, there are also a host of other elements. In general fly ash contains almost all the elements in the periodic table with the trace elements usually in the range of 1000 micrograms per gram or less. Of the trace elements the most common ones include; Pb, As, Se, Cd, Ni, Co, Mn, Zn and chromium (Suarez-Ruiz et al, 2008). These elements may have either inorganic or organic origins.

Based on the elemental composition the fly ash can be categorised as either Class C or Class F. According to the American Standards of Testing Materials (ASTM), Class C fly ash is produced when sub-bituminous or lignite coals are burnt. The sum of the silica, alumina and iron oxide content is set to a minimum limit of 50 %. The fly ash contains significant proportions of CaO, MgO and SO_3 (Punshon, et al, Sajwan et 2003). Class C ash is pozzolanic, meaning to say when mixed with calcium hydroxide it forms compounds with cementitious properties (Malhotra et al, 1996).

On the other hand Class F is produced when anthracite or bituminous coal is used. The ash is characterised by a minimum of 70% total of silica, alumina and iron oxides. The lime content of Class F is relatively low compared to that of Class C giving the former reduced or no cementitious value by itself. The physical properties of both classes are closely related in terms of the particle size and size (Daniel et al, 2005). The typical classification is presented in Table 2.1.

Usually fly ash also comes with significant amounts of calcium compounds with Class F containing calcium oxide in the range of 7 – 12 % and Class C having 15 – 24 % weight percentage (Giere et al, 2004).

Table 2.1: *Classification of coal fly ash (ASTM C 618 – 95) (Sheetz et al, 1998)*

Chemical components	Class F	Class C
$SiO_2 + Al_2O_3 + Fe_2O_3$ min %	70	50
SO_3 max %	5	5
Na_2O max %	1.5	1.5
LOI max %	6	6
moisture content max %	3	3

**LOI stands for loss of ignition; this is a measurement of the un-burnt carbon in the ash.*

2.1.2 Fly ash: The South African case

South Africa's economy largely rests on its mining industry, which is energy-intensive, and presents the country with high demands for power generation. To meet this ever increasing demand for power from the ever growing industry and increasing domestic demand, the country through its energy utility, Eskom, keeps on scaling up power generation. At present 77 % of the power is generated from coal powered stations. Apart from meeting domestic needs the power utility also supplies electricity to Lesotho, Botswana, Swaziland, and Namibia. In addition it also exports power to both Mozambique and Zimbabwe. The country is the 7th largest electricity producer and the 5th coal producing country globally, with a yearly output of 224 million tonnes marketable coal. It is estimated that Eskom generates two thirds of all the power generated in Africa and provides for 95 % of South Africa's power. Considering the fact that South Africa has limited capacity to turn to other energy sources such as hydro-electric and nuclear energy it is estimated that the country would rely largely on coal generated power up until 2020. South African coal reserves are estimated to be around 53 billion tonnes and at the current consumption rate this is expected to last for the next 200 years. There is also well established infrastructure for coal fired power stations. This reduces to the reality that coal might be relied on for some considerable period of time. Presented with this scenario it becomes apparently necessary to find means and ways to convert the accumulating fly ash into useful materials to ease the disposal constraints (Eskom 2012; Oxford Buss. Grp., 2008).

The coal produced in South Africa is dominantly bituminous and anthracite, however the country also does export large volumes of high quality coal and the low quality coal is used in South African power stations (Somerset et al., 2008). The burning of such

coal results in the formation of high volumes of ash because of the high inorganic content. In essence South African fly ash is classified as Class F (Daniel et al, 2005).

2.1.3 Environmental hazards of fly ash

The release of coal fly ash into the environment presents both direct and indirect human and ecological hazards (Frontasyeva et al, 2000). The microcrystalline nature of the coal fly ash particles enables it to absorb metals. Since the particles are minute and of size less than 1μm, they can easily be inhaled and find their way into the respiratory system (Speight, 2013). Chemical evaluation of fly ash has proved that it contains a range of toxic organic compounds, with the most common ones being phenanthrene, anthracene, pyrene, benz[a]anthracene, chrysene and benzo[a]pyrene. These organic compounds will be bioavailable since they are not photochemically degradable, and may eventually be taken up by organisms. Again the volatile compounds that are released during combustion may condense and get immobilised on the fly ash particles (Frontasyeva et al, 2000).

Fly ash also contains radionuclides mostly uranium and thorium (Sear, 2001). Uranium exists mostly as silicate minerals in the form of coffinite and uraninite. During coal combustion the coffinite usually remains at the bottom whilst the uraninite is vaporised and then later condenses on the fly ash particles. The existence of these radionuclides poses radiation exposure to human in the vicinity of the fly ash dams or landfills (Speight, 2013).

Due to the numerous metals found in the fly ash, when fly ash comes into contact with water it initiates salt enrichment of the soil due to solid phase dissolution reactions. This has the consequence of reducing the soil pH (Frontasyeva et al, 2000). The distribution of the various metals between the bottom ash and the fly ash is dependent on their degree of volatisation. Group 1 elements which include thorium (*which is radioactive*), remain condensed at coal combustion temperatures and partition equally between the bottom ash and the fly ash. The group 2 elements are quite volatile and most of them will condense on the fly ash (Speight, 2013). The elements of group 3 are very volatile and the greater proportion of these elements is associated with fly ash. This group also includes Hg, which has vast health consequences generally referred to as mercury poisoning or mercurialism (Mathieson, 2005).

2.1.4 Major applications of fly ash

Although being a waste product fly ash finds a range of applications worldwide. It can either be used in its raw state or modified. Since it contains a variety of major elements it is a suitable starting material for a range of products. Fly ash is the best known pozzolanic and this makes it a good additive to concretes and cement (Dhir et al, 2002). Portland cement contains about 65 % lime and during hydration part of the lime becomes free and available. This can then react with the fly ash to form additional cementitious materials (Rafalowski, 2003). The use of fly ash as an additive in production of Portland cement also reduces the emission of CO_2. It is estimated that for every ton of fly ash used instead of lime for a ton of Portland cement, a ton of CO_2 is prevented from entering the atmosphere. On the other hand the fly ash does not need to be treated in high temperature kilning processes unlike the case with Portland cement (Speight, 2013). It is has been proved that about 30 % CO_2 emission reduction can be achieved by the incorporation of fly ash to cements (Dhir et al, 2002).

Fly ash also finds application in the removal of heavy metals from water. A typical large scale water treatment in which fly ash has been successfully applied is in the removal of arsenic from drinking water in West Bengal in India and Bangladesh. The fly ash has the capacity to reduce arsenic levels within the concentration range of 0.3 – 100 ppm to low levels in the ppb range. The presence of unburnt activated carbon in the fly ash enables it to remove a host of other heavy metals from waters including Hg, Fe, Pb, Zn and Cu together with non-metallic compounds such as NH_3 (Samir, 2009) .

Although fly ash does not contain major macronutrients like nitrogen, it also can be applied in conjunction with other organic materials such as poultry litter and sewage sludge for soil enrichment. When combined with these organic materials it can create balanced soil enrichment comparable to that obtainable with conventional fertilisers and is used for non-food crops such as roses (Bogdanov, 2009). Fly ash is alkaline in its nature and this character can be advantageous if the ash is added to acidic soils (Samir, 2009). However the use of fly ash in agriculture has been hampered by the fact that it contains a variety of heavy metals which can easily be taken up by plants and end up in the food chain.

Low moisture fly ash has been used as a soil consolidating material in mine back-filling. It is usually a very convenient option for back-filling mining areas close to the coal mines. One of the most notable applications of fly ash is its use in road construction as a substitute to crushed aggregate materials (Dhir et al, 2002; Rafalowski, 2003).

Fly ash contains significant amounts of silica and alumina, and it has been used as a cheap source of silica and alumina in zeolite synthesis. Numerous research activities present reports on the synthesis of different zeolitic materials from fly ash. A comprehensive overview of zeolite synthesis from fly ash is presented in literature (Querol et al, 2002).

2.2 Zeolites

Zeolites are inorganic crystalline hydrated aluminosilicate generated from an infinite three dimensional network of AlO_4 and SiO_4 tetrahdra linked to one another by sharing of the oxygen atom (Georgiev et al, 2009).

2.2.1 Historical background and introduction to zeolites

The term zeolite was coined by amateur Swedish mineralogist Baron A.F. von Cronstedt, in 1756 upon the discovery that on rapid heating these stones release water and appear to boil. The term zeolite was then derived from a marriage of two Greek words, '*zeo*' meaning stone and *'lithos'* meaning to boil (Schwuger, 1996). In essence zeolites can be defined as inorganic crystalline hydrated alumonosilicates generated from an infinite three dimensional network of AlO_4 and SiO_4 tetrahdra linked to one another by sharing of the oxygen atom, forming a porous material with pore size in the range of (1 - 20 Å) in diameter. The SiO_4 tetrahedral is neutral whilst the AlO_4 tetrahedral is negatively charged and is charge balanced usually by either group 1A or group 2A metals like potassium, sodium, calcium, magnesium, strontium and barium. These cations together with water molecules occupy the interconnected void channels in the zeolite framework (Inglezakis and Poulopoulos, 2006).

The cations that are not held to fixed charge balancing positions are free to move within the confinements of the channels and they can also be readily interchanged with other cations. The water molecules can be reversibly removed, leaving voids that can amount to as much as 50% of the dehydrated crystal material (Haag et al, 1984).

Much attention has been given to the synthesis and application of zeolites. Their unique character enables them to find great use in ion exchange, adsorption and catalytic processes. Zeolites can be either natural or synthetic, but for most commercial purposes synthetic zeolites are preferred. The first commercially synthesised zeolites were Zeolite A, X and Y and later on the ZSM series. These zeolites have been applied in industrial processes such as purification and separation processes. They have also been applied successfully in the petrochemical industry in major processes such as catalytic cracking and the Friedel-Crafts alkylation of aromatics (Rebeiro et al, 1984). Further details with regard to their synthetic routes, major applications as well as their chemical and physical properties will be presented later in this chapter.

2.2.2 Zeolite framework structure and properties

The fascinating properties of zeolites emerge from their structures. The definition of zeolites has been given in section 2.4., they however can be described by the following empirical formula which depicts the general zeolite composition.

$$\mathbf{Mx/n\ [(AlO_2)x(SiO_2)y].zH_2O}$$

Where M is the exchangeable cation of valency *n*; z is the number of water molecules; with x and y being the stoichiometric ratios of Al and Si in the unit cell (depends on structure)

More Al in the lattice structure results in increased ion exchange capacity and hydrophilicity, whilst increased amounts of Si results in increased formation of surface silanol groups and hydrophobicity. In synthetic zeolites these ratios can be manipulated to effectively create a high field density, selectivity for water or polar and polarisable molecules to suit the specific application. The common exchangeable cations are Cu, Li, Mg, Zn, Pb, Ag, Cd and protons. Further modification of the zeolite surface chemistry can be enhanced by isomorphously replacement of framework elements such as Al with elements such as gallium, iron, phosphorus and germanium. Elements that are more electronegative than Al will result in decreased acid strength of Brønsted centres in the zeolite. The SiO_4 and AlO_4 tetrahdra, known as the T-atoms can be arranged in a variety of patterns resulting in a diverse range of pore structures (Breck, 1974). Figure 2.1 is a typical arrangement of the T-atoms.

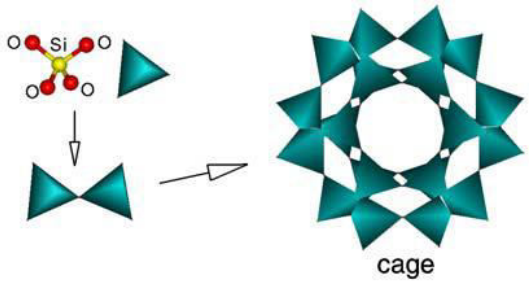

Figure 2.1: *Zeolite crystal framework structure (www.bza.org/zeolites.html)*

The T-atoms are referred to as the Primary Building Units and they then can arrange into hundreds of possible three dimensional frameworks or lattice structures. Almost all of the zeolites are constructed from Secondary Building Units SBUs (Wagner and Davis, 2000). Figure 2.2 presents the most common SBUs.

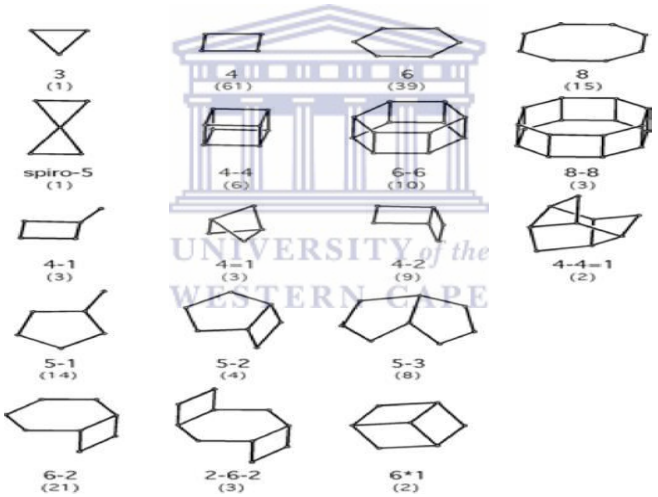

Figure 2.2*: Secondary building units, the polyhedral vertices represent tetrahedra atoms (Wagner and Davis, 2000)*

2.2.3 Classification of zeolites

There has been a lot of confusion with regard to zeolite nomenclature. In the past zeolites were named by the researcher who would have synthesised the zeolite. During this era it was apparently possible to have one particular zeolite having as many as 20 different names. To ease this confusion various attempts were made to classify zeolites in a more systematic manner. The nomenclature that has been now adopted is based on structure type code introduced by IUPAC (International Union of Pure and Applied

Chemistry), (Williams and Gagan, 2002). Table 2.2 presents a selected set of zeolites and the current nomenclature.

Table 2.2: IUPAC zeolite classification

zeolite type	structure code	pore size/nm	number of Si/Al tetrahedra in pore cross section
small pore			
zeolite A	LTA	0.41 (circular)	8
erionite	ERI	0.36 x 0.51	8
medium pore			
ZSM-5	MFI	0.53 x 0.56	10
ZSM-11	MEL	0.53 x 0.54	10
large pore			
zeolite X & Y	FAU	0.74 (circular	12
mordenite	MOR	0.65 x 0.75	12

Zeolite framework structures are described by a 3-lettered code usually derived from the material name. For interrupted frameworks the code is preceded by a (-) hyphen whilst an (*) asterisk precedes a framework of a hypothetical end member. Complete framework topology codes are assigned by the 'Structure Commission of the International Zeolites Association (IZA) and an updated classification is provided by IZA in the Atlas of Zeolite Framework types accessible on (http://www.iza-online.org). Selected 3-letter framework topology codes are presented in Table 2.3.

Table 2.3: Selected zeolite framework codes

Code	Abbreviated Name	Full Name
LTA	Linde type A	Zeolite A (Linde Division, Union Carbide)
LTL	Linde type L	Zeolite L (Linde Division, Union Carbide)
FAU	Faujasite	
MFI	ZSM-5	Zeolite Socony Mobil-five
-CLO	Cloverite	Four-leafed clover shaped pore opening
*BEA	Zeolite Beta	

2.4.3.1 Previous Zeolite Classification

Basically the classification of zeolitic materials was based on three schemes, two of which were based on the crystal structure whilst the third scheme was founded mostly on a historical basis, putting zeolites with common properties in the same group. In the first classification scheme the first zeolite to be discovered in the group is given priority in naming the group. The second framework classification is based on description given by Meier, (1968). This is based on the idea of Secondary building units (SBUs) as already presented in Figure 2.2. In this particular classification the distribution of Si-Al is neglected and there are basically seven groups in which zeolites are classified according to subunit structure. Table 2.4 shows the specific $(Al,SiO)_4$ tetrahedra arrays. Since the SBUs can be linked to form numerous polyhedra, many different zeolite structures can be created, with regular cavities and channel structures.

Table 2.4: Zeolite structural classification according to Breck. (1974).

Group	Secondary Building Unit (SBU)
1	single 4-ring, S4R
2	single 6-ring, S6R
3	double 4-ring, D4R
4	double 6-ring, D6R
5	complex 4-1, T_5O_{10} unit
6	complex 5-1, T_8O_{16}
7	complex 4-4-1, $T_{10}O_{20}$ unit

The third classification as proposed by Gottadi and Galli (1985) is almost the same as the one proposed by Breck (1974) based on the SBU concept. The difference with the third one is that it has a historical concept on the discovery and how the zeolites were named. This give rise to six structural classes, based on combining zeolite group names with specific SBUs and consisting of complex structural units either finite or infinite. Figure 2.3 presents the classification according to this concept.

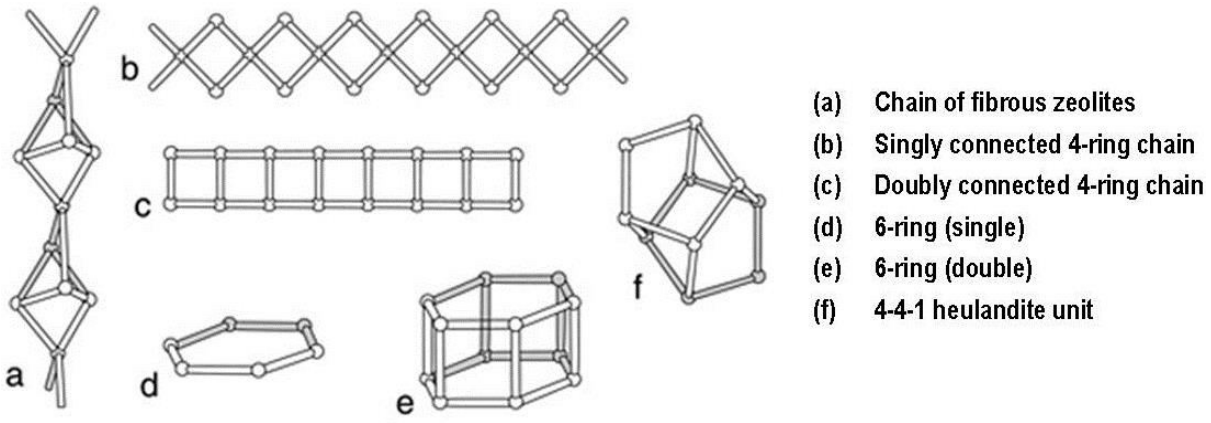

Figure 2.3: Finite or infinite structural units used to assemble zeolite frameworks (Breck, 1974; Gottard and Galli, 1985). The balls represent the SiO_4^{4-} or AlO_4^{5-} whilst the bars represent the oxygen atoms shared by the tetrahedra.

2.2.4 Framework density

The framework density (FD) is defined as the number of tetrahedra atoms (T-atoms) per 1000 Å^3. This parameter is directly related to the pore volume but does not reflect the pore size. The FD concept is used to differentiate between zeolites and zeolitic open material from denser tectosilicates. Zeolites with fully cross-linked frameworks have FD values in the range 12.1 to 20.6 T/1000 Å^3), whilst denser non zeolitic materials have FD values generally in the range 20 to 21 T/1000 Å^3. The FD values are dependent on the type and relative number of smallest rings in the tetrahedral framework, with the lowest densities arising from frameworks with a maximum number of 4-rings. Framework density increases as the size of the smallest network rings increases. FD values of less than 12 T/1000 Å^3 have been encountered in interrupted framework Cloverite (CLO) and some hypothetical frameworks. *Hypothetical frameworks are theoretically feasible frameworks that have not been physically observed*. To some extent the FD values are dependent on material chemical composition (Xu et al, 2007).

2.2.5 Pore structure

The peculiar zeolitic properties such as ion exchange, catalysis and molecular sieving arise from the interconnected regular three dimensional networks of micropores. The pore openings are described by 6, 8, 10, 12 and 14 membered oxygen –ring system forming tube-like structures interconnected to one another. The pore openings are further categorised according to ring sizes with an 8-ring being a small ring, 10-ring

being medium and a 12-ring considered large. Table 2.5 presents examples of the different zeolites with these pore variations.

Table 2.5: Zeolite pore size classification

Zeolite	Ring Members	Pore Diameter/Å	Category
GIS (NaP)	8	3.7	Small
MFI (ZSM-5)	10	5.4	Medium
FAU	12	7.4	Large

The shape and size of these pore openings are determined by the configuration of the T and O atoms relative to one another, the cation size, location of the cation and the Si/Al ratio. The n-ring apertures in zeolites and related porous materials are as depicted in Figure 2.4. The T-atoms are represented by the large black dots whilst the small dots represent the connecting oxygen atoms.

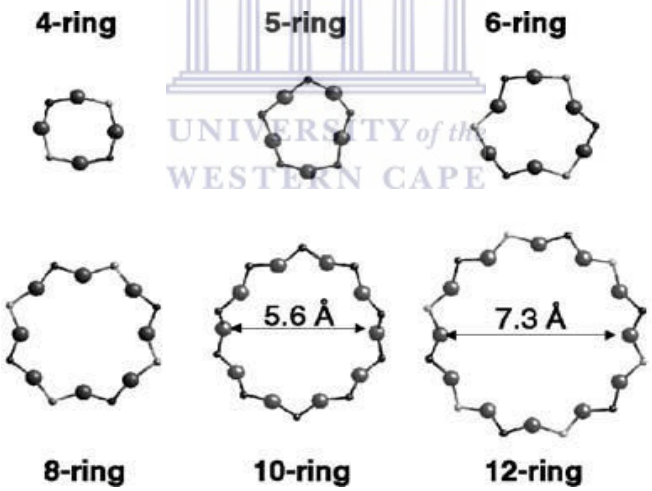

Figure 2.4: n-ring aperture structures in zeolites and related materials (Lobo, 2005)

The pore structures can also be described in terms of one, two or three dimensional channels as presented in Table 2.6. The short hand pore structure notation for the selected zeolites is also presented.

Table 2.6: Selected zeolites pore structure and respective short hand pore structure notation

Zeolite Code	Zeolite	Channel System	Pore Notation
CAN	Cancrinite	1-dimensional	[001] 12 5.9 x 5.9*
OFF	Linde T	2-dimensional	[001] 12 6.7 x 6.8* ↔ ⊥
GIS	NaP	3-dimensional	{[100] 8 3.1 x 4.5 ↔ [010] 8 2.8 x 4.8}***
MFI	ZSM-5	3-dimensional	{[100] 10 5.1 x 5.5 ↔ [010] 5.3 x 5.6}***
FAU	Faujasite	3-dimensional	<111> 12 7.4 x 7.4***
*BEA	Beta	3-dimensional	<100> 12 6.6 x 6.7* ↔ [001] 12 5.6 x 5.6*

The symbol (↔) denotes that the channel systems are interconnected while the symbol (⊥) represents a direction that is perpendicular to the crystallographic plane. The number of asterisks (*) represents the channel system dimensions i.e. (*) represents a 1-dimensional system whilst (**) represents a 2-dimensional system. The symbol <100> means that the channels are parallel to all crystallographic planes. In the case of CAN it has a 1-dimensional system parallel to the [001] plane, and having a 12 membered ring pore opening with a pore diameter of 5.9 Å (Xu *et al*, 2007).

2.2.6 Selected zeolite framework structures

In this work focus is centred on the synthesis of zeolites from fly ash and the Friedel-Crafts alkylation of benzene on metals supported on zeolites X (FAU), Beta (BEA) and mesoporous MCM-41. This section presents in-depth chemical and physical properties of the said zeolites. Some of the chemical and physical properties of these zeolites have been presented already. This section will present their respective framework topologies and their chemical composition.

2.4.6.1 Zeolite X

Zeolite X and Zeolite Y are synthetic analogues of naturally occurring mineral Faujasite (FAU). The Faujasite framework is built by the linkage of sodalite cages through double 6-rings. This linkage creates a large cavity in FAU referred to as the supercage (supercavity), which is accessible by a 3-dimensional 12-ring pore system. The natural Faujasite is generally represented by the chemical formula $(Na_2,Ca,Mg)_{3.5}[Al_7Si_{17}O_{48}].32H_2O$, with varying amounts of Na, Ca and Mg. The other synthetic members of the same group include zeolite X, zeolite Y and Na-Y. The FAU zeolite has a good ion exchange capacity and can be ion-exchanged with many different

ions (Na^+, K^+, Ba^{2+}, Cu^{2+}, Ni^{2+}, Rb^+, Sr^{2+}, Cs^+ and many others). The hydrated FAU unit cell can be represented by the formula, $[M_x(H_2O)_y][AlxSi_{192-x}O_{384}]$-FAU, where *x* represents the number of Al atoms per unit cell and M representing the monovalent cation (or one-half in case of a divalent cation) (Broach, 2010).

In FAU, the number of Al atoms per unit cell varies from 96 to less than 4 (Si/Al ratio of 1 to more than 50). This variation is then used in categorising the different FAU family members with zeolite X having a Si/Al ratio within the range of 96 to 77 Al atoms per cell (Si/Al ratio within the range of 1 and 1.5). Zeolite Y has less than 76 Al atoms per unit cell with a Si/Al ratio larger than 1.5. Figure 2.5 shows the FAU framework.

Figure 2.5: The FAU framework structure

The FAU framework is characterised by a 3-dimensional channel system and has a unit cell volume of 14428.77 $Å^3$, with a framework density of 13.3 T/1000 $Å^3$ (Broach, 2010). The FAU framework has the largest void volume known to zeolites, which constitutes about 50% of the dehydrated crystal (Kemball, 1977).

FAU (Zeolite X) has numerous industrial applications due to its excellent crystal structure, large surface area and pore volume. It was first used on an industrial scale in 1962 in the fluid catalytic cracking of heavy petroleum distillates (Weitkamp, 2000).

2.4.6.2 Zeolite HBEA

BEA (Zeolite beta) is an intergrowth of 3 polymorph types (Corma *et al,* 2008). The polymorphs are generated by different stacking of the same building layer as shown in

Figure 2.6. Zeolite beta is characterised by a 3-dimensional large pore channel system of 0.55 x 0.55nm and 0.76 x 0.64nm. The sodium form NaBEA has the general formula $Na_n\{Al_nSi_{64-n}O_{128}\}$, n < 7. The Si/Al ratio varies from 8 to more siliceous forms and eventually the aluminium free homologue (Meier et al, 1996). The high silicon content gives the zeolite high acid strength and thermal stability. Hence it finds great use as a catalyst support in processes that operate at high temperatures (Freese et al, 1999).

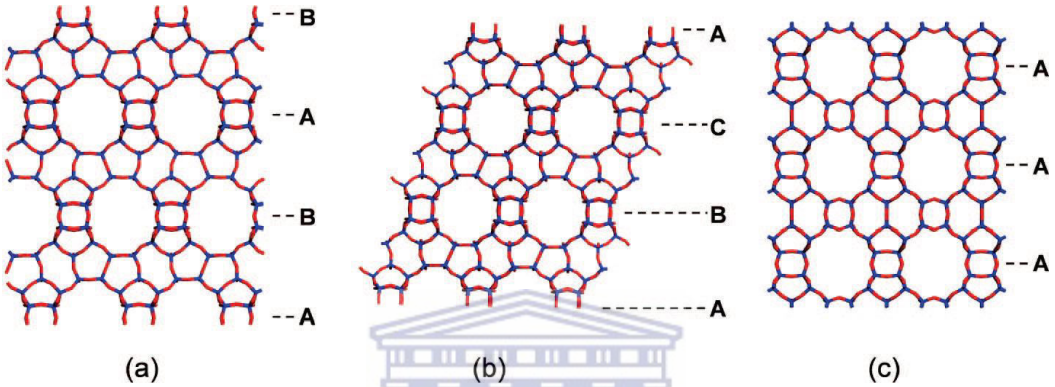

Figure 2.6: Framework structures of the three zeolite beta polymorphs (a) polymorph A (b) polymorph B and (c) polymorph C (Corma et al, 2008)

The three polymorphs are related and they all contain 12-membered oxygen rings. The pore dimensions are however not affected much by the intergrown polymorph hybrid. Zeolite beta has been applied in numerous industrial processes including transalkylation, epoxidation, isomerisation and acylation (Prasetyoko et al, 2006).

2.4.6.3 MCM-41

MCM-41 is a mesoporous siliceous material belonging to the M41S family and it was first synthesised by the Mobil Oil Corporation (Kong et al, 2004). It has a well organised structure resulting from a hexagonal arrangement of channels. In essence pure siliceous materials have low if any catalytic activity. However the catalytic activity of such material can be enhanced by the inclusion of Al^{3+} ions in the framework (Kovalchuk, 2005). This also increases the acidity of the material giving it properties similar to those of zeolites. MCM-41 has numerous industrial applications owing to its unique properties which include high specific surface area, high thermal and hydrothermal stability, hydrophobicity and acidity. It has been applied in such processes

as adsorption, ion exchange and as molecular sieves for large molecules. Metal incorporated MCM-41 such as Ti-MCM-41 has been used as an oxidation catalyst. Mn-MCM-41 has also been used for the epoxidation of stilbene with *t*-butyl peroxide (Thitsartarn et al. 2007). It was also found that Cu-MCM-41 is active for various oxidation reactions including oxidation of phenol, benzene, trimethylphenol and alcohols. The framework structure is presented in Figure 2.7.

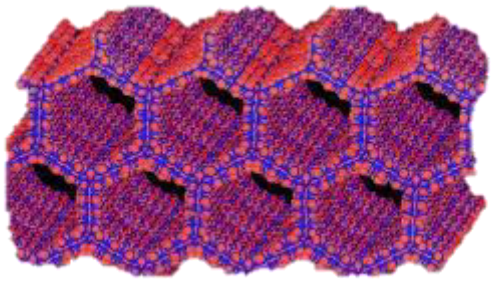

Figure 2.7: Framework structure of MCM-41showing the hexagonal channel arrangement (www.zeolite.utm.)

The MCM-41 framework presented in Figure 2.7 shows the parallel and ideally shaped cylindrical pore system with a high degree of pore symmetry. The pore sizes can be adjusted during synthesis and they range from 20 – 100 Å. This large mesopore size enables the material to be very effective in separation of large molecules. These pores are an order of magnitude larger than the pores typically found in zeolite structures.

2.2.7 Properties and applications of zeolites

Although it can be said that zeolites generally have the same chemical composition, each mineral has distinct chemical and physical properties based on its crystal structure. The most interesting zeolite chemical properties that make them useful in a wide variety of applications are their ability to dehydrate or rehydrate, and their applicability for adsorption and cation exchange (Eyde and Holmes, 2006). Zeolites differ from other aluminosilicates in that they accommodate water molecules within their structure. On heating, the water is rapidly released but the zeolite framework structure is retained leaving open angstrom sized channels from which a wide range of unique zeolite properties arise. In essence zeolites have a high degree of hydration and this consequently gives rise to a low density in the dehydrated crystal. Pure zeolite crystal

are colourless, however the presence of impurities may impact colouration, in the case of synthetic ones the presence of group 1A and/or 2A metals also accounts for colour (Breck, 1974). The crystal hardness is within the range of 4 – 5 on the Mohr scale. The dehydrated crystal is very stable both structurally and thermally and this has enabled their use as molecular sieves.

Molecular sieves are defined as materials that can selectively adsorb molecules based on their size, shape or electrical charge. Some of the most prominent applications of zeolites based on these properties are water and gas purification, treatment of waste waters, catalysis and a vast variety of other applications in the petrochemical industry.

Gas purification: the ability of zeolites to selectively adsorb polar compounds accounts for their application in gas purification. In addition the adsorptive properties can be enhanced by thermal treatment, ion exchange and structural changes. Commercial applications include purification of oxygen by pressure swing adsorption using LiX zeolites mainly, upgrading of natural gas to remove N_2 and /or CO_2 and water. In the petrochemical industry zeolites are also used to separate olefins from paraffins, n-paraffins from iso-paraffins. The most established processes are the PAREX, SOBEX and the BOC's petrofin processes. Acid treated clinoptilolite and mordenite zeolites are also widely applied in flue gas clean up (Ackley et al, 2002).

Removal of odours and pollutants: due to the anaerobic nature of manure and sewage waste noxious odours arise due to the release of NH_3, H_2S and some VOCs. Since zeolites can effectively capture polar molecules they are used in odour reduction in sewage systems in animal husbandry. In waste water treatment zeolites are also used to remove heavy metals. Using the zeolite clinoptiololite heavy metals have been successfully removed in accordance with the selectivity: $Pb^{2+} > NH_4^+ > Cd^{2+}$, Cu^{2+}, Sr^{2+}, $> Zn^{2+} > Co^{2+}$. This is based on the ion exchange ability of zeolites. The order may not be necessarily the same using a different zeolite and modification of the zeolite can also alter selectivity. Zeolites are also applied in the removal of radioactive fission products such as Cs and Sr (Sharadqah and Al-Dwairi, 2010).

Detergent builders: Modern detergents involve the use of surfactants, however their effectiveness is impaired by hard water and there is need to incorporate builders in detergents. Traditionally, polyphosphates have been used as builders, but due to rising

concerns about eutrophication there has been a marked reduction in their use and zeolites have taken their place. Zeolite A, X and P have proved to be very effective as water softeners and detergent builders (Klabunde and Richards, 2009).

Soil fertility: Zeolites have been used to enhance soil fertility by slow release of potassium, calcium, magnesium and other micronutrients. When loaded with ammonium it serves the same in slow release of nitrogen (Mohammad et al, 2004). Zeolites retain the nutrients in the root zone where plants can easily absorb them for use. The application of zeolites in enhancing soil fertility has been successfully applied in the production of crops such as apples, cereals, vegetables and grapes (Polat et al, 2004). Apart from nutrient release zeolites also control water balance due to their reversible sorption capacity for water without damage to the zeolite crystal structure (Ersoz and Barrott, 2012). This phenomenon is vital in avoiding waterlogging and enabling slow water release in periods of drought.

Catalysis: Various cations with specific catalytic activities can be ion exchanged on the zeolites giving rise to desired catalytic activity. This coupled with the possibility of pore size manipulation which allows for high selectivity has qualified zeolites for their numerous applications in heterogeneous catalysis. The most conspicuous applications include the Fluid Catalytic Cracking (FCC) where ZSM5 and zeolite Y are used. Mordenite is also used in paraffin isomerisation. These metal exchanged zeolites can also be used as oxidation or reduction catalysts for example Fe-ZSM5 for the catalytic reduction of NOx and Cu-ZSM5 for the oxidation of NH_3. The H-exchanged zeolites are solid acids with high acidity and are used in various organic reactions including fuel synthesis. Lately much research attention has been given to modification of zeolite catalytic properties for use in high value chemical synthesis such as cosmetics and pharmaceutical products. There has been considerable application of zeolites in other organic reaction as aromatic conversions, dewaxing and hydroisomerisation. Zeolites can be used either in their natural or synthetic forms (Xu et al, 2007). Some of the most prominent zeolite applications in industrial catalysis are presented in Table 2.7.

Table 2.7: Major industrial catalytic applications of zeolites (Bogdanov et al 2009).

Process	Zeolite	Product
catalytic cracking	Re-Y US-Y ZSM-5	gasoline fuels
Hydrocracking	Y Mordenite + Mo	kerosene, diesel, benzene
alkylation of aromatics	ZSM-5 Mordenite	p-xylene, ethyl-benzene
hydroisomerisation	Mordenite + Pt	i-pentane, i-hexane
xylene isomerisation	ZSM-5	p-xylene
catalytic dewaxing	Mordenite ZSM-5 +Ni	cold flow improvement
transalkylation	Mordenite	xylenes, cumene

2.2.8 Natural zeolites

Natural zeolites were discovered more than two centuries ago, and more than 23 frameworks and more than 40 types of natural zeolites are known. The most common natural occurring zeolites include chabazite, clinoptilolite, mordenite, heulandite, laumontite, analcime, natrolite, thomsite, and stilbite. Zeolites form in various sediments or rock material under different chemical and physical conditions and this gives rise to zeolite compositional variations which are commonly expressed as the ratio R=Si:(Si+Al+Fe) (Iijima, 1980). The ratio represents the Si percentage occupation of the tetrahedra. This parameter is important in describing the zeolite order-disorder relation as well as classification as 'basic' (0.50<R<0.625), intermediate (0.625<R<0.75) and acidic (0.75<R) (Gottard, Galli, 1985). Natural zeolites have a tendency of exhibiting a compositional variation even in the same species. The species formed are a direct influence of the original material such as pore water, acidic or basic volcanic glass and clays, together with pressure-temperature variations (Iijima, 1980). Geological explorations have led to the conclusion that zeolites are formed in accordance with the following generic types (Xu et al, 2007).

- Resulting from the hydrothermal or hot spring activity involving reactions between solutions and basaltic lava.
- Resulting from deposition of volcanic sediments in closed saline and alkaline systems

- Action of open freshwater or ground water systems on volcanic sediments
- Deposited volcanic material in alkaline systems
- Resulting from hydrothermal or low temperature alteration of marine sediments
- Formations as a result of low grade burial metamorphism

Due to the increasing industrial applications of zeolites there has been significant research in synthetic zeolites.

2.2.9 Synthetic zeolites

The discovery of the zeolite stilbite by Baron Cronstedt in 1756 opened a new chapter in the study of zeolitic material, especially their adsorption properties. More and more natural zeolites were discovered thereafter, however their applications were not prominent until their synthetic counterparts were produced. Apart from the fact that the natural zeolites could not meet the high industrial quality demand, synthetic zeolites have other advantages in comparison to natural ones. Synthetic zeolites have regular crystal structures and they have a high degree of purity since they are only constituted by precursor components. They also exhibit larger pore volumes and a more diverse framework composition due to the use of structure directing agents. The structure and properties of these synthetic zeolites can be tailored by manipulation of synthesis composition as well as conditions, to generate a synthetic product with specific properties designed for a particular purpose, in the diverse zeolite applications in areas such as adsorption, catalysis and ion exchange where there is a need for materials with high selectivity.

The study of the natural hydrothermal formation inspired early zeolite researchers to find possible synthesis routes that mimic natural processes. The earliest attempt to synthesis zeolites dates back to 1862 by St Claire-Deville, however a more definitive synthesis was done by R. Barrer in 1948. This breakthrough also marked the first synthetic zeolite (zeolite ABW) that did not have a natural analogue. The advent of low temperature hydrothermal techniques initiated an extensive industrial production of zeolites and by the end of 1954, zeolites A and X began to be commercially produced. The notable United States of America, pioneer companies to synthesise zeolites include, Linde, Mobil and Exxon. The most prominent industrial events in zeolite synthesis are highlighted in Table 2.8.

Table 2.8: Historical developments in commercial zeolite synthesis (Bogdanov et al, 2009)

Period	Zeolites Synthesised
Late 40's to Early 50's	Low Si/Al Ratio zeolites
Mid to Late 60's	High Si/Al ratio zeolites
Early 70's	SiO_2 Molecular sieves
Late 70's	$AlPO_4$ Molecular sieves
Early 80's	SAPO and MeAPO Molecular sieves
Late 70's	Metallo-silicates, aluminosilicates
Mid 80's	$AlPO_4$ based Molecular sieves
Late 80's	Large pore zeolites
Early 90's	Mesoporous molecular sieves

The use of zeolites in catalysis is rapidly increasing and more and more resources are being channelled in zeolite related research work. To date over 180 zeolite frameworks are known, however only a fraction of these have been used in industrial processes. About 95% of the commercial zeolites are used in fluid catalytic cracking with the other 5% being used in ion exchange, gas separation and purification and in the petrochemistry. The mostly synthesised zeolites include; LTA, FAU, MOR, LTL, MFI, BEA, MTW, CHA, FER, AEL, and TON. There also has been considerable attention given to zeolite-like materials such as aluminophosphate (AlPOs), silicoaluminophosphates (SAPOs) and metalloaluminophosphates (MeAPOs). The following section presents an overview of zeolite synthesis methods (Bogdanov et al, 2009).

2.3 Synthesis of zeolites

In general the synthesis of crystalline solids can be categorised into two main classes, one which involves solid state reactions and the other involving synthesis reaction in solution. Solid state reactions require high temperatures to overcome reactant transportation to the reaction site whilst transport in solution is achieved at much lower temperatures. The concept of using solvents in the materials synthesis is referred to as solvothermal, but since water is the mostly used solvent the special term *hydrothermal* is much used. Zeolitic materials are synthesised using the hydrothermal approach in

which an aluminosilicate suspension is mixed in an alkaline media resulting in gel formation or at times a clear solution. The alkali cation acts as a structure directing agent but in most cases an additional organic phase structure directing agent (SDA) is used. The nature of the SDA as well as the chemical composition of the aluminosilicate together with other reaction parameters such as temperature, pressure, water content as well as ageing time are crucial in determining the final product. The schematic representation of the hydrothermal synthesis of zeolites is presented in Figure 2.8.

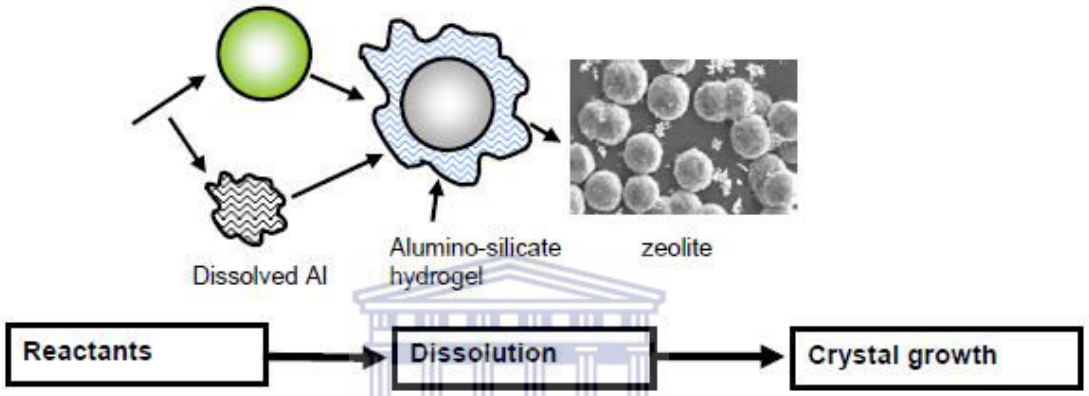

Figure 2.8: Zeolite synthesis (Brinker and Scherer, 1990).

2.3.1 Silica and alumina sources

The most commonly used silica source is sodium silicate (8.9 *wt%* Na_2O, 28.7*wt%* SiO_2) the purity of the silicate source does affect the range of possible zeolites that can be produced. In the case of the given composition a slight contamination can prevent the formation of zeolites with a SiO_2/AlO_3 ratio of above 600. Colloidal silica sources such as Ludox are often used when lower Al content zeolites are desired. In all solution preparation glass equipment is not to be used since glass participates in the reaction, hence polypropylene or Teflon containers are used (Kuhl, 2001).

On the other hand, the most preferred alumina source is sodium aluminate. When pure it is usually aged prior to zeolite synthesis. Aluminium salts can also be used but their strong electrolytic effect hinders gel formation. Both the alumina and silica must be in the appropriate ratios to create the zeolite of choice. The Si/Al ratio and impurities in the source material have a direct effect on the molar composition and type of the resultant zeolite, since each structure presents restrictions to the Al amount it can

accommodate. For synthesis of high silica zeolites the Al/Si ratio varies from 7 to infinity. In cases where the impure sources of silica and alumina are used e.g. kaolin and fly ash the starting material has to be assayed and appropriate adjustments to the Si/Al ratios done prior to gel formation. The concentration and nature of the mineraliser also plays an important role in determining the resultant zeolite type and composition. The gel composition is also to some extent affected by the presence of other cations (both inorganic and organic) and water content (Szostak, 1989).

2.3.2 Effect of mineraliser

In most conventional zeolite syntheses a high OH^- concentration is used to mineralise the silicates and alumina in the reactant gel. The OH^- dissolves the Si in such a way that the amorphous particles are depolarised resulting in oligomer species formation. The hydroxide concentration has to be appropriate since equilibrium is established between solution and gel solid species. A high concentration shifts the equilibrium far towards solution hence hindering crystallisation. On the other hand a low concentration is associated with formation of an amorphous product since particle transport to the growing crystal is limited by the reduced solubilisation of source material. During crystallisation the desired phase (metastable) crystallises first but on standing for longer periods of time may transform to dense phase material by Ostwald ripening. The OH^- concentration has to be fine-tuned to allow for the formation of the desired phase. It also affects the rate of crystallisation, crystal size, Si/Al ratio of resultant zeolite. In a study using a Si/Al ratio of 30, ZSM-12 was produced with gels of OH^-/Si ratio of ≤ 0.6, TNU-9 with OH^-/Si ratio of 0.79 and further adjustment to 1.0 resulted in the formation of STI.

The main source of OH^- is NaOH, but KOH can also be used, however in most cases NaOH is preferred since it is associated with a high conversion efficiency. On the other hand K^+ is associated with slow crystallisation rates. Apart from OH^-, the fluoride (F^-) can also be used, and is associated with defect reduction in highly siliceous zeolites (Strohmaier, 2010). The mostly used F^- sources are; NH_4F, NH_4HF_2 and HF, and where these sources are used the H-zeolite is formed on calcination and all the fluoride is removed (Kessler, 2001).

2.3.3 Structure directing agents SDAs

Structure directing agents (SDAs), also known as templates, are cationic species that are added to the reaction synthesis mixture during zeolite synthesis, to guide in the organisation of the anionic building units that form the framework. The commonly applied cations include; Na^+, Li^+, Cs^+, K^+, Rb^+, Ca^{2+}, Sr^{2+}, as well as organic structure directing agents such as tetra-alkyl-ammonium cations (TMA^+, TEA^+, TPA^+), di(hydroxyethyl) dimethyl ammonium), dialkyl and trialkyl amines and phosphonium compounds (Byrappa and Yoshimura, 2001). The cations play two significant roles, firstly in charge compensation of the alumina tetrahedra and secondly in guiding the polymerisation of the building blocks during framework formation. The obvious cation source is the alkali cations, however in certain cases their templating effect is not good enough to guide the formation of certain framework structure and organic cations are used to help in the templating. Apart from structure directing the cations also stabilise the structural subunits which in essence are nucleating species in crystallisation. Specific frameworks can only arise from specific synthesis cations (SDAs), e.g. MAZ and OFF structures cannot be generated in the absence of tetramethylammonium (TMA). The TMA facilitates the formation by templating action, of the aluminosilicate precursor gmelite cage building unit, which is found in the structures of both MAZ and OFF. Table 2.9 presents some of the well-studied cation-building unit relationships in zeolite synthesis.

Table 2.9: Cation-building unit relationship (Wilson, 2001)

Building Unit	**Structure-types containing building unit**	**Cation specificity for building unit**
A	LTA, KFI	Na
Sodalite	LTA, FAU	Na or TMA
Gmelite	GME, OFF, MAZ	Na or TMA
Cancrinite	ERI, OFF, MAZ	K, Ba, or Rb
D4R	LTA	Na
D6R	FAU, KFI, CHA, GME, ERI/OFF, LTL	Na, K, Sr, Ba

The use of complex organic cations which, apart from filling the cages also fill the channels has resulted in synthesis of other framework types which could not be

generated and examples include the use of 1,8-diaminooctane in ZSM-48 and tetrapropyl-ammonium in MFI syntheses. The application of quaternary ammonium polymers such as 1,4 diazabicyclo[2.2.2]octane-based polyelectrolytes results in crystallisation of larger pore zeolites where small pore species would otherwise result. In essence these complex organic cations can be applied to effect specific crystal formation as well as specific framework structures. The resultant organic/inorganic intergrowth needs to be detemplated in order to access the desired inorganic porous framework. This is accomplished either by ion exchange or thermal pyrolysis followed by combustion to remove the organic SDA.

2.3.4 The effect of pH

In zeolite synthesis alkalinity greatly influences supersaturation, kinetics, morphology, size, shape and crystallinity of resultant material. Increase of the [OH^-] accelerates crystal growth and in zeolite synthesis the pH is usually maintained within the range 8 – 12. The solubility of the amorphous aluminosilicate increases with increase in alkalinity but the crystalline phase is less soluble in alkaline media. This concept is largely responsible for the increased crystallisation rates observed with increase in pH. The hydroxide is a good complexing agent to bring amphoteric hydroxides and oxides into solution. In synthesis from industrial waste materials such as kaolin and fly ash the relative zeolite phase yields are dependent on the [OH^-] (Byrappa and Yoshimura, 2001).

2.3.5 Water content

Water has remarkable solvent powers that enhance transport and mixing of solid components. It also facilitates nucleation and crystal growth. During zeolite synthesis water acts as space filler, hence stabilising the porous lattices by formation of solid solution. The aluminosilicate will not form in the absence of a guest molecule, which can be a salt or water molecule. Specific amounts of water are required for specific zeolite syntheses. In calculating the amount of water to be used it is advisable to consider the water in hydrous reagents. All the hydroxides are considered as oxides plus water e.g.

$$NaOH = \frac{1}{2}Na_2O + \frac{1}{2}H_2O \text{ (this gives 22.5wt\% } H_2O)$$

In synthesis of some zeolites such as ZSM-5 water concentration or degree of dilution is of minor importance since ZSM-5 crystallises out of gels with an extremely wide range of H_2O/SiO_2 ratios. Ultra-pure water is recommended in order to avoid the complicating effects of such ions as calcium (Byrappa and Yoshimura, 2001).

2.3.6 Temperature

The synthesis temperature influences zeolite structure as well as the induction period. Temperature elevation increases both the nucleation rate and the linear growth rate (K) as expressed by the relationship;

$$K = 0.5\ \delta l/\delta t;\ \textit{where } l = \textit{the crystal size}$$

It follows that crystallinity of the sample increases with time, thus high temperatures result in reduced induction times. Usually zeolites are synthesised at temperatures below 350 ^{0}C with a few exceptions and generally the rise in temperature results in crystallisation of more dense products as the fraction of water filling the pores is significantly reduced. The use of non-volatile pore space fillers would in principle, allow high temperature synthesis of open porous structures. The rate of nucleation can be expressed with the following relationship (Byrappa and Yoshimura, 2001).

$$DN/\delta t = A[exp(E_t)^{-1}];\ R = Kt$$

Where K is the linear crystal growth rate, A and E are rates of nucleation *coefficients*

The coefficients K, A and E all increase with an increase in temperature. Heating during synthesis can be carried out by placing the autoclave in a heating oven or by surrounding it with a heating mantle. This approach is associated with inhomogeneous heating. Where the heat distribution is more homogeneous, this approach is associated with rapid synthesis. Another option is microwave heating in which the mixture is placed in a sealed vessel und heated under autogeneous pressure (pressure generated by the evaporation of the solution being heated). Microwave heating has the advantage that it is associated with rapid crystal growth and higher choice product selectivity (Byrappa and Yoshimura, 2001).

2.3.7 Reaction time

Using the same reactants and reaction conditions the products may vary according to the allowed reaction time. Zeolite synthesis by the sol-gel method rapidly gives rise to a

gel, which after some time separates into two phases, the solid and the liquid, with an increase in mixture density. The solid crystalline phase is usually a metastable phase which can undergo further dissolution leading to formation of more stable species. This phenomenon is described as the Ostwald's law of successive phase transformation (Nagy et al., 1998). In-depth understanding of the time factor as well as crystallisation parameters can be manipulated to optimise the product of choice.

2.3.8 Pressure

In general pressure variations do not have a great influence in zeolite synthesis, since crystallisation is usually carried out under autogeneous pressure (Weitkamp and Puppe, 1999). When synthesis is carried out in the presence of volatile reagents such as methane and ammonia, the pressure variations need to be carefully monitored. Syntheses at very high pressures might influence specific parameters such as liquid phase viscosity, which consequently affects crystallisation kinetics (Nagy et al., 1998).

2.3.9 Agitation and stirring

Agitation and stirring gives rise to gel temperature and compositional homogeneity, both of which have some marked influence on the synthesis outcome. The exercise allows for the following conditions to be established in the synthesis matrix; reagent dissolution, initial gel formation, maintaining a homogeneous gel, assisting with gel structure break-up, maintaining uniform temperature across the reactor, transferring ''nutrients'' to growing crystals and keeping the zeolite crystals in suspension on completion of the reaction (Casci, 2005).

Poorly mixed synthesis hydrogels result in the formation of impure phases, with impurity levels decreasing with improved mixing. The product crystal size is also affected by stirring for instance in the synthesis of zeolite beta and TS-1, stirred samples gave rise to smaller crystals whilst the unstirred samples gave rise to much larger crystals (Camblor et al, 1991). This observation can be described by the general tendency of zeolites to form large crystals in viscous systems where convective motion is hindered and mass transfer is diffusion controlled. Product selectivity is also observed with stirred and unstirred hydrogels. Zeolite A is the much preferred product relative to zeolite X with stirred hydrogels. Synthesis using 1.8-diaminooctane favours the

formation of the MEL structure rather than the obtainable TON structure with unstirred hydrogels (Casci, 2005).

2.3.10 Crystallisation

Zeolite synthesis is based mainly on two steps, nucleation and crystallisation, and nucleation happens to be the rate limiting step. By definition nucleation is a process in which small precursor aggregates give rise to germ nuclei. The precursor species are initiated by hydrolysis giving rise to reactive M – OH groups. This is then followed by condensation where the M-O-M bonds are formed. The condensation process occurs via two mechanisms namely olation and oxolation according to the following reactions:

$$M\text{-}OH^{\partial-} + M^{\partial+}\text{-}OH_2 \rightarrow M\text{-}OH\text{-}M^{\partial+}\text{-}OH_2^{\partial+} \rightarrow M\text{-}OH\text{-}M + H_2O \textit{ (olation)}$$

Olation progresses by the nucleophilic addition of a positively charged hydrated metal cation, whilst oxolation occurs via the condensation of two metal hydroxides as shown by the following schematic reaction (Jansen et al,1994).

$$M\text{-}OH + HO\text{-}M \rightarrow M\text{-}O\text{-}M + H_2O \textit{ (oxolation)}$$

Zeolite nucleation and crystallisation can be looked at through four sub divided processes namely; formation of simple and polymeric aluminosilicates, formation of embryo from the aggregation of the aluminosilicate complexes, formation of primary particles (well-ordered core and micelle formation) and aggregation of primary particles via oriented aggregation. These processes can be summarised by the scheme presented in Figure 2.9.

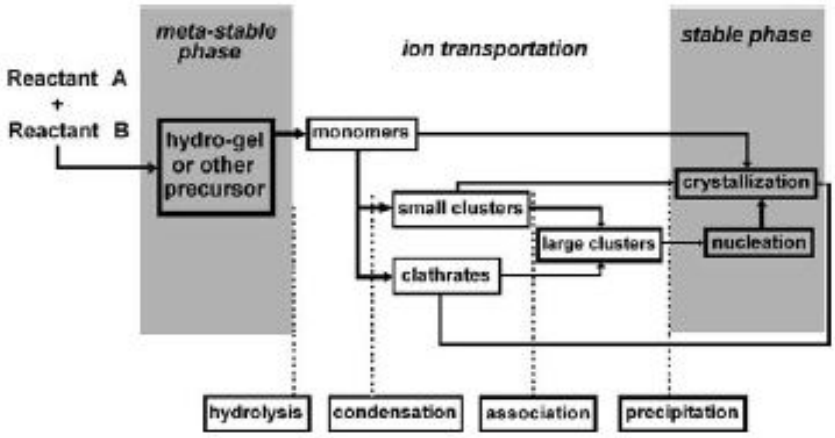

Figure 2.9: Zeolite crystallisation process (Singh and Dutta, 2003)

Crystallisation which occurs after nucleation is defined as the continued evolution of nuclei to macroscopic size. The process occurs much faster than nucleation, but is however also dependent on a number of reaction parameters such as; temperature, stirring/agitation, seeding, gel ageing, pH, water content, ratio and concentration of framework forming elements and template concentration.

Figure 2.10, presents a typical zeolite synthesis crystallisation curve, in which the nucleation rate and crystallinity of the system is plotted against synthesis time.

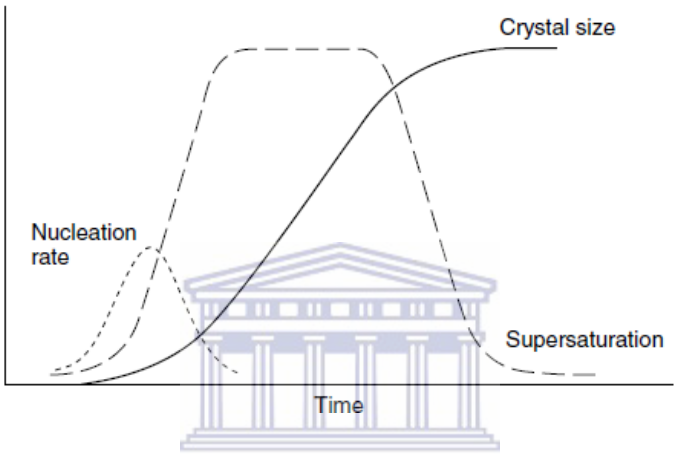

Figure 2.10: Evolution of nucleation and growth rates as well as supersaturation, as a function of synthesis time (Cubillas and Anderson, 2010)

As can be seen from the presented curve, the rate of nucleation rises fast and then falls to zero. As nucleation progresses and a threshold amount of nuclei is formed then crystallisation starts, and rises until a steady state is achieved when reactant ingredients diminish. Initially supersaturation increases resulting in nucleation and growth phase. It then levels off as the system reaches steady state, and finally drops off to zero as the reaction nutrients are depleted.

2.3.11 Recent developments in zeolite synthesis

Zeolite synthesis has evolved due to the increased need for specific zeolitic properties. This has been achieved by modification of the conventional hydrothermal approach by alteration of synthesis parameter and substitution of some reagents by other reagent which impart the desired framework and morphology. Some of the notable advances

include; ionothermal, dry gel conversion, low water synthesis, non-aqueous solvents and the application of computer aided synthesis.

Dry gel synthesis*:* the conventional hydrothermal approach is carried out in a medium containing aqueous dissolved ingredients and solid (gels and particles) species. The Dry Gel Conversion (DGC), the solid species is kept separate from the aqueous phase. The DGC can be subdivided into two i.e. Vapour Phase Transport (VPT) and Steam Assisted Conversion (SAC). In the VPT method, the dried amorphous aluminosilicate gel of appropriate composition is transformed into the desired zeolite by contact with vapours of amines and water or water alone. The amine serves to regulate the pH by absorbing into the hydrous phase and raising the pH. Xu et al, (2007) reports the synthesis of ZSM-5 from dry gels by contacting with water and volatile amines.

In the SAC method the gel is prepared containing the Site Directing Agent (SDA), before the drying step. The gel is then suspended over a small reservoir of water in an autoclave. Rao et al, (1998) synthesised self-bonded pellets of zeolite Beta by this approach.

Low water and non-aqueous syntheses: Conventional aluminosilicate syntheses use water levels of about $H_2O:SiO_2 > 25$ to permit for easy homogenisation as well as handling of the synthesis gels. In a review by Strohmaier, (2010) the synthesis of Zeolite Beta in the presence of fluoride was done without seeding using low water ratios of about $H_2O:SiO_2 < 10$. The review further goes on to mention that the first successful non-aqueous zeolite synthesis was reported back in 1985, in which ethylene glycol or propanol was used, with TMA as the SDA, to synthesise silica–sodalite. Later MFI, ZSM-39, ZSM-48 were synthesised using ethylene glycol, butanol, glycerol as solvents. Using pyridine/HF and triethylamine solvent systems giant crystals of MTN, FER and MFI zeolites are reported to have been successfully synthesised. Many other researchers have successfully synthesised different zeolite frameworks using organic solvents (Strohmaier, 2010).

Ionothermal and eutectic mixtures syntheses: Ionothermal synthesis is a solvothermal synthesis approach in which an Ionic Liquid (IL) is used as the solvent. ILs have negligible vapour pressures, hence they do not generate autogeneous pressure as is the case with volatile solvents. In essence ionothermal synthesis is carried out at ambient

pressure. Apart from acting as solvents they also act as SDAs providing a template around which the inorganic framework is ordered. Deep eutectic solvents (DESs) have almost the same properties as ILs but are much easier to prepare. They are produced by mixing two or more compounds generating a new mixture with a lower melting point than any one of its constituents. The first work of this nature was reported by Morris et al, (2004) in which 1-ethyl-3-methyl imidazolium bromide (EMIM Br) and urea/chlorine chloride (DESs) were used to prepare different zeolitic materials. The synthesis of TON and MFI zeolite frameworks using 1-butyl, 3-methyl imidazolium based ionic liquids with bromide-hydroxide counteranions was the first genuine ionothermal synthesis of zeolites (Wheatley et al, 2010). Figure 2.11, shows the generated product with the1-butyl, 3-methyl imidazolium (BMIM) clearly visible in the single-crystal X-ray diffraction structure of MFI. On the calcination the BMIM can be evacuated from the framework cavities.

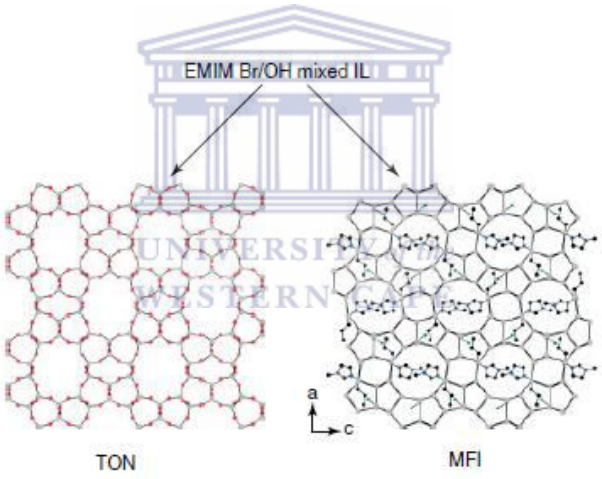

Figure 2.11: Ionothermal synthesised TON and MFI zeolites using BMIM based ILs with mixed bromide-hydroxide counteranions (Morris, 2010).

2.3.12 Computer simulations

Computer based simulations have helped a lot in determining the appropriate synthesis parameters as well as reagent composition. In a review by Wilson, (2001) it is reported that, computer based host/guest interactions and experimental data were combined in order to understand the interaction of organic templates on the zeolite structure. It was revealed that modelling can reveal details of the interaction of templates with zeolite framework structures and correctly determine the structure that can be generated from a

particular template. Successful predictions were reported for ZSM-5, ZSM-11 and SSZ-33. Using a computer programme ZEBEDDE, it was possible to predict that 4-piperidinopiperidine can be applied to produce an aluminophosphate with a CHA structure (Wilson, 2001).

2.3.13 Zeolite synthesis from fly ash

Coal fly ash contains significant amounts of silica and can be used as a starting material in zeolite synthesis.

2.5.13.1 Conventional zeolite synthesis from coal fly ash

Principally zeolites are synthesised from fly ash via a four step process (i) the fusion of fly ash with alkaline solution resulting in the formation of an aluminosilicate precursor with or without additives (organic SDAs or inorganic salts), (ii) pre-synthesis treatment including aging, homogenisation and seeding, (iii) hydrothermal crystallisation by subjecting the reaction mixture to elevated temperature and (iv) washing and drying (Meshram et al., 2004). The alkaline solution *(mineraliser)* is usually created by either hydroxide ions or fluorides with the commonly used sources being NaOH, KOH, NH_4F and NaF respectively (Tsuda et al., 2004).

In the first step silica and sodium aluminate are formed and their mixing in water results in a hydrolysis reaction taking place which consequently releases monomeric silica species into solution. The process is enhanced by the coordination of the OH^- ion with Si via a nucleophilic mechanism as presented in the following reaction. This weakens the Si-O bond in the gel (Meshram et al., 2004).

$OH^- + Si(OR)_4 \leftrightarrows HO....Si(OR)_4 \leftrightarrows HO\text{-}Si(OR)_4\text{-}RO \leftrightarrows Si(OR)_3OH \leftrightarrows Si(OR)_3OH + RO$

Where R is H, Si or alkoxy group.

At high pH a condensation reaction may occur in which a deprotonated silanol binds to a monomeric species according to the reaction:

$Si\text{-}O + Si(OR)_4 \leftrightarrows SiO\ Si(OR)_4 \leftrightarrows Si\text{-}O\text{-}Si(OR)_4 \leftrightarrows Si\text{-}O\text{-}Si(OR)_3 + OR$

The branched clusters formed by the condensation reaction will reorganise into large particles which are stabilised by the cations like Na^+ in solution. Increase in temperature results in increased rate of dissolution in which polymeric silicates break down into

monomeric and dimeric species. The growing clusters form zeolite nuclei large enough to be stable and the zeolite crystallisation begins. The nucleation follows four routes (Meshram et al., 2004)

i. homogeneous nucleation (which occurs in the clear solution and followed by crystallisation with a force driving equal in all directions
ii. heterogeneous nucleation on hydrogel that is followed by crystallisation with a driving force that extends in all directions
iii. heterogeneous (secondary) nucleation on a dispersed hydrogel which is then followed by crystallisation that proceeds into the gel.

Figure 2.12 shows a schematic representation of the described steps.

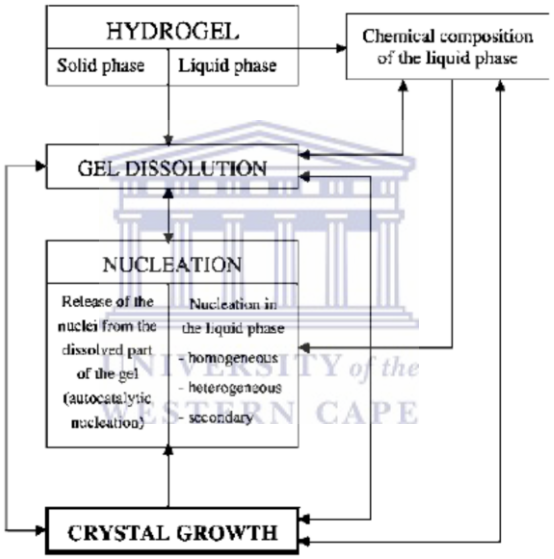

Figure 2.12: Schematic presentation of the processes interdependence in zeolite crystallisation (Subotic and Bronic, 2005).

Numerous authors have reported the synthesis of zeolites from fly ash for various applications, (Murayama et al, 2002; Wang et al, 2003; Molina and Poole, 2004; Adamczyk and Biaeck, 2005; Derkowski, 2006; Querol et al, 2007; Fiore et al, 2008; Ríos et al, 2009; Belviso et al, 2010; Musyoka et al, 2011; Chen et al,2012).

A modification of the described method was developed and reported by Hollman et al, (1999) in which there was the inclusion of an ageing step and a thermal activation step. The aging step presents the advantage of shortening the induction period due to an increased dissolution of the Al and Si precursor species. The second step involves

thermal activation, and since zeolite crystallisation takes place on the particle – alkali solution interface as the particle grows there is depletion in the supply of Al and Si from the gel this retards the rate of crystallisation. Thermal activation can then be employed to enhance precursor species transport and increase crystallisation (Murayama et al., 2002).

2.4.13.2 Two-stage synthesis

A two stage synthesis method has been developed and reported by Hollman et al., (1999) and is capable of synthesising zeolites of very high purity. The first stage involves the alkaline attack of fly ash resulting in a Si extract. The solution is then reacted with an Al bearing solution. The Si/Al ratios are controlled depending on the choice of zeolite. The residue from the extraction step can also be used to synthesise some classical zeolitic products using the traditional hydrothermal synthesis. Optimisation of this method was reported by Moreno et al., (2001), and zeolites of > 99 % purity were obtained from fly ash. Using this approach zeolite X, A, KM, chabazite and faujasite were synthesised. The approach allows for the synthesis of high Al/Si ratios which have high ion exchange potential.

2.4.13.3 Alkaline fusion approach

The alkaline fusion approach involves the treatment of fly ash with an alkaline solution and heating in an oven to form a fused sodium aluminate salt that is readily soluble in water. The Si/Al ratio is then moderated by reaction with a solution of sodium aluminate. This step is then followed by the conventional hydrothermal treatment and the zeolite of choice is thus generated. The approach has been reported in various articles (Somerset et al, 2008; Wajima and Ikegami, 2009; Kazemian et al, 2010; Zhang et al, 2011; Ríos et al, 2012), and applied for the synthesis of various zeolitic materials.

2.4.13.4 Modifications to zeolite synthesis

The microwave assisted synthesis is one modification that has resulted in accelerated crystallisation and reduction of synthesis time (Pathak and Srivastava, 2012; Querol et al,1997; Matlob et al, 2011; Kim et al, 2004; Inada et al, 2005). In conventional synthesis methods heating is non-homogeneous and slow, but the microwave approach

is much more homogeneous and rapid since it is the water molecules that absorb the microwave. The microwaves heat up the water by causing a dipole rotation in the molecule and consequently activating the molecules by the breaking of the hydrogen bond. In so doing microwave assisted zeolite synthesis has the following advantages over conventional hydrothermal synthesis (Pathak and Srivastava, 2012):

- It promotes nucleation and crystal growth, hence reducing treatment time.
- It presents a homogeneous heating throughout the reaction vessel.
- It reduces activation time to about 30 min. compared to 24 – 48 h. required in the conventional hydrothermal synthesis.
- It minimises the use of large volumes of digestion solutions.

Another modification that has been well applied is the synthesis from molten conditions without water, has been reported by Park et al. (2000a,b). Using the approach it was however not possible to obtain complete zeolitisation of the fly ash and only low cation exchange capacity zeolites were obtained due to the high temperatures required by this approach.

2.4.13.5 Zeolites and neomorphic phases synthesised from fly ash

Using the various approaches outlined in the previous section, a variety of zeolites and other *neomorphic* phases have been successfully synthesised from coal fly ash. Neomorphisim refers to the transformation of minerals that occurs in the presence of water, this includes processes of replacement by dissolution of one mineral with simultaneous formation of another mineral (Flugel, 2010). Table 2.10 presents some zeolites and other neomorphic phases that have been generated successfully from fly ash. Their respective Joint Committee Diffraction Standard (JCPDS) codes for XRD identification are presented as well.

2.5.13.2 Synthesis of zeolites from other silica and alumina sources.

Apart from pure chemicals and fly ash, zeolites can be synthesised from other sources of silica and alumina. The most commonly used starting materials are kaolinite, rice husk ash and blast furnace slag. Much work has been done applying the fore mentioned as starting materials.

Table 2.10: Zeolites and neomorphics synthesised from fly ash with the JCPDS codes (Querol, et al, 2002)

zeolitic product		JCPDS
NaP1 zeolite	$Na_6Al_6Si_{10}O_{32}.12H_2O$	39-0219
phillipsite	$K_2Al_2Si_3O_{10}.H_2O$	30-0902
K-chabazite	$K_2Al_2SiO_6.H_2O$	12-0194
zeolite F linde	$KAlSiO_4.1.5H_2O$	25-0619
herschelite	$Na_{1.08}Al_2Si_{1.68}O_{7.44}.1.8H_2O$	31-1271
faujasite	$Na_2Al_2Si_{3.3}O_{8.8}.6.7H_2O$	12-0228
zeolite A	$NaAlSi_{1.1}O_{4.2}.2.25H_2O$	43-0142
zeolite X	$NaAlSi_{1.23}O_{4.46}.3.07H_2O$	39-0218
zeolite Y	$NaAlSi_{2.43}O_{6.86}.4.46H_2O$	38-0239
perlialite	$K_9NaCaAl_{12}Si_{24}O_{72}.15H_2O$	38-0395
analcime	$NaAlSi_2O_6.H_2O$	19-1180
hydroxy-sodalite	$Na_{1.08}Al_2Si_{1.68}O_{7.44}.1.8H_2O$	31-1271
hydroxy-cancrinite	$Na_{14}Al_{12}Si_{13}O_{51}.6H_2O$	28-1036
kalsilite	$KAlSiO_4$	33-0988
tobermorite	$Ca_5(OH)_2Si_6O_{16}.4H_2O$	19-1364

Kaolinite. It is a layered silicate mineral of formula $Al_2Si_2O_5(OH)_4$. The clay has been successfully used as a starting material in the synthesis of zeolites. Numerous articles report the synthesis of a variety of zeolites from kaolinite, among them are; (Rocha, 1991; Murat et al, 1992; Chandrasekhar and Pramada, 1999; Park, 2001; Holmes et al, 2011; Hania et al, 2012).

Rice Husk Ash. The ash generated upon combustion of rice husks has significant amounts of silica. This makes it an interesting starting material in the synthesis of various zeolites and related materials. A number of articles in the open literature report on the use of rice husk as silica source (Bajpai et al, 1981; Wang et al, 1998; Mohamed, et al, 2008; Prasetyoko et al, 2010; Othman Ali et al, 2011; Dey et al, 2012).

Blast furnace slag. A range of zeolitic materials has been successfully synthesised from blast furnace slag. Of the numerous reports available in literature these include (Kuwahara et al, 2008; Anuwattana and Khummongkol, 2009; Kuwahara et al, 2010; Murakami et al, 2011).

2.5. Characterisation of zeolites

The morphology and pore structure of zeolitic material can be well understood by the application of various analytical techniques in characterising them. The most applied techniques in zeolite characterisation include XRD, SEM, TEM, ICP-OES and N_2-adsorption. The following section presents the operating principles of these analytical techniques.

2.4.1 X-ray diffraction (XRD)

Powder X-ray Diffraction (XRD) is a technique used to examine the physico-chemical make-up of powdered solid samples. X-rays are a form of electromagnetic radiation, and when they are irradiated on a material they give rise to radiation scattering (Woolfson, 1997). When certain geometrical pre-requisites are met this scattering gives rise to constructive and destructive interference. The interplanar distance in the crystal solid has to be comparable to the wavelength of the X-rays (in the Å range). The X-rays are usually generated by bombarding a metal surface mostly Cu, with a high energy electron beam, resulting in the emission of X-rays from the metal surface, which are then passed through a monochromator before being irradiated on the sample (Park, 2012). The following diagram shows a schematic presentation of the X-ray diffraction spectrometer.

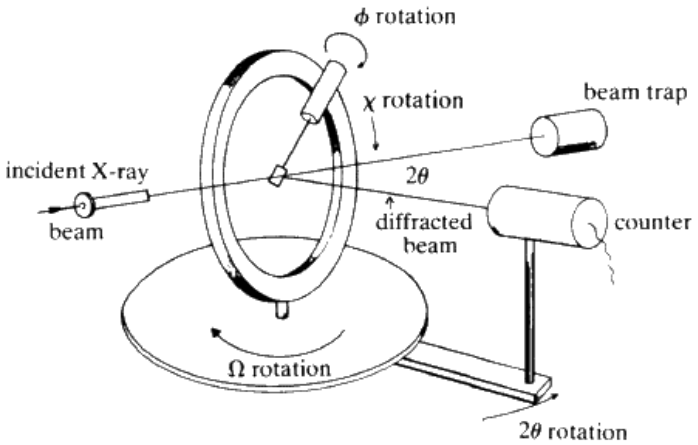

Figure 2.13: Schematic presentation of the XRD spectrometer (http://serc.carleton.edu)

Crystalline solids give characteristic X-ray diffraction angles, depending on the set of planes and their respective interplanar distances (Ertl et al, 1997). The Bragg's Law gives the relationship between the X-ray radiation wavelength, angle of diffraction and the interplanar distance, as expressed in the following equation.

$$\mathbf{n\,\lambda = 2}\boldsymbol{d}\mathbf{\cdot \sin\theta}$$

Where n is the order of reflection (0, 1 , 2, 3…), λ is the X-ray radiation wavelength (Å), d is the interplanar distance (Å) and θ is angle of diffraction (^{0})

After sample analysis the diffractometer generates a phase specific diffraction pattern that can be used to then identify the mineral phase composition of an unknown sample or to characterise the atomic scale structure of a known sample (Park, 2012). Each crystal has a distinct diffraction pattern at times referred to as crystal '*fingerprint*'. In the case of zeolitic materials the IZA has a collection of powder diffraction patterns that can be used as reference in the identification of unknown samples when a diffraction pattern is obtained (http://www.iza-online.org).

2.4.2 Scanning electron spectroscopy

The scanning electron microscopy (SEM) technique is used to establish the morphology and crystal size of solid materials (Yarimbiyik, 2007). Unlike traditional microscopes that use light waves, SEM uses a beam of high energy electrons to scan a sample and generate magnified images. Typically the electrons are generated by a thermionic, Schottky or field –emission, and are then accelerated through a potential difference of range (0.1keV – 50keV). The generated electron beam moves through a series of magnetic lenses which refines it into a fine spot (Reimer, 1998; Adriaens and Dowsett, 2004). Scanning coils will then move this electron spot to and fro, row by row across the sample. As the electrons hit the specimen there is generation of secondary electron (SE), characteristic X-rays, back scattered electrons (BSE), specimen current and electron beam induced current (EBIC). These signals are detected by different detectors. It however is unusual to have a microscope that is equipped with all the appropriate detectors. For imaging, the most useful of these signals are the secondary electrons, which are knocked off the surface of the specimen by the irradiated electron beam. The secondary electrons are then directed to a detector which counts them and generates an

amplified signal which then is used to create a 3-dimensional surface image (Reimer, 1998; Echlin, 2009).

Since the specimen is illuminated using electrons, it has to be conductive and non-conductive materials are coated with a thin film of a conductive material usually a thin gold film. The coating is done using a device known as a sputter coater (Reimer, 1998).

2.4.3 Transmission electron microscopy

Transmission electron microscopy (TEM) is a technique used to determine the morphology and content of crystalline phase in materials (Anderson and Pratt, 1985). An electron beam of uniform current density is irradiated on a thin film of the specimen, (typically 10 – 100 nm thickness). The beam is generated by thermionic, Schottky or field emission, and then accelerated through a voltage of typically 100 – 200 kV. The electron illuminating aperture is controlled by a 3 or 4 stage condenser-lens system. This also determines the area of the specimen to be illuminated (Reimer, 1998). Another set of (3 to 8) lens system is placed behind the specimen and is used to create an image based on the electron intensity distribution. The generated image is dependent on the density and thickness of the specimen, and is recorded digitally via a fluorescent screen coupled by an optic plate to a CCD camera. This produces a bright field image with thicker regions of the specimen appearing darker and the regions with no sample appearing light (Reimer, 1998).

In essence the image produced is a 2-dimensional projection of the specimen down the optic axis. The image then gives information with regard to size, shape and particle arrangement with relation to each other on the scale of atomic diameters. This also provides information on the degree of order and atomic scale defects within the specimen (Reimer, 1998).

2.4.4 Surface area determination by nitrogen-adsorption

The nitrogen-adsorption technique is based on the concept conceived by Brunauer, Emmett and Teller, that molecules such as N_2 do not adsorb on a surface by layer for layer fashion, but start by forming multilayers before making a complete monolayer. To reach this conclusion the following basic assumptions were made (Davis and Davis, 2003).

- The layers are densely packed
- The first layer has a greater heat of adsorption relative to the subsequent higher layers
- The heat of adsorption is constant for all molecules in the first layer
- The heat of adsorption for the second and higher layers is the same as the heat of liquefaction.

This mode of adsorption with the aforementioned assumptions led to the derivation of the linearised version of the isotherm, known as the BET equation (Davis and Davis, 2003):

$$\frac{P}{V_{ads}(P_0 - P)} = \frac{1}{cV_m} + \left(\frac{c-1}{cV_m}\right)\frac{P}{P_0}$$

Where P is the equilibrium pressure of gas with the surface, P_0 is the saturation vapour pressure, V_{ads} is the volume of gas (STP) adsorbed by sample, V_m is the volume of gas (STP) corresponding to monolayer formation and C is the fitted constant

A simplification of this equation is usually applied with the assumption that c is so large a value (not always the case though). This then reduces to:

$$\frac{P}{V_{ads}(P_0 - P)} = \frac{1}{V_m}\left(\frac{P}{P_0}\right)$$

A plot of the left hand side against P/P_0 gives a straight line and V_m can be found. Knowing the surface area of the nitrogen molecule together with the monolayer gas volume V_m the surface area can be calculated (Davis and Davis, 2003).

2.4.5 Fourier transform infrared spectroscopy

Attenuated total reflectance (ATR) fourier transform infrared spectroscopy (FTIR) is a technique used to study the materials of limited infrared transparency (Eagleton, 1993). The technique relies on the properties of light as it moves through materials with high reflective indices. The samples act as chemical mirrors reflecting non-adsorbed incident light back into the crystalline medium, repeatedly in series of reflection-adsorption steps within the ATR cell until the infrared radiation leaves the crystal bound for detection (Ayres, 2008). If the analyte solid sample contains substances that absorb IR, then

attenuation of radiation occurs at a wavelength at which the absorption occurs. A spectrum is then generated by plotting the intensity of the reflected radiation against the wavelength generating an absorption spectrum of the analyte (Eagleton, 1993). The sample preparation simply involves placing the powdered sample on the ATR material interface.

2.4.6 Inductively coupled plasma – optical emission spectroscopy

The inductively coupled plasma – optical emission spectroscopy (ICP-OES) technique is based on analysis of emission spectra of analyte atoms as they move back to their ground state after excitation by plasma. Plasma is a very hot gas in which a significant portion of the atoms or molecules are ionised (Pollard and Heron, 2008). The analyte sample, usually in aqueous solution is nebulised and passed into the plasma region as a fine mist. The plasma temperature can be as high as 10 000 ^{0}C, and at these temperatures atoms are left in electronically excited states (Dymott, 1995). Decay from these states results in spontaneous optical emission of radiation in the visible and ultra violet (UV) region, whose energy is given by the relationship:

$$\Delta E = E_j - E_0 = h\nu$$

Where E_j is the energy of highest level, E_0 is the energy of lowest level, h is the Plank's constant and ν is the frequency of radiation

The frequency is also related to the wavelength by the relationship;

$$\lambda = \frac{c}{\nu}$$

Where, c is the speed of light, ν is the frequency and λ the wavelength of the radiation (Dymott, 1995). The emission does not necessarily occur in a single step. It may progress via a series of intermediate steps. Each element has unique and characteristic transitions which give rise to spectral lines that then can be used to identify the element. The intensity of the spectra is proportional to its concentration. The plasma is generated in a quartz tube that is magnetised by a surrounding multi-turn copper induction coil, connected to a radiofrequency generator, operating at 20 – 50MHz. This set up then surrounds the plasma with a time varying magnetic field which induces electrical

currents in the ionised medium. The currents produce resistive heating that sustains the plasma (Dymott, 1995).

2.4.7 Temperature programmed desorption

Temperature programmed desorption (TPD) is based on the analysis of a probe gas such as NH_3, as it desorbs from a single crystal surface. In zeolite characterisation the technique can be applied to determine the density and the acid site strength using ammonia or pyridine as the probe gas (Damjanovic and Auroux, 2009). The probe gas is adsorbed via gas phase at low temperatures usually room temperature (25 ^{0}C). Ammonia is preferred since pyridine decomposes at high temperatures (Granger and Parvulescu, 2007). The probe-gas loaded zeolite is then heated at a linear rate using a stream of inert gas. The desorbed gas composition is determined by thermal conductivity detector (TCD) or mass spectroscopy and the temperature of the system by a thermocouple inserted in the catalyst bed (zeolite). The area under the desorption peak is proportional to the concentration of the acid sites, it has to be determined either by calibration with a standard sample with known acid site density or titrating the desorbed ammonia (Granger and Parvulescu, 2007).

2.4.8 Temperature programmed reduction

Hydrogen temperature programmed reduction (H_2-TPR) is a technique used to determine the reduction kinetics of metal oxides dispersed on support material. It also provides information on the available reducible species on the catalyst surface, their heterogeneity and the corresponding temperature at which reduction of the respective species occur (Uzio, 2001). This is achieved by passing a stream of hydrogen either pure or diluted, over the catalyst surface and monitoring the composition of the outlet gas using a thermal conductivity detector (TCD) system as the sample is heated up in a linear fashion, typically at a rate between 0.1 to 20 ^{0}C min^{-1}. The downstream gas composition is monitored by mass spectrometry or a thermal conductivity detector. The operating principle is based on the following reaction:

$$\mathbf{M_xO_y + yH_2 \longrightarrow xM + yH_2O}$$

The technique can also be used to measure the reproducibility of the catalytic surface, and can be used also as a quality control measure, since different synthesis routes give different reduction profiles (Cherkendorff and Niemantsverdiet, 2007).

The area under the H_2 consumption/concentration against temperature is integrated to give the total gas consumed and the peak corresponds to the temperature where there is maximum reduction rate of the metal oxide catalyst, the temperature also shows the oxidation state of the metal upon reduction.

2.4.9 Thermo-gravimetric analysis

Thermo-gravimetric analysis (TGA) is a technique that is used to measure the amount and the rate of weight changes in a material against time or temperature changes at a predetermined rate (Khopkar, 1998). This gives information on the composition as well as the thermal stability of the material concerned. There are two approaches that can be taken, i.e. dynamic thermo-gravimetric analysis in which the temperature is increased as the weight is measured and secondly static thermo-gravimetric analysis in which the temperature is kept constant while weight changes are monitored (Khandpur, 2006). When a sample is subjected to the heating process it produces distinct heating steps that form clearly defined temperature regions. A typical TGA instrument consists of a sensitive analytical balance on which the sample is placed and is heated from room temperature to about 1000 ^{0}C or more. The temperature is measured by a thermocouple that is placed very close to the sample. The heating chamber in which both the thermocouple and the sample are placed is purged with an inert gas. The accuracy of the method is enhanced by slow heating rates and low sample weight (Khandpur, 2006).

2.5 Metal loading on zeolites

In catalyst preparation or catalyst design the first step is to disperse the metal salt component on the support materials which in this study are zeolites, followed by the conversion of the supported metal salt into an oxide or a metallic form (Weckhuysen and Wacks, 2001; Acres et al, 1981). In most cases the salt of choice is usually the nitrate, due to its solubility and availability. Dispersion is achieved by various methods, chief among which are; impregnation or ion exchange, co-precipitation, deposition precipitation and adsorption from solution. The second step, calcination or reduction, is

achieved by thermally treating the supported metal salt in either an active or inert atmosphere (Acres et al, 1981). Proper catalytically active component dispersion on an inert support has the advantage of enabling effective utilisation of the metal as well as giving the catalyst an improved thermal stability. There are a number of processes that occur during metal loading by impregnation and ion exchange and they have to be fully understood in achieving a desired metal dispersion on the chosen support. One of the notable processes is the coulombic interactions between the active phase precursor and the support. These interactions are largely dependent on the selective adsorption of species by coulomb force, van der Waals forces or hydrogen bonds. These interactions can be manipulated or modified by pH adjustments, for instance, the use of an active phase precursor solution with a pH higher than the point of zero charge (PZC) or isolectric point of the charged solid surface enables the surface to attract positively charged precursor species, whilst the use of a solution with a lower pH than the PCZ of the charged solid surface enables it to attract negatively charged precursor species (Bitter and de Jong, 2009). In addition to this other complex reactions such as polymerisation/depolymerisation of species attached to the surface also occur alongside partial dissolution of the solid surface. In this work the metal loading methods employed are, incipient wetness impregnation, ion exchange and co-precipitation. These would be reviewed in detail while other metal loading approaches will be briefly reviewed (Acres et al, 1981).

2.5.1 Incipient wetness impregnation

In incipient wetness impregnation, the volume of the active phase precursor solution is less or equal to the support material pore volume. The approach is used to introduce the active component(s) into the pores of the support material. The first step is to determine the pore volume of the support (Richardson, 1989). This is usually done by an empirical approach in which the solvent is slowly added to a known amount of the powdered support material until it is just wet. To permit deeper solvent penetration into the pores the support is evacuated prior to solvent addition. This allows for uniform metal precursor distribution (Pinna, 1998). At first, when the solvent is added it moves into the pores of the support by capillary action, and the outside of the support looks dry. A known amount of the metal salt is then dissolved in the empirically determined solvent

volume and then mixed with the support in appropriate weight proportions. The solvent is then evaporated, followed by calcination in air which converts the metal salt to the metal oxide. In essence, active component species are physically retained inside the pores during drying rather than by specific solution/surface interactions (Ross 2012).

Metal loading is limited by the solubility of the metal salt in the chosen solvent and in cases where higher metal loadings are required the procedure is repeated several times until the required metal loading is achieved (Pinna, 1998). Quantification of the metal percentage loading is done using two approaches i.e. the actual metal loading obtainable by reduction/oxidation experiments and then the theoretical loading, calculated based on the quantity of metal salt used (Gupta et al, 2010). The technique is simple and very effective for loading expensive noble metals since it does not require bulk solutions, it however is complicated when applied in the preparation of mixed metal catalysts, since metal adsorption selectivity considerations have to be catered for, or else unexpected metal proportions would be observed (Acres et al, 1981).

However the final material may not be uniform due to collection of higher concentrations of the active phase component in larger pores resulting in formation of larger crystallines in those regions. Again the drying has to be carefully controlled in order to suppress the chromatographic effect, which would result in the creation of higher active phase concentration levels at the mouth of the pores or even on the outer surface of the support (Ross, 2012). Impregnation can also be effected via the following methods; impregnation by percolation, co-impregnation, successive impregnation and deposition by selective reaction with the support material (Haber et al, 1995).

2.5.2 Wet impregnation

The wet impregnation approach involves contacting the support material with an excess amount of the active phase precursor solution. The amount of the metal deposited is largely dependent on the solution/solid ratio (Richardson, 1989). The deposition process is quite slow requiring several hours to days in certain cases. The next step is elimination of the solvent, which is achieved by evaporation or filtration in cases where a large excess solution is used. The technique is characterised by large crystals on the outer surface of the support material since the bulk of the active component precursor solution is present in the solution outside the support pore system. The method allows

for the generation of a highly dispersed metal on the support and is very effective in cases where ion/solid interactions take place (Haber, 1995). Impregnation, both incipient wetness and wet, occurs via four stages; active phase precursor ion adsorption on support material, drying (filtration is carried out in the case where a large excess solution is used), nucleation and particle growth. Wet impregnation is also characterised by extensive surface restructuring when contacting the solid support with the active phase precursor solution, this consequently gives rise to surface area loss (Haber et al, 1995).

2.5.3 Ion exchange

When the triply-charged aluminium isomophorically replaces the quadri-charged silicon in the zeolite framework, it gives rise to a deficiency of positive charge and creates negatively charged centres (Kuhl, 1999). Singly or double charged atoms would then come into the structure to charge balance the system. These atoms can be exchanged by other cations and hence are referred to as exchangeable ions since they are not part of the zeolite framework. The amount of the exchangeable atoms for a particular zeolite is largely dependent on its charge density which in turn is governed by the SiO_2/Al_2O_3 ratio. The higher the SiO_2/Al_2O_3 ratio, the lower the charge density and the lower the amount of the exchangeable ions (Kuhl, 1999). When the zeolite is contacted with an external electrolyte, ion exchange between the cations on the solid support surface and the cations in the electrolyte takes place. The rate of ion exchange is generally governed by two main factors namely, the ion concentration and the size of the cation capable of penetrating the pore system of the zeolite. The size of a particular cation is determined by the degree of hydration as well as the charge density. An equilibrium exists between the fully hydrated ion with its partial hydrated states as well as the bare ion. This equilibrium is influenced mostly by temperature and concentration of co-solvent in cases where another solvent other than water is used (Kuhl, 1999). As the temperature is increased the hydration water molecules are stripped off the ions and the equilibrium shifts towards less hydrated ions which easily penetrate the zeolite pore and hence increased ion exchange rate is observed. The temperature commonly used is limited by the boiling point of the solution and since water is the commonly used solvent the ion-exchange is usually carried out within the temperature range 40-80 ^{0}C. The use of

pressure vessels allows the reaction to be carried out at even higher temperatures. Ions with a high charge density have a smaller hydration shell and hence are easily exchanged relative to those with a lower charge density (Kuhl, 1999).

When metal loading a zeolite with a particular ion the zeolite is contacted with a salt solution of the desired metal, either at ambient conditions or at elevated temperature to effect an increased ion-exchange rate. The anion associated with the metal is expelled by the repulsive forces exerted by the negative charge centres on the zeolite pore apertures. The following hypothetical reaction presents the equilibrium that is established when the zeolite is contacted with the active phase precursor solution (Kuhl, 1999).

$$b\mathrm{A}^{a+}{}_{s} + a\mathrm{B}^{b+}{}_{z} \rightleftharpoons b\mathrm{A}^{a+}{}_{z} + a\mathrm{B}^{b+}{}_{s}$$

Where A^{a+} is the ion initially in solution, B^{b+} is the ion initially in the zeolite pore system, *a* and *b* are the respective valences of the exchanging ions and *s* and *z* are designates for solution phase and the zeolite phase. Other factors controlling ion exchange are the zeolite topology, presence of counter ions, solution pH, presence of other exchangeable cations, location of the cation within the zeolite and the presence of extra-frame work cation (Armor, 2001). The zeolite framework can easily be damaged by acidic conditions, hence salts that form strong acidic solutions cannot be used unless pH adjustments are undertaken (Solt et al, 2008). However the metal solution concentration should not exceed 0.5 M or else significant imbibition of the salt is observed. This factor limits the approach when a higher metal loading is required, and in most cases successive ion exchange is performed to achieve higher metal loading (Kuhl, 1999). Another factor that limits the amount of metal loaded is the equilibrium that is established between the outgoing cation in solution and on the exchange site for instance when using the protonic zeolite; as the amount of H increases in solution it will reach a point where the rate at which the cation goes into solution is the same as the rate of re-deposition on the exchange site. This hinders further loading and a higher metal loading is only achievable by introducing the zeolite into a fresh solution of the metal precursor. To minimise this problem a large excess solution can be used. This can however pose a problem in dealing with the large waste electrolyte generated in the event that the process is up scaled (Price, 2007).

Ion exchange is characterised by uniform and optimal metal dispersion in the zeolite pore system, ability to generate mobile cations with various oxidation states and also the possibility of generating coordinatively unsaturated metal sites. For reproducibility purposes it is of paramount importance to mention the following synthesis parameters: (Armor, 2001).

- the solution pH before and after the ion exchange
- the source or origin of the zeolite as well as all the other material used in the ion exchange
- the SiO_2/Al_2O_3 ratio as well as the cation/Al ratio
- the composition of all source material and elemental analysis of the exchanged zeolite
- the order of addition together with time and exchange temperature
- all the other details pertaining to pre or post treatment

In comparison to other metal loading approaches ion exchange has a number of advantages and due to that it is widely applied. The method is however limited by the solubility of the metal salt and the exchange is also limited by steric constraints presented by the formation of bulky hydration shells and the thermodynamic equilibrium. Furthermore the exchange of multiply charged ions is difficult with this approach.

2.5.4 Solid state ion exchange

Solid state ion exchange (SSIE) takes place when the zeolite is contacted with a solid metal salt containing the ingoing metal. This is carried out in the absence of water or with little water. In most instances the contact is done by mechanical means usually grinding the zeolite together with the metal salt in a ball mill and finally introducing the metal in the zeolite cavities by a driving force (Price, 2007). The driving force is usually an elevated temperature, but in certain instances it is moisture induced or chemically induced using either an oxidising or reducing agent. The approach has been successfully applied to introduce transition metals into the cavities and channels of zeolites. In most cases the protonic form of the zeolite is preferred and the solid state reaction between the salt and the zeolite is characterised with the release of a volatile product that is then

swept away by purging or vacuum (Price, 2007; Solt et al, 2008). The general reaction between the stoichiometric quantities can be presented as follows;

$$MCl_n + nHZ \longrightarrow xMZ + (1\text{-}x)MCl_n + (n\text{-}nx)HZ + nxHCl(g) \longrightarrow MZ_n + nHCl(g)$$

Where M is the n-valent metal cation and Z is the monovalent zeolite fragment (ion exchange site). In cases where the metal precursor is a metallic oxide or a metallic hydroxide the off gas is water. The case presented in the equation above is irreversible, but if a zeolite which is not in its protonic form is used then there is no formation of a volatile product. This case however presents a setback since the ingoing cation competes with cations already on the exchange site, and extraframework cations and anions end up populating the zeolite pore system, a phenomenon referred to as occlusion.

As previously mentioned, the solid state ion exchange method involves the application of a driving force to enable the ingoing cations to break free from the precursor solid matrix. There are basically three conventional types of driving forces applied, namely (i) moisture induced (ii) high-temperature induced and (iii) reaction induced. Recently ultrasonic treatment has been used also as a driving force (Price, 2007).

2.5.5 Chemical vapour deposition

Chemical vapour deposition is a technique in which volatile inorganic and metal-organic precursors are introduced on a solid substrate in a vapour phase resulting in the dispersion of ordered crystals (Kodas and Hampden-Smith, 1994). Put in other words it can also be defined as the deposition of a solid film onto a substrate surface via chemical reaction in the gas phase species. The reactions are commonly carried out at temperatures around 1000 ^{0}C (Yan and Xu, 2010). The vapour phase is transported by a gas and the most commonly used carrier gases are inert carriers such as argon and nitrogen. The use of such gases enhances the rate of transport of the precursors to the reactor. In certain instances other reactive carrier gases such as ammonia, oxygen and hydrogen can be used in cases where the carrier has to participate in the film deposition chemistry by acting either as a reductant or oxidant. During deposition, gas phase reactions may occur depending on the reactivity of the participating species. These reactions usually lead to nucleation of solid particles which will be deposited together with the desired metal on the substrate. This phenomenon leads to the formation of

films containing impurities, defects, particulates and poor adhesion. There is also a chance of low metal deposition on the substrate due to depletion of precursor concentration before it reaches the substrate surface. To minimise these problems reactions are designed in such a way that gases are mixed just over the substrate surface. Lower operation pressures can also greatly reduce the gas-phase reactions. The underlying principle of the technique is that when the gas is flowed at relatively high pressure over the substrate, a boundary layer is created and temperature, velocity and concentration vary rapidly across the boundary. The gaseous species then diffuse through the boundary to reach the substrate surface on which they will chemisorb and deposit a solid film, with the release of volatile by-products that will diffuse back into the bulk gas flow, where they are swept away and leave the reaction chamber. The slowest of the two processes, chemisorption or desorption, will determine the overall rate of metal deposition (Kodas and Hampden-Smith, 1994).

Parise et al, (1998) reported on the deposition and characterisation of selenium on zeolites; A, X, Y and mordenite using this approach. It is relatively easy to deposit organometallic compounds on the zeolites due to the availability of charge balancing protons. The process can be presented by the following reaction.

$$ZO\text{-}H + (CH_3)_4M \longrightarrow ZO\text{-}M(CH_3)_3 + CH_4$$

The Z is the zeolite framework whilst the M is the metal to be loaded. After the organometallic species are grafted onto zeolite, H_2S is introduced into the system and reacts according to the following reaction scheme.

$$ZO\text{-}M(CH_3)n + nH_2S \longrightarrow ZO\text{-}M(SH)n + nCH_4$$

$$ZO\text{-}M\text{-}(SH/CH_3) + H_2S \longrightarrow ZOH + HS\text{-}M(SH/CH_3)$$

After the formation of the hydrogen sulphide compounds the material is thermally treated and this facilitates the formation of metal sulphide clusters within the zeolite pore system (Xu et al, 2007). Metal sulphide nanomaterials are used in energy conversion and storage, such as lithium-ion batteries, solar cells, fuel cells (Lai et al, 2012).

2.5.6 Deposition-precipitation

The deposition-precipitation technique involves the precipitation of a metal hydroxide on the substrate surface. This is achieved by raising the pH of the precursor solution. The substrate surface acts as the nucleating agent such that the precipitate crystallites form on the support. A good metal dispersion is enhanced by ensuring that the precipitation occurs very close to the substrate surface. This is achieved by avoiding local high concentration of hydroxide (Savage et al, 2009). The approach has the advantage of creating narrow particle distribution or high dispersion, but on the other hand it is also characterised by low metal loading in comparison to other metal loading methods such as ion exchange and incipient wetness impregnation (Nares et al, 2002). Conventionally the nitrate salt of the metal catalyst is mixed with an oxide based support material. In the case of zeolites, as reported by Nares et al., (2010), the OH groups on the zeolite surface are the nucleating sites where the metal particles form. In the same report Nares et al., (2010) presents the deposition of Ni on zeolite HBEA and it was found that the average particle sizes of the deposited metal particles ranged from 29 - 44Å, depending on the contact time.

2.5.7 Co-precipitation

Co-precipitation can be defined as the simultaneous precipitation of a normally soluble substance with a macro-component from the same solution by the formation of mixed crystals, by adsorption, occlusion or mechanical entrapment (McNaught and Wilkinson, 1997). Conventionally an aqueous solution containing the metal precursors is mixed with the nitrate form of the substrate under mild basic conditions. The pH of the solution is then adjusted by addition of a basic solution usually ammonium carbonate. It is expected that when two metals are in solution and the pH adjusted the two would precipitate at different pH values. The one which precipitates at a lower pH would precipitate first as the pH is gradually increased. When the pH approaches the stage where the second metal precipitates, the first metal re-dissolves and precipitates together with the second metal. A typical example is the co-precipitation of Al and Ni species. The Al precipitates at pH below 3 and the Ni at a pH above 6, but when the two are present together in solution the Al precipitates at a lower pH and as the pH is raised it

re-dissolves and precipitates together with Ni at a pH below 6. This results in the formation of a mixed layered hydroxide on the substrate surface (Ross, 2012).

The chemistry of co-precipitation is governed mostly by colloidal chemistry, and the most controlling factor which influences the bonding of the respective metal particles to form larger agglomerates is inter-particle force. The rate at agglomeration is dependent on the rate of particle collision per unit time (Jiang, 2003). Xia et al., (2011) presents a report in which the technique was successfully applied to introduce iron and copper onto MCM-41 support. Another interesting report is presented in which nanosized cerium-manganese ferrite particles were prepared using co-precipitation (Zhao et al., 2011).

2.6 Post loading treatment

Upon loading the catalysts using the range of available approaches, some of which were outlined in the previous section, the catalysts are usually treated further by washing them first to remove the excess salt and solvent used during loading. The next step is drying followed by calcination and reduction in certain cases. These three processes have an impact on the final catalyst generated and particular attention has to be taken depending on the nature of the catalysts and the desired properties that need to be imparted on the final catalyst. Every step creates an imprint on the final heterogeneous catalyst. These imprints can significantly determine the catalytic activity of the final catalyst (Perogo and Villa, 1997). This section will briefly look into the effects of these parameters.

2.6.1 Washing

This step is a traditional unit operation in catalyst preparation and the aim is to separate the catalyst from the mother liquor. It also enables the removal of certain impurities from the catalyst. In most cases it is simply done by adding an appropriate amount of distilled water to the solid catalyst and allowing the suspension to settle and the supernatant is decanted prior to further separation by either filtration or centrifugal means. With zeolitic support materials or any other crystalline substrate this step is less complicated. It however can pose a challenge when working with flocculants since they have long settling times (Perogo and Villa, 1997).

2.6.2 Drying

Upon washing the catalyst is usually dried in order to remove any remaining solvent entrapped in the pore system of the porous substrate. This is traditionally undertaken at temperatures in the range of 80 – 200 ^{0}C. Several factors influence the quality of the final catalyst and should be taken into consideration depending on the desired properties that need to be imparted on the catalyst. The major factors that can significantly alter the quality of the final catalyst are mainly the final temperature at which the catalyst is dried; the time the catalyst is exposed to the set condition (i.e. drying time); the atmosphere in which the drying is executed (i.e. either in vacuum or in the presence of a specific gas) and the rate of heating.

A slow rate of drying causes the solvent evaporation to start from the external surface of the substrate, which consequently causes diffusion of the metal salt into the deeper pore system of the zeolitic support. This results in an increased metal loading in the deeper pores than on the zeolite surface. On the other hand a high rate of heating would create temperature gradients, which results in the solution migrating to the outer surface of the support and metal precipitation takes place on the outer layer (Pinna, 1998). The removal of water from porous materials during this step is via evaporation, and if evaporation occurs and the moisture is blocked in the zeolite pore system, internal pressure of steam is created resulting in loss of pore volume and surface area due to dealumination. Therefore heating rates should be carefully controlled to ensure that the rate of evaporation is relatively higher than the rate of diffusion out of pore. It is also highly recommended to carry out this step in vacuum at low temperatures to avoid structural collapse (Perogo and Villa, 1997).

In a report by Zhu et al., (2006) mesoporous MCM- 41 was loaded with platinum and subjected to 3 different washing and drying conditions. The first catalyst was washed with water and oven dried at 100 ^{0}C, whilst the other two were washed with ethanol and vacuum dried at 30 and 100 ^{0}C. The result obtained from the XRD diffractograms as well as N_2-sorption measurements revealed that the ethanol washed and vacuum dried catalysts preserved the structure of the parent support whilst some structural collapse was observed on the catalyst that was water washed and oven dried.

2.6.3 Calcination

The calcination process involves heating the catalyst in an oxidising atmosphere at temperatures higher than those encountered during catalyst preparation as well as temperatures applied during the catalytic reaction and catalyst regeneration (Perogo and Villa, 1997). This decomposes the catalyst metal precursor with consequent formation of the oxide and removal of gaseous products. The process also removes organic and volatile impurities that might have been entrapped on the catalyst during synthesis (Pinna, 1998). In general during calcination the following occurs; loss of chemically bonded water; modification of texture through sintering; structure modification; active phase generation and stabilisation of mechanical properties (Pinna, 1998).

The extent to which the outlined processes alter the final catalyst are dependent on the treatment time, calcination temperature and the presence of stream (Perogo and Villa, 1997). Control of calcination temperature is of paramount importance when treating bimetallic catalysts in order to avoid formation of two separate oxides. Studies on the effect of calcination temperatures on Fe/HBEA prove that the calcination temperature affects the metal dispersion, pore volume and surface area of the catalyst (Ma et al, 2012). The study goes on to show that when Fe/HBEA prepared by impregnation was subjected to calcination temperatures above 850 ^{0}C, agglomeration occurred with consequent reduction in surface area and pore volume. The study also puts across the fact that calcination temperatures below 750 ^{0}C did not change the surface Lewis and Brønsted acidity of the zeolite.

The loading method applied also determines how the calcination temperature will affect the final catalyst. According to a report by Li et al, (2011) a study was carried out on copper catalysts supported on zeolite Y that were prepared via incipient wetness impregnation and ion exchange. The study found that catalysts prepared by impregnation can undergo solid state ion exchange during calcination at 400 ^{0}C, with the unexchanged Cu species dispersing on the zeolite surface. The same could not be observed in the catalyst prepared by ion exchange. For every catalyst there is an optimum calcination temperature that gives rise to a good dispersion on the substrate. Higher calcination temperatures enhance thermal motion of the metal atom and consequently improve the metal oxide dispersion. However excessive calcination temperatures lead to formation of large metal crystallites, which in turn reduces pore

volume as well as surface area, consequently reducing the catalyst activity (Chang et al, 2011).

2.6.4 Reduction

The calcination step results in the formation of metal oxide(s) on the surface and within the pore system of the zeolitic support material. However some catalytic systems would have better catalytic activity when the metal is dispersed on the support in its metallic and not oxide form. The conversion of the metal oxide to the metal is usually done by a reduction process. The reduction can either be undertaken by a thermal treatment of the catalyst in hydrogen flow or by chemical treatment using mostly formaldehyde or hydrazine (Zecca et al, 2008, Pinna, 1998). During thermal treatment factors such as heating rate, final temperature and contact time should be carefully controlled depending on the physicochemical properties that need to be imparted on the catalyst. These properties are determined by the specific catalytic reaction to be undertaken (Pinna, 1998).

In thermal treatment the hydrogen concentration and the flow rate are also of paramount importance, since the reduction step produces water, the flow should be high enough to sweep away the water vapour produced. The presence of water vapour results in poor metal dispersion and it should be kept as low as possible (Pinna, 1998). In cases where there are metal chlorides this approach might be detrimental since there is production of hydrogen chloride which in the presence of water can corrode the reactor. Catalysts bearing chlorides should be treated in carefully controlled environments and further treated with a diluted oxidant mixture usually (1-2% oxygen in an inert gas balance). This step stabilises the catalyst by forming a thin layer of oxide that can easily be removed in the reactor when the catalyst is to be used (Pinna, 1998).

Zeolite supported platinum catalysts are traditionally taken through a reduction process prior to their respective applications. In a report by Folefoc and Dweyer, (1992) an investigation on the platinum dispersion on zeolite ZSM-5 was undertaken. The study went further to look into the metal dispersion upon activation in oxygen prior to the reduction process and it was found that the different activation temperatures resulted in different metal dispersion. The choice of activation temperatures would then be determined by the catalytic system where the catalyst ought to be applied.

2.7 Friedel-Crafts alkylation of benzene

The background of the Friedel-Crafts (FC) alkylation of benzene as well as the uses of the products obtained in the reaction is presented in Chapter 1. The Friedel-Crafts alkylation of benzene involves the formation of a new C – C bond by an electrophilic substitution on the benzene ring in the presence of a Lewis or Brønsted acid as catalyst.

2.7.1 Alkylation of aromatics

The Friedel-Crafts reaction has proved to be much more complicated than it was originally thought to be at the time of its discovery. Further investigations of the reaction showed that the reaction is usually accompanied by isomerisation and polyalkyaltion processes. There are two types of isomerisation that may occur namely, rearrangement of the reactant alkylating agent and positional isomerisation. In certain instances some undesirable side reactions may occur. These include dealkylation, transalkylation and formation of saturated hydrocarbons.

The alkylation of aromatics is not only limited to benzene alone, but to other benzene homologues like fused polycyclic compounds such as naphthalene, anthracene, phenanthracene and indene. Polycyclic rings are also alkylable. These include compounds such as biphenyl, diphenyl methane, bibenzyl and tetraphenyls. However the polycyclic aromatics usually give low yields due to their own high reactivity under the FC operation conditions. Alkyl groups attached to the benzene ring are expected to be ortho and para directing to the incoming substituents. It was however established that it is possible to have a meta substitution in the event that the alkylbenzenes are monoalkylated. The meta substitution is not always caused by a low selectivity kinetic alkylation but by thermodynamically affected isomerisation. The respective quantities of the three dialkylbenzenes are affected by four factors namely; the type of the aromatic hydrocarbon, alkylating agent, catalyst and the reaction conditions. Given this background the mechanistic consideration of the FC reaction ought to be differentiated as kinetically controlled direct alkylation and thermodynamically controlled isomerisation (Olah and Molnar, 2003).

2.7.2 Kinetics and thermodynamics of the Freidel-Crafts reaction

There is limited data in literature that looks into the kinetics of the FC reaction (Carey and Sundberg, 2007). However there are some FC reactions that have been well studied, for instance, the alkylation of benzene with ethyl bromide in the presence of gallium chloride as catalyst. This particular reaction is first order with respect to each reactant in the catalyst. When aluminium chloride is used instead, the rate of reaction changes with time due to the heterogeneity of the reaction matrix. The initial rate is expressed according to the following expression.

$$\text{Rate} = k\,[\text{EtBr}][\text{benzene}][\text{AlBr}_3]^2$$

In the event that t-butyl benzene is used as the alkylating agent with $AlCl_3$ as catalyst and nitromethane as solvent, the reaction follows a third order kinetics as expressed by the following equation.

$$\text{Rate} = k[\text{AlCl}_3][\text{t-butylchloride}][\text{benzene}]$$

A mechanistic scheme for the FC reactions can be presented upon considering three fundamental factors namely:

- Complexation of the alkylating agent and the Lewis acid (in some instances ionisation of the complex occurs resulting in the formation of a discrete carbocation.
- Electrophilic attack on the aromatic reactant.
- Disproportionation.

The formation of the carbocation is held responsible for the rearrangement that is commonly observed in the alkyl halide. The rearrangement of the carbocation formed in the FC alkylation reaction arranges to more stable cations. The order of rearrangement is in the order primary > secondary > tertiary. It usually occurs via the migration of smaller groups on the adjacent carbon atom. This makes it difficult to introduce a primary alkyl group onto an aromatic ring. In the alkylation of benzene with n-propyl bromide the reaction gives mostly isopropylbenzene and less n-propyl benzene. Due to this fact most n-alkylbenzenes are prepared via acylation followed by reduction (Smith

and March, 2007). The rearrangement is usually accompanied by isomerisation, and this occurs via two processes; either through a 1,2 shift or through a dissociation to cation and readdition. Smith, (1946) reports that exposure of *sec*-butylbenzene to a mixed acid (HF-BF_3), produced a mixture of 36.7 % benzene, 10.9 % *n*-butylbenzene, 21.8 % of *sec*-butylbenzene and 30 % of di-*sec*-butylbenzene. A related reaction is also reported where *n*-butylbenzene is heated with $AlCl_3$ at 100 ^{0}C, for 3h, the resulting mixture comprised of 15.2 % of benzene, 27.7 % of di-butylbenzene (> 99.4 % *n*-butylbenzene and 0.6 % *sec*-butylbenzene), 15.2 % benzene and 27.7 % di-butylbenzene (> 90 % meta) and 11.9 % of polyalkylated benzene products. Based on these outcomes it could be established that the Lewis acid induced isomerisation of dialkylbenzenes usually favours the formation of the meta isomer based on its thermodynamic stability relative to the ortho and para isomers.

In the Friedel-Crafts alkylation of benzene with *t*-butyl chloride in the presence of $AlCl_3$, if a 1:1 mole ratio of benzene to the alkyl halide are reacted, the major product is the di-alkylated product (1,4-di-butylbenzene) whilst the monoalkylated product (*t*-butylbenzene) is much lower. This is due to the fact that when the first alkylation occurs the compound becomes more activated than benzene itself, leading to an almost unavoidable second alkylation. To avert this problem usually a large excess of benzene is used (McMurry, 2012). The use of zeolite supported catalysts has a significant influence in product selectivity.

Bidart et al, (2006) studied the alkylation of benzene over Fe loaded zeolite Y and proposed a possible mechanisim in which the first step involves a single electron transfer between the alkyl halide and the metal site resulting in the formation of a cation radical. In the second step, the cation radical interacts with the reduced metal species forming a chlorine atom and a carbocation, which will then alkylate the benzene. The following scheme represents the mechanistic view of the reaction.

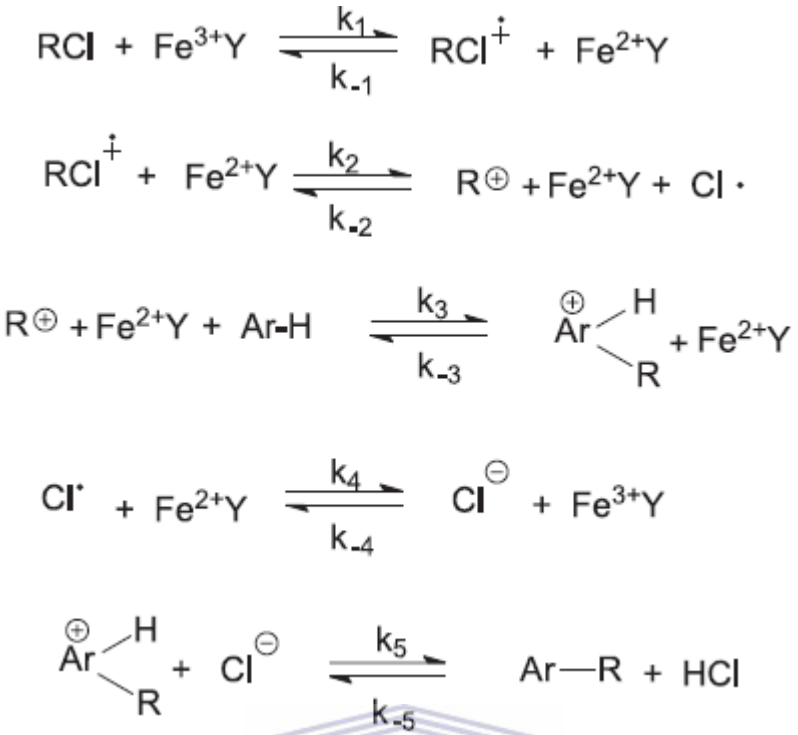

Scheme 2.1: Mechanistic view of the alkylation of benzene with t-butyl chloride over iron loaded Zeolite Y

2.7.3 Zeolites as catalysts for the FC reaction

Zeolites and aluminosilicates have proved to be efficient acidic supporting materials for metals (Kuhlmann, et al, 2004). The most seasoned zeolitic materials that have been applied in the FC alkylation of benzene include BEA, MOR, FAU, MCM-22, and MFI (Caeiro et al., 2006; Perego, et al, 1996; Degnan et al, 2001). Zeolite beta has proved to be more effective compared to Zeolite Y, due to the differences in the pore system. The Zeolite Beta openings are slightly larger than benzene and do not allow the formation of bulky molecules whilst the much larger pore system of Zeolite Y may allow formation of bulky by-products that are not sterically hindered. In a review, Perego and Ingallina, (2002) present a variety of materials that have been tested for the benzene alkylation, among them various zeolites, clays, heteropolyacids, sulphonated zirconia and immobilised ionic liquids.

The loading of metals on zeolites modifies the Brønsted acid sites as well as the metal state, which consequently changes the metal site density and acid strength distribution. The zeolites also greatly affect the dispersion of the metals, the overall reaction

mechanism as well as the adsorption of reactants on active sites (Stiles, 1987). To create an efficient catalyst there is a need to optimise the combination of both the chemical and physical factors of the catalyst. This has significant effects on both the reaction rate and selectivity (Dimian and Bildea, 2008).

2.7.4 Effect of aromatic/alkyl halide molar ratio

When using traditional catalysts such as $AlCl_3$, in the alkylation of benzene with alkyl halides, the benzene/alkyl halide molar ratio has a significant role in determining which by-products are formed. However the use of zeolitic materials of appropriate pore size can greatly improve the formation of the desired isomer with less or no dependence on the benzene/alkyl halide molar ratio. In a study carried out by Bidart and co-workers (2006), different stoichiometric ratios of benzene and *t*-butyl chloride over Fe-Y zeolite, were studied and it was observed that selectivity for monoalkylation was not influenced by the molar ratios. This is due to the fact that the reaction takes place in the pore system of the zeolite. It has to be noted though that there might be some slight influence since the reaction may also take place on the external surface. So in designing a catalyst for the Friedel-Crafts alkylation reaction, it is essential to modify the channel system of the zeolite to favour formation of a desired product (Bidart et al, 2006).

2.7.5 Advances in the Friedel-Crafts reaction

The alkylation of aromatics using alkyl halides is characterised by the release of acids, alongside the desired products. The main challenge faced with the reaction is to create more environmentally eco-friendly approaches. The use of alcohols as an alkylating agent is a promising avenue since water is the by product. On the other hand, activated double bonds and styrene when used produce no side products. The first attempt to use alcohols and styrene as alkylating agents was reported in 1996 in which $Sc(OTf)_3$ and then later $Mo(CO)_6$ were used as Lewis acids (Rueping and Nachtsheim, 2010).

Tian et al., (2008) presented a report in which the alkylation of benzene with propene over HBEA was carried out near super critical conditions. The outcome proved that the catalyst life can be greatly improved when the reaction is carried out under such conditions. The approach can also be viewed as an interesting way of improving throughput.

Yeh, (2008) presents a list of numerous patents in which a range of zeolites including, Zeolite Y, Zeolite X and ZSM-5, were used in the alkylation of benzene using olefins from C_2 – C_6. Alkylation of aromatics has also been successfully carried out via homogeneous catalysis using ionic liquids. It is another green approach and has received much attention and interesting outcomes were obtained (Sun and Zhao, 2006; Cai et al, 2008; Lee et al, 2010; Taylor et al, 2011, Xie et al, 2012))

2.7.6 Effect of temperature and time

Since alkylation reactions are exothermic, higher temperatures are undesirable, however very low temperatures may also slow down the reaction rate. There is always a need to compromise between the thermodynamic and kinetic factors (Sun and Zhao, 2006). Bidart and co-workers, (2001) studied the alkylation of benzene with a range of alkyl halides over Fe loaded Zeolite Y. It was noted that for primary halides the increase in temperature did not significantly improve the yield. With secondary and tertiary halides a slight increase was noted. These studies were carried out at moderate temperature ranges below 100 ^{0}C. Odedairo and Al-Khattaf, (2012) studied the alkylation of benzene with light alcohols over MOR and MFI zeolites at high temperatures and it was noted that using a temperature of 400 ^{0}C, the maximum conversion was achieved within a time period of 20 s. However temperatures within this range may have significant impacts on the catalyst itself. Laredo et al, (2012) reports that when HBEA was used at elevated temperatures in the alkylation of benzene with propylene, a marked deactivation of the catalyst was observed and was attributed to the formation of propene oligomers in the zeolite channel. Long reaction times also favour the formation of the most thermodynamically stable isomers. In the alkylation of benzene with alkyl halides, Bidart et al, (2001) report that prolonged reaction time of over 3 h favoured the thermodynamically more stable meta isomer.

2.8 Chapter summary

The scientific publications consulted in the present work have given the background information with regard to fly ash generation, its environmental hazards as well as its use in zeolite synthesis. An in-depth understanding of zeolite chemical composition, framework structure and nomenclature has been accrued. A large part of this chapter

was dedicated to present a detailed account of zeolite synthesis from both pure chemicals as well as waste materials such as fly ash, kaolin, rice husks and blast furnace slag. The effect of the respective parameters such as pH, temperature, water content, pressure, reaction time, agitation and stirring, crystallisation, addition of mineraliser and structure directing agents (SDAs) during synthesis have been presented. The chapter highlighted the recent developments in zeolite synthesis where non-conventional approaches or modification of conventional approaches have been successfully applied. Some of the most interesting new developments in zeolite synthesis that were reviewed including, the dry gel synthesis, low water and non-aqueous syntheses, ionothermal and eutectic mixture syntheses as well as the use of computer simulations in predicting suitable synthesis conditions for specific zeolitic materials. New approaches described in literature helped inform the synthetic routes used in this study.

A section of the literature review focused on the characterisation techniques applied for zeolitic materials. Various articles presented detailed information on the instrumental operating principles as well as the information on the nature of the zeolitic material that can be deduced from the respective analyses. The characterisation techniques reviewed were XRD, SEM, HR-TEM, N_2-adsorption, FTIR, ICP, NH_3-TPD, H_2-TPR and TGA. The combination of these characterisation techniques provided the necessary information to be applied in this study to determine the catalyst characteristics which consequently may influence the catalytic activity of the prepared catalyst.

The chapter went on to review the different metal loading approaches commonly applied in the preparation of zeolite supported metal catalysts. Much emphasis was put on the approaches applied in the present work namely liquid phase ion exchange and incipient wetness impregnation. Other metal loading approaches were reviewed namely wet impregnation, solid state ion exchange, chemical vapour deposition, deposition-precipitation and co-precipitation. The respective advantages and shortcomings of the respective approaches were also laid out. The methods chosen for the present work (ion exchange and incipient wetness impregnation) were found to be easy and reproducible based on outcomes presented in literature. Usually post synthesis modification is necessary to convert the metal catalysts to the desired state. In the case of the Friedel-Crafts alkylation the metal oxides are active and post modification steps are necessary to convert the metals to the respective oxide forms. This is achieved by washing the

prepared metal loaded catalyst followed by drying and the calcination in air. The effect of these post synthesis modification approaches on the nature of the catalysts were also reviewed and based on these principles suitable catalyst preparation conditions such as calcination temperature and drying rates were chosen.

The final part of the review focused on the Friedel-Crafts (FC) alkylation reaction, starting with the background of the reaction as well as the kinetics and the thermodynamics of the FC reaction. The FC alkylation of benzene to form alkylbenzenes is an essential industrial reaction since alkylbenzenes are useful in a number of reactions as either intermediates or solvents, with some of the prominent applications being their use in the plastic industry and as blending stocks in the increase of octane number in fuels. They are also used as solvents in paints, adhesives and pesticides and production of synthetic detergents. The traditional catalysts for the FC reaction were also reviewed and zeolites supported metal catalysts have recently gained much attention as green catalysts for the reaction and a review of the zeolites applied in the reaction has also been presented. Metal loaded HBEA and mesoporous MCM-41, have been used in the FC reaction and have proved to be versatile support materials, thus were chosen as baseline materials in this study.

Based on the literature reviewed it was found interesting to investigate the possibility of using fly ash based Zeolite X, and compare the activity to that of seasoned support materials such as HBEA and MCM-41 in the alkylation of benzene with *t*-butylchloride.. The fly ash based hierarchical Zeolite X has a new morphology and it has not been tested for the FC alkylation of benzene with alkyl halides. On the other hand, the activity of zeolite bimetallic catalysts consisting of Fe and Mn has not been investigated and the present work aims to investigate the effect of doping Fe catalysts with Mn and evaluate the effect it has on the catalytic activity. Both Fe and Mn are relatively cheap transition metals and are readily available.

CHAPTER 3

3.0 Experimental details

The chapter aims to present a detailed methodology of the experimental activities undertaken in catalyst preparation, characterisation and catalytic activity testing. The first section of this chapter focuses on the synthesis of the hierarchical Zeolite X from coal fly ash. The second section presents the experimental activities with regard to metal loading on the synthesised zeolite as well as on the commercial support materials used i.e. zeolite HBEA and MCM-41. The last section gives an overview of the characterisation as well as instrumentation conditions set up. A schematic flow diagram presented in Figure 3.1 summarises the experimental details.

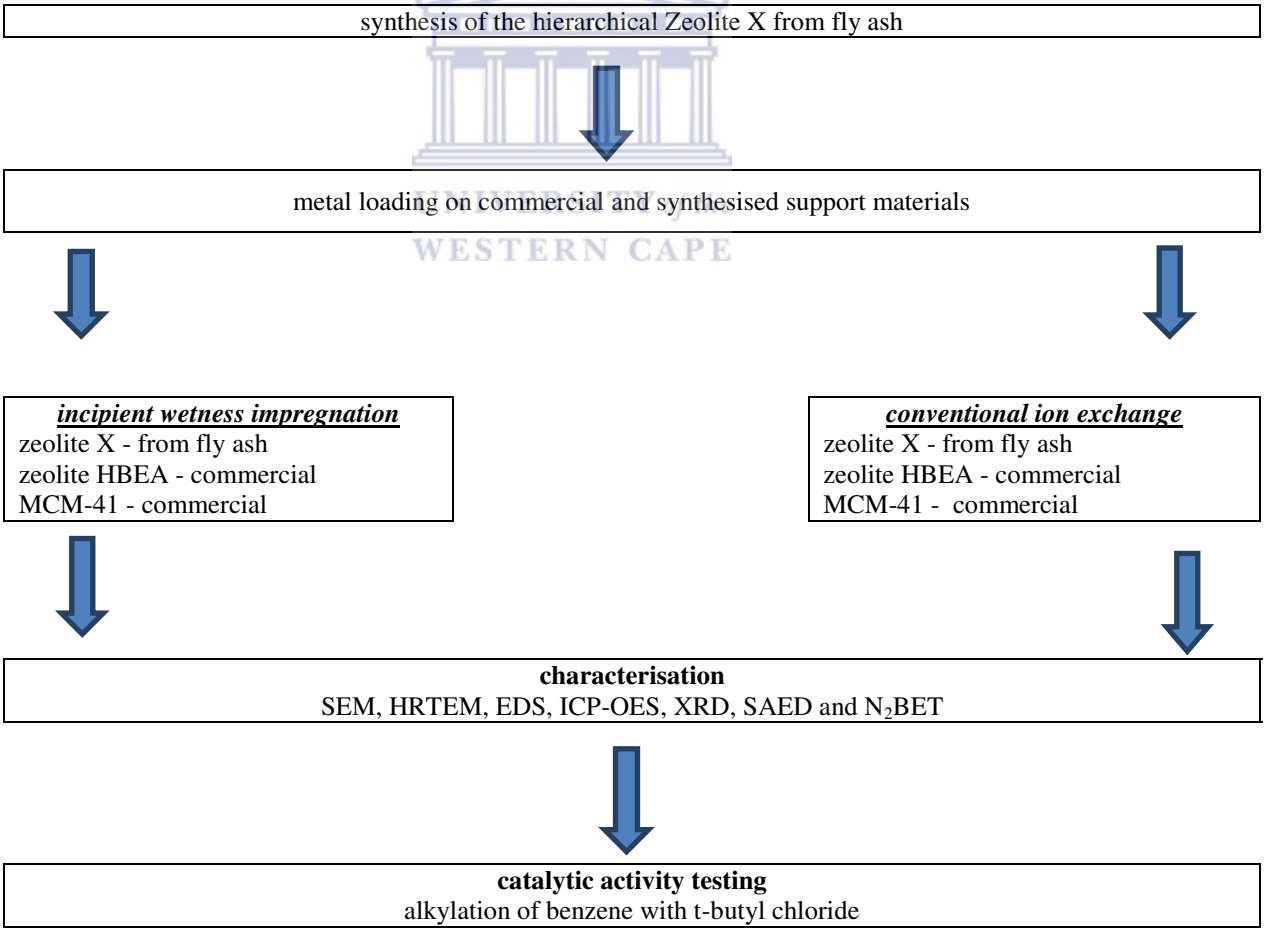

Figure 3.1: Schematic flow of experimental activities

3.1 Synthesis of the hierarchical Zeolites X from coal fly ash

The hierarchical Zeolite X was synthesised using fly ash obtained from Hendrina power station (South Africa). The set of equipment and reagents used for the synthesis of the zeolite, catalyst preparation and Friedel-Crafts alkylation of benzene with *t*-butylchloride are presented in Sections 3.1.1 and 3.1.2 respectively. The synthesis procedure of the zeolite is outlined in section 3.1.3.

3.1.1 Equipment used in the synthesis of Zeolite X

- Ball mill
- Muffle furnace (Gallenkamp)
- Polypropylene beakers
- Mortar and pestle
- Overhead stirrer
- Centrifuge
- Magnetic stirrer plate and magnetic bar
- Teflon bottles
- Oven (Scientific, Series 2000)
- Erlenmeyer flask and Buchner funnel
- Porcelain dishes
- pH meter
- Water de-ioniser (Purelab UHQ de-ionizer: ELGA)

3.1.2 Reagents

- Sodium hydroxide pellets (Kimix, SA, 99.9 %)
- Ammonium nitrate (Kimix, SA, 99.9 %)
- Iron (III) nitrate (Sigma Aldrich, SA. 99 %)
- Manganese (II) acetate (Sigma Aldrich, S.A, 98 %)
- Benzene (Sigma Aldrich, SA, 99 %)
- t-butylchloride (Sigma Aldrich, SA,)
- t-butylbenzene (Sigma Aldrich, SA,99 %)
- 1,2-di-t-butylbenzene (Sigma Aldrich, SA, 98 %)
- 1,3-di-t-butylbenzene (Sigma Aldrich, SA, 97 %)
- 1,4-di-t-butylbenzene (Sigma Aldrich, SA, 98 %)
- HBEA-25 (Sudie Chemie, SA)
- MCM-41 Mesoporous silica (Sigma Aldrich, SA)

3.1.3 Synthesis of the hierarchical Zeolite X

Sodium hydroxide pellets were ground to a fine powder using a ball mill. A ratio of 1:1.2 of coal fly ash (as obtained from Hendrina power station) and the powdered NaOH was fused in a muffle furnace for 1.5 h at a temperature of 550 ^{0}C. A 20 g sample of the fused fly ash was mixed with 50 mL of ultra-pure water. The mixture was stirred in a polypropylene beaker using an overhead stirrer for 2 h. The resultant slurry was then filtered and ~800 mL of the clear solution was subjected to hydrothermal treatment and crystallised for 9 h at a temperature of 94 ^{0}C. The product was filtered and washed until the filtrate pH was between 9 and 10. The crystallised zeolite product was dried at 100 ^{0}C for a period of 12 h (Musyoka et al, 2011).

3.2 Zeolite conversion to protonic form

The hierarchical Zeolite X synthesised from fly ash was obtained in the Na-Zeolite form and was converted to the H-Zeolite form via ion exchange using a 2.0 M NH_4NO_3 solution with a solid to solution ratio 100:1 (100 mL of solution per 1 g of zeolite sample). The solution was stirred under reflux at a temperature of 80 ^{o}C for 2 h. The mixture was then filtered and washed with deionised water until the suspension's pH was in the range of 4.5 – 5. The solid product was then dried at 100 ^{o}C for a period of 10 h followed by calcination in a muffle furnace at a temperature of 550 ^{o}C, for 4 h in air. The resultant H-Zeolite was then loaded with Fe/Mn via ion exchange and incipient wetness impregnation as described in the following sections.

3.3 Metal loading on zeolitic support materials

In this particular research two conventional metal loading approaches were applied with the intent of establishing which one of the methods gives better metal loading and catalytic activity. The loading was performed via incipient wetness impregnation or ion exchange. For comparison purposes, two established commercial support materials i.e. zeolite HBEA and MCM-41 were metal loaded alongside the fly ash generated Zeolites X. Using the two loading methods a total of 15 catalysts were prepared, both monometallic and bimetallic (Fe/Mn). The following sections present a detailed account of the experimental details with regard to the manner in which the metal was introduced onto the respective support materials.

3.3.1 Incipient wetness impregnation

Metal precursor salts ($Fe(NO_3)_3.4H_2O$ and $CH_3COO)_2.Mn.4H_2O$) of appropriate amounts were dissolved in appropriate volume (empirical support pore volume, refer to Section 3.3.1.2), to achieve 5 and 10 % metal weight loading. The metal precursor solution of appropriate volume was added to 2.5 g of the zeolite sample and thoroughly mixed to form a paste using a spatula. The mixture was left standing for a period of 1 h to allow the solution to penetrate the pore system of the zeolite support. The resultant solid material was dried for 10 h in an oven at 100 ^{0}C, and then calcined at 550 ^{0}C at a heating rate of 10 ^{0}C/min for a period of 4 h, after which the catalyst was ground into a fine powder using a mortar and pestle and finally labelled and sealed in a sample bottle ready for characterisation and application.

3.3.1.1 Empirical Pore Volume Determination

Each of the respective support material has a different pore volume and this was empirically determined, to obtain the appropriate amount of solution to be used for the required metal loading. To 2.5 g of the zeolite support, ultra-pure water was added from a burette drop-wise followed by mixing using a spatula. The addition of water was done until the support was just wet and the volume recorded. To the obtained volume 0.1 mL was subtracted and the new value was taken to be the empirical pore volume of the support. Appropriate metal precursor amounts were then calculated and dissolved in the ultra-pure water of corresponding pore volume for each of the 3 support materials. The following tables present the respective catalyst coding and the amount of metal salt used to achieve the corresponding metal loadings. The empirical pore volumes of the support materials were 2.8, 1.2 and 0.8 mL per g of support for MCM-41, HBEA and Zeolite X respectively.

3.3.1.2 Catalyst coding and amount of metal salt used

The following set of tables present the catalyst coding used in this study. The coding is based on the theoretical metal loading for instance 10%FeH refers to a catalyst supported on HBEA and loaded with a calculated amount of 10 % Fe weight. A typical calculation applied in determining the amount of metal salt to be used is presented in the Appendix Section A1.

Table 3.1: HBEA supported catalysts prepared via Incipient Wetness Impregnation

Sample code	Theoretical Fe wt/ %	Theoretical Mn wt /%	Calculated Fe salt wt/g zeolite	Calculated Mn salt wt/g zeolite
5%FeH	5	-	0.3885	-
10%FeH	10	-	0.8204	-
10%MnH	-	10	0.5008	-
10%Fe/MnH	5	5	0.4101	0.2504

Table 3.2: MCM41 supported catalysts prepared via Incipient Wetness Impregnation

Sample code	Theoretical Fe wt/ %	Theoretical Mn wt /%	Calculated Fe salt wt/g zeolite	Calculated Mn salt wt/g zeolite
5%FeM	5	-	0.3885	-
10%FeM	10	-	0.8204	-
10%MnM	-	10	0.5008	-
10%Fe/MnM	5	5	0.4101	0.2504

Table 3.3: H-form Zeolite X supported catalysts prepared via Incipient Wetness Impregnation

Sample code	Theoretical Fe wt/ %	Theoretical Mn wt /%	Calculated Fe salt wt/g zeolite	Calculated Mn salt wt/g zeolite
5%FeX	5	-	0.3885	-
10%FeX	10	-	0.8204	-
10%MnX	-	10	0.5008	-
10%FeMnX	5	5	0.4101	0.2504

3.3.2 Ion exchange

The metal precursor solution used for liquid phase ion exchange was 0.25 M $Fe(NO_3)_3$. The liquid to solid (support weight) used was 10:1 (25 mL of solution was used for 2.5 g of zeolite sample). The mixture was stirred under reflux overnight at a temperature of 80 ^{0}C over an oil bath. The metal loaded support material was washed with 500 mL cold deionised water followed by another 500 mL hot water. In each case the resultant suspension was centrifuged and then vaccum filtered over nylon membrane filter papers

(0.45 μm). The solid zeolite was dried overnight in an oven at 100 ^{0}C and calcined at 550 ^{0}C at a heating rate of 10 ^{0}C/min. for 4 h. Upon cooling down to ambient temperature the prepared metal loaded catalysts ware packed, labelled and sealed in a sample bottle. The catalyst coding for the different catalysts prepared via ion exchange are presented in Table 3.4

Table 3.4: Catalyst coding for ion exchange prepared catalysts

Sample code	Metal precursor	Support material
0.25FeH	0.25 M Fe	HBEA
0.25FeM	0.25 M Fe	MCM-41
0.25FeX	0.25 M Fe	Zeolite X

3.4 Catalyst Characterisation

This section presents the catalyst characterisation procedures undertaken with particular emphasis on the sample pre-treatment and instrumental set up conditions for each respective technique applied.

3.4.1 High resolution transmission electron microscopy

The crystallographic analysis of the catalyst samples studied was carried out by high resolution transmission electron spectroscopy (HRTEM), according to the following steps.

3.4.1.1 Sample pre-treatment

A small amount of each powdered catalyst sample was immersed in a 5 mL aliquot of methanol. The resultant suspension was vigorously shaken and placed in an ultrasonic vessel (Labcon Ultra-Sonic 5019U) for a period of 15 min. A fine drop of the mixture was then dropped on a copper grid and allowed to air dry at room temperature. The sample was finally placed in the HRTEM machine (Technai G2 F 20 X-Twin MAT) which was operated at the conditions presented in Table 3.9.

3.4.2.2 Instrument operation conditions

The instrumental set up conditions applied in the high resolution transmission electron microscopy analysis are presented in Table 3.5.

Table 3.5: Instrument set up conditions for transmission electron microscopy

Name of the instrument	Technai G^2 F 20 X-Twin MAT
Applied voltage	200 kV
Emission current	48 µA
Illumination angle	15 °
Magnification	Varied depending on sample
Resolution	0.24 nm
Exposure time	Varied depending on sample

3.4.2 Scanning electron microscopy and electron dispersive spectroscopy

The morphology of the synthesised catalysts was analysed using high resolution scanning electron microscopy (HRSEM) on a Nova NanoSEM 230 machine. The same instrument was used to determine the qualitative elemental composition of the catalysts by electron dispersive spectroscopy (EDS) and selected area electron diffraction (SAED) analysis.

3.4.2.1 Sample preparation

A carbon tape was placed on top of a specimen holder and a small representative amount of fine powder was dusted on the tape, and the specimen was introduced into the HRSEM instrument. The HRSEM was coupled with an EDS detector using GENESIS software for elemental analysis.

3.4.2.2 Set up conditions

The instrumental set-up conditions are detailed on the micrographs presented in section 4.1.

3.4.3 X-ray diffraction spectroscopy

The X-ray diffraction analyses were carried out on a Phillips PW 3830/40 Generator. Only the wide angle analysis was performed on the samples. The instrumental conditions are presented in Table 3.6.

3.4.3.1 Sample preparation

The samples were first ground into a fine powder using mortar and pestle. The powdered samples were placed onto a sample holder using a spatula. The samples were then introduced in the X-ray diffractometer.

3.4.3.2 Set up conditions

The instrument operating conditions for the X-ray diffractometer are presented in Table 3.6.

Table 3.6: X-ray diffractometer set up conditions for the wide angle analysis

Name of the instrument	Phillips PW 3830/40 Generator with PW 3710 mpd
X- ray detector	X pert data collector
Generator voltage	40 kV
Generator current	25 mA
Scanning range (2θ)	2.01 ° to 45.99 °
Scan type	Continuous
Scan speed per step	0.50 seconds
Scan time	40 minutes
Step size	0.02 °
Synchronous rotation	No

3.4.4 Inductively coupled plasma-optical emission spectrometry

The amount of metal on the catalysts was determined by inductively coupled plasma-optical emission spectrometry (ICP-OES) on a Varian 710-ES series spectrometer equipped with a CCD detector, axially-viewed plasma, a cooled cone interface, and ICP Expert II software.

3.4.4.1 Sample Digestion

The sample digestion was achieved by adding a volume of 5 mL of aqua regia and 2 mL of HF to 0.1 g of sample in a Teflon beaker. The mixture was sealed and then heated in an oven for 2 h, at a temperature of 100 ^{o}C. The mixture was then taken out and cooled to room temperature after which 1 g of boric acid was added followed by filtering over a nylon membrane filter paper (0.45 μm). The resultant solution was further heated for

another 15 min again at a temperature of 100 ^{o}C. The solution was cooled to room temperature and diluted to a volume of 50 mL with deionised water.

3.5.5 Nitrogen adsorption

The N_2-adsorption analysis was performed on a TriStar machine (3000 Analyser, 060), to determine the surface area and porosity of the solid powdered samples. A 0.36 g of the solid sample was weighed and degassed in flowing He at a temperature of 90 ^{o}C for a period of 1 h. The sample was then held at 350 ^{o}C for a period of 16 h to desorb the water from the surface as well as the pores of the sample. The sample was then weighed and cooled and the N_2-adsorption was performed based on a 39 point analysis. The summary of the instrumental set up conditions applied are presented in Table 3.7.

3.5.6.1 Instrumental set up conditions

The instrumental set up conditions for the N_2-adsorption analysis are presented in Table 3.7.

Table 3.7: Instrumental set up condition for the N_2-adsorption analysis

Instrument model	Micrometrics Tri Star 3000 Analyser
Gas	N_2
Pressure table	39 points (20 adsorption and 20 desorption)
Pressure range	0 to 999 mmHg

3.5 Benzene alkylation with t-butyl chloride

The synthesised catalysts were tested for their activity in benzene alkylation reaction with t-butyl chloride. Benzene was used as a solvent in the reactions studied according to the outline presented in the following section.

3.5.1 Catalyst Pre-treatment

Using an analytical balance a quantity of 250 mg of the catalyst was weighed and transferred to a round bottom flask. The catalyst was activated by heating in a muffle furnace at a temperature of 250 ^{o}C for a period of 2 h. The catalyst was then cooled to room temperature before the reactants were added according to the following procedure.

3.5.2 Alkylation procedure and testing

A volume of 10 mL of benzene was mixed with a volume of 1 mL of the alkyl halide and transferred to a round bottomed flask containing the activated catalyst. The mixture was stirred using a magnetic bar with reflux apparatus and the reaction temperature was maintained at 45 ^{0}C over an oil bath. Samples were taken at 30 min, 1, 2, 3, 4 and 5 h. Sample aliquots taken at the aforementioned intervals were diluted with acetone and analysed using a GC equipped with FID and HP-5 (phenylmethylsilicon) capillary column, (Agilent technologies). Product identification was achieved by injecting pure standards of both reactants and anticipated products.

3.5.3 Activity testing

The data generated from the catalyst testing was treated and calculations for conversion, selectivity and yield were performed according to the following equations.

$$conversion = \frac{[\%\ t{-}BB] + [\%\ int.A] + [\%\ int.B] + [\%\ 1,4{-}di{-}t{-}BB]}{[\%\ t{-}BC] + [\%\ t{-}BB] + [\%\ 1,4{-}di{-}t{-}BB] + [\%\ int.A] + [\%\ int.B]}\ x\ 100\% \quad \text{(i)}$$

$$selectivity = \frac{[\%\ t{-}BB]}{[\%\ t{-}BB] + [\%\ 1,4{-}di{-}t{-}BB] + [\%\ int.A] + [\%\ int.B]}\ x\ 100\% \quad \text{(ii)}$$

$$yield = conversion\ (\%)\ x\ selectivity\ (\%)/100 \quad \text{(iii)}$$

**{t-butyl benzene (t-BB); 1,4-di-t-butyl benzene (1,4-di-t-BB); intermediate A (int. A); intermediate B (int. B); t-butyl chloride (t-BC)}*

The intermediates A and B could not be identified since appropriate standards were not available. They however are thought to be transient carbonium intermediates. Further discussion on the nature of the intermediates is presented in Section 5.2.3.

CHAPTER 4

The chapter presents a detailed account of the catalyst characterisation undertaken in this research and the chapter will also present a discussion on the outcomes. An outline of the characterisation and metal loading achieved for each of the supported catalysts are laid out.

4.0 Characterisation of metal supported catalysts

In order to create a comparison basis, catalysts were prepared from both commercial porous support materials and fly ash based hierarchical Zeolites X. The commercial supports used herein were HBEA and MCM-41 while Zeolite X support was synthesised from fly ash. The introduction of the metals to the support were done via two conventional approaches namely, ion exchange and incipient wetness impregnation. Using the latter approach both monometallic and bimetallic catalysts were prepared with manganese acetate and iron nitrate as the metal precursors. Only monometallic Fe catalysts were prepared via ion exchange using iron nitrate as metal precursor. The procedure used in the preparation of catalysts via incipient wetness impregnation and the catalysts coding used are presented in Sections 3.3.1 and 3.3.2 respectively. The sample preparation and coding for the catalysts prepared via ion exchange are presented in Section 3.3.3. Physicochemical properties of HBEA, MCM-41 and Zeolite X supported metal catalysts were characterised using a range of techniques namely SEM, EDS, HRTEM, XRD, ICP-OES, SAED and N_2 adsorption.

4.1 Morphological studies of metal loaded commercial HBEA

The morphology of HBEA supported metal catalysts was examined with high resolution scanning electron microscope (HRSEM). The analysis was performed on Nova NanoSEM 230 machine. These catalysts were prepared via two approaches namely ion exchange (IE) and incipient wetness impregnation (IWI). The ion exchanged catalysts were prepared using commercial 0.25 M Fe salt ($Fe.(NO_3)_3.9H_2O$) as metal precursor. The catalysts prepared via incipient wetness impregnation were loaded using $Fe.(NO_3)_3.9H_2O$ and $(CH_3COO)_2.Mn.4H_2O$ as metal precursors.

4.1.1 Morphological studies of commercial HBEA catalysts prepared via ion exchange

The typical scanning electron microscopy (SEM) image obtained of the metal loaded HBEA supported (0.25FeH) catalysts prepared via ion exchange (IE) are presented in Figure 4.1.

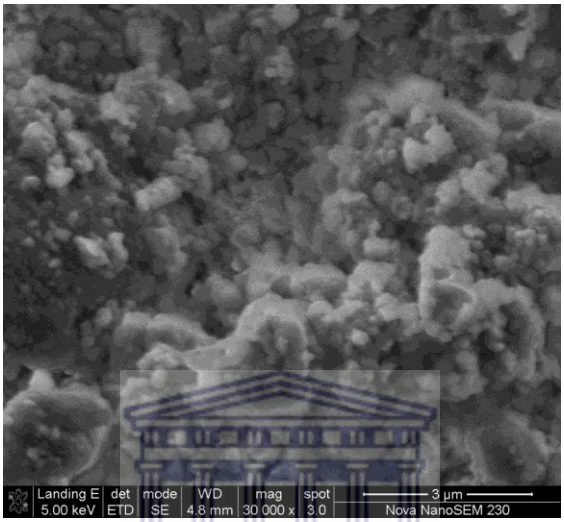

Figure 4.1: SEM image of 0.25FeH prepared via ion exchange

The observed agglomerated morphology for metal loaded HBEA was irregular in shape as can be seen on the SEM image in Figure 4.1. Akbar, (2010) mentioned that the morphology of HBEA does not exhibit any particular crystal habit. This is in agreement with the observed morphology obtained in this analysis. Previous experimental work on metal catalysts supported on HBEA prepared via liquid phase ion exchange, reported in literature obtained comparable results (Yang et al, 2010; Akbar, 2010).

4.1.2 Morphological studies of HBEA supported metal catalysts prepared via incipient wetness impregnation

The SEM micrographs of the commercial HBEA, supported metal catalysts (10%FeH and 10%FeMnH) prepared via incipient wetness impregnation (IWI) are presented in Figure 4.2. Using this loading approach both monometallic and bimetallic catalysts were synthesised. Only two micrographs are presented. The other micrographs were found to be similar to the ones shown.

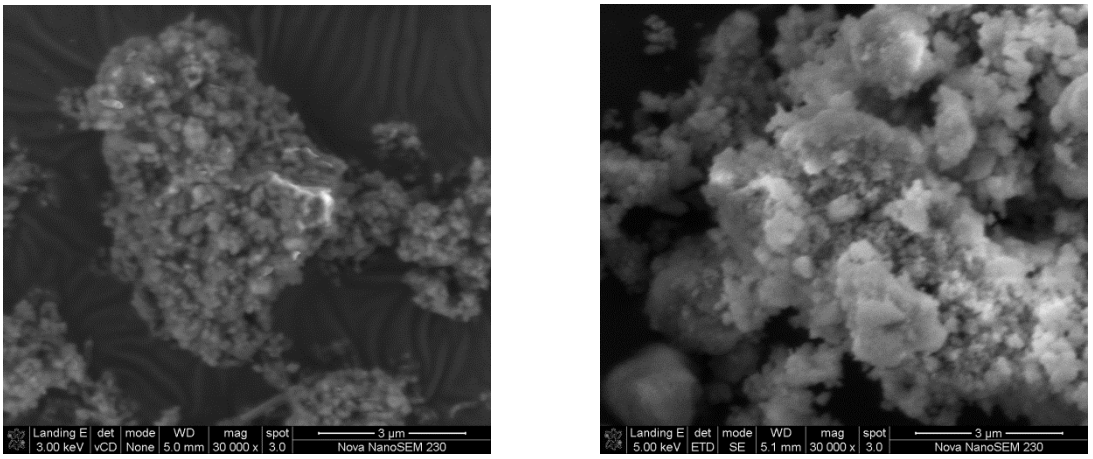

(a) (b)

Figure 4.2: SEM images of (a) 10%FeH and (b) 10%FeMnH; HBEA supported metal catalysts prepared via incipient wetness impregnation

Again the SEM micrographs obtained showed an agglomerated morphology with irregular shape. There was not much difference observed between the morphology of the catalysts prepared via liquid phase ion exchange or incipient wetness impregnation. The micrographs presented are comparable to those presented in previous related work in which HBEA was metal loaded via incipient wetness impregnation (Van Steen et al, 2005; Ausavasukhi et al, 2012).

4.1.3 Morphological studies of commercial MCM-41 catalysts prepared via ion exchange

The metal loaded MCM-41 catalysts (0.25FeM) prepared via liquid phase ion exchange (IE) were also examined with SEM. The loaded support (MCM-41) exhibited an agglomerated morphology as can be seen from the SEM image presented in Figure 4.3.

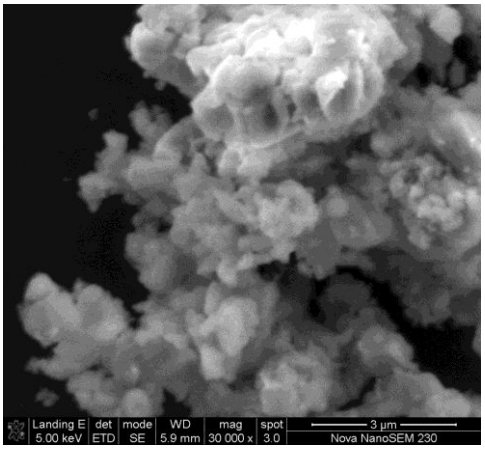

Figure 4.3: SEM image of 0.25FeM prepared via ion exchange.

The morphology of the metal loaded MCM-41 falls in line with similar results reported by Parvulescu et al, (2002). In their particular study transition metals were incorporated into the MCM-41 molecular sieve. The SEM images produced showed aggregates of small particles, similar to those generated in this research.

4.1.4 Morphological studies of MCM-41 supported metal catalysts prepared via incipient wetness impregnation

The SEM micrograms for the MCM-41 supported metal catalysts (10%FeM and 10%FeMnM) prepared via incipient wetness impregnation (IWI) are presented in Figure 4.4.

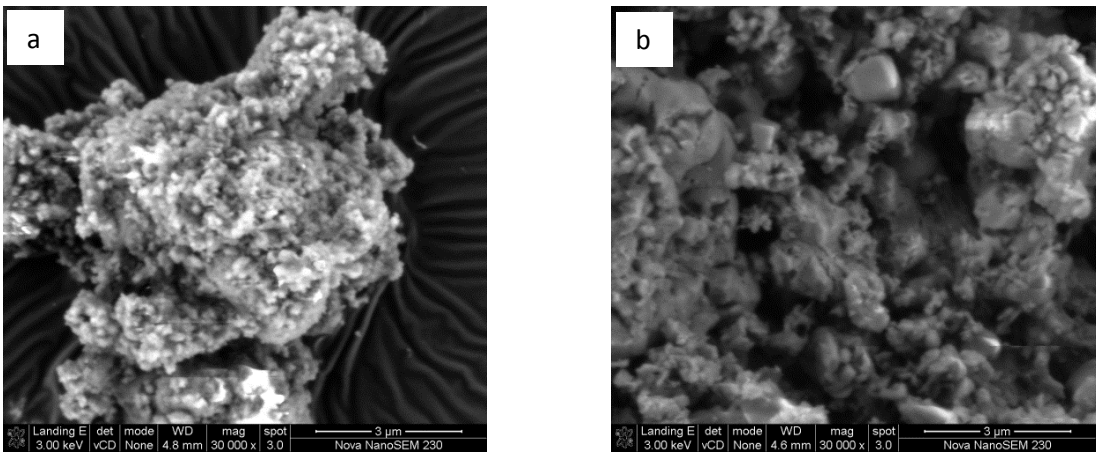

Figure 4.4: SEM images of (a) 10%FeM and (b) 10%FeMnM; MCM-41 supported metal catalysts prepared via incipient wetness impregnation

The images obtained also showed the agglomerated morphology. There were no significant differences in the morphology for the MCM-41 supported catalysts prepared using the liquid phase ion exchange and incipient wetness impregnation.

4.1.5 Morphological studies of metal loaded Zeolite X

Zeolite X was synthesised from coal fly ash collected from Hendrina power station in South Africa. The synthesis of Zeolite X was done in accordance with the procedure and conditions outlined in section 3.1.1. In this research the zeolite was synthesised according to conditions reported by Musyoka et al, (2012). Figure 4.5 shows the morphology of the synthesised zeolites at two different magnifications.

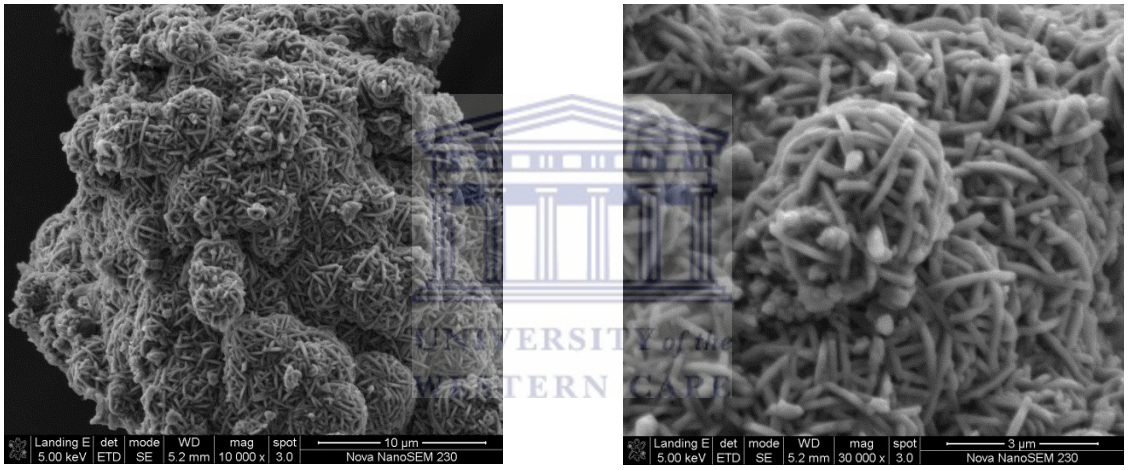

Figure 4.5: SEM images of the hierarchical Zeolite Na-X synthesised from fly ash at two magnifications

The SEM micrographs presented in Figure 4.5 show the morphology of the coal fly ash based Na-X zeolite support which was characterised by a hierarchical morphology and plate like interwoven crystals. The same morphology was obtained and reported by Babajide et al, (2012). Literature presents a vast amount of work with regard to the synthesis and characterisation of zeolite X, both from waste material and pure chemicals. A typical zeolite X synthesis from pure chemicals is presented by Htun et al., (2012). In the reported work pure chemicals were used in the synthesis of zeolite X and the resultant zeolite morphology was octahedral. In general that is the characteristic morphology for the zeolite. Several other attempts to synthesise the zeolite from waste materials such as coal fly ash are also reported in literature and a typical report is presented by Ojha et al, (2004). In their study Zeolite X was successfully synthesised

and it exhibited the same typical octahedral morphology, a comparison was also made with a commercial zeolite X. In a related report Franus, (2011) reported a needle like morphology of zeolite X synthesised from coal fly ash. This morphology can be said to lie between the characteristic octahedral morphology and the hierarchical morphology obtained in this particular research, which is a novel morphology.

4.1.6 Morphological studies of Zeolite X supported metal catalysts prepared via ion exchange

The synthesised hierarchical Na-X zeolite was firstly converted to the protonic form (H-X) in accordance to the procedure and experimental conditions outlined in section 3.2. The H-X zeolite was then loaded with Fe using a 0.25 M Fe solution as metal precursor according to experimental procedure presented in section 3.3.3. Conversion of the loaded metal to the oxide form was done by calcination in air at 550 ^{o}C. Figure 4.6 presents the micrographs on the ion exchanged metal loaded H-X zeolites (0.25FeX).

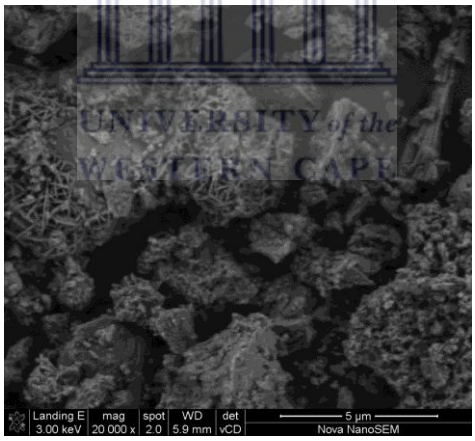

Figure 4.6: SEM micrograph of 0.25FeX prepared via ion exchange.

The micrograph presented in Figure 4.6 shows that there was a reduction in the network of the integrated hierarchical Zeolite X structure. The parent zeolite presented in Figure 4.5, shows a well integrated plate like structure. The XRD patterns obtained for the Zeolite X supported metal catalysts and presented in Section 4.3.3 attest to the fact that the porous structure of the zeolite remained intact. However there was a marked reduction in the peak intensities, which may be attributed to excessive metal loading.

4.1.7 Morphological studies of Zeolite X supported metal catalysts prepared via incipient wetness impregnation

The SEM images of the hierarchical Zeolite X supported metal catalysts prepared via incipient wetness impregnation are presented in Figure 4.7. The 10%FeX was loaded with Fe only whilst the 10%FeMnX was prepared by co-impregnation with Fe and Mn to create a bimetallic catalyst. The preparation procedure is presented in section 3.3.1. Conversion of the metal to the oxide form was achieved by calcination in air at 550 ^{o}C.

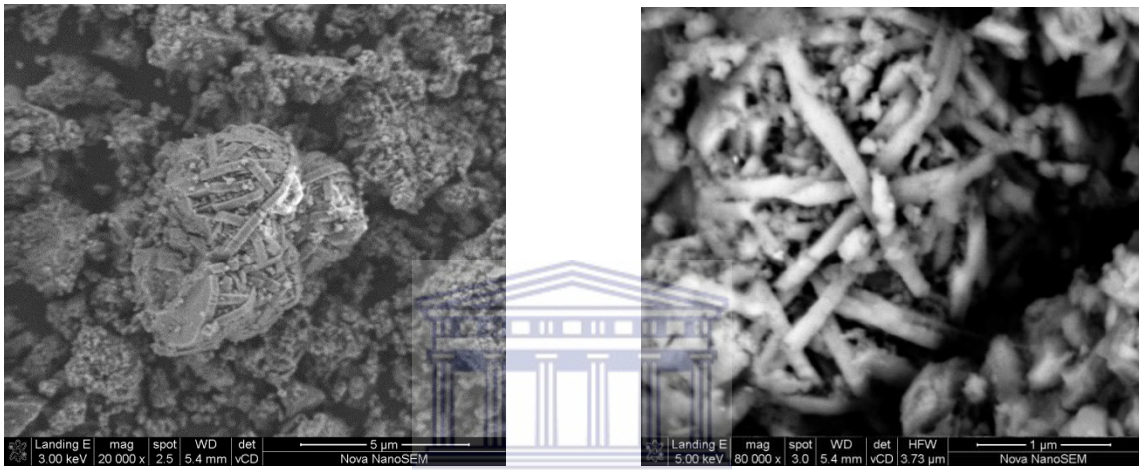

(a) (b)

Figure 4.7: SEM micrographs of (a) 10%FeX and (b) 10%FeMnX; Zeolite X supported metal catalysts prepared via incipient wetness impregnation

The micrographs presented in Figure 4.7 show that the small white specks of the metal oxide(s) on the external surface of the zeolite. The integrated morphology of the fly ash based hierarchical Zeolite X was reduced upon metal loading. This was further confirmed by the loss of external surface area of the loaded zeolite in comparison to that of the parent material (H-X). The surface area from N_2-adsorption studies are presented in Section 4.7.3. The images in Figure 4.7 (a) and (b) show some of the plate like structures of the hierarchical zeolite. The same observation was made with the catalysts prepared via liquid phase ion exchange.

4.2 Surface structure and topology studies

High resolution transmission electron microscopy (HRTEM), was used to determine the crystallographic structure of the loaded support materials in order to make an assessment of whether the crystallinity and micropore structure of the parent material was retained upon metal loading and determine the metal dispersion on the support. The analysis was performed according to the procedure outlined in chapter 3. The analysis was carried out on a Technai G2 F 20 X-Twin MAT.

4.2.1 Morphological analysis of HBEA supported catalyst prepared via ion exchange

The morphology and crystallinity of the BEA zeolite loaded (0.25FeH) prepared via ion exchange was done by HRTEM. The micrograph is presented in Fig. 4.8.

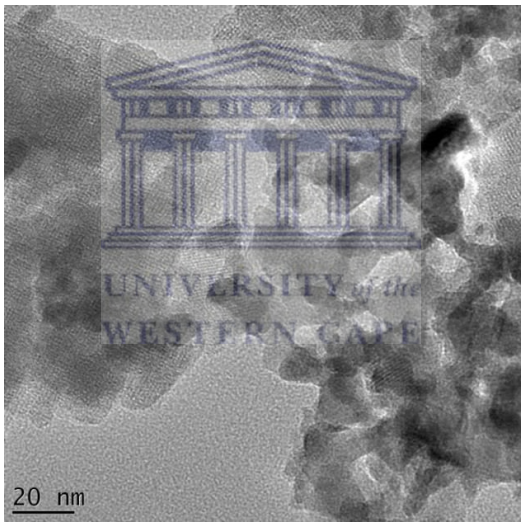

Figure 4.8: HRTEM images of 0.25FeH prepared via ion exchange.

The HRTEM micrograph presented in Figure 4.8 shows the microporosity and lattice of the parent HBEA material was retained upon metal loading. It however has to be noted that the metal deposited inside the zeolite pore channels could not be visualised, since this would require high energy electron beam, which consequently would destroy the zeolite (Balle et al, 2009). To further confirm the presence of the metal an electron dispersive spectroscopy (EDS) analysis was also performed on the sample using the same instrument. The outcomes are presented in section 4.3. Bisio et al, (2006) reported

and presented similar micrographs on Cs exchanged HBEA loaded via liquid phase ion exchange.

4.2.2 Morphological analysis of HBEA supported catalysts prepared via incipient wetness impregnation

The analysis of the morphology and crystallinity of the HBEA supported metal catalysts was also done by HRTEM on the 10%FeH and the 10%FeMnH prepared by incipient wetness impregnation. These two catalysts had the highest theoretical weight metal percentage of 10 %. It was then presumed that if the catalyst retained the crystallinity and morphology of the parent zeolite then the other catalysts of lower metal loading should retain the morphology and crystallinity of the parent support as well. Figure 4.9 presents the HRTEM micrographs of the two catalysts.

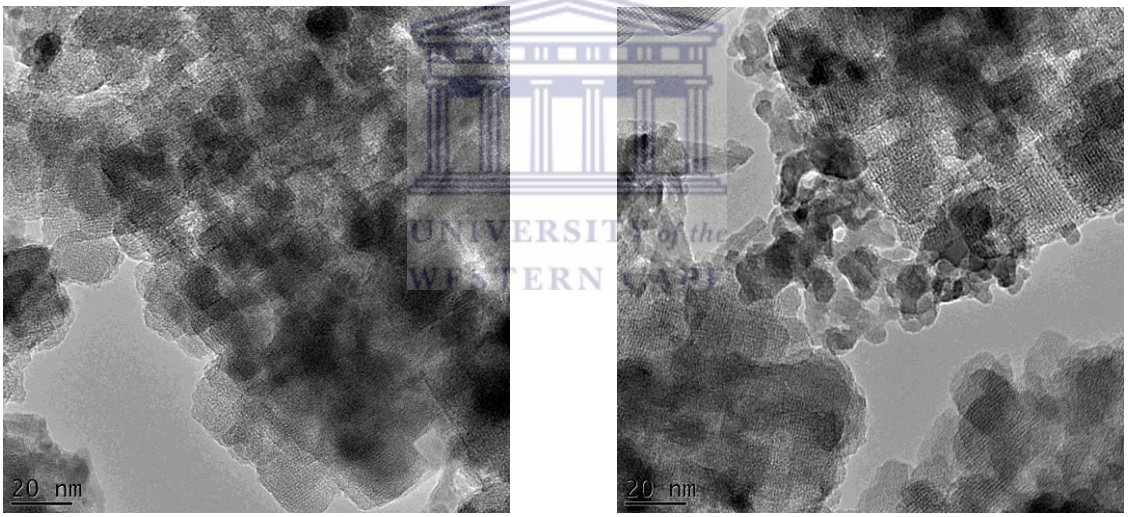

(a) (b)

Figure 4.9: (a) 10%FeH and (b) 10%FeMnH; HRTEM micrographs for HBEA supported metal catalysts prepared via incipient wetness impregnation.

The HRTEM micrographs in Figure 4.9 show that the crystal lattice and the microporous structure of the parent zeolite was retained upon metal loading. The same was observed with the catalysts prepared via liquid phase ion exchange. Both the bimetallic and monometallic catalysts showed some dark fringes due to the presence of the Fe/Mn metal oxide crystallites. Similar outcomes were reported and presented by Balle et al, (2009). In their study Fe was loaded on HBEA and the TEM micrographs

generated were similar to those obtained in this study. To further confirm that the integrity of the parent material was retained upon metal loading powder X-ray diffraction analysis was performed on the samples and the patterns are presented in Section 4.3.1.

4.2.3 Morphological analysis of MCM-41 supported catalyst prepared via ion exchange

HRTEM analysis for MCM-41 supported metal catalyst prepared via ion exchange. The obtained micrograph for the 0.25FeM catalyst is presented in Figure 4.10.

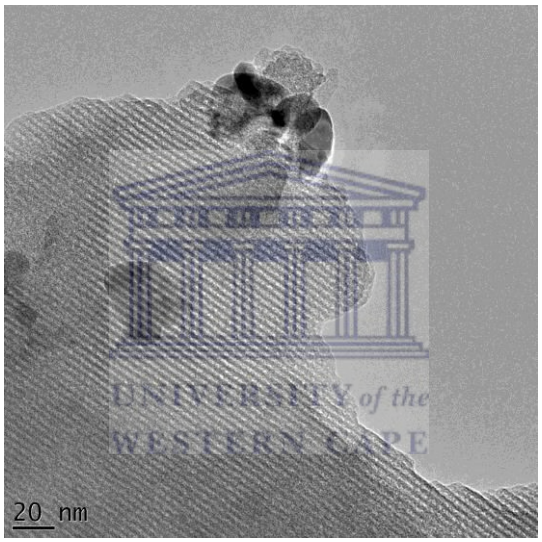

Figure 4.10: HRTEM micrograph of 0.25FeM prepared via ion exchange

It could be established from the generated HRTEM image for the MCM-41 supported metal catalyst that the porosity and crystallinity of the parent MCM-41 support was retained upon metal loading. The HRTEM micrograph clearly shows the characteristic honeycomb structure of the MCM-41, with pores in the nanometre range.

The micrograph also affirm that there was clustering of the excess metal as crystallites on the external surface of the support, this is evinced by the visibility of the dark fringes on the image. To further substantiate the presence of the metal on the support an EDS analysis was performed on the very sample and the spectrum generated confirmed the presence of the loaded metal. The EDS spectrum is presented in section 4.3.3. Related research activities also generated similar outcomes, for instance Mokhonoana et al,

(2009); Li et al, (2012), although different approaches were used to introduce the metal onto the MCM-41support. The X-ray diffraction patterns obtained on the samples also showed that the integrity of the parent material was retained upon metal loading.

4.2.4 Morphological analysis of HBEA supported catalysts prepared via incipient wetness impregnation

The MCM-41 supported metal catalysts prepared via incipient wetness impregnation were subjected to analysis by HRTEM. The analysis was done on the 10%FeM and the 10%FeMnM. These catalysts had the highest metal loading of all MCM-41 supported catalysts prepared using this approach. Figure 4.11 presents the HRTEM micrograms for the said catalysts.

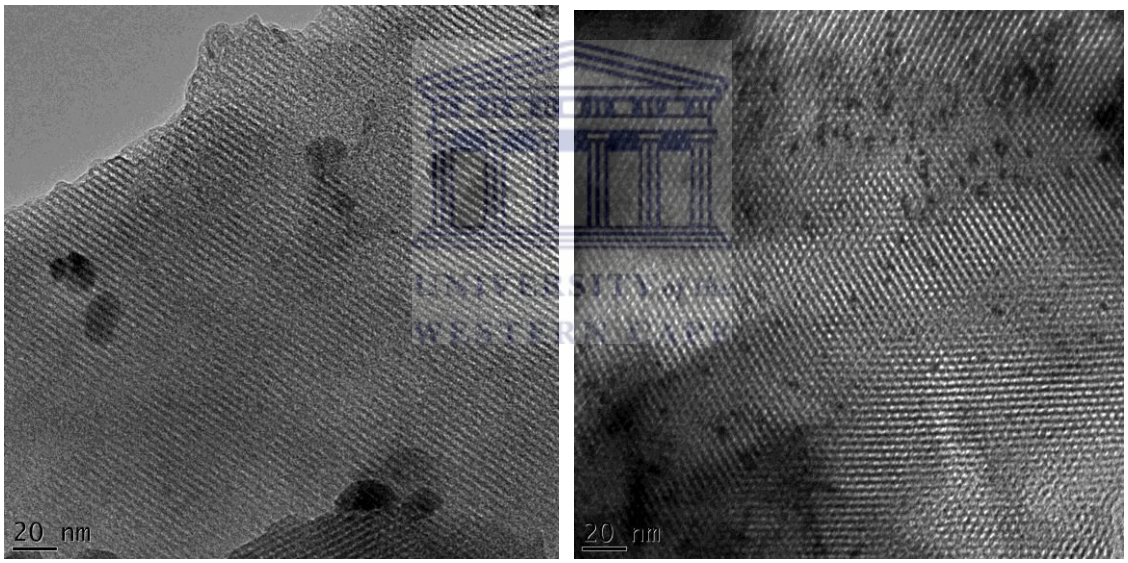

(a) (b)

Figure 4.11: HRTEM micrographs of (a) 10%FeM and (b) 10%FeMnM; MCM-41 supported metal catalysts prepared via incipient wetness impregnation.

The micrograms obtained for both catalysts showed that the nanoporous structure of the MCM-41 parent support remained intact upon metal loading. The same observation was made on the catalysts prepared via ion exchange. Again the metal oxide crystallites could be seen as dark fringes on the micrograms. An elementary qualitative analysis was also performed on the same samples by EDS. The analysis further established the presence of the metals on the support. The EDS analysis is presented in section 4.3.4.

Similar micrograms as the ones presented in Figure 4.11 were also presented and reported by Mokhonoana et al, (2009); Li et al, (2012).

4.2.5 Morphological analysis of Zeolite X supported catalyst prepared via ion exchange

Morphological and crystallographic analysis was performed using HRTEM on the fly ash based hierarchical Zeolite X supported catalyst prepared via ion exchange. The micrograph obtained for the 0.25FeX is presented in Figure 4.12.

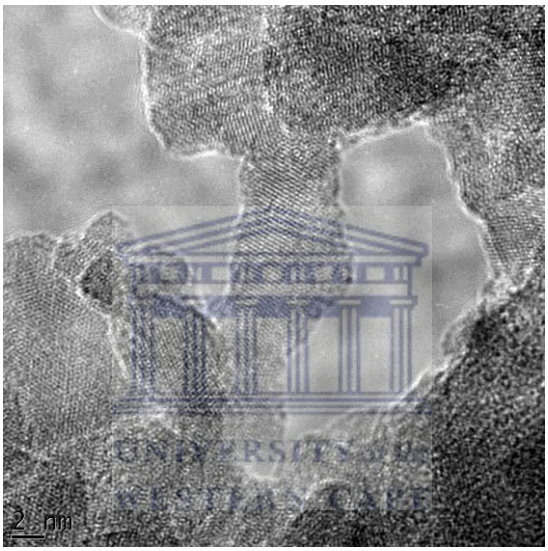

Figure 4.12: HRTEM micrograph of 0.25FeX; fly ash based Zeolite X supported metal catalyst prepared via ion exchange.

The HRTEM micrograph presented in Figure 4.12 attests to the fact that the crystallinity and microporous structure of the parent zeolite X support was retained upon metal loading. The dark fringes due to the iron oxide crystallites could be seen on the micrograph. Further confirmation of the presence of the metal on the zeolite was done qualitatively and quantitatively by EDS and ICP-OES. The compositional results obtained are presented in Sections 4.4.4 and 4.5.4 respectively. Similar micrographs were reported and presented by Hincapie et al, (2005). In their study Cu was loaded on faujasite (FAU) type zeolite.

4.2.6 Morphological analysis of Zeolite X supported catalysts prepared via incipient wetness impregnation

The fly ash based Zeolite X supported metal catalysts prepared via incipient wetness impregnation were also analysed for their crystallographic and morphological structure by HRTEM. The micrographs presented are for the 10%FeX and 10%FeMnX. These catalysts had the highest metal loading and it was presumed that the other catalysts of lower loading should have more or less the same crystallographic and morphological structure. The micrographs for the said catalysts are presented in Fig. 4.13.

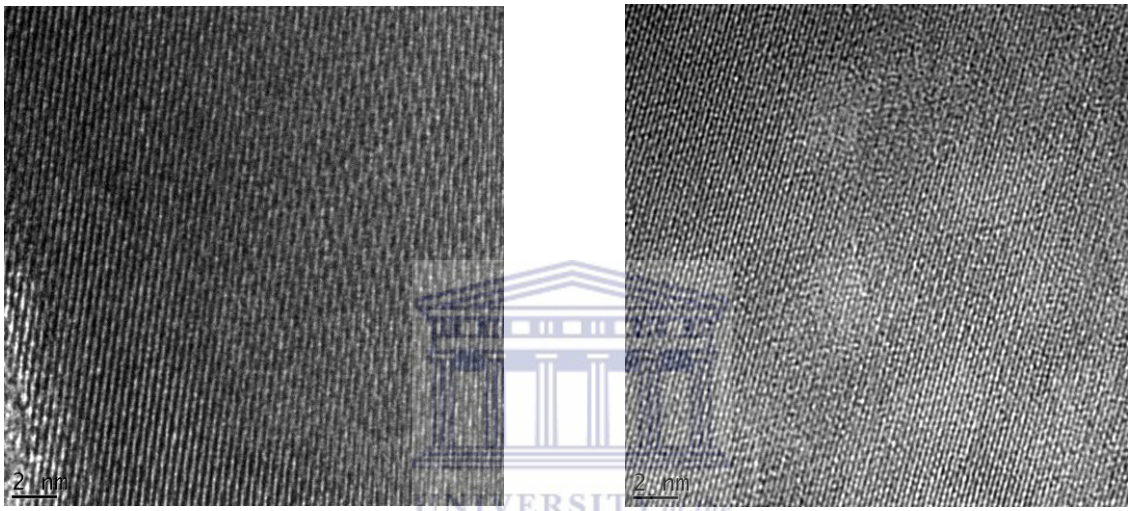

(a) (b)

Figure 4.13: HRTEM micrographs of (a) 10%FeX and (b) 10%FeMnX, fly ash based hierarchical Zeolite X supported metal catalysts prepared via incipient wetness impregnation.

The generated micrographs in Figure 4.13 attested to the fact that the crystallinity and microporous structure of the fly ash based hierarchical Zeolite X support material was retained upon metal loading. The hierarchical zeolite was composed of micropores seen in these micrograms. The micrographs obtained with the incipient wetness impregnation prepared catalysts are well defined implicating that the structure of the parent support is preserved. To further confirm the crystallinity of the supported metal catalysts X-ray diffraction analysis was performed and the diffractograms are presented and discussed in Section 4.3.3.

In comparison to the other supported metal catalysts, the hierarchical fly ash based Zeolite X supported catalysts did not show much metal clustering on the surface of the zeolite as could be deduced from the lack of prominent dark fringes on the HRTEM

images. This may be due to the fact that most of the metal was not on the surface but attached to the exchange sites within the zeolite pore system as expected and well dispersed at an atomic level. Some small metal crystallites may have formed within the zeolite channels but this could not be visualised from the generated micrographs, since an attempt to do such would require the use of a high energy electron beam, which consequently may disrupt the zeolite structure itself completely. Qualitative and quantitative elemental analysis was also carried out to confirm the presence of the metals on the zeolite by EDS and ICP-OES and the outcomes are presented in sections 4.4.4 and 4.5.2 respectively.

4.3 Crystallographic studies by X-ray diffraction spectroscopy

The sample analysis by XRD was performed according to the procedure outlined in Section 3.4.3. The intent was to determine the crystallinity of the parent support material as well as to confirm whether there was formation of metal crystallites upon metal loading. It was also intended to determine whether the loaded material still retains its crystallinity after being loaded with the metal. The wide angle XRD analysis was performed on a Phillips PW 3830/40 machine between 3 – 60° 2θ, for all the metal loaded supports as well as the parent materials. The analysis was done in accordance with the procedure set out in Section 3.4.3.2.

4.3.1 X-ray diffraction spectra for HBEA supported catalysts

The X-ray diffraction (XRD) profiles of the HBEA supported metal catalysts were carried out in accordance with the procedure outlined in Section 3.4.3.2. The objective of the analysis was to determine whether there was formation of new crystalline phases on the support. Comparison was made against the parent commercial support HBEA. The XRD profiles for the commercial HBEA supported catalysts together with the parent zeolite are depicted in Figure 4.14.

The X-ray diffraction profiles presented in Figure 4.14 show the characteristic peaks for HBEA and demonstrate that the HBEA crystalline phase was not changed over the series of HBEA supported metal catalysts studied. The XRD profiles for the 5%FeH and the 10%FeMnH prepared via incipient wetness impregnation show almost the same profile as the parent support HBEA. The absence of the Fe_2O_3 signals in the XRD

spectra of the said catalysts may be indicative of the fact that the metal was well dispersed on the support. However the same could not be said with the profile obtained with the 10%FeH since the α-Fe_2O_3 peaks were well pronounced on the profile giving rise to signals at, 33, 35, 40, 49 and 53 ^{o} 2θ values. The confirmation that these signals were indeed due to the Fe_2O_3 was done using PANalytical X'pert pro software. The α-Fe_2O_3 has hcp lattice structure, and from the SEM images presented in Section 4.1.2. Weak peaks of the Fe_2O_3 were also noted on the profile of the 0.25FeH at 33, 35 and 49 ^{o} 2θ values. The catalyst was prepared via ion exchange and had a Fe wt % loading of 7.2. As the metal loading increases the Fe_2O_3 crystallites become a major component of the catalysts. The XRD spectra of all the HBEA supported metal catalysts attested to the fact that both liquid phase ion exchange and incipient wetness impregnation may be used to introduce metals on the support and the pristine character and features of the parent material are retained.

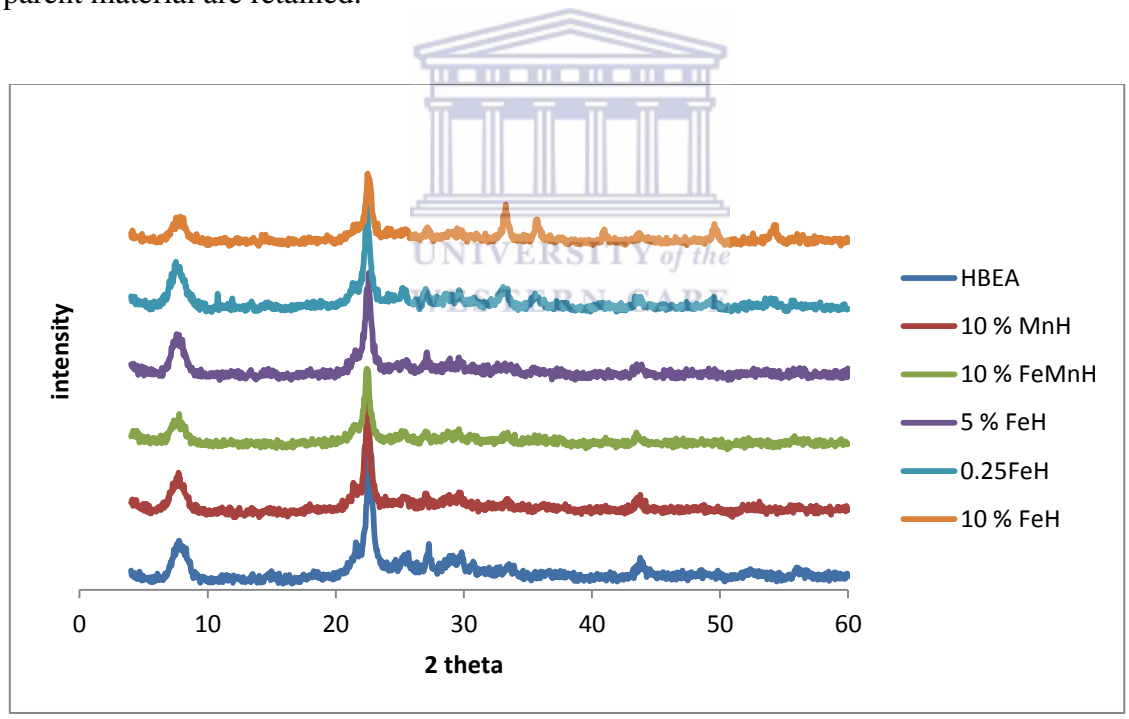

Figure 4.14: X-ray diffraction profiles for the HBEA supported metal catalysts

Ma et al, (2012) carried out a study in which low Fe metal loadings were obtained on HBEA via incipient wetness impregnation. The XRD profiles of the catalysts did not exhibit the Fe_2O_3 signals. In a different study carried out by Balle et al, (2009), different

Fe catalysts of various loadings were prepared via incipient wetness impregnation. The profiles of the catalysts with a Fe wt % loading of less than 10 did not exhibit the Fe_2O_3 signals whilst the signals due to the oxide were exhibited with the catalysts with more than Fe wt % of 10. In both research activities it was found that the crystalline phase of the HBEA support was retained upon metal loading and calcination. The outcomes in this research are similar to those found and reported in the previously cited research activities.

4.3.2 X-ray diffraction spectra for MCM-41 supported catalysts

The crystalline phase of the metal catalysts supported on the commercial mesoporous silica MCM-41, was also carried out via the procedure presented in section 3.4.3.2. The 0.25FeM was prepared via liquid phase ion exchange as described in section 3.4.2. The other catalysts were prepared via incipient wetness impregnation as presented in section 3.4.1. The XRD spectra for the MCM-41 supported metal catalyst are presented in Figure 4.15. The patterns are arranged with the catalyst with the highest metal loading at the top.

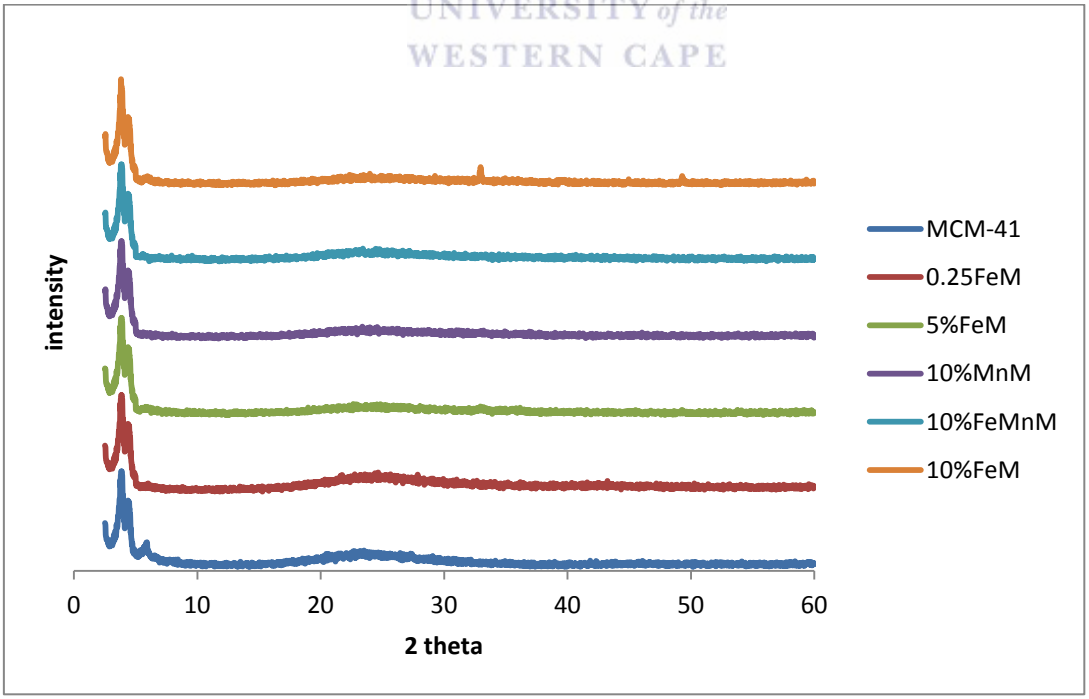

Figure 4.15: X-ray diffraction profiles for the MCM-41 supported metal catalysts

The X-ray diffraction (XRD) spectra of all the metal catalysts supported on MCM-41 in Figure 4.15 resembled the spectrum of the pristine MCM-41 support material except in the case of the 10%FeM. The characteristic peaks of the parent support MCM-41 were observed at 2.7 and 3.6 ^{o} 2θ values. The same spectra were obtained for all catalysts prepared via both liquid phase ion exchange and incipient wetness impregnation. This shows that both metal loading approaches did not cause structural collapse of the support. However the spectrum obtained with the 10%FeM exhibited signals of the Fe_2O_3 (at 32 and 49 ^{o} 2θ values) leading to the conclusion that at this particular loading there was agglomeration of the oxide species on the external surface as was visible in HRTEM images as well. Loadings of less than 10 wt % Fe did not have pronounced peaks of the metal oxide. This leads to the conclusion that there was no agglomeration of the metal oxides on the support in those cases to form metal crystallite oxides. The 10%FeMnM had a total metal weight percentage of 10 %, however the bimetallic oxide signals were not observed, as each metal loading was only ~ 5 %.

The spectra of the MCM-41 supported metal catalysts obtained were in agreement with those found by Mokhonoana, (2005). In their study Fe was loaded onto MCM-41 via incipient wetness impregnation and loadings of as high as 50 wt % Fe were characterised. Lower metal loadings of less than 5 % did not give out the oxide peaks. In another related research by Sirotin et al, (2011) in which MCM-41 was impregnated with wt % Fe of 6, 7 and 11 % were prepared, the XRD spectra for the 6 wt % Fe did not exhibit any peaks due to the metal oxide. The peaks for Fe were however observed with catalysts of Fe wt % above 7.

4.3.3 X-ray diffraction spectra for the hierarchical fly ash based Zeolite X supported metal catalysts

The crystalline phase of the fly ash based hierarchical Zeolite X supported metal catalysts was analysed by X-ray diffraction and the XRD profiles are presented in Figure 4.16.

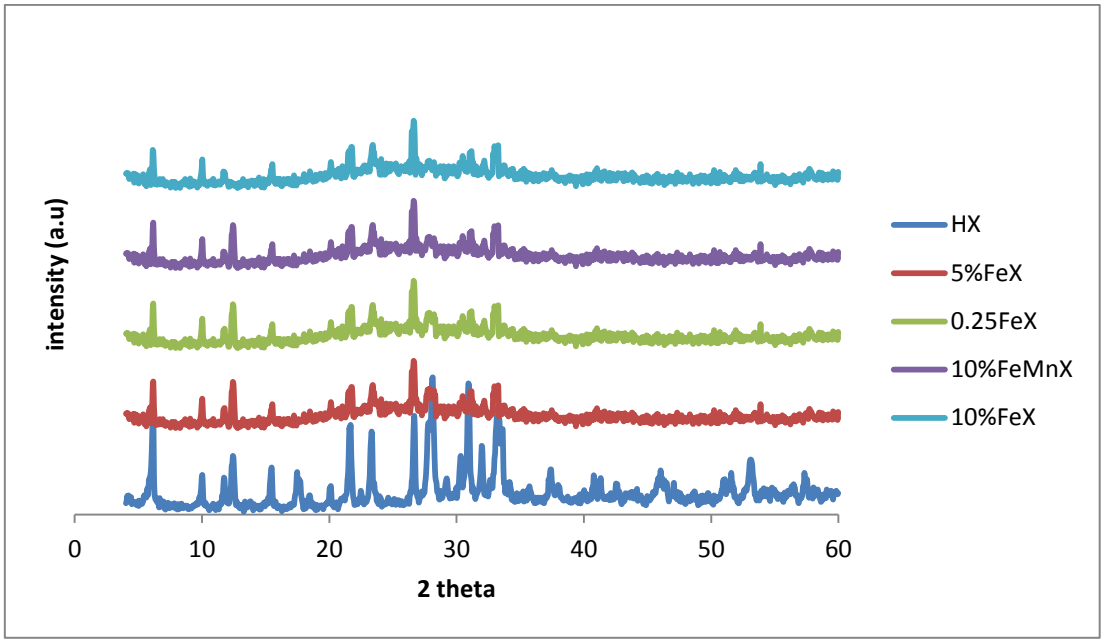

Figure 4.16: X-ray diffraction profiles for the fly ash based hierarchical Zeolite X supported metal catalysts

The X-ray diffraction profiles for the fly ash based hierarchical Zeolite X supported metal catalysts presented in Figure 4.16 show that there was a reduction in the peak intensities upon metal loading alongside disappearance of some peaks especially in the region of 37 – 60 ^{o} 2θ values. From the outcomes it could be seen that there was significant peak reduction in the intensity of the loaded support. The catalysts with a Fe wt % loading of 10 supported on HBEA and MCM-41 showed some signals due to the Fe_2O_3, at (33, 35, 40, 49 and 53 ^{o} 2θ values) and (32 and 49 ^{o} 2θ values) respectively. However the same cannot be said of the catalysts supported on the hierarchical Zeolite X. This may be an indication that part of the Fe_2O_3 was amorphous or the metal was highly distributed on the support. Pearce et al, (1981) loaded Fe on Zeolite Y which has the FAU structure; the same as Zeolite X and in their findings precipitation of amorphous iron oxides were indicated.

The XRD patterns testify to the fact that the microporous structure was maintained (from low angle peak below ± 8 ^{o} 2θ). Ronchetti et al, (2010) loaded Fe on zeolite X and they concluded that as the metal wt % loading increases there is a reduction in the peak intensities. High metal loading can cause structural damage to the zeolite structure. On the other hand the acidic nature of the hydrated Fe complex may cause zeolite

framework disruptions (Canfield, 2010) and to preserve the zeolite structure there may be a need to regulate the pH of the precursor solution.

4.4 Qualitative elemental composition

The supported catalysts were analysed for their elemental composition by electron dispersive spectroscopy (EDS). The analyses were performed alongside SEM and HRTEM analyses, and the objective of the exercise was simply to confirm the presence of the loaded metal on the support. Although the technique is a qualitative one it can however provide an insight of the qualitative elemental composition of the catalyst.

4.4.1 Qualitative elemental composition on HBEA supported metal catalysts

The qualitative elemental composition of the series of HBEA supported metal catalysts were analysed using Electron dispersive spectroscopy (EDS) on the same SEM instrument and on the same samples analysed for morphological and crystallographic structure. A 6 spot EDS analysis was done and Figure 4.17 presents the EDS results for the 10%FeMnH prepared incipient wetness impregnation. With the other samples only the mean values for the EDS qualitative elemental composition are presented in Table 4.2. The reason why the catalyst was chosen for discussion is that the HBEA support was loaded with both Fe and Mn.

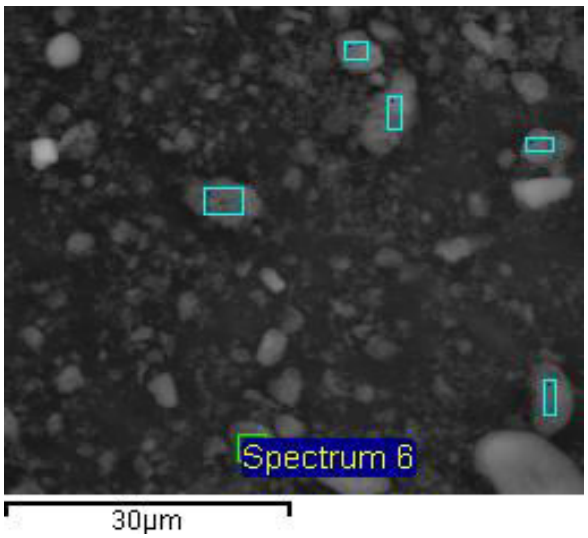

Figure 4.17: The 6 spot EDS analysis of the 10%FeMnH prepared via incipient wetness impregnation.

The objective of the EDS analysis was simply to confirm the presence of the metals on the support material. The catalyst was loaded with Fe and Mn and these were the only expected elements apart from Al and Si, which constitute part of the zeolite framework. The elemental composition of the catalyst is presented in Table 4.1.

*Table 4.1: Elemental composition of the 10%FeMnH prepared via incipient wetness impregnation. (*All results in weight % and n = 6)*

Spectrum	In stats.	O	Al	Si	Mn	Fe	Total
Spectrum 1	Yes	50.28	3.27	37.23	4.98	4.24	100
Spectrum 2	Yes	49.35	3.04	40.13	3.44	4.04	100
Spectrum 3	Yes	51.46	2.78	37.13	4.64	3.99	100
Spectrum 4	Yes	45.31	3.28	42.35	4.05	5.01	100
Spectrum 5	Yes	57.01	1.73	33.08	4.25	3.93	100
Spectrum 6	Yes	52.59	2.37	37.98	3.87	3.19	100
Mean		51	2.75	37.98	4.21	4.07	100

**(Si/Al = 13.81)*

From the data presented in Table 4.1 it could be seen that each spot analysed gave a different elemental composition in terms of weight percentages of the respective elements. From the mean values obtained the Si/Al ratio of the HBEA support was found to be 13.8. It could be established that the Fe and Mn were indeed present on the zeolite from the EDS analysis carried out. On a qualitative basis the technique confirmed the expected outcomes. The presence of the metals was further substantiated by a quantitative elemental analysis carried out by ICP-OES and the outcomes are presented in Section 4.4.2. Table 4.2 presents the mean values obtained from the 6 spot EDS analysis for the other HBEA supported metal catalysts. The details of the sample coding used in the table are presented in Sections 3.3.2 and 3.3.3.

The results presented in Table 4.2, attest to the fact that the intended metals were indeed introduced onto the support material. The 0.25FeH was prepared via liquid phase ion exchange while the other catalysts were prepared via incipient wetness impregnation. The outcomes also lead to the conclusion that both loading approaches can effectively introduce the metals onto the support. In general the EDS underestimated the metal wt % loading in comparison to the outcomes obtained from ICP-OES analysis, except in

the case of the 10%MnH which had a higher value from EDS relative to the value obtained from ICP-OES analysis. Quantitative elemental measurements were done by ICP-OES and are presented in Section 4.5.2.

*Table 4.2: Elemental composition of the HBEA supported metal catalysts (*All results in weight % and n = 6)*

Sample	O	Al	Si	Mn	Fe	Total
0.25FeH	53	1.12	39.56	0	6.32	100
5%FeH	57.07	2.77	36.5	0	3.66	100
10%FeH	51.24	2.89	37.45	0	8.42	100
10%MnH	42.33	2.79	39.22	15.67	0	100
10%FeMnH	51	2.75	37.98	4.21	4.07	100

4.4.2 Qualitative elemental composition on MCM-41 supported metal catalysts

Qualitative elementary analysis of the series of MCM-41 supported catalysts was also undertaken by EDS on the same samples prepared and analysed for SEM. Details of the 10%FeMnM, the bimetallic catalyst prepared via incipient wetness impregnation are presented. Only the mean values for the other catalysts are presented, for the same reasons cited for the HBEA supported catalysts in the previous section. Figure 4.18 presents the 6 spot EDS analysis of the 10%FeMnM.

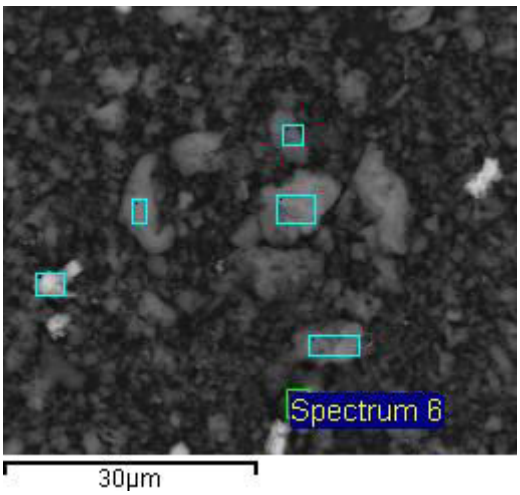

Figure 4.18: The 6 spot EDS analysis of the 10%FeMnM prepared via incipient wetness impregnation

The data generated from the elementary composition of the marked spots in Figure 4.18 are tabulated in Table 4.3.

*Table 4.3: Elemental composition of the 10%FeMnM prepared via incipient wetness impregnation. (*All results in weight % and n = 6)*

Spectrum	In stats.	O	Al	Si	Mn	Fe	Total
Spectrum 1	Yes	45.35	0.57	44.56	5.13	4.39	100
Spectrum 2	Yes	50.04	0	40.06	4.21	5.69	100
Spectrum 3	Yes	59.46	0.14	32.33	4.36	3.71	100
Spectrum 4	Yes	47.78	0.22	43.4	1.85	6.75	100
Spectrum 5	Yes	57.63	0	38.08	3.54	0.75	100
Spectrum 6	Yes	58.32	0.78	31.54	4.67	4.69	100
Mean		53.10	0.29	38.33	3.96	4.33	100

The data presented in Table 4.3 attest to the fact that the metals Fe and Mn were indeed present on the support material. Although MCM-41 does not contain Al, traces of the metal were detected and this could be from the stub used to mount the sample. The lack of Al would lead to no exchange sites, and hence a catalyst prepared via ion exchange with MCM-41 as the support is likely to have a much lower metal loading than could be achieved using IWI. The introduction of the metal on the MCM-41 is via grafting rather than ion exchange. The ICP-OES results obtained on the ion exchanged MCM-41 catalyst indeed showed low metal loading. The results are presented in section 4.5.1.

The mean elemental composition obtained with the 6 spot EDS analysis for the other MCM-41 supported metal catalyst are presented in Table 4.4.

Table 4.4: Elemental composition of the MCM-41 supported metal catalysts (All results in weight % and n = 6)

Sample	O	Al	Si	Mn	Fe	Total
0.25FeM	58.01	0.89	40.44	0	0.66	100
5%FeM	50.36	1.13	41.41	0	7.1	100
10%FeM	51.47	0.93	39.25	0	8.35	100
10%MnM	42.33	2.79	39.21	15.67	0	100
10%FeMnM	53.1	0.29	38.33	3.96	4.33	100

The results presented in Table 4.4 confirmed the presence of the respective metals on the support material. However in certain instances the loadings were found to be higher than expected or lower than expected. The theoretical loading of the 10%MnM was 10% but the EDS data obtained gave a value of 15.67 %. Again the 10%FeMnM was expected to have a 5 % Fe and 5 % Mn. However the weight percentage loading of the respective metals obtained was approximately 4 % thus were lower than expected. Further quantitative analysis of the metal loading on MCM-41 was done by ICP-OES and the data is presented in Section 4.5.

4.4.3 Qualitative elemental composition on Zeolite X supported metal catalysts

A qualitative analysis of the elemental composition of the fly ash based hierarchical Zeolite X supported metal catalysts was also undertaken on the samples analysed for SEM. A 6 spot EDS analysis was performed on the catalysts and the results obtained with the 10%FeMnX are discussed in detail whilst the mean values obtained for the other catalysts are presented. Figure 4.19 presents the 6 spot EDS analysis of the 10%FeMnX, synthesised via incipient wetness impregnation, and loaded with both Fe and Mn.

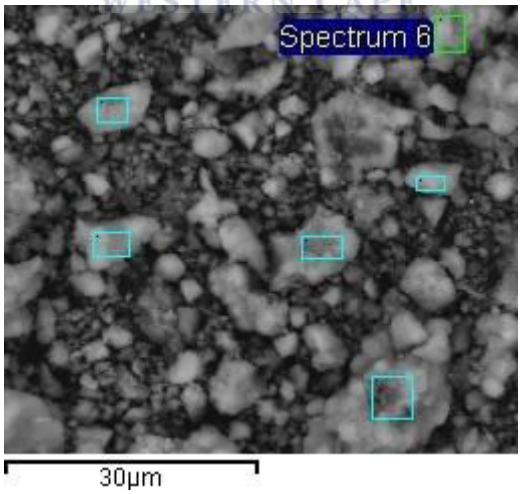

Figure 4.19: The 6 spot EDS analysis of the 10%FeMnX prepared via incipient wetness impregnation

The EDS data generated was based on the elemental composition of the highlighted spots on the image presented in Figure 4.19. The values for the respective spots are

presented in Table 4.5. It should be noted that the number of spots taken are too low to give a quantitative elemental composition of the catalyst. However the EDS analysis was used to give an insight of whether the loaded metals were indeed on the support. A 50 spot analysis would have given a more accurate composition of the catalysts, because EDS is not a bulk technique and it is to be expected that complete homogeneity would not be possible at the spot scale of 5 – 10 μm that was analysed.

Table 4.5: Elemental composition of the 10%FeMnX prepared via incipient wetness impregnation. (All results in weight % and n = 6)

Spectrum	In stats.	O	Al	Si	Mn	Fe	Total
Spectrum 1	Yes	52.87	13.47	21.48	7.11	5.07	100
Spectrum 2	Yes	53.54	14.38	23.77	4.89	3.42	100
Spectrum 3	Yes	54.74	14.8	21.71	3.97	4.78	100
Spectrum 4	Yes	54.08	13.56	22.61	4.15	5.6	100
Spectrum 5	Yes	55.8	12.07	19.06	6.67	6.4	100
Spectrum 6	Yes	53.63	13.02	21.08	4.31	7.96	100
Mean		54.11	13.55	21.62	5.18	5.54	100

**Si/Al ratio = 1.6*

The data presented in Table 4.5 indeed confirms the presence of the metals Fe and Mn on the 10%FeMnX coal fly ash based hierarchical Zeolite X support. The Si/Al ratio was 1.6, this value was lower than that of Zeolite HBEA of 13.8, which indicated that the zeolite has more exchange sites compared to that of Zeolite HBEA. The absence of Na from the elemental composition of the Zeolite X supported metal catalyst proved that the conversion of the synthesised Zeolite Na-X to the H-Form using NH_4OH according to experimental procedure presented in section 3.2 was effective. If the conversion to the H-form was not complete then some residual Na would have been detected on the EDS analysis..

The calculated ratio of Fe to Mn in the catalyst was 1. However for each spot the ratio differed. This discrepancy may be ascribed to the sample inhomogeneity. It could be seen that the mean actual ratio of Fe : Mn attained was close to 1. From the data presented the ratio was 1.07 : 1 (5.54 : 5.18). However since the EDS analysis is qualitative, it could be said that the EDS technique was relatively effective in determining the elemental ratios of the catalyst, provided an average of 6 or more analyses were performed. Further analysis with ICP-OES was undertaken in order to

determine the exact quantitative elemental composition. The ICP-OES data and discussion are presented in section 4.3. The EDS data for the other Zeolite X supported metal catalysts is presented in Table 4.6 and only the mean values are tabulated.

The other metal catalysts supported on the coal fly ash hierarchical Zeolite X were also analysed for their respective elemental composition by EDS and the mean values obtained for a 6 spot analysis are presented in Table 4.6.

*Table 4.6: Mean values of the elemental composition of the Zeolite X supported metal catalysts. (*All results in weight % and n = 6)*

Sample	O	Al	Si	Mn	Fe	Total
0.25FeX	53.61	17.77	24.38	0	4.24	100
5%FeX	55.5	16.66	21.83	0	6.01	100
10%FeX	53.99	17.53	20.3	0	8.18	100
10%MnX	52.31	16.46	21.37	9.86	0	100
10%FeMnX	54.11	13.55	21.62	5.18	5.54	100

On all the catalysts tested the EDS data obtained confirmed the presence of the loaded metals on the Zeolite X support. The absence of the Na from the elemental composition of the catalyst gave an indication that the sodium was effectivelly exchanged during the conversion of the synthesised Na-X to the protonic form H-X. Since the technique is a qualitative one further quantitative elemental analysis was necessary. The technique could however provide an insight in the amount and ratio of metals on the support if many spots on the sample are analysed. To fully establish the exact quantitative elementary composition of the prepared catalyst analysis was done by induced coupled plasma – optical emission spectroscopy (ICP-OES) and the outcomes are presented in the next section.

4.5 Quantitative Elemental Composition

The quantitative elemental composition was determined by inductively coupled plasma spectroscopy (ICP-OES). The catalysts had been prepared via two methods namely liquid phase ion exchange and incipient wetness impregnation. The ICP-OES data obtained is presented in the following sections. The sample digestion and dilutions were performed in accordance with the procedure outlined in chapter 3.4.4.

4.5.1 Catalysts loaded via liquid phase ion exchange

The actual Fe loading on the supports were determined by ICP-OES and the results are presented in Table 4.7. The details of the catalyst coding used in the table are presented in Table 3.4.

Table 4.7: Actual Fe weight percentage on monometallic catalysts prepared via ion exchange (ICP-OES analysis)

	catalyst		
	0.25FeH	0.25FeM	0.25FeX
wt % Fe	7.2	2.2	11.4

Although the same solutions and conditions were used to ion exchange the respective support materials it could be established from the outcomes that the loading was not the same with each support material. The metal wt % loading followed the order Zeolite X > HBEA > MCM-41. Metal loading via liquid phase ion exchange is mainly influenced by the CEC of the zeolite which is dependent on the Si/Al ratio. As the Si/Al ratio increases the CEC reduces. The Si/Al ratios of the respective materials followed the order MCM-41 (+ ∞) > HBEA (13.8) > Zeolite X (1.6).

4.5.2 Catalysts loaded via incipient wetness impregnation

Table 4.8 presents the actual loading on HBEA supported metal catalysts as determined by ICP-OES.

Table 4.8: Actual Fe/Mn weight percentage loading on HBEA supported catalyst prepared via IWI.

	catalyst			
	5%FeH	10%FeH	10%MnH	10%FeMnH
wt % Fe	4.8	12.4	-	5.1
wt % Mn	-	-	12.5	5.8

The ICP-OES data obtained proved that the IWI method is an effective method to obtain the desired metal loading and the actual metal loadings were close to the theoretical value. A typical calculation to determine the amount of metal added to achieve a specific loading is presented in Appendix (Section A1). The intended ratio of Fe : Mn in the 10%FeMnH was intended to be 1 : 1 however the actual ratio obtained was 0.87 : 1.

The actual metal loading for the MCM-41 supported metal catalyst is presented in Table 4.9. It can again be seen from the data that the intended loading is quite close to the actual value. The actual ratio of Fe : Mn in the bimetallic 1.02 : 1.

Table 4.9: Actual Fe/Mn weight percentage loading on MCM-41 supported catalyst prepared via IWI.

	catalyst			
	5%FeM	10%FeM	10%MnM	10%FeMnM
wt % Fe	4.8	12.2	-	4.9
wt % Mn	-	-	9.5	4.8

Table 4.10 presents the elemental composition of the Zeolite X supported catalysts. In this instance it can again be seen that the actual values were closer to the calculated values obtained upon analysis.

Table 4.10: Actual Fe/Mn weight percentage loading on Zeolite X supported catalyst prepared via IWI.

	catalyst			
	5%FeX	10%FeX	10%MnX	10%FeMnX
wt % Fe	5.3	9.6	-	5.2
wt % Mn	-	-	9.8	4.7

The Fe : Mn ratio in the bimetallic catalyst 10%FeMnX was found to be 1.11 : 1, again in this case the desired calculated ratio was 1. It can be concluded from the ICP-OES data generated that incipient wetness impregnation is an easy and reproducible approach of metal loading zeolitic materials since the calculated values always are closer to the actual results. On the contrary the liquid phase ion exchange approach gave different values on different supports even though the same metal solution concentration was

used. This may be attributed to the differences in the respective CECs of the supports, that is related to the Si/Al ratio of the support matrix.

4.6 Crystalline phases study by selected area electron diffraction

The crystalline phase studies of the loaded support materials were carried out by selected area electron diffraction (SAED) analysis on a Technai G^2 F 20 X-Twin MAT on the same samples prepared for HRTEM in accordance to the procedure outlined in Section 3.4.1.1. In this section only two catalysts for each respective support were chosen for discussion, one prepared via liquid phase ion exchange and one prepared via incipient wetness impregnation. The decision was reached after it was observed that there was no marked difference in the SAED diffraction patterns for the respective catalysts despite their different metal wt % loading.

4.6.1 Crystalline phase studies of HBEA supported metal catalysts

The selected area electron diffraction (SAED) pattern of the 0.25FeH (prepared via liquid phase ion exchange) and the 10%FeH (prepared via incipient wetness impregnation) are shown in Figure 4.20 (a) and (b) respectively.

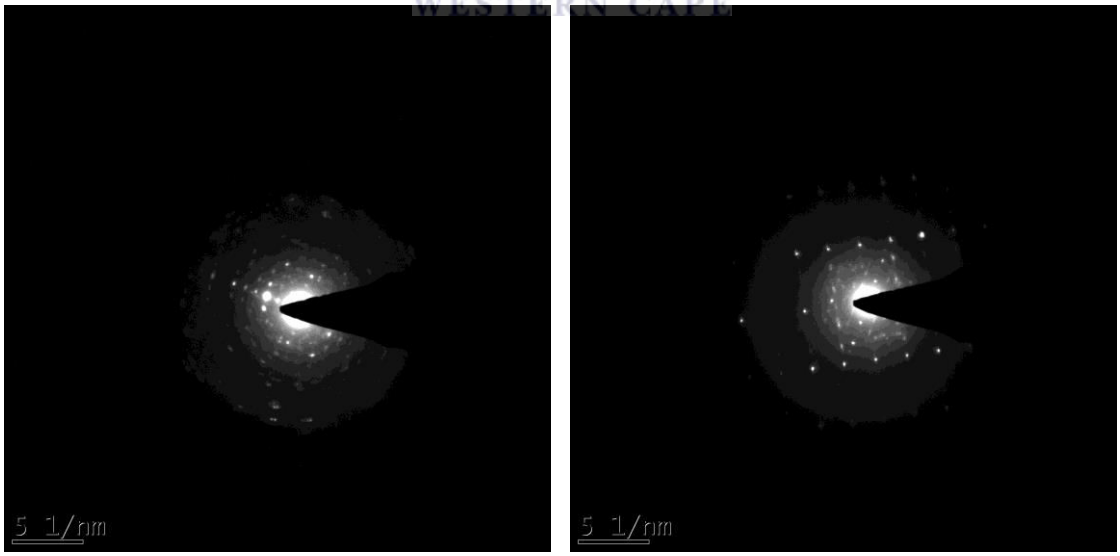

(a) (b)

Figure 4.20: Selected area electron diffraction pattern of (a) 0.25FeH (b) 10%FeH

The SAED patterns for the 0.25FeH and 10%FeH show the presence of the dispersed metal particles on the HBEA support. The small grains are attributed to the presence of the metal oxide species (Fe_2O_3). In the case of the 10%FeH the presence of the crystalline Fe_2O_3 was confirmed by the presence of characteristic peaks on the X-ray diffraction pattern presented in Figure 4.14.

4.6.2 Crystalline phase studies of MCM-41 supported metal catalysts

The SAED patterns for the 0.25FeM (prepared via ion exchange) and the 10%FeM (prepared via incipient wetness impregnation) are presented in Figure 4.21.

(a) (b)

Figure 4.21: Selected area electron diffraction pattern of (a) 0.25FeM (b) 10%FeM

The SAED patterns for both the 0.25FeM and the 10%FeM in Figure 4.21, attested to the presence of the metal crystallites on the mesoporous MCM-41 support. These can be seen as the small spots on the images. The parent material MCM-41 is amorphous and the diffraction pattern is characterised by diffuse rings (Goodhew, 2001). It could be however noted that the metal oxide species on the 0.25FeM was lower relative to that observed over the 10%FeM. This outcome was anticipated since the 0.25FeM had a lower metal wt % loading of 2.2 compared to that of 12.2 on the 10%FeM. The XRD patterns presented in Figure 4.9 also confirmed the crystallinity of these respective

catalysts. In the case of the 10%FeM, the XRD pattern was characterised by Fe_2O_3 peaks.

4.6.3 Crystalline phase studies of Zeolite X supported metal catalysts

The SAED patterns for the 0.25FeX (prepared via ion exchange) and the 10%FeX (prepared via incipient wetness impregnation) are presented in Figure 4.22.

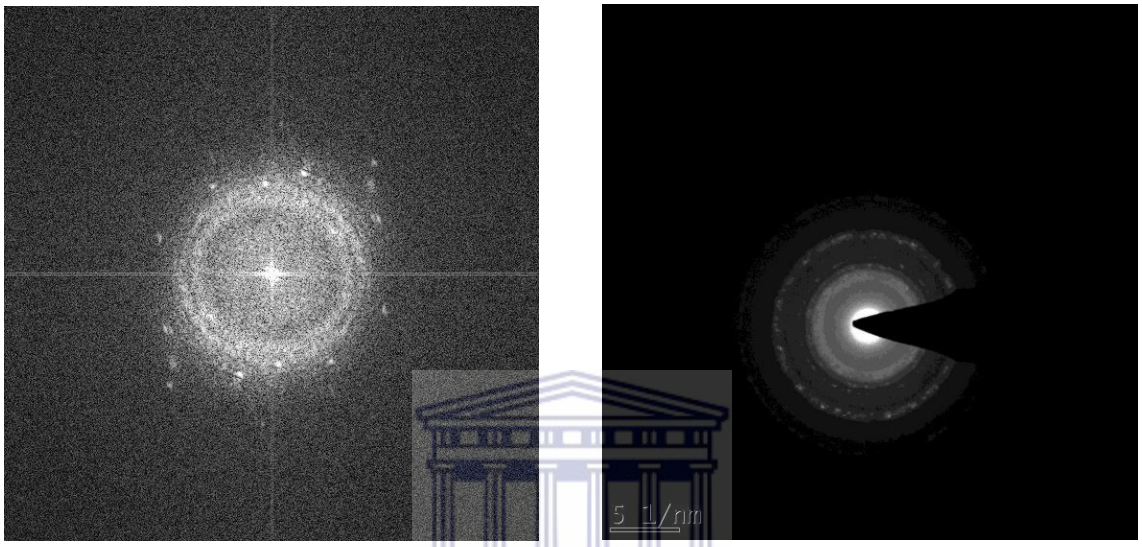

(a) (b)

Figure 4.22: Selected area electron diffraction pattern of (a) 0.25FeX (b) 10%FeX

The SAED patterns for both the 0.25FeX and the 10%FeX attested to the presence of the metal oxide (Fe_2O_3) species on the hierarchical Zeolite X support as evidenced by the presence of the small dots on the images. Comparing the two images presented in Figure 4.22, it could be seen that the image of the 0.25FeX was of poor quality. This may be ascribed to the high Fe wt % loading on the catalyst. The 0.25FeX had a Fe wt % loading of 11.4 and the 10%FeX had Fe wt % of 9.6. Since Fe_2O_3 is ferromagnetic, a high Fe loading on the sample may deflect and distort the electron beam due to the effect of Lorentz forces (*the orthogonal force on a charged particle traveling in a magnetic field*), (Fultz and Howe, 2002; Koyama et al, 2012). This could have affected the quality of the SAED pattern for the 0.25FeX.

The diffuse rings on the diffraction patterns indicate zeolite polycrystallinity and that the metal was highly dispersed on the support.

The XRD patterns for the metal catalysts supported on Zeolite X (Figure 4.16) also confirmed that the loaded catalysts retained the crystallinity of the pristine Zeolite X although the XRD peaks were characterised by reduction in peak intensities. Catalysts with Fe wt % of 10, supported on both HBEA and MCM-41 exhibited characteristic peaks due to the presence of the Fe_2O_3 crystallites, but this was not the case with the Zeolite X supported metal catalyst counterpart. This may be indicative of the possibility that part of the metal oxide was amorphous or there was formation of crystallites that were smaller than the nanoscale.

4.7 Surface area and pore size distribution studies

The N_2-adsorption studies were carried out on both the parent support as well as the metal loaded support materials in order to determine the surface area as well as the pore size distribution of the catalysts. The Brunauer- Emmet-Teller (BET) equation was employed to calculate the surface area while the Barrett, Joyner, Halenda (BJH) equation was employed in determining the pore size distribution. Both analyses were carried out on a Micrometrics Tri Star 3000 Analyser under experimental conditions outlined in Section 3.4.5. For each of the three support materials used only three samples were analysed, namely the parent support, the 5%Fe and the 10%Fe. The outcomes obtained are presented and discussed in the following sections.

4.7.1 Surface area studies over HBEA supported metal catalysts

The BET surface area and the pore diameter of the HBEA supported metal catalyst are presented in Table 4.11.

Table 4.11: Nitrogen adsorption surface area and pore size of the HBEA supported metal catalysts

catalyst	pore diameter (nm)	BET surface area (m^2/g)	micropore area (m^2/g)	external surface area (m^2/g)
HBEA	67.1	485	332	153
5%FeH	66.5	443	304	139
10%FeH	68.2	379	246	132

The data presented in Table 4.11 shows that there was a reduction on the BET surface area with increasing metal loading. The parent material HBEA had a BET surface area

of 485 m^2/g whilst the 10%FeH with an actual Fe wt % of 12.4 had a BET surface area of 379 m^2/g. The micropore surface area was decreasing with increasing metal loading. This may be ascribed to the formation of Fe_2O_3 crystallites that are bigger than the micropores of the zeolite. The nitrogen sorption isotherms for the Fe loaded HBEA prepared via incipient wetness impregnation are presented in Figure 4.23.

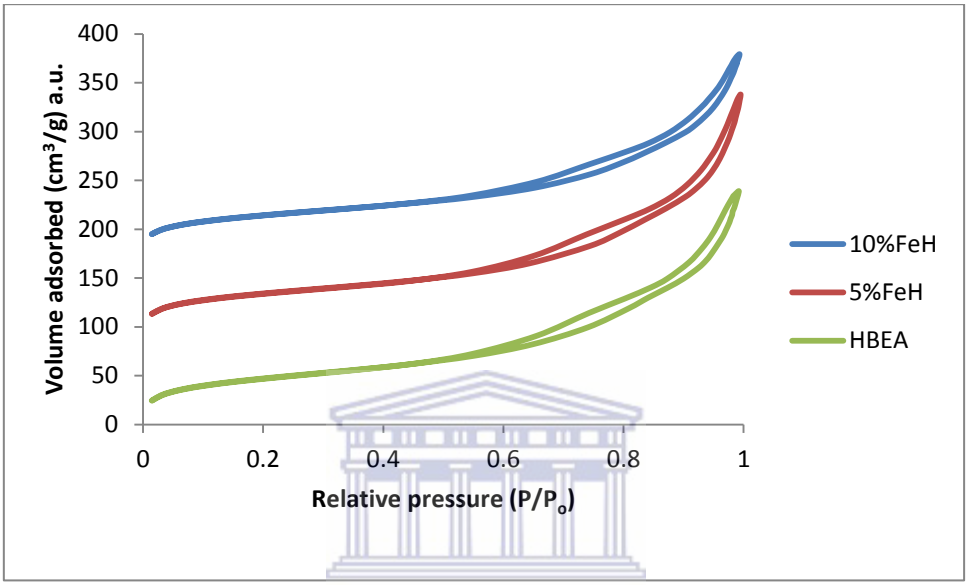

Figure 4.23: Nitrogen sorption isotherms at 77 K of the 5%FeH and 10%FeH catalysts prepared via incipient wet impregnation in comparison with the of parent HBEA isotherm.

The hysteresis loops presented in Figure 4.23, show that the isotherm of the parent support HBEA was almost unaltered by the inclusion of the metal. It could be seen that there was no marked difference in both the inflection point as well as the sharpness of the loop between the parent HBEA and the metal loaded catalysts. According to the IUPAC empirical classification of hysteresis loops the loops in Figure 4.23 are categorised as type B. Generally the inflection points of type B hysteresis loops are found above a relative pressure of 0.4 mmHg (Savidha, 2004). This is characteristic of microporous materials that have high adsorption capacities at low pressures (Lima et al, 2011). The fact that the metal loaded support had a hysteresis loops as the parent material attest to the fact that the porosity of the support was not altered by the introduction of the metal on the support. From Table 4.11, it could be seen that as the metal loading was increased there was a systematic decrease in both the micropore and

external surface area, but this did not hamper the porosity of the support. Comparable outcomes in related research activities were generated and reported (Lima et al; Konnov et al, 2008)

4.7.2 Pore diameter distribution of HBEA supported metal catalysts

The pore distribution of the HBEA supported metal catalysts is presented in Figure 4.24.

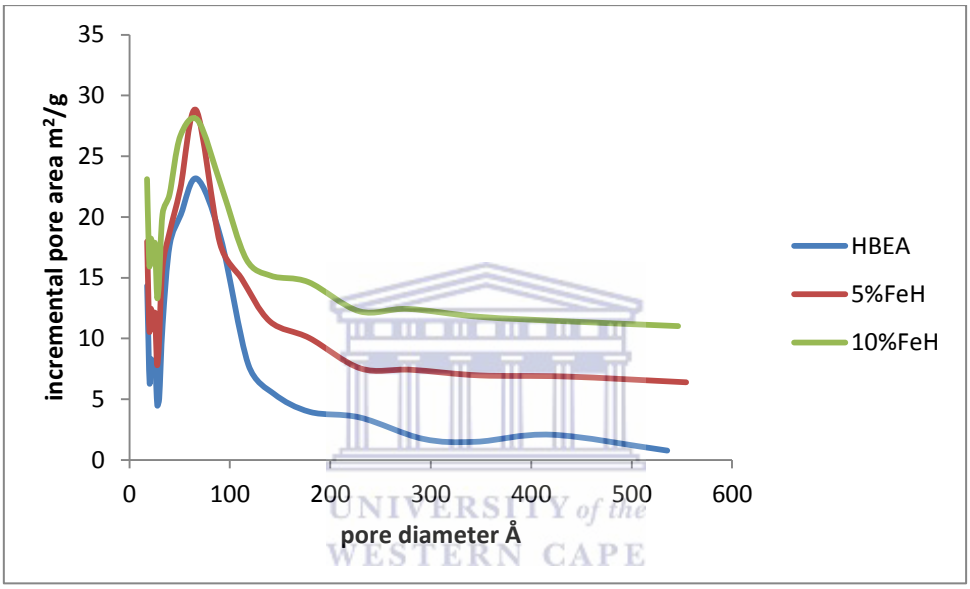

Figure 4.24: Pore distribution of the HBEA supported metal catalyst prepared via incipient wetness impregnation

From the pore distribution data presented in Figure 4.24, it could be seen that the introduction of the metal did not significantly alter the pore diameter of the parent HBEA support. The average pore size of the parent material was 67.1 Å, while the metal loaded catalysts 5%FeH and the 10%FeH had average pore sizes of 66.5 Å and 68.2 Å respectively.

4.7.3 Surface area studies over MCM-41 supported metal catalysts

The BET surface area and the pore diameter of the MCM-41 supported metal catalyst are presented in Table 4.12.

Table 4.12: Nitrogen adsorption surface area and pore size of the MCM-41 supported metal catalysts

catalyst	pore diameter (Å)	BET surface area (m^2/g)	micropore area (m^2/g)	external surface area (m^2/g)
MCM-41	25.6	867	52	815
5%FeM	23.8	812	-426	1238
10%FeM	23.8	794	-453	1247

The BET surface area of the parent material MCM-41 was found to be 867 m^2/g, as presented in Table 4.12. The introduction of the metal on the support material resulted in a reduction on the BET surface area. Incipient wetness impregnation is said to be associated with extensive surface restructuring which consequently gives rise to surface area loss after metal loading. The micropore surface area was found to decease as the metal loading was increased. This outcome was anticipated since MCM-41 is a mesoporous and the limited micropores in the support may easily be filled up with the Fe_2O_3 crystallites, resulting in a complete mesoporous material. The nitrogen sorption isotherms for the MCM-41 supported Fe catalysts prepared via incipient wetness impregnation are presented in Figure 4.25.

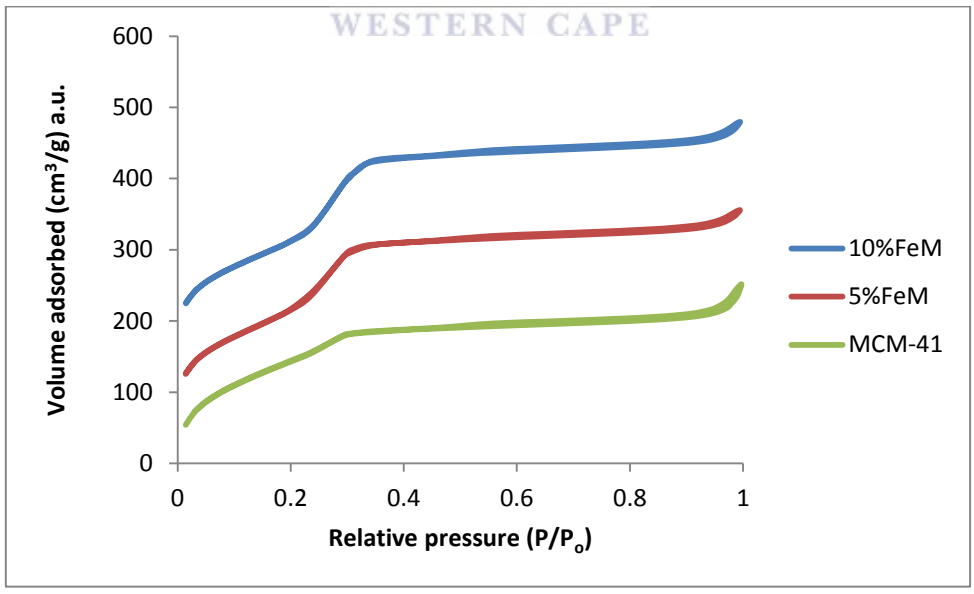

Figure 4.25: Nitrogen adsorption/desorption isotherms at 77 K of the 5%FeM and 10%FeM catalysts prepared via incipient wet impregnation in comparison with the parent MCM-41 isotherm.

The hysteresis loops for both the Fe loaded supports resembled the hysteresis loop of the pristine HBEA support. This was a confirmation that the metal introduction did not alter the porosity of the support material. The inflection points for both the metal loaded supports and the parent HBEA were within the range of 0.2 – 0.4 mmHg (P/P_0) values. The range in which the inflections occur is characteristic of mesoporous materials and according to the IUPAC classification the isotherms are categorised as type A and D. The surface area of the MCM-41 catalyst series were in the range of 867 – 794 (refer to Table 4.12), which also is characteristic of mesoporous materials (Savidha and Pandurangan, 2004). The isotherms presented in Figure 4.23 are characterised by three well defined regions, with the first region characterised by an initial increase in the nitrogen uptake at low relative pressure values. This may be ascribed to monolayer-multilayer adsorption on the pore walls. The second region at intermediate relative pressure values was characterised by a sharp gradient which may be ascribed to capillary condensation in the mesopores. The final region (the plateau) at higher relative pressure values is characteristic of multilayer adsorption on the external surface of the MCM-41 support material. On the other hand the hysteresis loops for the three catalysts presented in Figure 4.25 are comparable, this further suggested that there were no major changes in the meosporosity of the parent upon metal loading. These outcomes put together were indicative that the mesoporosity of the pristine MCM-41 was well maintained upon metal loading.

4.7.4 Pore diameter distribution of MCM-41 supported metal catalysts

The pore distribution of the MCM-41 supported metal catalysts prepared via incipient wetness impregnation is presented in Figure 4.26. The pore distribution data presented shows that the pore diameter of the parent material was not significantly altered. The parent Zeolite HBEA had a pore diameter of 25.6 Å whilst 5%FeM and the 10%FeM both had a pore diameter of 23.8 Å.

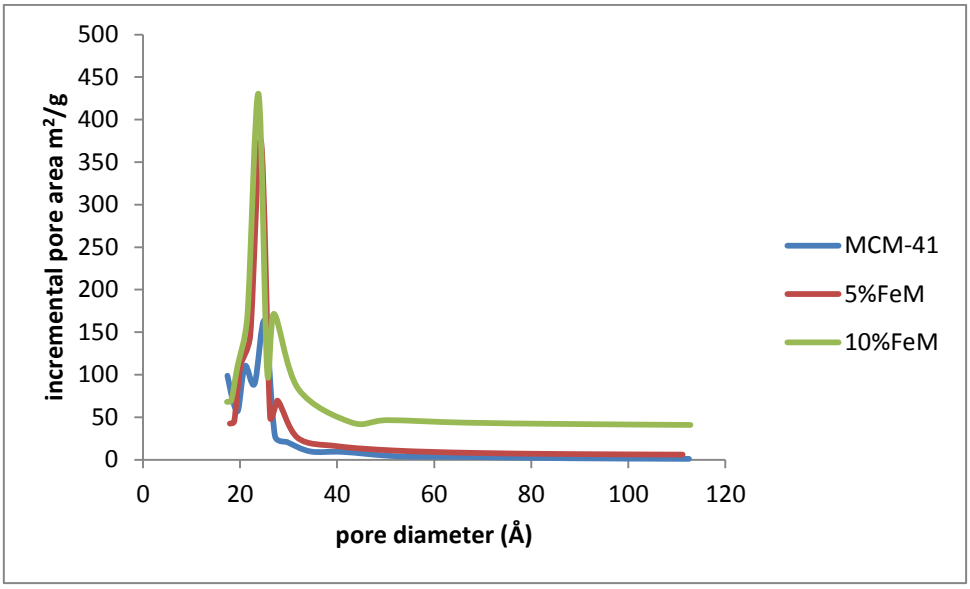

Figure 4.26: Pore distribution of the MCM-41 supported metal catalyst prepared via incipient wetness impregnation

4.7.5 Surface area studies over the hierarchical Zeolite X supported metal catalysts

The BET surface area and the pore diameter of the fly ash based hierarchical Zeolite X supported metal catalyst are presented in Table 4.13.

Table 4.13: Nitrogen adsorption surface area and pore size of the Zeolite X supported metal catalysts

catalyst	pore diameter (nm)	BET surface area (m^2/g)	micropore area (m^2/g)	external surface area (m^2/g)
HX	32.6	221	189	32
5%FeX	51.8	135	87	48
10%FeX	40.1	95	38	57

The data presented in Table 4.13 showed that the BET external surface decreased as the metal loading was increased. The same outcomes were observed with the HBEA and the MCM-41 supported metal catalyst series. The same attributes made for the HBEA can be said of the observed outcomes in the case of the fly ash based hierarchical Zeolite X. The zeolite X however had a lower surface area in comparison to the HBEA. The parent Zeolite X had a BET surface area of 221 m^2/g whilst the parent HBEA had a BET surface area of 485 m^2/g which was more than twice as much. The nitrogen sorption

hysteresis loops for the Fe loaded Zeolite X prepared via incipient wetness impregnation are presented in Figure 4.25.

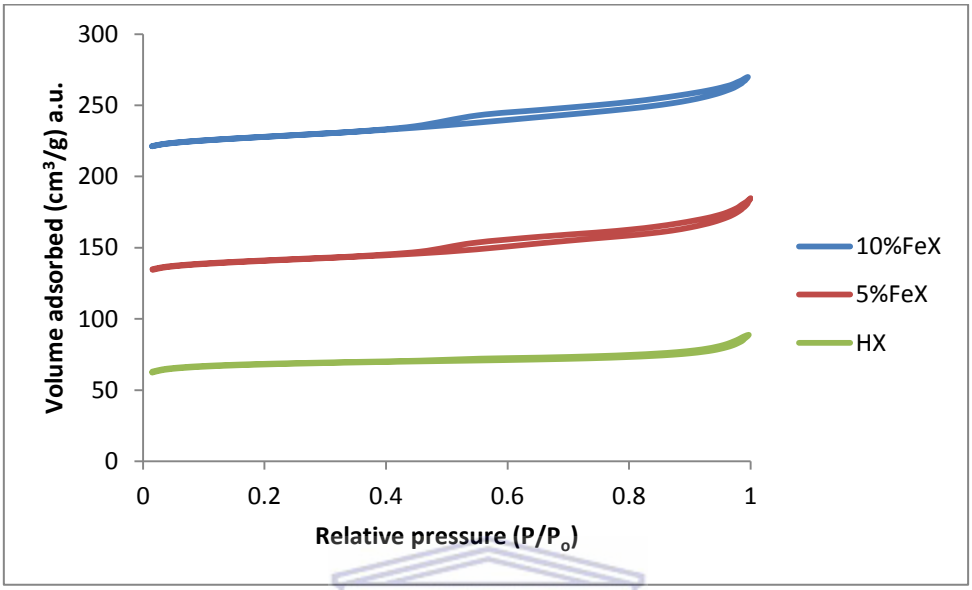

Figure 4.27: Nitrogen adsorption/desorption isotherms at 77 K of the 5%FeX and 10%FeX catalysts prepared via incipient wet impregnation in comparison with the of parent Zeolite X isotherm.

The hysteresis loops presented in Figure 4.27 showed that the porosity and texture of the parent hierarchical Zeolite X was retained upon metal loading. The hysteresis loops are categorised as type A according to IUPAC classification and are typical of microporous materials. The loop for all the three catalysts appear from intermediate to high relative pressure values, which may be ascribed to capillary condensation effect usually associated with creation of mesopores (Bouvy et al, 2007). It could be seen from Table 4.13, that the increase in metal loading resulted in a reduction in surface area. Based on the sorption isotherms presented in Figure 4.27 it could be seen that the porosity of the hierarchical Zeolite X was retained upon metal loading, since the hysteresis loops of the metal loaded support resembles that of the parent zeolite.

4.7.6 Pore diameter distribution of the Zeolite X supported metal catalysts

The pore distribution of the fly ash based hierarchical Zeolite X are presented in Figure 4.28.

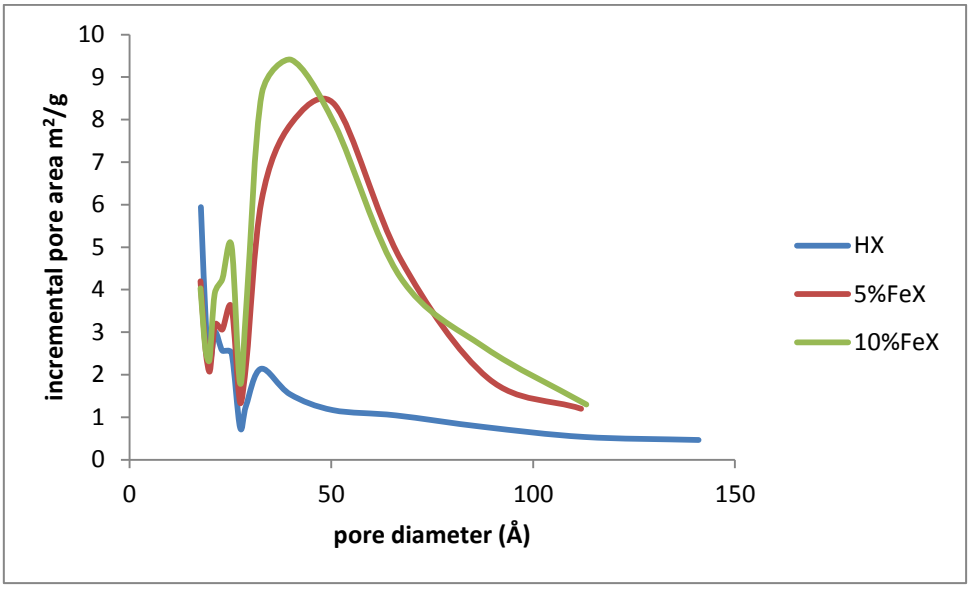

Figure 4.28: Pore distribution of the Zeolite X supported metal catalyst prepared via incipient wetness impregnation

The pore distribution of the fly ash based hierarchical Zeolite X showed that there were significant changes in the average pore size of the zeolite as the metal was introduced. The parent Zeolite X had an average pore size of 32.6 Å but upon metal loading the average pore size of the 5%FeX and the 10%FeX were 51.8 Å and 40.1 Å respectively.

CHAPTER 5

5.0 Catalyst Testing

This chapter presents the catalyst testing outcomes for the synthesised and characterised supported metal catalyst in the Friedel-Crafts alkylation of benzene with t-butyl chloride under experimental conditions outlined in chapter 3. This chapter is broken down into four sections with the first three sections focusing on the catalytic activity of HBEA supported metals followed by MCM-41 and then by Zeolite X supported metal catalysts. The fourth and final section presents the effects of four parameters namely, reaction time, amount of metal on support, doping with Mn and pore system of support on the conversion, selectivity, product distribution and yield of the primary product (t-butylbenzene). The chapter then closes with a brief summary of the overall catalytic activity of all the catalysts studied.

5.1 Introduction

The catalytic activity of the prepared supported metal catalysts was tested for the Friedel-Crafts alkylation of benzene with t-butyl chloride, which proceeds as follows:

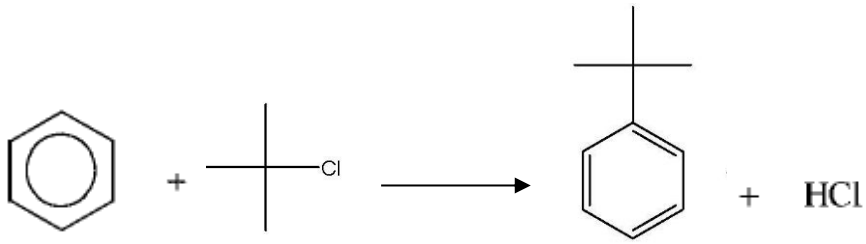

The reaction however results in other by products as well as the *t*-butyl benzene. Alkylation reactions are generally associated with transalkylation polymerization and polyalkylation. The reaction may also give rise to a variety of reaction intermediates as shown in the mechanistic view presented in Section 2. 7. 2. In this study the desired end product was *t*-butyl benzene. In most parts of this chapter this compound is referred to as the monoalkylated product. The reaction could possibly produce significant amounts of the dialkylated product, 1,4-di-*t*-butyl benzene and in this section the compound is

usually referred to as the *para* isomer. The reaction was carried out in a liquid batch reactor at a temperature of 45 ^{o}C, under reflux and stirring using a magnetic bar as detailed in Section 3.5.2. Sample aliquots were taken at time intervals over 5 h and analysed by gas chromatography as set out in Section 3.5.2.

The studies for conversion of the t-butyl chloride, selectivity towards the formation of the monoalkylated product, and yield of the monoalkylated product were then calculated using equations presented in section 3.5.4. A total of 18 catalysts supported on HBEA, MCM-41 or Zeolite X were studied, as set out in Tables 3.4 and 3.5.

5.2 Catalytic activity studies over the HBEA supported metal catalysts

The conversion, selectivity, product distribution studies and yield over the HBEA supported metal catalysts were carried out at a temperature of 45 ^{o}C over a reaction time of 5 h. The outcomes are presented in the following sections**.**

5.2.1 Conversion Studies on HBEA Supported Metals

The results for the conversion over the various samples of metal loaded HBEA prepared via liquid phase ion exchange and incipient wetness impregnation as set out in sections 3.3.1 and 3.3.3 respectively are presented in Figure 5.1. The percentage conversion of *t*-butyl chloride is plotted as a function of reaction time.

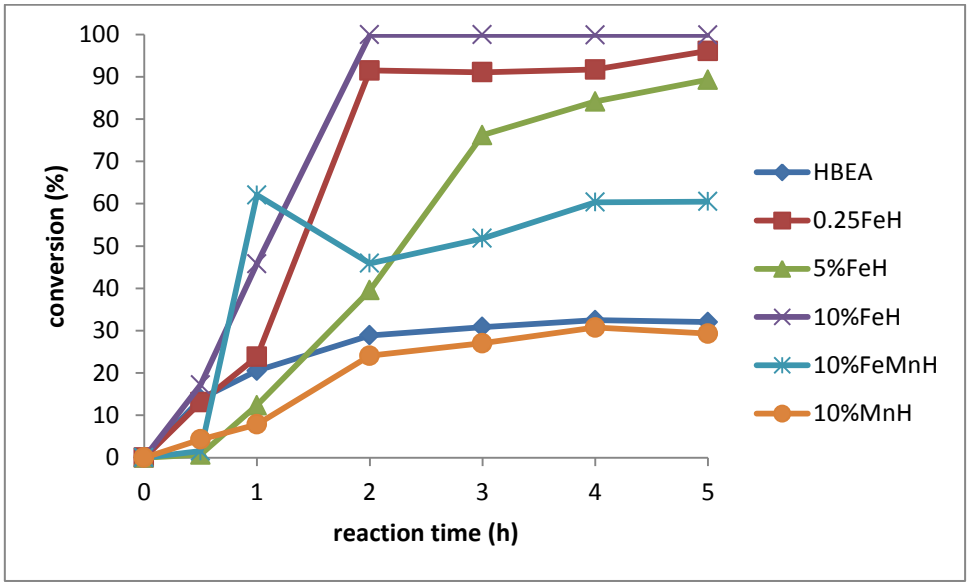

Figure 5.1: Conversion of t-butyl chloride over the series of HBEA supported Fe/Mn catalysts at 45 ^{o}C

Figure 5.1 shows the conversion trend of *t*-butylchloride as a function of reaction time. There was a general rapid increase in conversion within the first 2 h. The maximum conversion obtained over the parent HBEA was 30.8 % after 3 h time on stream. The low conversion obtained over the parent support HBEA may be attributed to the absence of Lewis acid sites in the parent zeolite. On the other hand Fe loaded catalysts had high conversion due to the presence of both the Brønsted and Lewis acid sites, which actually play a synergic role in the alkylation reaction. The Brønsted acid sites are responsible for the formation of the carbonium ion while the deprotonation to form the alkylated product occurs mainly on the Lewis acid sites (Nur et al, 2011).

The 10%FeH prepared via incipient wetness impregnation (refer to code in Table 3.1) reached a steady state giving a conversion of 100 % after a reaction time of 2 h. The high conversion may be ascribed to the high Fe loading on the HBEA support. The BET surface area data presented in Table 4.11 showed that as the metal loading was increased there was a reduction in surface area. However the high activity observed over the 10%FeH may be ascribed to increased active sites. The catalyst had a Fe wt% of 12.4 determined by ICP-OES and presented in Table 4.8.

The second highest conversion of 99 % was observed with the 0.25FeH (refer to code in Table 3.5) prepared via liquid phase ion exchange. The catalyst had an actual Fe wt% loading of 7.2 determined by ICP-OES (presented in Table 3.9). The high conversion may again be attributed to the high metal loading on the support.

The results in Figure 5.1 show that there was a general increase in conversion of the *t*-butyl chloride with increasing Fe loading. The 5%FeH had a maximum conversion of 89 % which was achieved after a reaction time of 5 h. After a reaction time of 2 h, the conversion was only 40 % compared to a conversion of 99 % achieved with the 10%FeH which had about twice as much the amount of Fe. The effect of doping the Fe catalyst with Mn was also investigated, and it was found that the inclusion of Mn reduced the conversion of the *t*-butyl chloride. In the present work, 10%FeMnH, (5%Fe and 5%Mn), was compared with 5%FeH, (5%Fe). Both catalysts had comparable amounts of Fe, with the former doped with an equal amount of Mn. The conversion profile observed with the 5%FeH had a rapid increase in conversion between 0.5h to 3h after which there was a gradual increase observed, reaching a conversion of 89 %.

After the first 2 h it had a higher conversion relative to that of the bimetallic catalyst (10%FeMnH) of only 60 %. The effect of metal loading is further discussed in Section 5.7.1.

On the other hand the 10%FeMnH catalyst initially showed a rapid increase in the conversion within the first hour, and the conversion gradually increased to 60 % after the second hour. The trend was different from the general trends observed with the other catalysts. During the initial stages Mn can possibly dealkylate the formed alkylated products back to the reactants. This may give rise to an increased concentration of the alkyl halide and hence a decrease in the conversion from the first hour to the second. After this decrease the conversion started to rise steadily and almost reached steady state after 4 h. A monometallic catalyst loaded with Mn alone was also tested (10%MnH), and it had a low conversion characterised with a rapid increase reaching steady state after 2 h. The conversion obtained over the 10%MnH catalyst was slightly lower than that obtained over the parent HBEA which was not loaded with metal. This attests to the fact that Mn is not active for the alkylation of benzene with *t*-butylchloride. When Mn was loaded on MCM-41 (catalyst code 10%MnH), which has no Brønsted acid sites, there was no activity observed. Hence the activity observed with the 10%MnH could be ascribed to the acid sites on the zeolite HBEA, and not due to the metal loaded.

Another possible factor that could have enhanced the conversion of the 0.25FeH over the other catalysts supported on HBEA could be the good metal dispersion that is said to be associated with the liquid phase ion exchange (Armor, 2001; Ross, 2012). Metals loaded on zeolites via ion exchange tend to have a better metal dispersion relative to those created via incipient wetness impregnation. Incipient wetness impregnation is usually characterised by the formation of large metal crystallites within the zeolite pore system as well as on the external surface of the zeolite (Kinger et al, 2000). Yazaki et al, (1997) loaded Rh on Zeolite Y via ion exchange and incipient wetness impregnation, each of the catalyst had a metal loading of 2 %, however when they were tested for their activity in the decomposition of N_2O, the ion exchanged catalyst gave a higher conversion and this was attributed to the dispersion of the metal on the support. Formation of large metal crystallites associated with incipient wetness impregnation

may partially block the pores of the zeolite, presenting some diffusional constraints to reactants or products.

5.2.2 Selectivity Studies on HBEA Supported Metals

The alkylation of benzene with t-butyl chloride can give rise to numerous products. The desired product in this study was the monoalkylated product (t-butyl benzene). However the reaction can give rise to dialkylated products (1.2-di-t-butyl benzene, 1.3-di-t-butyl benzene and 1,4-di-t-butyl benzene), trialkylated product as well as some intermediates. Since the desired product was the monoalkylated product, selectivity studies were based on the formation of the monoalkylated product. The selectivity towards the formation of the *t*-butyl benzene was studied over the series of metal catalysts supported on HBEA (catalysts presented in Sections 3.3.1 and 3.3.3.) The general trend for the selectivity-time plots given in Figure 5.2, were characterised by a rapid increase of selectivity to a maximum reaching steady state.

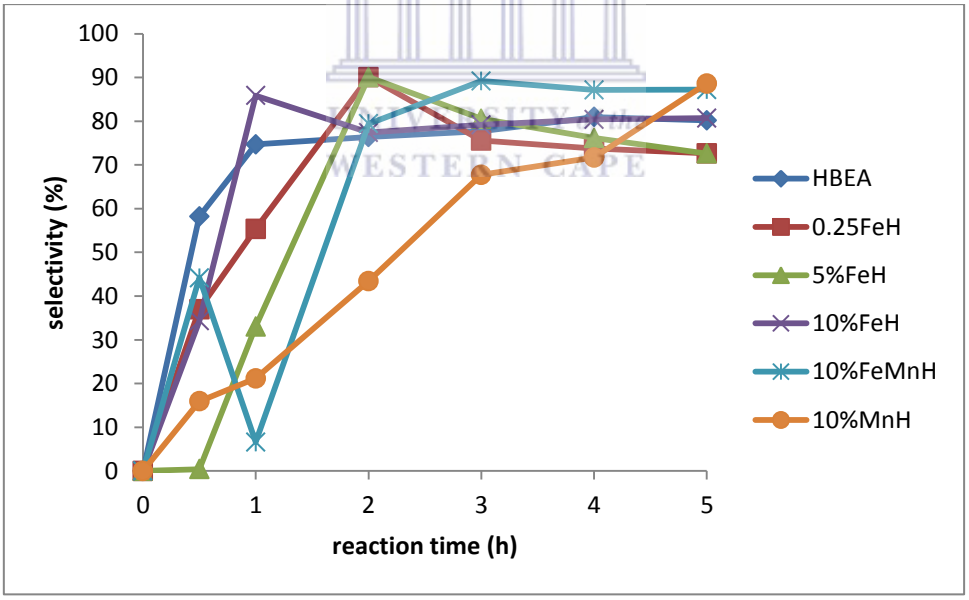

Figure 5.2: The monoalkylated selectivity-time curve for HBEA supported metal catalysts in the alkylation of benzene with t-butyl chloride at 45 °C.

The parent zeolite HBEA, had a high selectivity of 80.9 % after 4 h time on stream. The selectivity over the parent support material, HBEA was slightly lower than that obtained over the metal loaded support. This may be indicative of the fact that the metals do

influence the reaction progression and consequently the product distribution. The *para* isomer was not formed over the HBEA within the 5 h time on stream studied. The conversion over the parent HBEA zeolite was low compared to the Fe loaded catalysts. However the parent zeolite gave a reasonably high selectivity, this may be indicative of the fact that selectivity is largely influenced by the zeolite pore system rather than the metal loaded onto the zeolite.

The highest selectivity of 90 % was obtained over the 5%FeH prepared via incipient wetness impregnation after a reaction time of 2 h. The catalyst had an actual Fe wt % of 4.8 % (refer to Table 4.8). The selectivity was better than the selectivity given by the 10%FeH which had an actual metal loading of 12.4 %. The higher selectivity obtained over the 5%FeH could be attributed to its higher micropore surface area (304 m^2/g) relative to that of the 10%FeH (246 m^2/g), since there was no significant differences in the pore diameters of the respective catalysts as could be seen in the data presented in Section 4.7.1.

Comparison can be made between the 10%FeH and the 10%FeMnH, the total metal wt% was comparable (12.4 and 10.9 % respectively). After the catalysts reached steady state at a reaction time of 3 h, the 10%FeMnH had a higher selectivity of 89 % compared to 79 % obtained over the 10%FeH. This may be due to the dispersion of the metals on the support. It is said that bimetallic catalysts prepared via co-impregnation have a tendency to form alloys rather than large metal crystallites (Caelho et al, 1995). However the nature of the metal dispersion was not studied in this research. Caelho et al, (1995) also reported that introducing Fe and Mn on porous supports via co-impregnation improves the dispersion.

However the trend observed with the 10%FeMnH was different, the selectivity towards formation of the monoalkylated product increased within the first hour and then decreased and then increased again reaching steady state after 3 h. This discrepancy could be attributed to the presence of Mn. In related research by Wang et al, (2012) in which the alkylation of phenol was studied over Mn supported on silica, it was found that Mn suffers a partial reduction of the Mn_2O_3/MnO_4, which may result in the decrease in acid strength, which consequently might affect product selectivity. Another discrepancy was observed with the 10%MnH. In general all the catalysts had an increase in selectivity until steady state was achieved within a time period of 5 h.

However with this particular catalyst the selectivity was still increasing at 5 h, this may be due to the poor alkylating activity of Mn. The trends observed are generally comparable to other alkylation selectivity-time curves reported in literature (Da, et al, 2001; Kondamudi et al, 2010; Wang et al, 2012), although different alkylation reactions were studied over various zeolite based catalysts.

5.2.3 Product Distribution over HBEA Supported Catalysts

In the alkylation of benzene the first stages of the reaction are characterised by the formation of various dialkylated products, together with intermediates, but long reaction times would be characterised by the thermodynamic more stable products. In this instance Mn favoured the formation of two intermediates, which could not be identified, since product identification was done by injecting standards of the expected monoalkylated product as well as the polyalkylated isomers. They are thus identified as intermediate A and B. Since their retention times were close to the retention of the monoalkylated product they may be transient intermediates that form prior to the completion of the first alkylation that results in the formation of the monoalkylated product. The alkylation of benzene with *t*-butyl chloride proceeds via the formation of the *t*-butyl cation, which will then react with the benzene giving a π-complex of similar stability to the σ-complex, with the 2 complexes separated by a small energy barrier (McClelland, 2006). It is also well known that alkyl halides (*t*-butylchloride inclusive) have the property of producing alkyl groups as intermediates or at least as transient intermediates in alkylation reactions (Rosenwald, 1949). Haw, (2002) probed the transformations of benzene over Zeolite HY using ^{13}C solid state NMR and confirmed that there was the formation of the benzinum/carbenium intermediate. In most cases in the present work the intermediates were detected in the product mixture before steady state was achieved and this may be indicative of the fact that they may be transient intermediates. However standards for the suspected possible carbocations or alkyl groups were not available to ascertain the exact nature of the intermediates. The only dialkylated product identified in the analyses carried out was the *para* isomer (1,4-di-*t*-butyl benzene). It is generally accepted that the exact nature of the intermediates formed during alkylation of aromatics over solid acid catalysts such as zeolites is not well understood (Craciun, et al, 2007).

The highest conversion of *t*-butyl chloride was obtained over the 10%FeH as presented in Section 5.2.1. The product distribution obtained over the catalyst is presented in Figure 5.4. The other Fe catalysts had the same trends except for the amounts of the relative products, and they are not going to be discussed. However the product distribution data for the catalysts are presented in Table 5.1. For comparison purposes the product distribution obtained over the parent HBEA zeolite is presented as a baseline in Figure 5.3. The Mn containing catalysts had a different product distribution trend and they are discussed in Sections 5.2.3.3 and 5.2.3.4.

5.2.3.1 Product Distribution over parent HBEA

The product distribution obtained over the parent HBEA zeolite is presented in Figure 5.3.

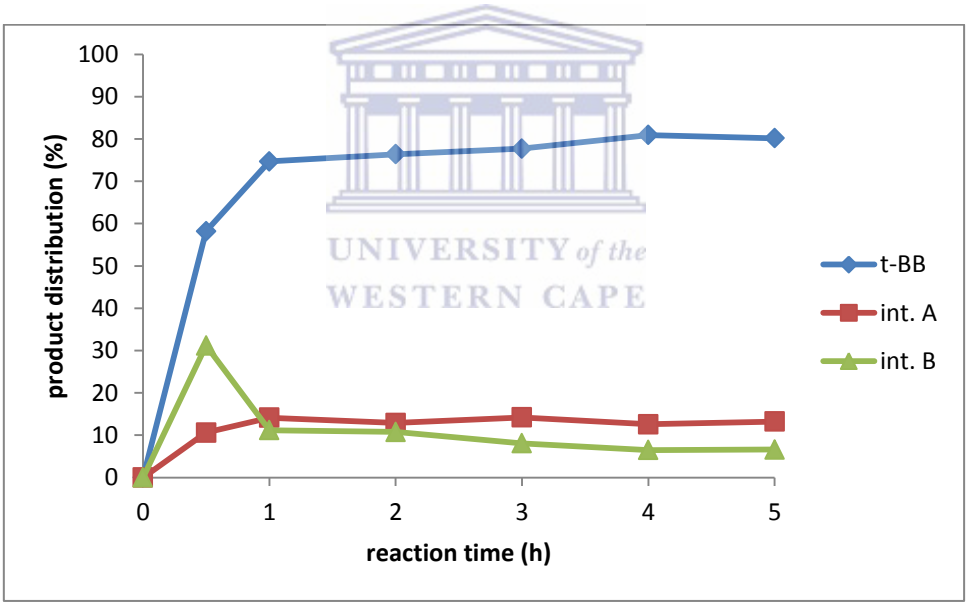

Figure 5.3: Product distribution for benzene alkylation with t-butyl chloride over the parent HBEA at 45 ^{o}C.

**{t-butyl benzene (t-BB); 1,4-di-t-butyl benzene (1,4-di-t-BB); intermediate A (int. A); intermediate B (int. B)}*

The primary product obtained in all of the reactions carried out with the HBEA supported metal catalysts was *t*-butylbenzene (coded t-BB on graphs). However some transient intermediates were also observed (int. A and int. B). With the Fe loaded HBEA catalysts the intermediates disappeared from the product mixture between 0 – 2

h, during the start-up transient period before steady state conditions were achieved. However the product distribution obtained over the parent HBEA presented in Figure 5.3 shows that the intermediates were still present in the product mixture over the 5 h time on stream studied. The persistence of the intermediates in the product mixture may be attributed to the absence of Lewis acid sites on the parent zeolite. Lewis acid sits are generally responsible for the deprotonation of the carbonium intermediates to form the alkylated product. The tri-alkylated product was not observed to form in any of the experiments undertaken.

5.2.3.2 Product Distribution over 10%FeH Catalyst

The product distribution obtained over the 10%FeH catalyst (refer to code in Table 3.1) is presented in Figure 5.4.

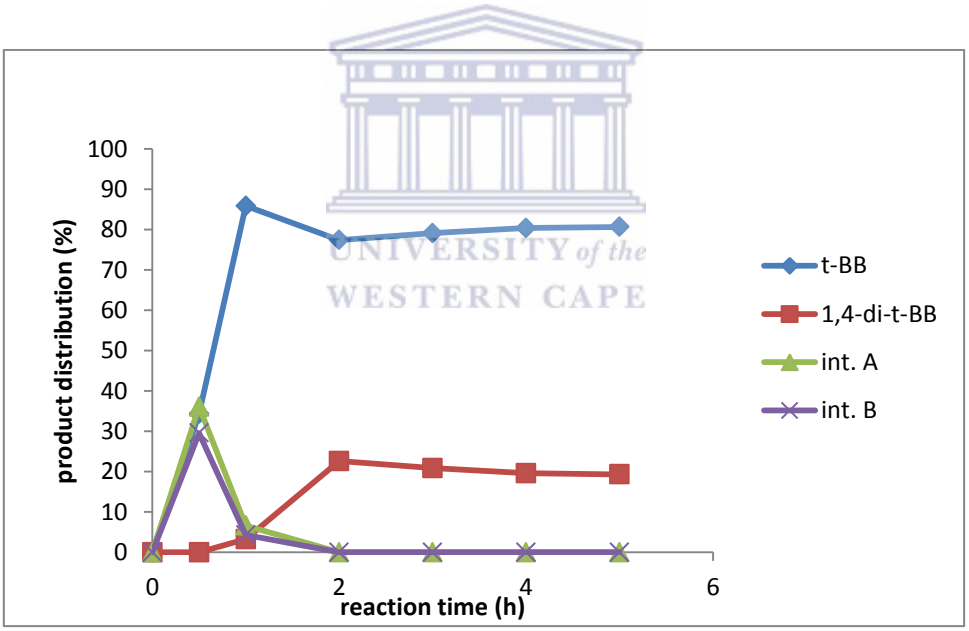

Figure 5.4: Product distribution for benzene alkylation with t-butyl chloride over the 10%FeH at 45 °C.

The general outcome observed with the HBEA supported metals was characterised by a mixture of the primary product (t-BB) and the intermediate products in the initial stages of the reaction. The later stages were characterised by the formation of the *para* isomer, with the disappearance of both the intermediate A and B. This is due to the fact that the first alkylation activates the *para* position. Although the selectivity obtained over the

parent HBEA and the 10%FeH are comparable, the product distribution was found to be different. The HBEA product distribution was characterised by the presence of both intermediates A and B in the product mixture even after 5 h time on stream. This outcome indicated that the addition of Fe favoured the formation of the *para* isomer with disappearance of the intermediates from the product mixture. The difference in the nature of the acidity of the Fe loaded catalyst and the parent HBEA may be attributed to have caused the different product distribution trends observed over the two catalysts. The parent HBEA has more Brønsted acid sites which tend to promote the formation of the carbonium intermediates and the alkylation of the carbonium ion mostly occurs on the Lewis acid sites which do not exist in the parent zeolite (Nur et al 2011).

During the first hour (transient state) the amount of both intermediates over the 10%FeH began to decrease whilst the formation of the primary product continued to increase reaching steady state after 2 h. The decrease of the intermediates can be attributed to their low thermodynamic stability. After the first hour the formation of the *para* isomer was observed. The amount increased and reached steady state after 2 h. Longer reaction times gave two products in the reaction mixture namely the primary product t-BB and the *para* isomer. The findings here are consistent with related findings reported by Bidart et al (2001). The same trend was generally observed with the other HBEA supported catalysts with the exception of those trends observed with the 10%FeMnH and 10%MnH. With the other catalysts the product distributions obtained after a reaction time of 3 h are tabulated in Table 5.1.

5.2.3.3 Product distribution on 10%FeMnH catalyst

The inclusion of Mn as an active metal changed the product selectivity and distribution compared to the generally observed and well reported trends in literature. The product distribution over the 10%FeMnH is presented in Figure 5.5. The trends generated with 10%FeMnH show that the inclusion of Mn in the catalyst tended to favour formation of both intermediate A and B during the initial transient stages of the reaction. The amounts of both intermediates being formed were higher than that of the primary product during the first hour. The amount of the primary product tended to increase within the first 0.5 h and then decreased after 1 h. It then increased to steady state after 2 h on stream.

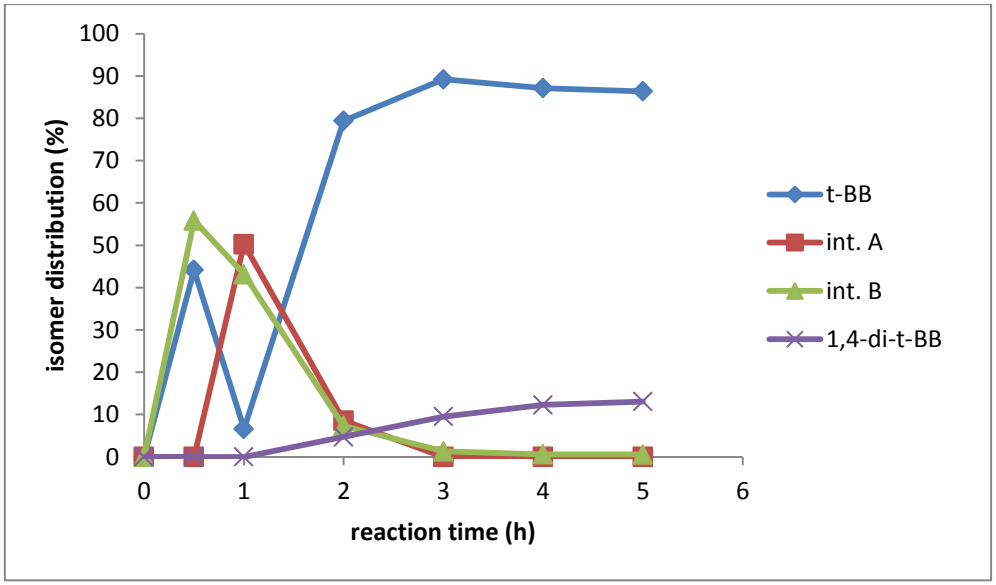

Figure 5.5: Product distribution in the benzene alkylation with t-butyl chloride over 10%FeMnH at a temperature of 45 °C.

The decrease in the percentage of the monoalkylated product is basically due to the fact that there is an increase in the formation of both intermediates A and B during the first hour. It could be said that Mn tended to favour the formation of the intermediates. However since these intermediates are not thermodynamically stable they then disappeared from the reaction mixture, and the selectivity improved towards the monoalkylated product. With longer reaction times it could be seen that the formation of the *para* isomer became more pronounced increasing to a maximum of 13 % after 5 h. However the amount of the *para* isomer formed over the Mn containing catalysts was relatively lower than that observed with catalysts that contained Fe alone. This phenomenon can be manipulated to reduce the formation of the *para* isomer. Although the conversion obtained over the Mn containing catalysts was lower in comparison to that obtained over the monometallic Fe catalysts, the inclusion of Mn did improve the selectivity towards the monoalkylated product. In liquid phase alkylation reaction product separation is a challenge and a catalyst that gives a high selectivity towards the formation of the desired product is of great advantage. However the Mn doped catalysts (10%FeMnH) was found to be less active overall since steady state was reached after a reaction time of 3 h contrary to observations made with the Fe monometallic catalysts

which reached a steady state after 2 h. It may be said that the Mn blocks the Brønsted acid site and hence reduces the active sites for the formation of the carbonium ion, which forms mainly on the Brønsted acid sites (Nur et al, 2011). The formation of the carbonium ion is the rate determining step in the alkylation of benzene (Craciun et al, 2007) hence the observed slow attainment of steady state over the Mn doped catalyst.

5.2.3.4 Product distribution on 10%MnH catalyst

To further ascertain the effect of Mn on the product distribution, a catalyst that contained Mn only was tested and the product distribution obtained is presented in Figure 5.6.

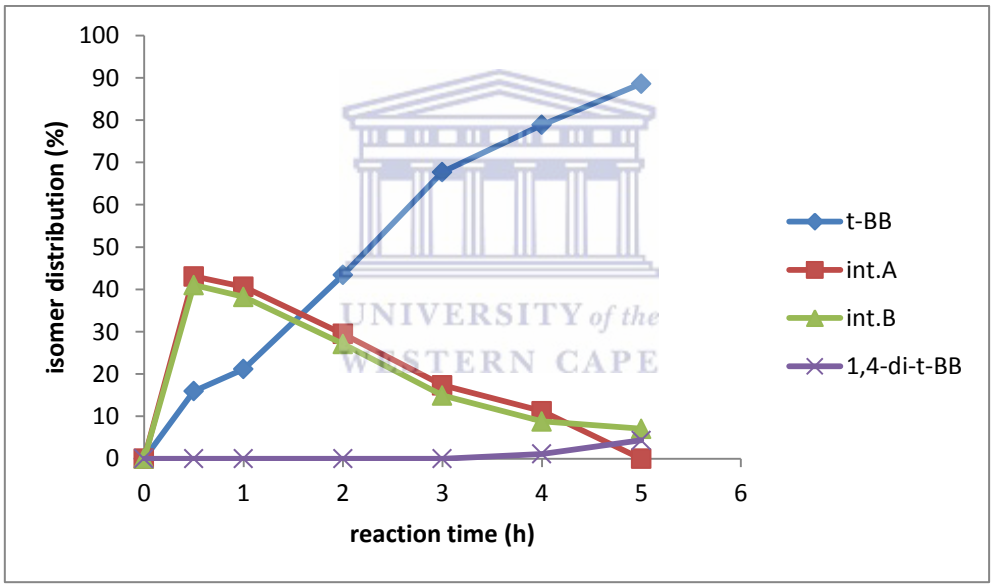

Figure 5.6: Product distribution for benzene alkylation with t-butyl chloride over 10%MnH at a temperature of 45 ^{o}C

The product distribution curve, over 10%MnH presented in Figure 5.6 shows that steady state was not achieved in the 5 h window but transient state was extended significantly. Very small amounts of the *para* isomer were produced. However the effect of Mn can only be further ascertained upon making comparison with the various metal loadings on other supports since the Brønsted acid sites in the zeolite can also act as alkylating sites (Da et al, 2001). Although the percentage conversion of the 10%MnH was relatively low (29.2 % after 5 h) compared to the Fe loaded counterpart the

10%FeH (99.9 % after 5 h), it could be seen that the selectivity of the catalyst towards formation of the monoalkylated product was quite high (88.6 % and 85.9 % respectively). However the catalyst took much more time to establish such a product distribution and did not reach steady state during the time on stream. This could be attributed to the reduction in the active sites, since Mn itself is not an active alkylating catalyst but the Brønsted sites in the HBEA zeolite are. The inactivity of Mn was determined when the metal was loaded on MCM-41 which does not contain Brønsted acid sites and the catalyst was found to be inactive. The outcomes are presented in Section 5.3.1. Again the observations made with the 10%MnH showed that Mn improves the selectivity towards the formation of the monoalkylated product.

5.2.3.5 Product distribution over the HBEA supported metal catalysts

Steady state was reached for all the HBEA supported metal catalysts after 3 h time on stream. The product distribution for the HBEA supported catalysts after 3 h is presented in Table 5.1

Table 5.1: Product distribution for HBEA supported metal catalysts HBEA after 3 h at 45 ^{o}C.

catalyst	**product distribution (%)**			
	t-BB	*1,4-di-t-BB*	*int. A*	*int. B*
HBEA	77.7	-	14.2	8.1
0.25FeH	75.6	24.4	0	0
5%FeH	80.5	19.4	0	0.1
10%FeH	79.1	21	0	0
10%FeMnH	89.2	9.5	0	1.3
10%MnH	67.7	0	17.3	14.9

In all the cases after 3 h, the monoalkylated product was predominant with all the catalysts. However the initial stages of the reaction was characterised by the presence of the two intermediate products and later stages showed an increasing selectivity towards the *para* isomer. The *para* isomer was not detected in the reaction mixture over the parent HBEA support.

5.2.4 Product Yield over HBEA Supported Catalysts

One of the most important parameters in considering the activity of a catalyst is the yield of the desired product. The percentage yield of the desired product (*t*-butyl benzene) was determined over the set of HBEA supported catalysts studied and presented in Figure 5.7.

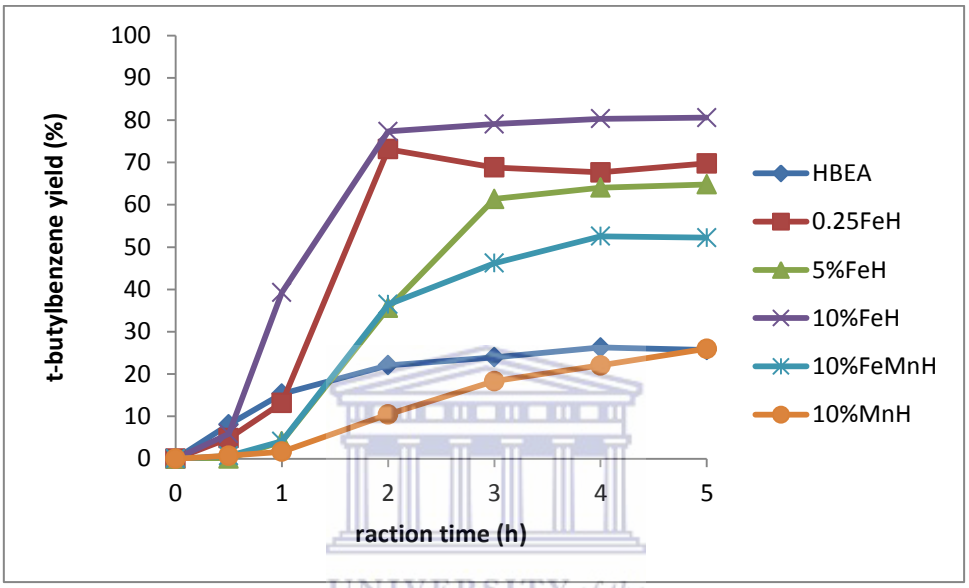

Figure 5.7: Percentage yield of t-butyl benzene as a function of reaction time over HBEA supported metal catalysts at 45 °C.

The highest yield obtained was 80.6 % achieved over the 10%FeH catalyst after a reaction time of 5 h. The lowest yield of 26 % after the same time on stream was obtained over the 10%MnH catalyst. It could be ascertained that a high conversion does not always lead to a high yield. The general trend observed was characterised by a rapid initial increase and steady state was achieved in the yield percentage at 2 h. The Mn containing catalysts had a lower yield in comparison to the monometallic Fe catalysts. Although the inclusion of Mn enhanced the product selectivity it reduced the conversion of the *t*-butyl chloride. The lower conversions resulted in the low yields (refer to equation 3 in Section 3.5.3). Since Fe catalysts tended to give high conversions and Mn doped catalysts gave high selectivities, this may lead to the belief of the existence of a specific Fe:Mn ratio that may give optimum yield. Generally the trends obtained in this study were in agreement with the normally observed trends associated with alkylation

reactions. Related trends in alkylation of aromatics were obtained and presented by Shimizu et al, (2008).

5.2.5 Summary of the Catalytic Activity of HBEA Supported Metals

For the first time the doping of Fe-HBEA catalysts with Mn for the alkylation of benzene with *t*-butyl chloride was studied and the general outcomes attested to the fact that the inclusion of Mn affected the product distribution and consequently the selectivity towards the formation of the monoalkylated product. Product selectivity in alkylation reaction is mainly influenced by the pore size of the support, however in this study it was found that the Mn tended to favour the formation of intermediates A and B (by-products) contrary to the formation of the *para* isomer (by-product) with Fe loaded HBEA, within the 5 h reaction time studied. In general the selectivity of the HBEA supported catalysts reached steady state after a reaction time of 3 h, and the highest selectivity of 89.2 % was obtained with the 10%FeMnH. The 10%MnH, which did not contain Fe did not reach steady state within the 5 h during which the reactions were studied.

In general the conversion, selectivity and yield reached a steady state after 3 h, so comparison of the catalytic activity is based on the outcomes generated after this reaction time. For the HBEA supported catalysts the conversion percentage ranged from 27 – 99.9 % at 3 h. The 10%FeH gave the highest and 10%MnH gave the lowest conversion. The selectivity range was from 67.7 – 89.2 % with 10%FeMnH giving the highest and 10%MnH the lowest. The product distribution for all the HBEA supported catalysts with the exception of 10%MnH, were characterised predominantly by two products, namely the primary product (*t*-butyl benzene) and the *para* isomer (1,4-di-*t*-butyl benzene). The 10%MnH had three products namely the primary product as well as the two intermediates A and B. Although the metal loaded catalyst gave rise to three products in the reaction mixture, it was noted that the formation of the *para* isomer was supressed. The percentage yield ranged from 18.3 – 79.1 % with the 10%FeH giving the highest yield and the 10%MnH giving the lowest. Assessment of these outcomes can lead to the conclusion that the 10%FeH was the most active of the HBEA supported catalysts. Table 5.2 presents the activity outcomes of the catalysts mentioned in this summary.

The outcomes showed that the alkylation of benzene under mild conditions can successfully be carried out with high conversion, selectivity and yields achievable. This may be a possible green alternative to the traditionally applied approaches that employ the use of $AlCl_3$ or mineral acids as catalysts. The use of strong mineral acids poses a lot of environmental hazards and corrosion to equipment, while the use of $AlCl_3$ is characterised with separation constrains. The selectivity of the desired product is also a great challenge and zeolite HBEA has proved to give a high selectivity towards the formation of the *t*-butylbenzene.

Table 5.2: Comparison of catalytic activity of metal centres supported on HBEA at 3 h time on stream at a temperature of 45 °C.

catalyst	**conversion %**	**selectivity %**	**product distribution**			**yield %**
			1,4-di-t-BB	*int. A*	*int. B*	
HBEA	30.8	77.7	0	14.2	8.1	23.9
10%FeH	100	79.1	20.9	0	0	79.1
10%FeMnH	51.8	89.2	9.5	0	1.3	46.2
10%MnH	27	67.7	0	17.3	14.9	18.3

The effect of the metal wt % on selectivity, conversion, product distribution and yield is discussed in broader details in Section 5.7.1.

5.3 Catalytic activity of MCM-41 supported metal catalysts

The conversion, selectivity, product distribution studies and yield over the MCM-41 supported metal catalysts were carried out at a temperature of 45 °C during a reaction time of 5 h. The outcomes are presented in the following sections**.** The conversion, selectivity and yields were calculated using equations presented in Section 3.5.4. The parent support MCM-41 was found to be inactive and the outcomes were therefore omitted in this discussion.

5.3.1 Conversion Studies on MCM-41 Supported Metals

Conversion studies for the MCM-41 supported metal catalysts were carried out over 5 catalysts of different metal loading and composition alongside the parent mesoporous MCM-41. The catalysts were prepared via two approaches namely incipient wetness

impregnation and ion exchange as presented in Section 3.3.1 and 3.3.3 respectively. The catalyst coding is presented in Tables 3.2 and 3.5. The benzene alkylation with t-butyl chloride reaction was carried out at a temperature of 45 ^{o}C as presented in Section 3.5.2. The conversion of *t*-butylchloride as a function of reaction time is presented in Figure 5.8.

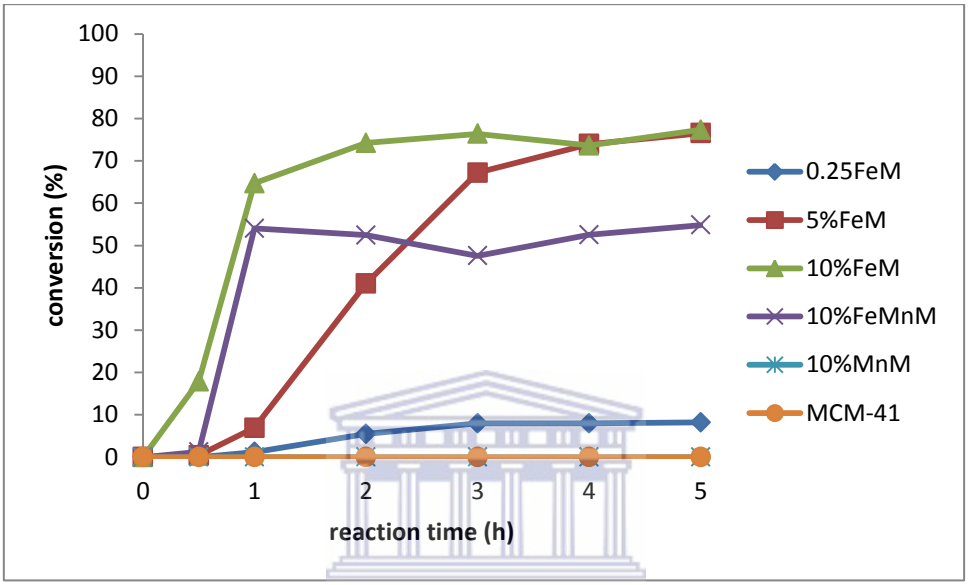

Figure 5.8: Conversion of t-butyl chloride over the series of MCM-41 supported Fe/Mn catalysts at 45 ^{o}C.

The parent MCM-41 was found to be inactive and the activity obtained over the MCM-41 supported metal catalysts can be attributed to the presence of the metal. In general the conversion trends obtained over the series of MCM-41supported metal catalysts were characterised by a rapid initial increase and then steady state was achieved within the first 3 h. The only catalyst that did not follow this trend was the 10%MnM, which was observed to be inactive. When Mn was supported on HBEA the catalyst was active however when the same metal was introduced on MCM-41 the resultant catalyst was inactive for the alkylation of benzene with *t*-butyl chloride. This can confirm that Mn by itself is not the active centre for this particular alkylation reaction. The activity of the Mn supported on HBEA can be ascribed to the presence of the Brønsted acid sites of the zeolite, which do not exist in MCM-41. Generally Mn is not applied for the alkylation

reaction and its inactivity is not surprising, Rueping and Nachtsheim, (2010) list a range of metals that are used for the FC alkylation of aromatics and Mn is not part of this list.

The highest conversion observed for this MCM-41 series was 77 % obtained over the 10%FeM, which had an actual Fe wt % loading of 12.2. A comparison of the 10%FeM (Figure 5.8) with the 10%FeH (Figure 5.1) indicates that the HBEA supported catalyst was more active despite the fact that the MCM-41 supported metal catalyst had a higher BET surface area compared to the corresponding HBEA supported metal catalyst. The BET surface area data for HBEA and MCM-41 is presented in Tables 4.11 and 4.12 respectively.This can be ascribed again to the additional presence of Brønsted sites within the HBEA framework which do not exist in MCM-41. It can be concluded that all MCM-41 supported metal catalysts prepared via incipient wetness impregnation gave a lower conversion relative to the corresponding metal catalysts supported on HBEA.

The 0.25FeM prepared via ion exchange gave a low selectivity relative to the other catalysts. This can be attributed to the fact that MCM-41 does not have Brønsted sites. Kim et al, (1995) reported that pure MCM-41 does not ion exchange, so the introduction of the metal can be said to occur via grafting. This leads to a low metal loading on the support in comparison to that which is obtainable with HBEA. This explains why the 0.25FeM had a conversion of 8 % compared to a conversion of 96 % with the 0.25FeH (Figure 5.1). The 0.25FeM had an actual Fe wt % loading of 2.2.

The introduction of Mn together with iron did not enhance the conversion over the MCM-41. The same trend was observed with the corresponding Mn containing bimetallic catalyst supported on HBEA. In terms of Fe content the 5%FeM and 10%FeMnM are comparable (refer to ICP-OES data in Tables 4.10 and 4.11) but the conversion differed a great deal. As discussed previously the introduction of Mn was to enhance the metal dispersion, but this did not improve the conversion.

Apart from the trend obtained over the 10%MnM, the general trends observed with the other 4 catalysts are in agreement with other trends obtained in related research activities although different alkylating agents and experimental conditions were applied (Van Bekkum and Kloetstra, 1998; Okumura et al, 2001; Choudhary and Jana, 2002; Mantri et al, 2005; Ahmed and Adam, 2009; Pineda et al, 2012).

5.3.2 Selectivity Studies on MCM-41 Supported Metals

The trends of the selectivity towards the formation of the monoalkylated product (t-butylbenzene) over the MCM-41 supported metal catalysts are presented in Figure 5.9.

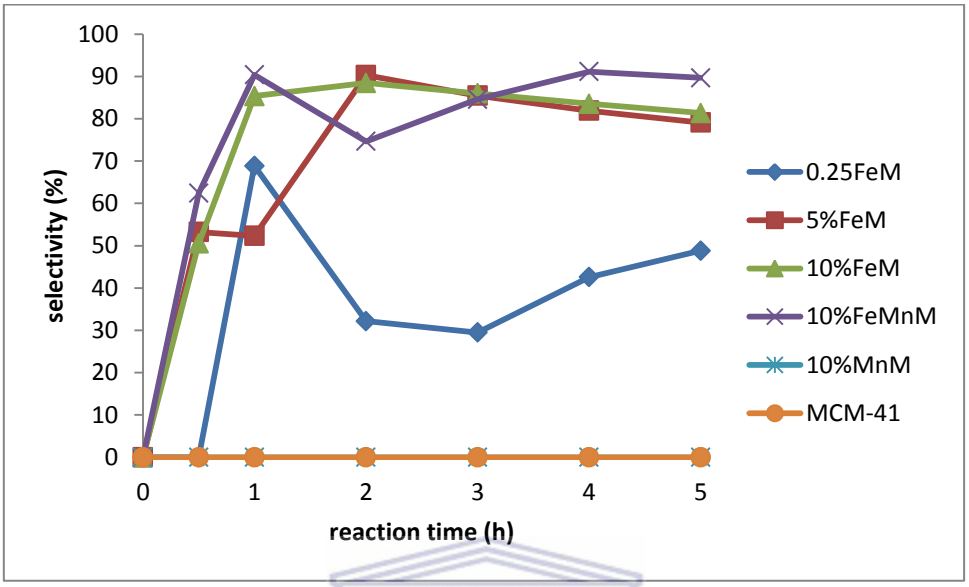

Figure 5.9:The monoalkylated selectivity-time curve for MCM-41 supported metal catalysts in the alkylation of benzene with t-butyl chloride at 45 °C.

The parent support material MCM-41 was found to be inactive and only the Fe supported catalysts were found to be active. The selectivity was characterised by a rapid initial increase towards the formation of the monoalkylated product whereafter the system reached a steady state after 2 h on stream. The trend obtained with the 0.25FeM was not similar to the other MCM-41 supported catalysts. The catalyst was prepared via ion exchange and had a low Fe weight percentage of 2.2 %.

The selectivity towards the formation of the monoalkylated product increased rapidly from 0.5 h to 1 h and then decreased in some cases followed by further increase in selectivity towards the formation of the monoalkylated product. The discrepancy observed in the trend for the 0.25FeM could be attributed to the low amount of metal loaded on the support. This would imply that there would be limited active sites leading to a reduction in the formation of the *t*-butylbenzene. This may slow down the full conversion of the intermediates to the monoalkylated product. The product distribution obtained over the 0.25FeM and presented in Figure 5.10 showed that there was significant formation of the intermediates within the first 2 h on stream.

The 10%FeMnM had an almost similar selectivity trend to that of the 0.25FeM, although it gave much higher selectivity than the 0.25FeM. This could be due to the fact that Mn tended to enhance the formation of intermediate products A and B as could be seen from the product distribution of the 10%FeMnM presented in Figure 5.11. The same was observed with the corresponding HBEA supported catalyst (10%FeMnH).

The highest selectivity obtained over the MCM-41 supported metal catalysts series was 91.1 % obtained over the 10%FeMnM after 5 h time on stream. The catalysts also gave a very high selectivity of 90.4 % after just 2 h on stream. This may lead to the conclusion that the inclusion of Mn does increase the selectivity towards formation of the monoalkylated product. However the pore system of the support material does have a significant role in product selectivity. A comparison of the selectivity obtained after 3 h time on stream for the 10%FeMnM, 10%FeM and 5%FeM were 85.5 %, 86 % and 84.6 % respectively. Although the metal content was different, with long reaction times the selectivity of the two catalysts was comparable. This further confirms the fact that the selectivity is dependant mostly on the pore system of the support rather than the amount of metal. However the effect of doping with Mn may be said to enhance the selectivity as well. In general the selectivity obtained over the MCM-41 supported metal catalysts was higher compared to the selectivity obtained over the HBEA supported metal catalysts. This may be ascribed to the differences in the pore system of the support materials. MCM-41 has external pockets and if the reaction occurs in these pockets there are reduced chances of having consecutive reactions like dialkylation due to the absence of confinement effects. In all the cases it was found that the amount of the *para* isomer was higher over the HBEA series than over the MCM-41 series. The effect of support material to selectivity is further discussed in broader detail in Section 5.6.2.

The selectivity curves obtained with the 10%FeM and 5%FeM follow the general trend observed in most alkylation reactions. Similar trends have been obtained in related research activities and reported in various articles (Udayakumar et al, 2004; Rac et al, 2007; Zhang et al, 2012). The trends were characterised by rapid initial increase and then steady state was reached. Bidart et al, (2006) studied the alkylation of aromatics over Zeolite Y and concluded that the reaction occurred in the pore system of the zeolite, hence selectivity was found to be mainly determined by the pore system of the

support and bulky molecules are suppressed from forming unless the support has large pores.

Although the trend obtained over the 0.25FeM was different it is however typical of alkylation reactions, a similar trend was presented by Selvaraj et al, (2005). In their study they reported the alkylation of toluene with *t*-butylalcohol over Al modified MCM-41. The decrease in the selectivity towards the formation on the 4-t-butyltoluene was attributed to insufficient acid sites to convert the reactants to the product (4-t-butyltoluene). The same could be said of the 0.25FeM since the amount of metal (Fe) on the catalyst was low (2.2 wt %, refer to ICP-OES data in Table 4.9).

5.3.3 Product distribution over MCM-41 Supported Catalysts

In the alkylation of benzene with *t*-butylchloride over the series of MCM-41 supported metal catalysts, the first stages of the reaction (< 2 h time on stream) were characterised by the formation of the monoalkylated product (*t*-butylbenzene), together with intermediates A and B, but long reaction times were characterised by the disappearance of the intermediates and the formation of the *para* isomer (1,4-di-t-butylbenzene) alongside the monoalkylated product. The parent MCM-41 was found to be inactive. On the other hand the Mn doped catalyst (10%FeMnM) tended to favour the formation of two intermediates A and B. The 10%MnM containing only Mn was found not to be active. The general trend observed over the series of MCM-41 supported metal catalysts was characterised by a rapid initial increase in the formation of the monoalkylated product together with intermediates which would then disappear within the first 2 h time on stream. However the 0.25FeM and the 10%FeMnM had slightly different product distribution trends and the outcomes are discussed in Sections 5.3.3.1 and 5.3.3.2 respectively. All the other Fe containing catalysts had the same trend as observed with the 10%FeM but with different product percentages. The product distribution obtained over the 10%FeM is presented in section 5.3.3.3. The product distribution obtained over other catalysts is presented in Table 5.3.

5.3.3.1 Product distribution over 0.25FeM

The product distribution obtained over the 0.25FeM was slightly different from the

other trends obtained over the other MCM-41 supported metal catalysts. The product distribution is presented in Figure 5.10.

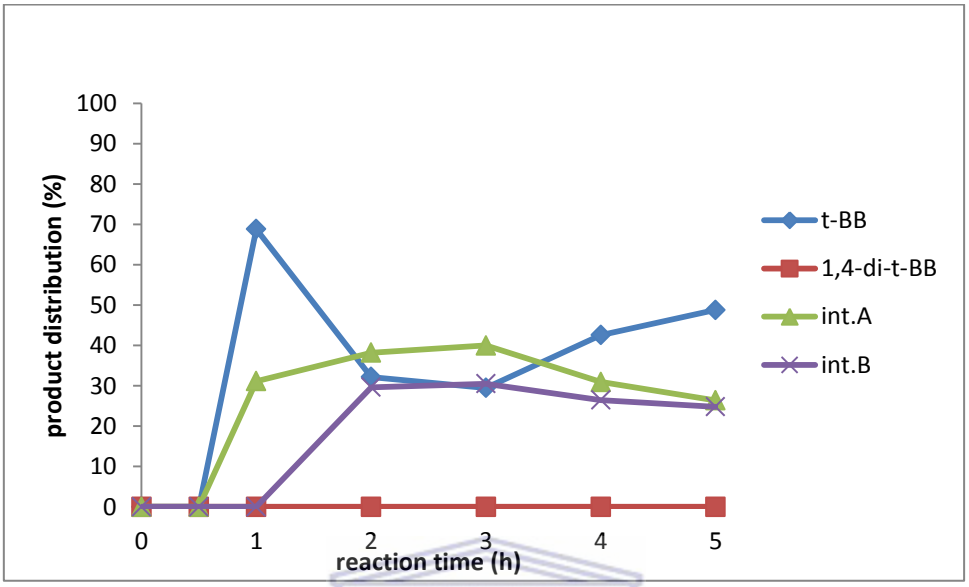

Figure 5.10: Product distribution for benzene alkylation with t-butyl chloride over 0.25FeM at 45 °C.

The 0.25FeM was prepared via liquid phase ion exchange and had an actual Fe wt % loading of 2.2 % (refer to ICP-OES data in Table 4.9). The reason for the low metal loading on the support may be attributed to the fact that the MCM-41 did not have Brønsted acid sites which are essential for the introduction of the metal on the exchange sites. The absence of Brønsted acid sites combined with the low metal loading may be attributed to the low selectivity of the monoalkylated product. The product distribution obtained over the 0.25FeM catalyst showed that there was a rapid initial increase during the first 1 h transient period of the reaction and this period was characterised by the formation of both the monoalkylated product as well as intermediate A. The percentage of the monoalkylated product reached a maximum of 68.8 % after 1 h time on stream. After 2 h there was a marked decrease in the percentage of the monoalkylated product which was then followed by a gradual increase after 3 h. Intermediate B increased rapidly between the first and second hour. The formation of significant amounts of the intermediates over this catalyst may be attributed to the low metal loading which consequently would reduce the number of active sites. It then may be said that the active sites were not sufficient to convert the intermediates into the monoalkylated product. It

should also be noted that within the 5 h reaction time studied over the catalysts the *para* isomer was not formed. This may be due to the low amounts of the monoalkylated product in the reaction mixture. The *para* isomer is formed via second alkylation of the monoalkylated product and since the levels of the monoalkylated product was low this could have hampered the formation of the *para* isomer which was observed after 3 h time on stream over the other catalysts supported on MCM-41 as well as the HBEA supported counterpart (0.25FeH).

5.3.3.2 Product distribution over 10%FeMnM

The product distribution obtained with the 10%FeMnM was a bit different from the trends obtained over the Fe monometallic catalysts supported on MCM-41. The trends obtained over the 10%FeMnM are presented in Figure 5.11.

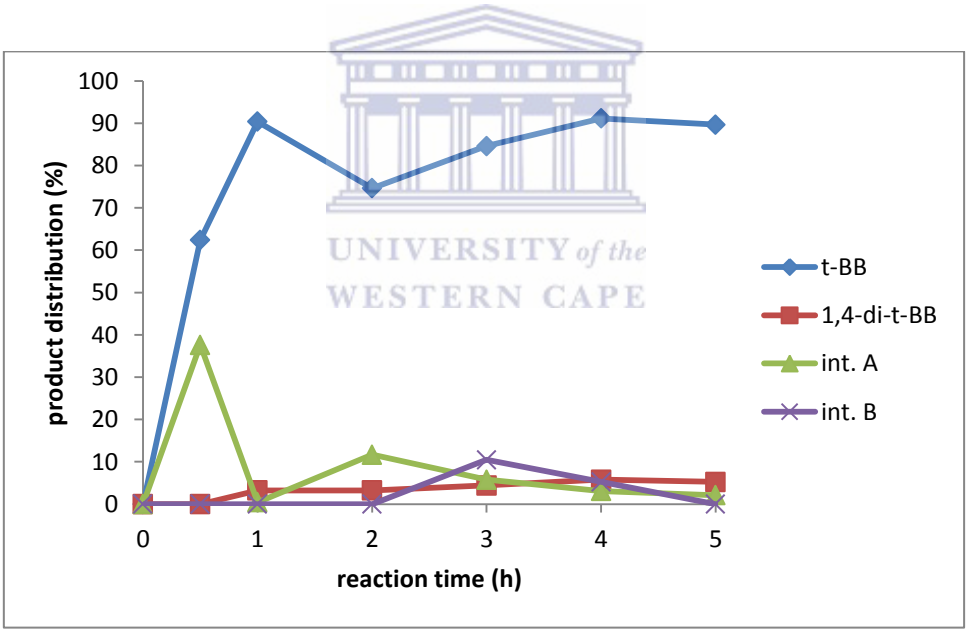

Figure 5.11: Product distribution for benzene alkylation with t-butyl chloride over 10%FeMnM at 45 °C.

The initial stages (<1 h time on stream) were characterised by a rapid increase in the percentage of both the monoalkylated product and intermediate A. The percentage of the monoalkylated product reached a maximum of 90.4 % after 1 h. This was the highest selectivity obtained over all the catalysts tested within this reaction time. This may then lead to the conclusion that the inclusion of Mn, although it does not enhance

the conversion, however enhanced the selectivity. The highest selectivity of 91.1 % over the 5 h time on stream was also obtained over the 10%FeMnM catalyst. It should however be noted that the MCM-41 pore system was found to have a significant effect on selectivity. Further discussion on the effect of support material on the selectivity is presented in Section 5.6.2. The tendency of Mn to favour the formation of the intermediates A and B could also be observed over the catalyst. The intermediates would form over Fe monometallic catalysts and disappear within 3 h time on stream. However with the Mn doped catalysts the intermediates persisted in the reaction mixture over the 5 h time on stream studied.

5.3.3.3 Product distribution over 10%FeM

Both product distribution curves generated with the 5%FeM and the 10%FeM had the same trend save for the percentages of the respective products. The 10%FeM had the highest conversion of the MCM-41 supported metal catalysts and it is discussed in this section. The product distribution obtained over the other catalysts supported on MCM-41 after 3 h time on stream is presented in Table 5.3. The complete product distribution data over the entire 5 h time on stream studied for the other catalyst are tabulated in the Appendix (A2). Figure 5.12 presents the product distribution obtained over the 10%FeM.

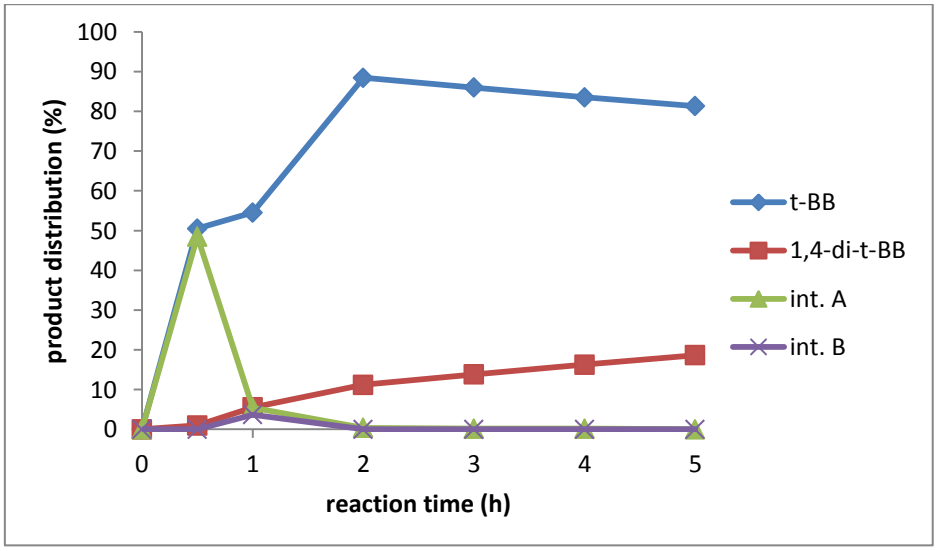

Figure 5.12: Product distribution for benzene alkylation with t-butyl chloride over 10%FeM at 45 °C.

During the first 0.5 h time on stream the percentage of both the monoalkylated product and intermediate A increased rapidly. The levels of the intermediate in the product stream began to decrease after this period whilst the monoalkylated product increased, reaching a maximum of 88 % after 2 h time on stream. After 2 h time on stream the levels of both intermediates A and B were very low, almost insignificant and the product mixture was mainly composed of the monoalkylated product and the *para* isomer as the only two products in the product stream. Once the monoalkylated product reached a maximum the relative amount began to decrease gradually, accompanied by a gradual increase in the formation of the *para* isomer. The increase in the *para* isomer may be attributed to the fact that the *para* position is activated after the first alkylation of the benzene ring, hence longer reaction times tended to favour the formation of the isomer.

A comparison of the product distribution curves obtained over the 10%FeMnM and the 10%FeM clearly depicted the influence that Mn doping had on the selectivity. In terms of metal loading both catalysts had about 10 % wt % metal loading. However the product distribution obtained over these two catalysts were found to be different. The inclusion of Mn tended to favour the formation of the intermediate products A and B whilst the monometallic Fe catalyst tended to favour the formation of the *para* isomer. Although it cannot be disputed that product selectivity and hence product distribution are largely dependent on the pore system of the support, the interaction of the respective metals studied resulted in different product distributions, and hence affected selectivity to an extent.

5.3.3.4 Product distribution over the MCM-41 supported metal catalysts

In general for benzene alkylation steady state was achieved after 3 h time on stream with all the catalysts supported on MCM-41. The product distribution of the catalyst supported on MCM-41 after 3 h at a temperature of 45 ^{o}C is presented in Table 5.3.

The selectivity to the monoalkylated product after 3 h time on stream for the metal loaded catalysts prepared via incipient wetness impregnation was almost comparable, giving an indication that the support does influence the selectivity. However at different points during the 5 h time on stream studied the product distribution varied and maximum selectivity for t-BB were obtained with the Mn doped catalyst (10%FeMnM).

The product distribution curves of each of the MCM-41 supported catalysts over the 5 h time on stream are presented in the Appendix (A1).

Table 5.3: Product distribution for benzene alkylation with t-butyl chloride over MCM-41 supported catalysts obtained after 3 h at 45 °C.

catalyst	**product distribution (%)**			
	t-BB	*1,4-di-t-BB*	*int. A*	*int. B*
MCM-41	0	0	0	0
0.25FeM	29.5	0	40.0	30.5
5%FeM	85.5	14.2	0.3	0
10%FeM	86.0	13.8	0.2	0
10%FeMnM	84.6	5.8	5.2	4.4
10%MnM	0	0	0	0

5.3.4 Product Yield over MCM-41 Supported Catalysts

The percentage yields of the *t*-butyl benzene produced over the MCM-41 supported metal catalysts are presented in Figure 5.13.

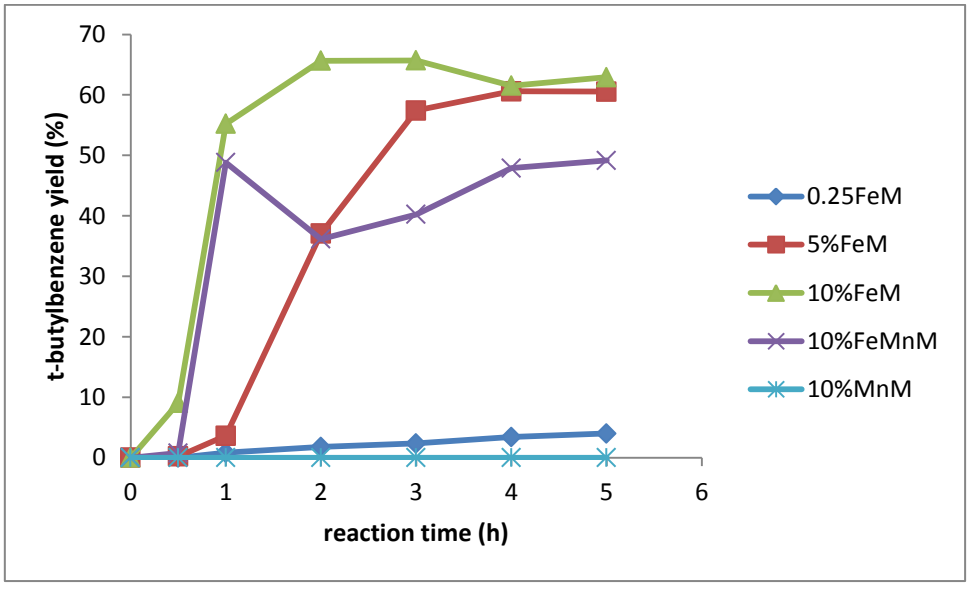

Figure 5.13: Percentage yield of t-butyl benzene as a function of reaction time over MCM-41 supported metal catalysts.

In general after 3 h time on stream, the yield of *t*-butylbenzene reached steady state and the 10%FeM gave the highest yield of 65.6 %. The second highest yield of 57.4 % at the same time on stream was obtained over the 5%FeM. It can be seen in Figure 5.13 that the monometallic Fe catalysts gave a higher yield of t-BB in comparison to the Mn doped catalysts. The lower yields obtained over the 10%FeMnM was due to the low conversion of the catalyst. Although the catalyst had a high selectivity it also had a low conversion. The percentage yield was calculated from both the conversion and selectivity according to equation 3 presented in Section 3.5.3. The inclusion of Mn on the MCM-41 support thus did not enhance the yield but rather reduced it. The 10%FeMnM had a comparable amount of Fe loaded as in the case of the 5%FeM, but at 3 h the 5%FeM had a yield of 57.4 % compared to a yield of 40.2 % obtained over the10%FeMnM. After 4 h, both the 10%FeM and the 5%FeM had comparable yields even though the 5%FeM contained about half the amount of active metal. This might be indicative that there is a threshold amount of Fe that is required to achieve the maximum yield of t-BB and any further increase would not enhance the yield.

In general the yields obtained over the HBEA supported metal catalysts were higher than those obtained over the MCM-41 supported metal catalysts. The conversion over the HBEA supported metal catalysts were relatively higher compared to the conversions obtained over the corresponding MCM-41 supported catalysts. The selectivity over the MCM-41 supported catalysts was relatively higher compared to the HBEA supported metal catalysts. The higher selectivity over the MCM-41 supported metal catalysts may be attributed to the lack of Brønsted acid sites on the MCM-41. The Brønsted acid sites are largely responsible for the formation of the arenium ions (rate determining step). Rapid formation of the arenium ions may lead to high rates of alkylation, which also paves way for the formation of dialkylated products since after the first alkylation the ring becomes activated.

The general trend was characterised by a rapid initial rise followed by steady state conversion. This is in agreement with related curves presented in literature on studies related to the present one although different alkylating agents and experimental conditions were applied (Okumura et al, 2001; Mantri et al, 2005).

5.3.5 Summary of the Catalytic Activity of MCM-41 Supported Metals

In this study for the first time, the combination of bimetallic Fe and Mn metals supported on MCM-41 have been tested for the alkylation of benzene with t-butyl chloride at a reaction temperature of 45 ^{o}C. As in the case of metal loaded HBEA, it was found that the inclusion of Mn did not enhance the conversion of the *t*-butyl chloride. Although the selectivity towards the formation of *t*-butylbenzene was enhanced by doping the Fe catalyst with Mn the yields were not high due to lower conversions. The same observation was made over the metal catalysts supported on HBEA. In general steady state was reached for all the catalyst after 3 h time on stream and comparison of the respective activities of the metal catalysts was based on the outcomes obtained after a reaction time of 3 h. The highest conversion, selectivity and yield were obtained over the 10%FeM, which were 76.4 %, 86 % and 66 % respectively. No conversion, selectivity and yield were obtained with the 10%MnM and the parent MCM-41, which were found to be inactive. In terms of product distribution the 5%FeM and the 10%FeM gave one dialkylated product, the *para* isomer whilst the other active catalysts produced intermediate products A and B in the reaction mixture. A good catalyst should give less by-products to avoid separation constraints. It could then be said that the 10%FeM performed better than any of the other catalysts prepared by supporting metals on MCM-41.

The HBEA supported metal catalysts gave better conversions relative to their metal counterparts supported on MCM-41. The lower conversions obtained over the MCM-41 supported metal catalyst series may be attributed to the absence of Brønsted acid sites in the MCM-41 mesoporous support. The Brønsted acid sites were found to be active when the parent HBEA was tested. The unloaded MCM-41 was tested and found to be inactive in the alkylation of benzene with t-butylchloride. However the MCM-41 supported metal catalysts generally gave a better selectivity towards the formation of the monoalkylated product when compared to the HBEA supported catalysts but with lower yields.

Again metal catalysts supported on MCM-41 may be a viable alternative for the traditionally employed $AlCl_3$ and mineral acid catalysts. The MCM-41 supported metal catalysts have the advantages of higher selectivity, easy separation from reaction

mixture as well as being a green synthesis route in the Friedel-Crafts alkylation reaction.

The effect of metal wt % loading on the catalytic activity is discussed in Sections 5.7 and 5.8. A summary of the respective catalytic activity after 3 h time on stream together with the highest activity achieved at different times are presented in Tables 5.8 and 5.9 respectively.

5.4 Catalytic activity of metal catalysts supported fly ash synthesised Zeolite X

The conversion of *t*-butylchloride over the fly ash synthesised Zeolite X was carried out at a mild temperature of 45 ^{o}C according to the procedure outlined in Section 3.5.2. The conversion was calculated using equation (i) in Section 3.5.3. The selectivity and percentage yield of t-butylbenzene was calculated using equations (ii) and (iii) presented in the same section.

5.4.1 Conversion Studies on Zeolite X Supported Metals

The trends obtained in the conversion studies of *t*-butyl chloride over metal catalysts supported on Zeolite X are presented in Figure 5.14.

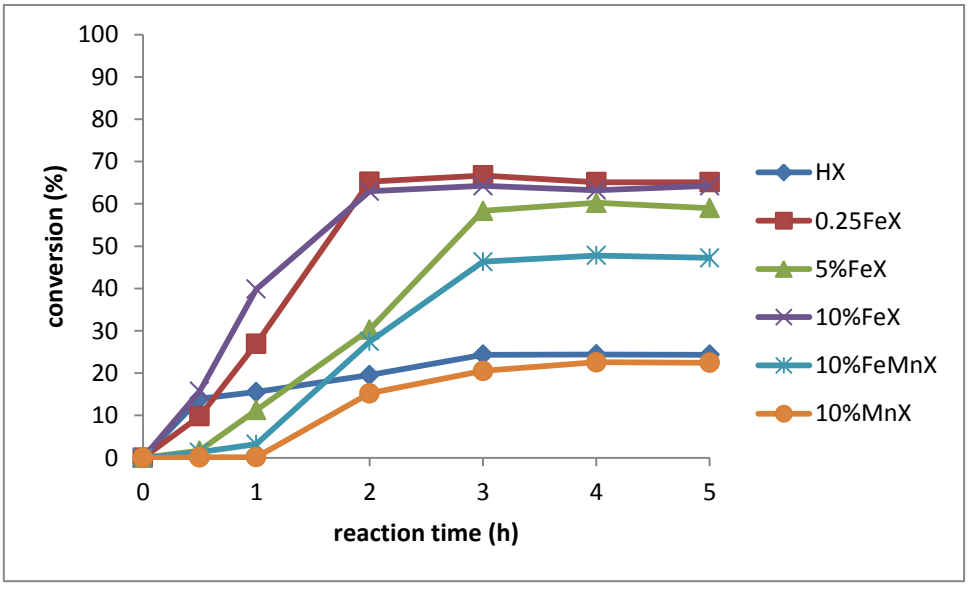

Figure 5.14: Conversion of t-butyl chloride over Zeolite X supported Fe/Mn at 45 ^{o}C

The trends were again characterised by a rapid initial increase reaching steady state between 2 – 3 h. The parent support (hierarchical Zeolite X) had a maximum conversion of 24 % after 4 h. The conversion obtained over the parent zeolite was higher than the conversion obtained over the Mn loaded zeolite. This indicates that the Mn is not active and the lower conversion may be attributed to the Mn blocking the Brønsted sites. This was also the case with HBEA. The highest conversion of 66.7 % was obtained over the 0.25FeX loaded via ion exchange, after 3 h time on stream. The Zeolite X supported catalyst had a Fe wt % of 11 (actual loading determined by ICP-OES and presented in Table 4.1). This amount of metal was comparable with the amount of Fe on the 10%FeX prepared via incipient wetness impregnation which had a Fe wt % loading of 12. The two catalysts gave comparable conversions. The conversion obtained over the parent Zeolite HX (maximum 24 %) was lower than that obtained over the parent HBEA (maximum 30.8 %). The difference may be attributed to the lower surface area of the Zeolite HX of 221 m^2/g against that of HBEA of 485 m^2/g. Another contributing factor might have been the difference in the acid strength of the respective zeolites. Zeolite X has weaker Brønsted acid sites compared to HBEA due to its low Si/Al ratio (HX = 1.6 ; HBEA = 13.8 from EDS data presented in Sections 4.4.3 and 4.4.1 respectively). Since the Brønsted acid sites take part in the rate determining step (arenium ion formation), their strength may influence the conversion. Due to the same attributes the conversions obtained over the metal loaded hierarchical Zeolite X were lower relative to those obtained over metal loaded HBEA. For all the metal catalyst prepared via incipient wetness impregnation and supported on Zeolite X, the conversions were found to be lower compared to those obtained over the corresponding metal catalysts supported on MCM-41. The higher conversion obtained over the MCM-41 may be ascribed to the high surface area of the mesoporous MCM-41 support (parent MCM-41 = 867 m^2/g). These outcomes lead to the conclusion that both the acid strength and the surface area influence the conversion.

It could again be seen from the trends presented in Figure 5.14 that the inclusion of Mn did not enhance the conversion of the *t*-butychloride. Comparison of the 10%FeMnX and the 5%FeX which contained comparable amounts of Fe showed that the monometallic catalyst gave a better conversion relative to the bimetallic counterpart. The lowest conversion after steady state was given by the 10%MnX. The Mn could be

said to be inactive as has been shown by the results obtained over the MCM-41 supported Mn catalyst. It however should be noted that the activity of the 10%MnX may be ascribed to the Brønsted acid sites in the zeolite rather that the Mn itself.

Bidart et al, (2001) studied the alkylation of benzene with *t*-butylchloride over Fe supported on Zeolite Y and obtained similar trends, which were characterised by a rapid initial increase followed by steady state. In their work they obtained a highest conversion of 86 % over Zeolite Y with a Fe wt % loading of 7. Zeolite Y is a member of the FAU zeolite family to which Zeolite X also belongs, hence it was expected to behave in a similar manner, but their catalyst had the characteristic hexagonal FAU morphology and a high BET surface area of 728 m^2/g.

5.4.2 Selectivity Studies on Zeolite X Supported Metals

The selectivity curves for the formation of t-butylbenzene obtained over the Zeolite X supported Fe/Mn catalysts are presented in Figure 5.15.

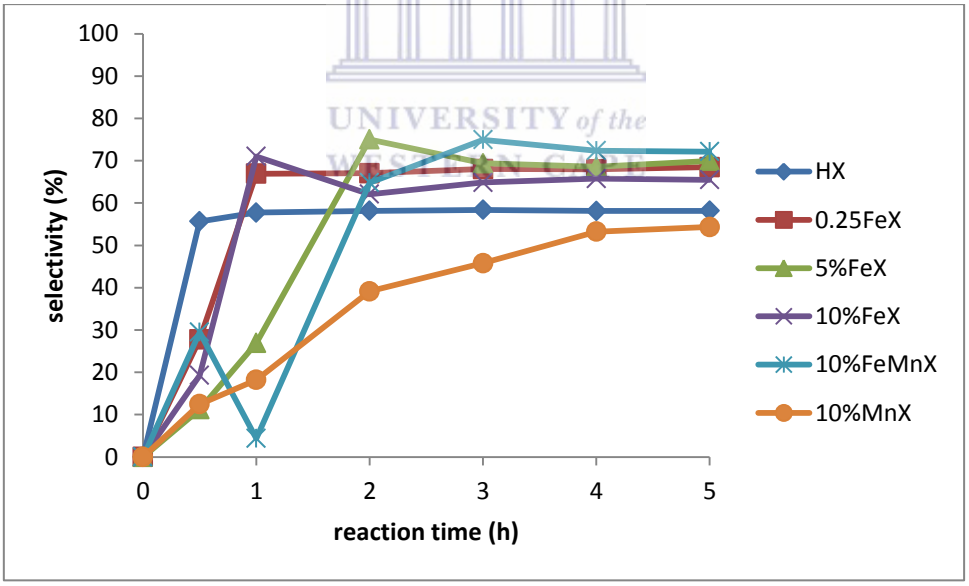

Figure 5.15: Selectivity studies towards the formation of t-butylbenzene over Zeolite X supported metal catalysts at 45 °C.

The selectivity trends obtained over the Zeolite X supported metal catalyst series presented in Figure 5.15, were again characterised by a rapid initial increase towards the formation of the monoalkylated product during the first 2 h reaching a steady state

thereafter. The parent zeolite HX gave a maximum selectivity of 58 % after 3 h time on stream. Metal incorporation only improved the selectivity slightly. Selectivity is mainly influenced by the pore system of the support rather than the metal loaded. The highest selectivity of 75 % was obtained over the 10%FeMnX. The same observation was made with the corresponding catalyst supported on HBEA, and the same reasons attributed to the outcome presented in Section 5.2.1 could be applied to the 10%FeMnX. The dealkylating nature of the Mn when co-impregnated with Fe was also observed as was the case with the HBEA supported bimetallic catalyst. The 10%FeMnX selectivity curve rose initially during the first 0.5 h, and then decreased followed by another rise and finally reaching a steady state. The same attributes of the HBEA counterpart can be said to apply for this particular catalyst.

The lower selectivity generally obtained over the series of the hierarchical Zeolite X supported metal catalysts may be attributed to the non-shape selectivity surface area in the meso and macropores of the hierarchical structure. Again zeolite X has a caged structure in the microporous region which may favour poly alkylation due to confinement effects. This will increase the formation of the dialkylated product and hence reduction in the selectivity towards the monoalkylated product. From the product distribution obtained over the Zeolite X supported metal catalysts it could be deduced that there was more of the dialkylated *para* isomer formed than on the other support materials HBEA and MCM-41. The product distribution obtained over the Zeolite X supported metal catalysts is presented in the following section.

Related research activities reported in literature brought up comparable outcomes where the selectivity trends for the monoalkylated product were characterised by a rapid increase followed by steady state. Bidart et al, (2001) studied the alkylation of benzene with t-butylbenzene over Fe loaded Zeolite Y and obtained a maximum conversion of 81 %. The surface area and morphology are cited in Section 5.4.1.

5.4.3 Product Distribution over Zeolite X Supported Catalysts

The reaction over the Zeolite X supported metal catalysts were characterised by the formation of both intermediate A and B in the initial stages of the reaction. The *para* isomer was then produced with longer reaction times alongside the disappearance of both intermediates. The disappearance of the intermediates could be attributed to their

low thermodynamic stability whilst the existence of the *para* isomer in the reaction mixture at longer reaction times could be attributed to its relatively high stability.

The product distribution curves obtained over the 0.25FeX, 10%FeMnX and the 10%FeX are presented in this section and the tables presenting the product distribution obtained over the other catalysts are presented in the Appendix.

5.4.3.1 Product distribution over 0.25FeX

The product distribution obtained over the 0.25FeX prepared via ion exchange is presented in Figure 5.16.

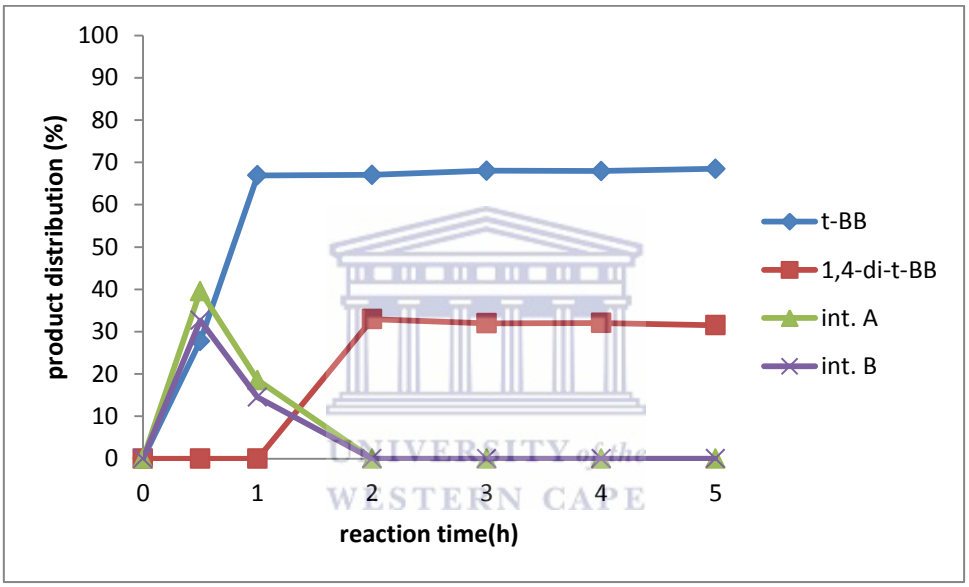

Figure 5.16: Product distribution for benzene alkylation with t-butyl chloride over 0.25FeX at 45 ^{o}C

It was observed that during the first hour, the reaction mixture was composed of four products. After 2 h time on stream, the mixture was entirely composed of the monoalkylated product and the *para* isomer. The highest percentage of the monoalkylated product obtained with the 0.25FeX was 68 % after a reaction time of 3 h. All the monometallic Fe catalysts had a similar product distribution trend except for the yields of the respective products. In comparison to the HBEA supported metal catalysts it could be seen that in general the Zeolite X supported metals gave a higher concentration of the dialkylated *para* isomer. This could be due to the non-shape selective active sites on the external surface area of the hierarchical Zeolite X

5.4.3.2 Product distribution over 10%FeMnX

The product distribution of the bimetallic catalyst the 10%FeMnX is presented in Figure 5.17.

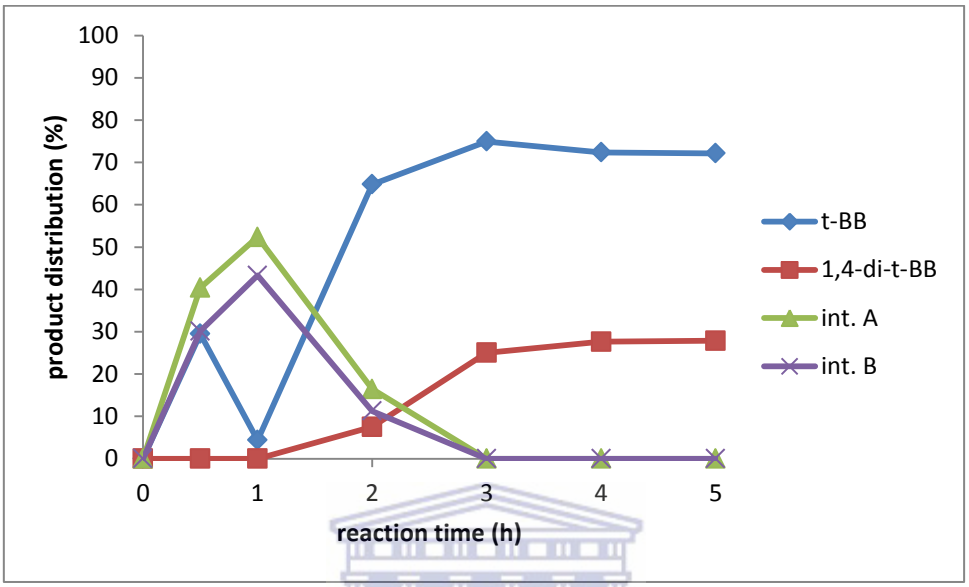

Figure 5.17: Product distribution for benzene alkylation with t-butyl chloride over 10%FeMnX.

The product distribution trend is closely related to the one obtained over the HBEA supported counterpart (10%FeMnH). It could be seen from Figure 5.17 that during the first 3 h, the product distribution was composed of all the 3 by-products together with the primary product (monoalkylated), but after this period the intermediates A and B disappeared from the product mixture with an increase in the levels of the *para* isomer as was the case for the ion exchanged sample (0.25FeX). Compared to the monometallic Fe catalysts supported on Zeolite X it could be seen that the production of the intermediate products were high over the bimetallic 10%FeMnX. The same was observed over the HBEA supported metal catalysts series. It can be seen that the inclusion of Mn slowed down the achievement of steady state and increased the length of transient start up.

5.4.3.3 Product distribution over 10%FeX

The monometallic Fe catalysts prepared via incipient wetness impregnation had a similar product distribution trend as those obtained over the 0.25FeX (prepared via ion

exchange), with varying amounts of the by-products. The same trends were observed over the HBEA supported Fe catalysts. The product distribution obtained over the 10%FeX is presented in Figure 5.18

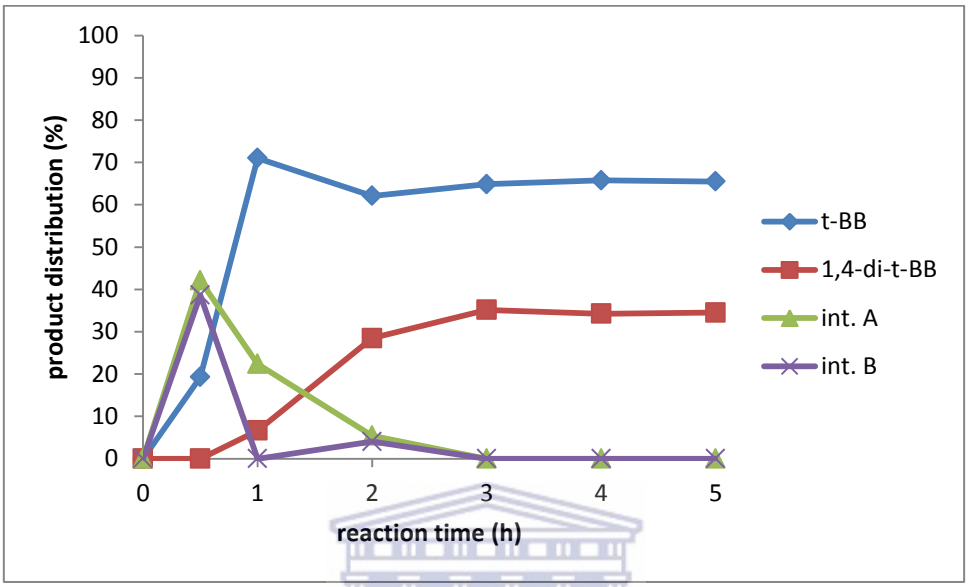

Figure 5.18: Product distribution for benzene alkylation with t-butyl chloride over 10%FeX.

Figure 5.18 shows that the highest percentage concentration of the monoalkylated product over the 10%FeX was 71 %, obtained after a reaction time of 1 h. It again could be seen that the initial stages of the reaction was characterised by a mixture of the two intermediates and the monoalkylated product. The intermediates disappeared from the reaction mixture with longer reaction times and the formation of the *para* isomer increased to a constant, at which the ratio of the monoalkylated product to the *para* isomer remained almost constant. Making a comparison with the HBEA supported analogue it could be established that the Zeolite X gave rise to more of the dialkylated product (*para* isomer), and this is attributed to the hierarchical structure of Zeolite X. The structure may have enhanced the formation of the *para* isomer on the external surface as the zeolite.

In general the product distribution curves obtained over the fly ash based Zeolite X supported metal catalysts were quite comparable with those obtained over the commercial HBEA supported catalysts.

5.4.3.4 Product distribution over the Zeolite X supported metal catalysts

Table 5.4 shows the reaction products obtained in the alkylation of benzene with *t*-butyl chloride over Zeolite X supported catalysts after a reaction time of 3 h, when steady state was achieved.

Table 5.4: Product distribution for benzene alkylation with t-butyl chloride over Zeolite X supported catalysts after 3 h.

catalyst	**product distribution (%)**			
	t-BB	*1,4-di-t-BB*	*int. A*	*int. B*
HX	58.5	0	23.2	18.3
0.25FeX	68	32	0	0
5%FeX	69.4	30.6	0	0
10%FeX	64.8	35.2	0	0
10%FeMnX	75	25	0	0
10%MnX	45.8	2.1	26.5	25.6

The monometallic Fe loaded Zeolite X catalysts gave the monoalkylated product together with intermediates A and B during the first 3 h. The parent HX gave a product distribution that was composed of the monoalkylated product and the intermediates only. This outcome was anticipated based on the generally accepted mechanism for the alkylation of benzene which suggests that the carbonium ion forms on the Brønsted acid sites and the deprotonation of the carbonium ion to form the alkylated product occurs on the Lewis acid sites. The 10%MnX gave rise to the formation of both the intermediate products and the *para* isomer was not detected in the reaction mixture after a reaction time of 3 h. In the case of the 10%FeMnX it could then be said that the Mn suppressed the formation of the *para* isomer. The same observation was made with the bimetallic catalysts supported on HBEA and MCM-41. The 5%FeX was found to be more selective towards the formation of the t-BB, than the 10%FeX. This outcome may be attributed to the loss in micropore surface area (shape selective area) with increased metal loading. The respective micropore surface areas for the 5%FeX and the 10%FeX were 87 m^2/g and 38 m^2/g. Incipient wetness impregnation was used to load the two catalyst (5%FeX and 10%FeX) and this approach is usually associated with surface restructuring and loss of surface area (Haber et al, 1995).

5.4.4 Product Yield over Zeolite X Supported Catalysts

The percentage yield of the monoalkylated product as a function of reaction time for the respective Zeolite X supported metal catalysts are presented in Figure 5.19.

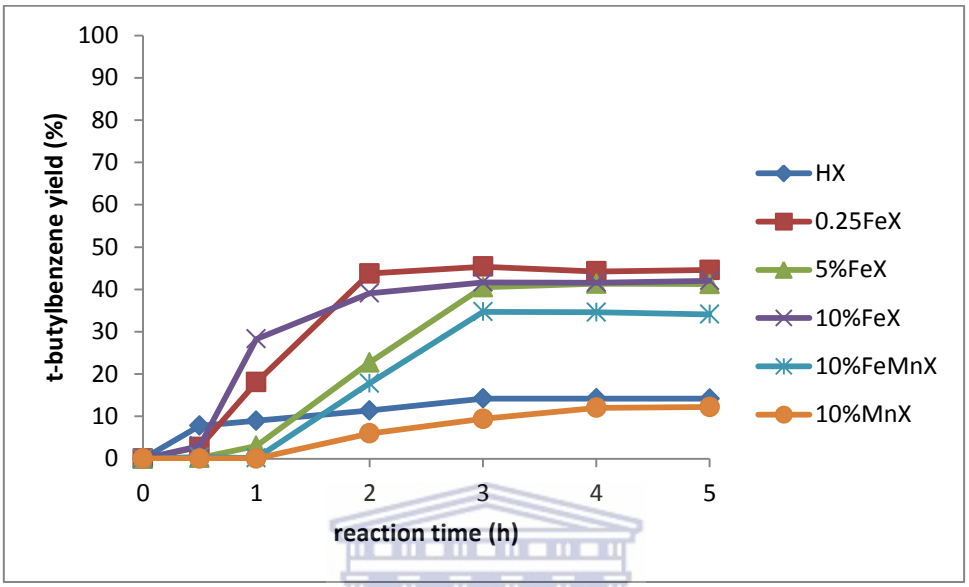

Figure 5.19: Percentage yield of t-butyl benzene as a function of reaction time over Zeolite X supported metal catalysts

The generated trends had a relatively rapid initial increase in the first 2 - 3 h reaching steady state at 3 h. The parent Zeolite X had a maximum yield of 14.2 % after 3 h time on stream. The highest percentage yield of 45.4 % after 3 h time on stream was obtained over the 0.25FeX prepared via ion exchange. This could be attributed to the good metal dispersion associated with the metal loading approach. The 5%FeX and the 10%FeX gave comparable yields of 40.5 % and 41.6 % respectively after 3 h time on stream. Despite the differences in the metal loading the yields were comparable. This may be attributed to the loss of surface area as the metal loading was increased. From the BET data the respective surface areas were 135 m^2/g and 95 m^2/g for the 5%FeX and the 10%FeX respectively. The lowest yield 9.4 % after a reaction time of 3 h, was obtained with the 10%MnX, this low value could be due to the inactivity of Mn as an alkylating catalyst. However the parent zeolite support itself has Brønsted sites which could have given it the alkylating activity observed. The fact can be further substantiated by the observed activity over the parent H-X zeolite. Generally the yields obtained over the

Zeolite X supported metal catalyst series were lower compared to the yields obtained over the HBEA supported metal catalysts of comparable metal wt % loading. The higher yields obtained over the HBEA series may be attributed to the larger surface area of HBEA as well as the higher acid strength.

5.4.5 Summary of the Catalytic Activity of Zeolite X Supported Metals

The activity of Fe/Mn supported on the fly ash based hierarchical Zeolite X has been studied for the first time in the alkylation of benzene with *t*-butylchloride. The highest conversion obtained over the Zeolite X supported metal catalysts after a reaction time of 3 h was 66.7 % obtained over the 10% FeX. The lowest conversion of 20.5 % was obtained over the 10%MnX. The inclusion of Mn enhanced the selectivity of the catalyst towards formation of the monoalkylated product but with low yields. The highest selectivity of 75 % after a reaction time of 3 h, was given by the bimetallic catalyst 10%FeMnX whilst the monometallic 10%MnX gave the lowest selectivity of 45.7 %. In general the product distribution obtained over the Zeolite X supported metal catalysts series showed that there was an increase in the amounts of the dialkylated product (*para*) relative to those obtained with the corresponding HBEA supported catalyst. This could be attributed to the larger cages of the Zeolite X relative to that of HBEA. The caged structure enhances the formation of bulky molecules due to the confinement effect. The Zeolite X also had a lower surface area and the conversions were lower on the zeolite X relative to the conversions obtained over the corresponding HBEA supported metal counterparts. After 3 h all the monometallic Fe catalyst gave the monoalkylated product alongside the *para* isomer. The existence of the *para* isomer is characteristic of the benzene alkylation reaction since the first alkylation activates the *para* position. The initial stages of the reaction was however characterised by the formation of both intermediates A and B. The highest percentage yield obtained was 45.4 % given by the 0.25FeX. The lowest percentage yield of 9.4 % was obtained over the 10%MnX. In general the catalytic activity of the Zeolite X catalysts was generally lower than that of the corresponding HBEA supported catalysts.

Based on the outcomes the fly ash based hierarchical Zeolite X can be an alternative support material that can be applied for the alkylation of benzene with *t*-butylchloride under mild conditions. Further optimisation studies ought to be carried out to determine

the most suitable conditions to load metal on the zeolite. Fly ash based supports will present a cheaper and green route in the synthesis of Friedel-Crafts alkylation catalysts. It is noteworthy that a fly ash based zeolite made from waste could be utilized for this reaction, showing the potential to create high value from waste beneficiation.

5.5 Effect of support on the catalytic activity

The effect of the nature of the support material on the conversion of the t-butyl chloride could be presented by making comparison with supported metal catalyst with related percentage metal loading.

5.5.1 Effect of support on conversion

To establish the effect of the nature of the support material on the conversion of *t*-butylchloride after 3 h time on stream, catalysts with 10 % Fe, 5 % Fe and 10% Fe/Mn supported on the respective supports are compared. The outcomes are presented in Table 5.5, showing the highest conversion achieved and the conversion obtained at 3 h. The comparison at 3 h was taken since it was noted that steady state was achieved for almost all the catalysts after 3 h time on stream.

Table 5.5: Effect of support material on the percentage conversion of t-butyl chloride

	catalyst support					
	HBEA		**MCM-41**		**Zeolite X**	
	highest con. %	*con. at 3 h %*	*highest con. %*	*con. at 3 h/ %*	*highest con. %*	*con. at 3 h/ %*
parent material	32	30.8	0	0	24.4	24.3
10%Fe	100	100	77	76	62	64
10%FeMn	62	62	23	22	48	46
5%Fe	89	76	77	67	60	58

In this study conversion was basically determined by three main factors; namely, surface area, Brønsted acidity and the amount of metal loaded on the zeolite. A comparison of catalysts with comparable metal loading should then differ in their conversions due to their differences in surface area and acidity of the respective support

materials used herein. The outcomes presented in Table 5.5, shows that the HBEA supported catalysts gave the highest conversion for each of the three different metal loadings. Generally the conversions obtained could be said to be fairly good with all the catalyst with the exception of the bimetallic (10%FeMnM) catalyst supported on MCM-41. The low conversion given by this catalyst could be attributed to the lack of Brønsted acid sites in the MCM-41. Another contributing factor might be the reduction in acid strength that could be induced by the partial reduction of Mn_2O_3/MnO_4, as discussed in previous sections.

The major differences between HBEA and the hierarchical Zeolite X are the respective surface area and acidity. The HBEA (485 m^2/g) had a higher surface area compared to Zeolite X (221 m^2/g). The larger surface area on HBEA could be said to have influenced the high conversions obtained over the HBEA supported metal catalyst series. On the other hand the Brønsted acidity of the HBEA was stronger than that of Zeolite X based on the Si/Al ratios obtained from EDS analysis. Although the MCM-41 did not have Brønsted acid sites, it had a fairly large surface area of 867 m^2/g, which was higher than either HBEA or Zeolite X. The high surface area may be ascribed to be responsible for the high conversions obtained over the MCM-41 supported metal catalyst series because of better dispersion of the metal. The conversion on the three tested support materials followed the order HBEA > MCM-41 > Zeolite X.

5.5.2 Effect of support on t-butylbenzene selectivity

The shape selectivity of a catalyst is said to be mainly influenced by the zeolite pore size, although metal composition, acidity of the support and reactant molar ratios are also major contributing factors. In this study the reactant molar ratios were kept relatively constant and the catalysts being compared had the same theoretical metal wt % loading. However the actual metal wt % loading was not necessarily the same. It has to be mentioned that to fully appreciate the effect of the support on the selectivity, different reactant molar ratios and the effect of the acidity of the support should be studied. The selectivity outcomes for the selected catalyst are presented in Table 5.6.

Table 5.6: Effect of support material on the percentage selectivity of t-butyl benzene

	catalyst support					
	HBEA		**MCM-41**		**Zeolite X**	
	highest sel %	*sel at 3 h %*	*highest sel %*	*sel at 3 h %*	*highest sel %*	*sel at 3 h %*
parent material	81	78	0	0	58	58
10%Fe	85	79	88	86	71	65
10%FeMn	89	89	91	85	75	75
5%Fe	90	81	90	86	75	69

The general outcomes reflected that both MCM-41 and HBEA gave comparable selectivity percentages even though the pore channels and surface area of the two supports were different. Hence the effect of the support on the selectivity cannot be fully ascribed to the size of the support pore channels or surface area. In the present work, benzene was used in excess, both as a reactant and as solvent. The use of excess benzene has an influence over the selectivity since it favours formation of the monoalkylated product (Bidart et al, 2001). Hence the effect of the support on the selectivity could not be well defined based on the outcomes generated in the present work. However the selectivity obtained over the Zeolite X supported was lower and this may be attributed to the presence of cages in the Zeolite X that may present confinement effects which generally favour polyalkylation (Dupuy et al, 2012).

5.5.3 Effect of support on yield of t-butyl benzene

The percentage yields of *t*-butyl benzene, obtained over the selected catalysts are presented in Table 5.7. The highest yield of 81 % was obtained over the 10%FeH, with the lowest yield given by the bimetallic catalyst supported on Zeolite X. Considering HBEA and MCM-41, the high yields obtained over the HBEA metal catalyst series may be attributed to the presence of the Brønsted acid sites on the HBEA which was not the case with MCM-41. Lewis and Brønsted acid sites are said to play a synergistic role in the alkylation of aromatics (Nur et al, 2011). On the other hand the hierarchical Zeolite X has both the Lewis and Brønsted acid sites but the yields obtained over the Zeolite X supported metal catalyst series were relatively lower in comparison to those obtained over both MCM-41 and HBEA.

Table 5.7: Effect of support material on the percentage yield of t-butyl benzene

	catalyst support					
	HBEA		**MCM-41**		**zeolite X**	
	highest yield/ %	*yield at 3 h/ %*	*highest yield/ %*	*yield at 3 h/ %*	*highest yield/ %*	*yield at 3 h/ %*
parent material	26	24	0	0	13	12
10%Fe	81	79	66	66	42	42
10%FeMn	55	55	49	40	35	35
5%Fe	65	61	61	57	41	41

The low yield may be attributed to the lower surface area of Zeolite X as well as the caged structure of the zeolite which is said to favour polyalkylation due to confinement effect. This reduces the selectivity and consequently the yield, since the yield was calculated from both the selectivity and conversion percentages. Generally the yield given by the Fe monometallic catalysts was in the order HBEA > MCM-41 > Zeolite X.

5.6 Effect of metal loading on catalytic activity

The effect of the amount of Fe wt % loading on the support to the catalytic activity can be depicted by following the HBEA series. A total of 3 monometallic Fe supported catalysts supported on HBEA were tested namely 5%FeH, 0.25FeH and the 10%FeH. The listed catalysts had the following Fe wt %; 4.8, 6.2, 7.2, and 12.4 respectively. To create a good comparison these catalysts were compared with the parent HBEA which was assumed to have a Fe wt % of zero. Figure 5.20 presents the effect of metal loading on the conversion of *t*-butylchloride, selectivity towards formation of t-butylbenzene and the yield of t-butylbenzene as a function of Fe wt % on the HBEA support.

The conversion of t-butylchloride was found to correlate positively with the amount of metal on the support material. It can be seen from Figure 5.20 that as the amount of Fe was increased the conversion also increased in almost a linear fashion. Hence the metal centres play a role in increased activity for the Friedel-Crafts alkylation of benzene with t-butylchloride. The selectivity was not affected by the amount of metal loaded on the support. The introduction of Fe on the HBEA support did not significantly alter the pore diameter of the zeolite, hence there were no diffusional constraints brought about by metal loading.

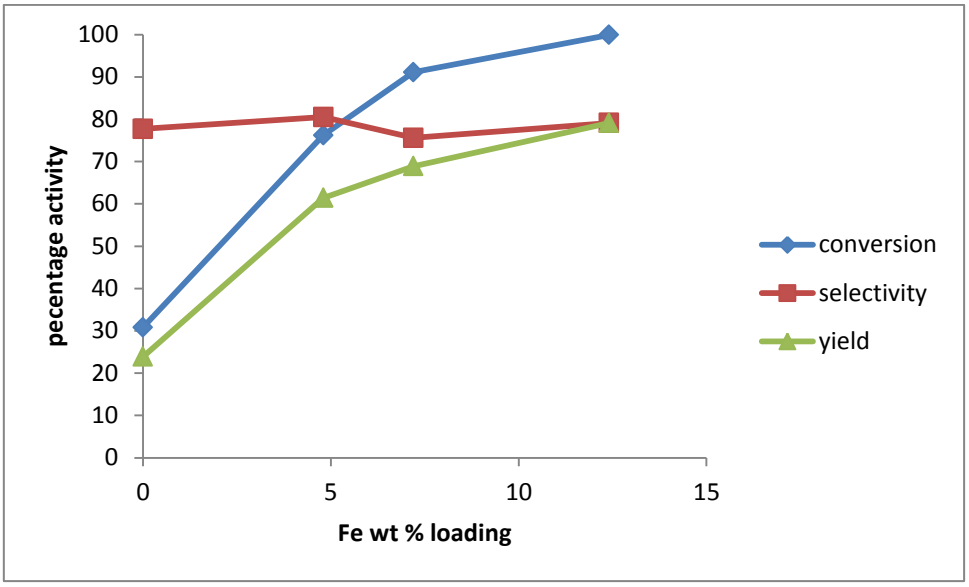

Figure 5.20: The correlation of metal loading with the conversion, selectivity and yield over HBEA supported metal catalysts after 3 h time on stream.

The percentage yield of *t*-butylbenzene obtained over the Fe supported on HBEA catalyst series also correlated positively with the amount of metal loaded. It has to be noted that the yield is calculated from both the conversion and selectivity. Since the selectivity was not much influenced by the amount of metal on the support it implies that the conversion affected the yield to a great extent hence the similarity in the obtained trends for both yield and conversion.

5.7 Effect of doping with Mn on the catalytic activity

The effect of doping the Fe catalyst with Mn was investigated on 3 catalysts supported on HBEA one with Mn alone, one with both Fe and Mn and one with Fe alone. The catalysts are, the 10%MnH (with actual Mn wt % of 12.5), 10%FeMnH (with actual Fe and Mn wt % loading of 5.1 and 5.8 respectively) and the 10%FeH (with Fe wt % of 12.4). The HBEA series was chosen for discussion since the catalysts gave high yields relative to metal catalysts supported on both MCM-41 and Zeolite X. Figure 5.21 presents the effect of Mn on the conversion, selectivity and yield. It however should be noted that the plots were made based on actual Mn : Fe wt % ratios on the catalysts.

The inclusion of Mn was found to decrease the conversion of t-butylchloride. From the trend in Figure 5.21 it can be seen that as the amount of Mn increased there was a decrease in the conversion. The decrease was almost linear and the same observation

was made over the other Mn doped catalysts supported on both MCM-41 and Zeolite X. The catalyst prepared with Mn alone also showed very low conversions and the 10%MnM was found to be inactive for the alkylation of benzene with t-butyl chloride. It can be concluded that Mn is not active in this particular reaction.

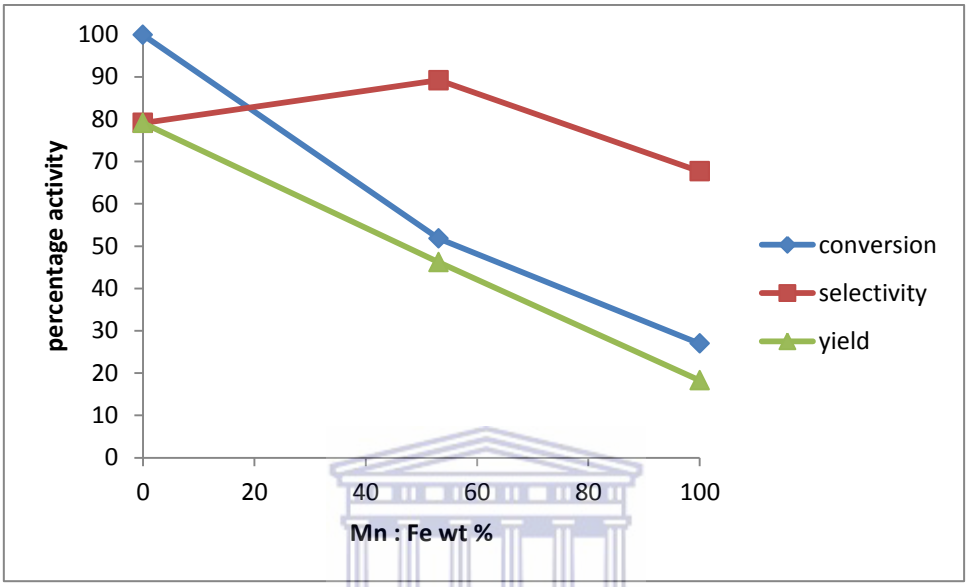

Figure 5.21: The effect of Mn inclusion on the conversion, selectivity and yield over HBEA supported metal catalysts after 3 h time on stream.

The selectivity towards the formation of the *t*-butyl chloride was found to increase slightly when the ratio of Fe:Mn was ~ 50:50. The selectivity then decreased over the HBEA supported catalyst that had Mn alone. It however would be difficult to draw a concrete conclusion on the exact effect of the bimetallic catalyst with Mn on the selectivity since only 3 catalysts are compared. A conclusive deduction would be possible if the ratio of Fe:Mn were varied and the selectivity trend followed. However the outcomes obtained herein may suggest that there is a ratio of Fe:Mn that might give optimum selectivity. However it cannot be disputed that the inclusion of Mn has an effect on the selectivity. The fact is further confirmed by the differences in the product distribution between the monometallic Fe catalysts and the Fe/Mn catalysts. The Mn bearing catalysts tended to favour the formation of the intermediate products at the expense of the *para* isomer. It could be said that the Mn blocks the active Fe sites that are largely responsible for the conversion of the arenium ion to the alkylated product.

It may be said that the inclusion of Mn slowed down the rate of reaction as the transient intermediates persisted for longer periods in the product mixture in comparison to the observed outcomes with the Fe monometallic catalysts. However looking at the selectivity percentages after a reaction time of 3 h, it could be established that the bimetallic catalyst gave a higher selectivity relative to the monometallic counterpart. The bimetallic catalyst (10%FeMnM) gave a selectivity of 90 % after a reaction time of 2 h. The inclusion of Mn may be thought to have influenced the outcome.

5.8 Effect of reaction time on catalytic activity

The general outcome obtained from the conversion and selectivity was such that the curves were characterised by transient start up during the first 2 – 3 h, which was followed by steady state. During the transient start up period the reaction mixture was composed of the monoalkylated product together with the two intermediates A and B. Longer reaction times were characterised by the disappearance of the intermediates and an increase in the amount of the *para* isomer. The *para* isomer was usually detected in the reaction mixture after a reaction time of 1 h, with most catalysts. The level of the *para* isomer gradually rises reaching a constant value which was mostly maintained to a period of 5 h. The same outcomes are reported by Bidart et al, (2001).

5.9 Chapter summary

The highest conversion achieved over the supported metal catalysts tested was 100 %, after a reaction time of 2 h, over the 10%FeH. The 10%MnM was found to be inactive in the benzene alkylation with *t*-butylchloride. A selectivity of 91 % was achieved over the 10%FeMnM after a reaction time of 4 h. Although selectivity is mainly ascribed to the pore system of the support, comparison with other catalyst of comparable metal loading supported on MCM-41 may lead to the conclusion that the inclusion of Mn enhanced selectivity towards the formation of the monoalkylated product but with low yields. However further investigations ought to be undertaken to establish the exact effect Mn has on the selectivity. The 10%FeH gave the highest yield of 81 %. The study also indicated that the amount of metal on the support correlated positively with higher conversion. It was established that the increase in the Fe wt % resulted in an increased conversion within the Fe wt % loading studied. The results also showed that the nature of the support chiefly influenced selectivity, and the MCM-41 was found to have a

better selectivity relative to the other two support materials HBEA and the fly ash based hierarchical Zeolite X.

The summary of the activity after 3 h time on stream (steady state was reached) of the supported metal catalysts studied are presented in Table 5.8. The highest activities of the respective catalyst achieved at various times on stream within the 5 h reaction time studied are presented in Table 5.9.

Table 5.8: Catalytic activity of supported metal catalysts after 3 h time on stream

catalyst	**conversion**	**selectivity**	**product distribution (%)**				**yield**
	(%)	(%)	*t-BB*	*1,4-di-t-BB*	*int. A*	*int. B*	(%)
HBEA	30.8	77.7	77.7	0	14.2	8.1	23.9
0.25FeH	91.1	75.6	75.6	24.5	0	0	68.9
5%FeH	76.2	80.5	80.5	19.3	0	0.1	61.4
10%FeH	99.9	79.1	79.1	20.9	0	0	79.1
10%FeMnH	51.8	89.2	89.2	9.5	0	1.3	46.2
10%MnH	27	67.7	67.7	0	17.3	14.9	18.3
MCM-41	0	0	0	0	0	0	0
0.25FeM	8	29.5	29.5	0	40	30.5	2.4
5%FeM	67.2	85.5	85.5	14.2	0.4	0	57.4
10%FeM	76.4	86	86	13.8	0.2	0	65.7
10%FeMnM	47.6	84.6	84.6	4.4	5.8	10.4	40.3
10%MnM	0	0	0	0	0	0	0
HX	24.3	58.4	58.4	0	23.5	18.2	14.2
0.25FeX	66.7	68	68	32	0	0	57.3
5%FeX	58.3	69.4	69.4	30.6	0	0	39.1
10%FeX	64.2	64.8	64.8	35.2	0	0	56.2
10%FeMnX	46.3	75	75	25	0	0	43.7
10%MnX	20.5	45.8	45.8	2.1	26.5	25.6	13

Table 5.9: Highest achieved catalytic activity of the supported metal catalysts within 5 h time on stream

catalyst	highest conversion	time (h)	highest selectivity	time (h)	highest yield	time (h)
	(%)		(%)		(%)	
HBEA	32	5	80.9	4	26.2	4
0.25FeH	96.1	5	90.1	2	73.1	2
5%FeH	89.3	5	90.1	2	64.8	5
10%FeH	99.9	2	85.9	1	80.6	5
10%FeMnH	62	1	89.2	3	55.3	3
10%MnH	30.7	4	88.6	5	26	5
MCM-41	0	n/a	0	n/a	0	n/a
0.25FeM	8.2	5	68.8	1	4	5
5%FeM	76.5	5	90.3	2	62.9	5
10%FeM	77.3	5	88.4	2	65.7	3
10%FeMnM	54.8	5	91.1	4	49.2	5
10%MnM	0	n/a	0	n/a	0	n/a
HX	24.4	4	58.4	3	14.2	3
0.25FeX	66.7	3	68.5	5	45.4	3
5%FeX	60.2	4	75	2	41.3	4
10%FeX	64.2	3	71	1	42.1	5
10%FeMnX	47.7	4	75	3	34.7	3
10%MnX	22.6	4	54.3	5	12.1	5

CHAPTER 6

6.0 Conclusion and recommendations

This chapter presents an overall conclusion of the outcomes generated in the present work. The chapter further presents some recommendations for further research as inspired by the very outcomes accrued in the present work.

6.1 Conclusion

The present study has shown that the hierarchical Zeolite X can be synthesised from fly ash via a hydrothermal treatment approach. The synthesised zeolite was characterised by a hierarchical morphology and plate like interwoven crystals. The conversion of the synthesised Na-form to the H-form was almost 100 % since no residual Na was detected by EDS analysis. The H-form had a BET surface area of 221 m^2/g. The HX zeolite was successfully loaded with Fe/Mn via two conventional approaches namely, liquid phase ion exchange and incipient wetness impregnation. The metal loading brought about some notable surface changes as the surface area was decreased upon metal loading. The XRD peak intensities also decreased when the metals were loaded onto the HX zeolite.

Using the same metal loading approaches commercial support materials, HBEA and MCM-41 were loaded with the same metals under the same conditions. The respective catalysts generated as well as the respective parent support materials were subjected to a range of characterisation techniques namely, SEM, HRTEM, XRD, EDS, SAED, ICP-OES and N_2-adsorption. Generally the integrity of the respective pristine support materials was retained upon metal loading. Analysis by EDS and ICP-OES showed that the loaded metals were indeed present on the respective support materials. In the case of the HBEA and MCM-41 supported metal catalysts the XRD patterns largely resembled the patterns of the parent support except in the case of the 10%FeH and the 10%FeM which exhibited peaks due to Fe_2O_3 crystallites. The HRTEM micrographs for all the metal loaded support materials were characterised by some dark fringes due to the metal crystallites formed on the external surface of the support. The metal crystallites were also visible on the SEM images obtained. The surface area studies by N_2-sorption attested to the fact that there was reduction in surface area upon metal loading.

Although the BET surface area reduced with increasing metal loading, there was increase in the number of active sites which consequently increased activity.The pore diameters of the HBEA and the MCM-41 largely remained unchanged upon metal loading. The parent HBEA had a pore diameter of 67.1 Å while the parent MCM-41 had a pore diameter of 25.6 Å. The parent HX had a pore diameter of 32.6 Å, but when loaded the diameter changed and in in the case of the 5%FeX and the 10%FeX the pore diameters were 51.6 Å and 40.1 Å respectively.

The synthesised catalysts were then tested for the alkylation of benzene with *t*-butychloride. The highest conversion of *t*-butylchloride of 100 % was obtained over the 10%FeH. The 10%MnM as well as the parent MCM-41were found to be inactive leading to the conclusion that Mn is not an active metal centre in the reaction. The Mn loaded Zeolite HBEA and HX were found to be active giving conversions of 32 % and 24.4 % respectively. The activity over these catalysts was due to the presence of the Brønsted acid sites on the zeolites and not due to the presence of Mn.

The highest selectivity towards the monoalkylated product (*t*-butylbenzene) of 91.1 % was obtained over the 10%FeMnM. The inclusion of Mn slightly enhanced the selectivity although the conversions obtained over the Mn doped catalysts were relatively lower in comparison to those obtained over monometallic Fe catalysts. Catalysts of comparable metal loading loaded on the respective support materials gave different selectivity. The selectivity followed the order MCM-41 > HBEA > Zeolite X.

The highest yield of the 80.6 % was obtained over the 10%FeH. In general the yields obtained over the Zeolite X supported metal catalyst series were relatively lower in comparison to the yields obtained over the HBEA supported metal catalysts. For the catalysts prepared via incipient wetness impregnation the yields followed the order HBEA > MCM-41 > Zeolite X. In the case of the catalysts prepared via liquid phase ion exchange the yields followed the order HBEA > Zeolite X > MCM-41.

It was also observed that the conversion of *t*-butylchloride had a positive correlation with increase in metal loading. Increase in metal loading did not significantly affect the selectivity over the respective support materials studied. Overall the supported metal catalysts studied proved to be a viable alternative to the traditionally applied catalysts which are usually non-porous Lewis acid or strong mineral acids. The use of solid acid catalysts would ease separation constraints and the environmental hazards associated

with both non-porous Lewis acids and minerals acids. In addition the supported metal catalysts give higher selectivity towards the formation of the monoalkylated product under mild conditions. Generally when either non-porous Lewis acid or mineral acids are used as catalysts the product distribution is composed more of the dialkylated product than the monoalkylated product. The application of the fly ash based hierarchical Zeolite X would present an additionl advantage since it creates high value from waste beneficiation.

6.2 Recommendations

The outcomes generated in this research encourages further research to ascertain and optimise a number of parameters in order to have a solid understanding of the scientific background of the observations as well as to create a catalyst that has higher activity. From the outcomes it was found that the inclusion of Mn does not enhance the conversion but it does slightly increase the selectivity towards the monoalkylated product. It is in this vein that future work should focus on studying the effect of varying the Fe:Mn ratio with intent to find the composition that gives optimum selectivity.

Other metal loading approaches need to be investigated as well and a comparison drawn with the outcomes herein. It was also observed that the Zeolite X suffered significant loss in surface area upon metal loading. Since the fly ash based hierarchical Zeolite X has a new morphology, the loading and post loading conditions may need further optimisation in order to come up with appropriate loading conditions. One of the primary factors that may be investigated is to load the zeolite at various pH values, or rather at a pH closer to the point of zero charge (PCZ) of the zeolite in the case of catalysts prepared via ion exchange. Calcination temperature and drying rates have a significant influence on the nature and character of resultant catalyst and these should be further investigated.

A sound understanding of the mechanistic progression of the reaction studied can be enhanced by investigating the kinetics of the reaction. The inclusion of Mn is believed to weaken the acid strength of the catalyst, so there is need to understand the extent to which the acid strength is weakened with each particular support.

The present study did not investigate the effect of varying the molar ratios of benzene to the *t*-butylchloride and the effect of varying the temperature. These two concerns should also be further explored to ascertain the optimum conditions.

CHAPTER 7

7.0 Appendix

A 1: Calculation for metal loading via incipient wetness impregnation

A typical calculation used to determine the amount of Fe salt [$Fe(NO)_3.9H_2O$] added to zeolite support in order to prepare a 1 g catalyst of Fe wt % loading of 10.

Worked example

10 % Fe loading on HBEA/MCM-41/Zeolite X

$Fe(NO)_3.9H_2O$ Mr = 404.00

To prepare 1 g of catalyst 10 % should be Fe

$$\frac{10}{100}\ x\ 1\ g = 0.1g$$

Mr of Fe = 55.845

404.00 g of salt has 55.845 g Fe

$$\frac{0.1}{55.845}\ x\ 404.00 = 0.7234\ g$$

Purity consideration

The salt was 98 % pure

$$\frac{100}{98}\ x\ 0.7234 = 0.7382\ g$$

1 g of catalyst should contain 90 % of support material, thus

$$\frac{90}{100}\ x\ 1\ g = 0.9\ g$$

Thus 0.9 g of support material should be mixed with 0.7382 g of $Fe(NO)_3.9H_2O$ to prepare a catalyst of 1 g with Fe wt % of 10.

A2: Product distribution over supported metal catalysts

The product distribution data obtained over some of the metal supported catalysts were not presented in Chapter 5 and the outcomes are tabulated in this section.

Table A2.1. Product distribution for benzene alkylation obtained over 0.25FeH at 45 ^{o}C

		product distribution			
catalyst	**TOS**	t-BB	1,4-di-t-BB	int. A	int. B
0.25FeH	0	0	0	0	0
	0.5	36.9702	0	33.361	29.6688
	1	55.355	0	23.4223	21.2227
	2	90.0605	9.9395	0	0
	3	75.5755	24.4245	0	0
	4	73.7456	26.2544	0	0
	5	72.6248	27.3752	0	0

Table A2.2. Product distribution for benzene alkylation obtained over 5%FeH at 45 ^{o}C

		product distribution			
catalyst	**TOS**	t-BB	1,4-di-t-BB	int. A	int. B
5%FeH	0	0	0	0	0
	0.5	0.3914	19.3114	36.1254	44.1718
	1	33.0242	0	35.2811	31.6947
	2	90.1169	7.6629	1.1194	1.1008
	3	80.5481	19.3128	0	0.1391
	4	76.1474	23.8526	0	0
	5	72.6052	27.29	0	0.1048

Table A2.3. Product distribution for benzene alkylation obtained over 5%FeM at 45 ^{o}C

		product distribution			
catalyst	**TOS**	t-BB	1,4-di-t-BB	int. A	int. B
5%FeM	0	0	0	0	0
	0.5	53.2258	0	46.7742	0
	1	52.3391	0	47.6609	0
	2	90.3129	8.0874	1.5997	0
	3	85.4534	14.1966	0.351	0
	4	81.9198	17.9455	0.1348	0
	5	79.1162	20.8838	0	0

Table A2.4. Product distribution for benzene alkylation obtained over 5%FeX at 45 ^{o}C

		product distribution			
catalyst	**TOS**	t-BB	1,4-di-t-BB	int. A	int. B
5%FeX	0	0	0	0	0
	0.5	51.142	0	0	48.858
	1	26.92	0	37.7586	35.3214
	2	75.0188	23.4454	1.07799	0.4578
	3	69.3789	30.6211	0	0
	4	63.5682	36.4318	0	0
	5	69.953	30.047	0	0

Table A2.5. Product distribution for benzene alkylation obtained over 10%MnX at 45 ^{o}C

		product distribution			
catalyst	**TOS**	t-BB	1,4-di-t-BB	int. A	int. B
10%MnX	0	0	0	0	0
	0.5	12.4587	0	45.3659	42.1754
	1	18.2001	0	42.1548	39.6451
	2	39.1289	0	31.269	29.6021
	3	45.7819	2.1345	26.454	25.6296
	4	53.236	4.1253	21.2389	21.3998
	5	54.3264	4.23659	20.20141	21.2356

Table A2.6. Product distribution for benzene alkylation obtained over the parent HX at 45 ^{o}C

		product distribution			
catalyst	**TOS**	t-BB	1,4-di-t-BB	int. A	int. B
HX	0	0	0	0	0
	0.5	55.6719	0	23.7457	20.5824
	1	57.7209	0	24.1886	18.0905
	2	58.1588	0	23.7448	18.0964
	3	58.3746	0	23.4659	18.1595
	4	58.1104	0	23.6741	18.2155
	5	58.1588	0	23.7448	18.0964

REFERENCES

Ackley, M.W., Rege, S.U. & Saxena H. (2002). Application of natural zeolites in the purification and separation of gases. Micro. & Meso. Mater. 61, p. 25–42.

Acres, G.J.K., Bird, A.J., Jenkins, J.W. and King, F. (1981) Catalysis Vol. 4. Kemball, C & Dowden, D.A. (eds). Royal Society of Chemistry, Great Britain, p. 1-5.

Adamczyk, Z. and Biaeck, B. (2005) Hydrothermal synthesis of zeolites from polish coal fly ash. Polish Journal of Environmental Studies Vol 14, No 6, p. 713-719.

Adams R. (1946) Organic Reactions, Vol. 3, John Wiley and Sons Inc. New York, p. 2.

Adriaens, A. & Dowsett M.G. (2004) Electron microscopy and its role in cultural heritage studies, *in* Non-destructive Micro Analysis of Cultural Heritage Materials, (eds) Janssens, K. & Van Grieken, R. Elsevier B.V., Amsterdam, p. 92 – 100.

Ahmed, A.E., & Adam, F. (2009) The benzylation of benzene using aluminium, gallium and iron incorporated silica from rice husk ash. Micro. & Meso. Mater, Vol. 118, Issues 1–3, p. 35–43.

Akbar, S. (2010) Characterisation of Beta Zeolites by X-ray diffraction, scanning electron microscopy and refractive index techniques. J. Chem. Soc Pakistan. 32, No 5.

Anderson, J.R. & Pratt, K.C. (1985) Introduction to characterization and testing of catalysts. Academic Press, Australia, p. 355-359.

Anuwattana, R. & Khummongkol, P. (2009) Conventional hydrothermal synthesis of Na-A zeolite from Cupola slag and aluminum sludge. J. Hazardous Mater., 166(1), p 227-232.

Armor, J.N., (2001). Ion exchange of non-framework cations in zeolites for catalysis, *in* Catalysis by unique metal ion structures in solid matrices from science to application. Centi, G., Wichterlova, B. and Bell, A.T., (eds). Nato Sciences Series, Neitherlands, p. 22- 26.

Ausavasukhi, A., Huang, Y., Ahn, T., Sooknoi, T., & Resasco, D,E. (2012). Hydrodeoxygenation of *m*-cresol over gallium-modified beta zeolite catalysts. Journ. of Cat. Vol. 290, p. 90–100.

Ayres, P.R. (2008) Investigating bacterial interactions with polymer surfaces using attenuated total reflectance fourier transform infrared spectroscopy. ProQuest LLC, USA, p. 9 – 10.

Babajide, O., Musyoka, N., Petrik, L. & Ameer, F. (2012). Novel zeolite Na-X synthesized from fly ash as a heterogeneous catalyst in biodiesel production. Cat. Tod. 190, p. 54– 60.

Bajpai, P. K., Rao, M. S. & Gokhale, K. V. G. K., (1981). Synthesis of mordenite type zeolite using silica from rice husk ash. IEC, PRD., 20(4), p. 721-726.

Balle, P., Geiger, B. & Kureti, S. (2009) Selective catalytic reduction of NOx by NH_3 on Fe/HBEA zeolite catalysts in oxygen-rich exhaust. App. Cat. B: Envin. 85, p. 109–119.

Bandini M., & Umani-Ronchi, A. (2009) Catalytic asymmetric Friedel-Crafts alkylations, Wiley-VCH. Weinheim, p. 3 – 10.

Belviso, C., Cavalcante, F. & Fiore, S. (2010) Synthesis of zeolite from Italian coal fly ash: Differences in crystallization temperature using seawater instead of distilled water. Waste Manag. 30(5), p. 839-847.

Bidart A.M.F., Borges A.P.S, Chagas H.C., Nogueira L.,Lachter E.R., & Mota C.J.A. (2006) Mechanistic Aspects of Friedel-Crafts Alkylation over FeY Zeolite. J. Braz. Chem. Soc, Vol. 17, No. 4, p. 758-762.

Bidart, A.M.F., Borges, A.P.S., Nogueira, L., Lachter, E.R. & Mota, C.J.A., (2001). Iron-exchanged zeolite as effective catalysts for Friedel–Crafts alkylation with alkyl halides. Cat. Letters. Vol. 75, No. 3–4.

Bisio, C., Massiani, P., Fajerwerg, K., Sordelli, L., Stievano, L., Silva, E.R., Coluccia, S. & Martra' G. (2006) Identification of cationic and oxidic caesium species in basic Cs-overloaded BEA zeolites. Micro. & Meso. Mater, Vol. 90, Issues 1–3, p. 175–187.

Bitter, J.H. & de Jong, K.P., (2009). Preparation of carbon-supported metal catalysts, *in* Carbon Materials for Catalysis. Serp, P. and Figueiredo, J.L., (eds). John Wiley and Sons, Inc, New Jersey, p. 158.

Bogdanov, B., Georgiev, D., Angelova, K. & Hristov, Y. (2009). Synthetic zeolites and their industrial and environmental applications review, International Science conference 4th - 5th June, Stara Zagora, Bulgaria.

Breck D.W. (1974) Zeolite molecular sieves, John Wiley & Sons, New York.

Brinker, C. J. and Scherer, G.W. (1990) Sol-gel science: The physics and chemistry of sol-gel processing. Academic Press, Boston.

Broach, R.W. (2010). Zeolite types and structures, *in* Zeolites in industrial separation and catalysis. Kulprathipanja, S., (ed). Wiley-VCH, Weinheim, p. 36-39.

Byrappa, K. and Yoshimura, M. (2001) Handbook of hydrothermal technology: A technology for crystal growth and materials processing. Noyes Publications New Jersey, p. 348.

Cahn, A. (1994) Proceedings of the 3rd world conference on detergents: Global pespectives. AOCS, Montreux, p. 162.

Cai, X., Cui, S., Qu, L., Yuan, D., Lu, B., & Cai, Q. (2008) Alkylation of benzene and dichloromethane to diphenylmethane with acidic ionic liquids. Cat. Comm. 9(6), p. 1173-1177.

Camblor, M. A., Mifsud, A. & Perez-Pariente J. (1991) Influence of the synthesis conditions on the crystallization of zeolite beta. Zeolites 11 p. 792.

Canfield, G.M., Bizimis, M. & Latturner, S.E. (2010) Transition-metal ion exchange using poly(ethylene glycol) oligomers as solvents. Chem. Mater. 22, p. 330-337

Carey, F.A. & Sundberg, R.J. (2007) Advanced organic chemistry: Part A: Structure and mechanisms. Springer, New York, p. 805 – 806.

Casci, J.L. (2005) Zeolite molecular sieve: Preparation and scale up. Micro. & Meso. Mater. 82 p. 217-226.

Chandrasekhar, S. & Pramada P.N. (1999) Investigation on the synthesis of zeolite NaX from Kerala kaolin. J. Porous Mater. 6, p. 283–297.

Chang, N., Gu, Z., Wang, Z., Liu, Z., Hou, X. & Wang, J. (2011) Study of Y zeolite catalysts for coal tar hydro-cracking in supercritical gasoline. J. Porous Mater. 8, p. 589–596.

Chen, X., Wendell, K., Zhu, J., Li, J., Yu, X., & Zhang, Z. (2012) Synthesis of nano-zeolite from coal fly ash and its potential for nutrient sequestration from anaerobically digested swine wastewater. Biores. Techn. 110, p. 79-85.

Cherkendorff, I. & Niemantsverdiet, J.W. (2007) Concepts of modern catalysis and kinetics, 2nd revised and enlarged edition. Wiley-VCH, Weinheim, p. 154.

Choudhary, V.R. & Jana S.K. (2002) Benzylation of benzene and substituted benzenes by benzyl chloride over $InCl_3$, $GaCl_3$, $FeCl_3$ and $ZnCl_2$ supported on clays and Si-MCM-41. J. Mol. Catal. A: Chem. 180, p. 267–276.

Clark J.H., (1998) Green chemistry: challenges and opportunities, Green Chemistry February 1999.

Coelho, M.A., Resasco, D.E., Sikabwe, E.C, & White, R.L. (1995) Modification of the catalytic properties of sulfated zirconia by addition of metal promoters. Cat. Letters 32, p. 253-262.

Corma, A., Moliner, M., Cantín, A., Díaz-Cabañas M.J., José L. Jordá, J.L., Zhang, D., Sun, J., Jansson, K., Hovmöller, S., & Zou, X. (2008) Synthesis and structure of polymorph B of Zeolite Beta. Chem. Mater. 20, p. 3218–3223.

Cornils B. & Herrmann W.A. (2006) Aqueous-phase organometallic catalysis: concepts and applications, 2nd completely revised and enlarged edition, Wiley-VCH p. 4.

Craciun, I., Reyniers, M-F., Guy B. & Marin, G.B. (2007) Effects of acid properties of Y zeolites on the liquid-phase alkylation of benzene with 1-octene: A reaction path analysis. J. Mol Catal A: Chemical 277, p. 1–14.

Cubillas, P. & Anderson, M. (2010) Synthesis mechanism: Crystal growth and nucleation, *in* Zeolites and Catalysis: Synthesis, Reactions and Application. Cejka, J., Corma, A. and Zones, S., (eds). Wiley-VCH, Weinheim, p. 12-27.

Da, Z., Han, Z., Magnoux, P, & Guisnet, M. (2001) Liquid-phase alkylation of toluene with long-chain alkenes over HFAU and HBEA Zeolites. App. Catal. A General 219, p. 45–52.

Damjanovic, L. & Auroux, A. (2009) Determination of acid/base properties by temperature programmed desorption. *in* Zeolite Characterization and Catalysis: A Tutorial. (eds) Chester, A.W. and Derouane, E.G. Springer, Heidelberg, p. 107 -123.

Daniel D.G. & Lobo C.L. (2005) User's Guide to ASTM Specification C94 on Ready-mix Concrete, ASTM International, pp. 29.

Davis, M.E. & Davis, R.J. (2003). Fundamentals of chemical reaction engineering. Mc-Graw companies Inc, Boston, p. 133-135.

Degnan, T. F., Smith, C. M. & Venkat, C. R. (2001) Alkylation of aromatics with ethylene and propylene: Recent developments in commercial processes. App.Catal. A; General, 221, p. 283 – 294.

Derkowski, A., Franus, W., Beran, E., & Czímerová, A., (2006). Properties and potential applications of zeolitic materials produced from fly ash using simple method of synthesis. Powder Techn. 166(1), p. 47-54.

Dey, K. P., Ghosh, S. & Naskar, M. K. (2012) A facile synthesis of ZSM-11 zeolite particles using rice husk ash as silica source. Mater. Letters, Vol. 87, p. 87–89.

Dhir R.K., Dyer T.D. & Halliday J.E. (2002) Sustainable Concrete Construction, Thomas Telford, USA.

Duke C.B. & Plummer E.W. (2002) Frontiers in Surface and Interface Science, Elsevier Science B.V. Amsterdam, p. 930-937.

Dupuy, B., Laforge, S., Morais, C., Bachmann, C., Magnoux, P. & Richard, F. (2012) Alkylation of 3-methylthiophene by 2-methyl-1-pentene over HY, HBEA and HMCM-22 acidic zeolites. App. Catal. A: General. Vol. 413–414, p. 192–204.

Dutta, P.K., Long, J.F., Williams, M.V. & Waldman W.J. (2008) Biological activity of mineral fibers and carbon particulates: implications for nanoparticle toxicity and the role of surface chemistry, in Nanoscience and nanotechnology:Environmental and health impacts. (ed) Grassian, V.H. Wiley and Sons Inc, New Jersey, p. 221.

Dymott, T.C. (1995) Application of ICP-OES techniques in environmental QC, *in* Quality Assurance in Environmental Monitoring: Instrumental Methods. Subramanian, G., (ed), VCH, Weinheim, p. 96 -97.

Eagleton, M. (1994) Concise encyclopedia chemistry. Walter de Gruyter and Co, Berlin, p. 535.

Eary, L. E, Rai, D., Mattigold, S.V & Ainsworth, (1990) Geochemical factors controlling the mobilization of inorganic constituents from fossil fuel combustion residues: II. Review of the minor elements" J. Environ. Qual. 19, p. 202 – 214.

Echlin, P. (2009) Handbook of sample preparation for scanning electron microscopy and X-ray microanalysis. Springer, New York, p. 2 -10.

Ersoz, M. & Barrott, L. (2012) Best practice guide on metal removal from drinking water by treatment. IWA Publishing, United Kingdom, p. 63.

Ertl, G., Knözinger, H. & Weitkamp, J. (1997) Hand book of heterogeneous catalysis, Volume 2, Wiley-VCH, Weinheim, p. 1997.

Eskom Holdings Limited (2012) available at http://www.eskom.co.za; [accessed on 27th September 2012.

Eyde, T.H. & Holmes, D.A. (2006) Commodities, *in* Industrial minerals and rocks: Commodities, markets and uses, 7th edition. Kogel, J.E., Trivedi, N.C., Barker, J.M., & Krukowski, S.T., (eds). Society for Mining Metallurgy and Exploration Inc, Colorado, p. 1041.

Fiore, S., Cavalcante, F. & Belviso, C. (2008) U.S. Patent Application 12/101,362.

Flugel, E. (2010) Microfacies of carbonate rocks: Analysis, interpretation and application, 2nd edition. Springer, Heidelberg, p. 321.

Folefoc, G.N. & Dweyer, J. (1992) Dispersion of platinum in Pt/ZSM-5 zeolites. J. Catal. Vol. 136, Issue 1, p. 43–49.

Fox M.A. & Whitesell J.K. (2004) Organic Chemistry, 3rd edition, Jones and Barlett Publishers, p. 530.

Freese, U., Heinrich, F. & Roessner, F. (1999). Acylation of aromatic compounds on H-beta zeolites. Catal. Tod. 49, p. 237–244.

Fultz, B. & Howe, J.M. (2002) Transmission electron microscopy and diffractometry of materials, 2nd edition. Springer, Heildelberg, p. 109.

Georgiev, D., Bogdanov, B., Angelova, K., Markovska, I. & Hristov, Y. (2009) Synthetic zeolites and their industrial and environmental applications review, International Science conference 4th - 5th June, Stara Zagora, Bulgaria.

Goodhew, J.P., Humphreys, J. & Beanland, R. (2001) Electron Microscopy and Analysis, *in* Electron Microscopy and Analysis. ed. Taylor and Francis, Taylor and Francis, London, p. 47-48.

Gottardi, G., & Galli, E. (1985) Natural Zeolites, Springer-Verlag, Berlin, p. 409.

Gupta, P., Li, F., Velazqueq, L., Sridhar, D., Iyer, M., Ramkumar, S. & Fan, L.-S. (2010) Chemical looping particles, *in* Chemical looping systems for fossil energy conversions. Fan, L.-S. (ed). John Wiley and Sons, p. 82-84.

Haber, J., Block, J.H. & Delmon, B. (1995) Manual of methods and procedures for catalyst characterisation, technical report. Pure & App. Chem. Vol. 67, Nos 8/9, p. 1257-1306.

Hancock E. G. (1975) Benzene and its industrial derivatives. London: Ernest Benn Limited.

Hania, H. A., El-Sayeda, M. M. H., Mostafab, A. A., El-Defrawya, N. M. & Soroura, M. H., (2012). Removal of Cr (III) in batch and pilot scale dynamic systems using Zeolite NaA prepared from egyptian kaolin. Int. Journ. 3(3).

Harmer M.A. & Sun Q. (2001) Solid acid catalysis using ion-exchange resins, App. Catal. A: General 221, p. 45–62.

Haw, J.F. (2002) Zeolite acid strength and reaction mechanisms in catalysis. Phys. Chem. Chem. Phys, 4, p. 5432 – 5441.

Hincapie, B.O., Garces, L.J., Gomez, S., Ghosh, R. & Suib, S.L. (2005). Direct synthesis of copper faujasite. Catal. Tod. Vol. 110, Issues 3–4, p. 323–329.

Hollman, G. G., Steenbruggen, G., & Janssen-Jurkovičová, M., (1999). A two-step process for the synthesis of zeolites from coal fly ash. Fuel, 78(10), p. 1225-1230.

Holmes, S.M, Khoo, S.H. & Kovo, A.S., (2011). The direct conversion of impure natural kaolin into pure zeolite catalysts. Green Chem., 13, p. 1152-1154.

Horňáčeka, M., Hudeca, P., Smiešková̱a, A. & Jakubíkb. T. (2009). Alkylation of benzene with 1-alkenes over Zeolite Y and Mordenite. ActaChimicaSlovaca, Vol.2, No.1, p. 31 – 45.

http://scienceworld.wolfram.com (visited 02/05/2013)

http://serc.carleton.edu (visited 30/04/13)

http://www.iza-online.org (visited 02/11/2012)

http://www.bza.org/zeolites.html (visited 02/11/2012)

http://www.zeolite.utm. (visited 11/06/2013)

Htun, M.M.H., Htay, M.M. and Lwin, M.Z. (2012) Preparation of zeolite (NaX, Faujasite) from pure silica and alumina sources, International conference on chemical processes and environmental, Issues, July 15-16, Singapore.

Hunger, M., (2009) Catalytically active sites: Generation and characterisation, *in* Zeolites and Catalysis: Synthesis, Reactions and Application. Cejka, J., Corma, A. and Zones, S., (eds). Wiley-VCH, Weinheim, p. 502.

Iijima, A., (1980). Geology of natural zeolites and zeolitic rocks, Pure & Appl.Chem., Vol. 52, p. 2115 - 2130.

Inada, M., Tsujimoto, H., Eguchi, Y., Enomoto, N. & Hojo, J. (2005) Microwave assisted zeolite synthesis from fly ash in hydrothermal process. Fuel. 84, p. 1482 - 1486.

Inglezakis, V.J. & Poulopoulos, S.G. (2006) Adsorption, ion exchange & catalysis: Design of operations & environmental applications. Elsevier, Amsterdam, p. 248 – 254.

Jiang, Y., (2003) Handbook of nanophase and nanostructured materials : Synthesis. Wang, Z.L., Lui, Y. and Zhang, Z. (eds). KluwerAcademic, New York, p. 67.

Kazemian, H., Naghdali, Z., Ghaffari Kashani, T. & Farhadi, F., (2010). Conversion of high silicon fly ash to Na-P1 Zeolite: Alkaline fusion followed by hydrothermal crystallization. Adv. Powder Technol,, 21(3), p. 279-283.

Kemball, C. (1977) Special Periodical Reports: Catalysis Volume 1, The Chemical Society, London, p. 88.

Kessler, H. (2001) Synthesis of high-silica zeolites and phosphate-based materials in the presence of fluoride, *in* Verified Synthesis of Zeolitic Materials, 2nd Revised Edition. Robson, H. (ed). Elsiever Science, Netherlands, p. 25.

Khandpur R.S. (2006) Handbook of analytical instruments. Tata McGraw Hill Publishing Co., New Dehli, p. 450 –451.

Khopkar, S.M. (1998) Basic concepts of analytical chemistry, 2nd edition. New Age International Publishers, New Dehli, p. 364.

Kim, D.S., Chang, J., Hwang, J., Park, S. & Kim, J.M. (2004) Synthesis of zeolite beta in fluoride media under microwave irradiation. Micro & Meso Mater. 68 (1-3), p. 77-82.

Kim, J.M, Kwak, J.H., Jun, S. & Ryoo, R. (1995) Ion exchange and thermal stability of MCM-41. Journal of Physical Chemistry 99, p. 16742-16747.

Kinger, G., Lugstein, A., Swagera, R., Ebel, M., Jentys, A. & Vinek, H. (2000) Comparison of impregnation, liquid- and solid-state ion exchange procedures for the incorporation of nickel in HMFI, HMOR and HBEA Activity and selectivity in n-nonanehydroconversion. Micro & Meso Mater. 39, pages 307 – 317.

Klabunde, K.J. & Richards, R.M. (2009) Nanoscale Materials in chemistry, 2nd Edition. John Wiley & Sons, Inc, New Jersey, p. 348.

Kodas, T. & Hampden-Smith, (1994) The chemistry of metal CVD, VCH Weinheim, p. 30

Kondamudi, K., Elavarasan, P., Dyson, P.J. & Upadhyayula, S. (2010) Alkylation of p-cresol with tert-butyl alcohol using benign Brønsted acidic ionic liquid catalyst. J. Mol Catal A: Chem. 321, p. 34–41.

Kong, Y., Zhu, H., Yang, G., Guo X., Hou W., Yan, Q., Gu, M. & Hu, C. (2004) Investigation of the structure of MCM-41 samples with a high copper content. Adv. Func. Mater. 14, No.8.

Konnov, S.V., Sushkevich, V.L., Monachova, Y.V, Yushcenkov, V.V., Panomareva, O.A. & Ivanova, I.I. (2008) Hydroisomerisation of n-octane over Pt-containing micro/mesoporous molecular sieves, *in* Zeolites and Related Materials: Trends Targets and Challenges. Gedeon, A., Massiani, P. & Babonneau, F. (eds), Elsevier, Amsterdam, p.1169.

Koster, A.J., Ziese, U., Verkleij, A.J., Janssen, A.H. & De Jong, K.P. (2000) Three-dimensional transmission electron microscopy: a novel imaging and characterization technique with nanometer scale resolution for materials science, J. Phys. Chem. B, 104, p. 9368-9370.

Kovalchuk, T.V., Sfihi, H., Korchev, A.S., Kovalenko, A.S., Il'in, V.G., Zaitsev, V. N. & Fraissard J. (2005) Synthesis, structure, and acidic properties of MCM-41 functionalized with phosphate and titanium phosphate groups. J. Phys. Chem. B, 109, p. 13948-13956.

Koyama, T., Takayanagi, K., Togawa, Y., Mori, S. & Harada, K. (2012) Small angle electron diffraction and deflection. American Institute of Physics, Advances 2, 012195

Kuhl, G., (2001). Source materials in Zeolite synthesis, *in* Verified Synthesis of Zeolitic Materials, 2nd Revised Edition. Robson, H. (ed). Elsiever Science, Netherlands, p. 19 - 20.

Kuhl, G.H., (1999). Modification of zeolites, *in* Catalysis and Zeolites: Fundamentals and Applications. Weitkamp, J., and Puppe, L., (eds). Springer, Heidelberg, p. 82-83.

Kuwahara, Y., Ohmichi, T., Kamegawa, T., Mori, K. & Yamashita, H. (2010) A novel conversion process for waste slag: synthesis of a hydrotalcite-like compound and zeolite from blast furnace slag and evaluation of adsorption capacities. J. Mater. Chem. 20(24), p. 5052-5062.

Kuwahara, Y., Ohmichi, T., Mori, K., Katayama, I. & Yamashita, H. (2008) Synthesis of zeolite from steel slag and its application as a support of nano-sized TiO_2 photocatalyst. J. Mater. Sci. 43(7), p. 2407-2410.

Kwakye-Awuah, B., Williams, C., Kenward, M. A. & Radecka, I. (2008) Antimicrobial action and efficiency of silver-loaded zeolite X. J. App. Microbiol. 104(5): p. 1516 – 1524.

Lai, C-H., Lu, M-Y. & Chen, L-J. (2012) Metal sulfide nanostructures: synthesis, properties & applications in energy conversion and storage. J. Mater. Chem. 22 p. 19-30.

Lee, C., Liu, S., Juang, L., Wang, C., Lin, K. and Lyu, M. (2007) Application of MCM-41 for dyes removal from wastewater. J. Hazard. Mater. 147, p. 997–1005.

Lee, J. W., Shin, J. Y., Chun, Y. S., Jang, H. B., Song, C. E., & Lee, S. G. (2010) Toward understanding the origin of positive effects of ionic liquids on catalysis: formation of more reactive catalysts and stabilization of reactive intermediates and transition states in ionic liquids. Acc. Chem.l Res., 43(7), p. 985-994.

Lerado, G.A., Castillo, J.J., Navarrete-Bolaños, J., Perez-Romo, P. & Lagos, F.A. (2012) Benzene reduction in gasoline by alkylation with olefins: comparison of beta and MCM-22 catalysts. App. Catal. A. General Vol. 413–414, p. 140–148.

Li, X., Yu, H., He, Y. & Xue, X. (2012) Synthesis of Fe-MCM-41 using iron ore tailings as the silicon and iron source. J Anal Methods Chem, Article ID 928720.

Li, Z., Fu, T.J., & Zheng, H.Y. (2011) Effect of preparation method on catalytic active center of CuY for oxidative carbonylation of methanol. Chin J Inorg Chem, Volume 27, Issue 8, p. 1483-1490.

Lima, P.M., Garetto, T., Cavalcante, C.L. & Cardoso, D. (2011) Isomerization of n-hexane on Pt–Ni catalysts supported on nanocrystalline H-BEA zeolite. Catal. Tod. 172, p. 195– 202.

Lobo, R.F, (2005) Introduction to the Structural Chemistry of Zeolites, *in* Handbook of zeolite science and technology. Auerabach, S.M., Carrado, K.A., & Dutta, P.K., (eds). Taylor and Francis, New York, p. 86.

Ma, L., Li, J., Arandiyan, H., Shi, W., Liu, C. & Fu, L. (2012) Influence of calcination temperature on Fe/HBEA catalyst for the selective catalytic reduction of NOx with NH_3. Catal. Tod. 184, p. 145– 152.

Malhotra V.M. & Mehta P.K. (1996) Pozzolanic and cementitious materials, Gordon and Breach Publishers.

Mantri, K., Komura, K., Kubota, Y. & Sugi, Y. (2005) Friedel–Crafts alkylation of aromatics with benzyl alcohols catalyzed by rare earth metal triflates supported on MCM-41 mesoporous silica. J. Mol. Catal. A: Chem. 236, p. 168–175.

Mathieson P.W. (1995) Mercury: God of TH2 Cells. Clin. Exp. Immunol. 102 (2), p. 229–230.

Matlob, A.S., Kamarudin, R.A., Jubri, Z. & Ramli, Z. (2011) Response Surface Methodology for a Green Synthesis of Zeolite Na-A. Eur J Sci Res. Vol. 60 No.4, p. 540-550.

McClelland, R.A. (2006) Carbocations, *in* Organic reaction mechanisms, Knipe, A.C. (ed). John Wiley & Sons, England, p. 241.

McMurry J.E. (2012) Organic Chemistry, 8th Edition, Brooks/Cole, p. 575 – 576.

McNaught, A.D. & Wilkinson, A. (1997) Compendium of Chemical Terminology, 2nd Edition. (the "Gold Book" IUPAC). Blackwell Scientific Publications, Oxford, p. 86.

Meier, W. M., Olson, D. H., & Baerlocher, C. (1996) Atlas of zeolite structure types, fourth edition. International Zeolite Association, Netherlands.

Meier, W.M., (1968) Zeolite structures, in molecular sieves. Society of Chemical Industry, London, p. 10 -27.

Meshram, S.U., Rayalu, S.S. & Kumar, P. (2004) Influence of crystallisation time on synthesis of fly ash based Zeolite A. *in* Advances in life sciences. Kumar, A. & Singh L.K. (eds) A.P.H. Publishing, New Dehli, p. 436 – 437.

Mohamed, M. M., Zidan, F. I. & Thabet, M. (2008) Synthesis of ZSM-5 Zeolite from rice husk ash: Characterization and implications for photocatalytic degradation catalysts. Micro & Meso Mater. 108(1), p. 193-203.

Mohammad, M.J., Karam, N.S. & AI-Lataifeh, N.K. (2004) Response of croton grown in a zeolite-containing substrate to different concentrations of fertilizer solution. Comm Soil Sci Plant Anal, Vol. 35, Nos. 15 and 16, p. 2283-2297.

Mokhonoana, M.P. (2005) PhD Thesis. The synthesis and study of some metal catalysts supported on modified MCM-41. University of the Witwatersrand, Johannesburg, p.168-177

Mokhonoana, M.P. & Coville, N.J. (2009) Highly loaded Fe-MCM-41 materials: Synthesis and reducibility studies, Materials, 2, p. 2337-2359.

Molina, A. & Poole, C. (2004) A comparative study using two methods to produce zeolites from fly ash. Minerals Engineering, 17(2), p. 167-173.

Morris, R.E. (2010) Ionothermal synthesis of zeolites and other porous materials. *in* Zeolites and catalysis: Synthesis, reactions and application. Cejka, J., Corma, A. and Zones, S., (eds). Wiley-VCH, Weinheim, p. 93.

Morris, R.E., Wormald, P., Webb, P.B., Wheatley, P.S., Andrews, C.D. & Cooper, E.R. (2004) Ionic liquids and eutectic mixture as solvent and template in synthesis of zeolite analogues. Nature 430, p. 1012-1016

Mortensen A. (2007) Concise Encyclopaedia of Composite Materials, 2nd Edition, Elsevier Ltd (UK)

Murat, M., Amokrane, A., Bastide, J.P. & Montanaro, L. (1992) Synthesis of zeolites from thermally activated kaolinite. Some observations on nucleation and growth. Clay Minerals 27, p. 119-130.

Murayama, N., Yamamoto, H. & Shibata, J. (2002) Mechanism of zeolite synthesis from coal fly ash by alkali hydrothermal reaction. Int. J. Min. Proc, 64(1), p. 1-17.

Musyoka N, MSc Thesis (2009) Hydrothermal synthesis and optimisation of zeolite Na-P1 from South African coal fly ash, Department of Chemistry, University of the Western Cape.

Musyoka, N.M, Petrik, L.F. & Hums, E. (2011) Ultrasonic assisted synthesis of zeolite A from coal fly ash using mine waters (Acid mine drainage and circumneutral mine water) as a substitute for ultra pure water. Mine Water – Managing the Challenges. Aachen, Germany.

Musyoka, N.M., Petrik, L. & Hums, E. (2012) Pending patent, University of the Western cape, South Africa.

Nagy, J.B., Bodart, P., Hannus, I. & Kiricsi, I. (1998) Synthesis, characterization and use of zeolitic microporous materials. Deca General Ltd, Szeged, Hungary.

Nares, R., Ramirez, J., Gutierrez-Alejandare, A., Louis, C. & Klimova, T. (2002) Ni/Hβ-Zeolite catalysts prepared by deposition-precipitation, J. Phys Chem B, 106, p. 13287-13293

Nur, H., Ramli, Z., Efendi, J., Rahman, A.N.A., Chandren, S. & Yuan, L.S. (2011) Synergistic role of Lewis and Brönsted acidities in Friedel–Crafts alkylation of resorcinol over gallium-zeolite beta. Catal. Comm. 12, p. 822 – 825.

Odedairo, T. & Al-Khattaf, S. (2012) Comparative study of zeolite catalyzed alkylation of benzene with alcohols of different chain length: H-ZSM-5 versus Mordenite. Cat. Letters. Vol. 204, p. 73–84.

Ojha, K., Pradhan, N.C. & Samanta, A.N. (2004) Zeolite from fly ash: Synthesis and characterization, B Mater Sci. Vol. 27, No. 6, p. 555–564.

Okumura, K., Nishigaki, K. & Niwa M. (2001) Prominent catalytic activity of Ga-containing MCM-41 in the Friedel-Crafts alkylation. Micro. & Meso Mater. 44-45, p. 509-516.

Olah, G.A. & Molnar, A. (2003) Hydrocarbon chemistry, 2nd Edition. John Wiley and Sons Inc, New Jersey, p. 230 - 232.

Othman Ali, I., Hassan, A. M., Shaaban, S. M. & Soliman, K. S. (2011) Synthesis and characterization of ZSM-5 zeolite from rice husk ash and their adsorption of Pb< sup> 2+</sup> onto unmodified and surfactant-modified zeolite. Sep. Pur. Technol, Vol. 83, p. 38

Oxford Business Group (2008) The Report: South Africa, the Oxford Business Group.

Parise, J.B., MacDoughall, J.E., Herron, N., Farles, R., Sleight, A.W., Wang, Y., Bein, T., Moller K. & Moroney, L.M. (1998). Characterisation of Se-Loaded Molecular Sieves A, X, Y, AlPO-5 and Mordenite. Inorg. Chem. 27 p. 221-228

Park, J., Kim, B. C., Park, S. S. & Park, H. C. (2001) Conventional versus ultrasonic synthesis of Zeolite 4A from Kaolin. J Mater Sci, 20(6), p. 531-533.

Park, J-K. (2012) Principles and applications of lithium secondary batteries. Wiley-VCH, Weinheim, p. 263

Park, M., Choi, C.L., Lim, W.T., Kim, M.C., Choi, J. & Heo, N.H. (2000). Molten-salt method for the synthesis of zeolitic materials: I. Zeolite formation in alkaline molten-salt system, Micro & Meso Mater. 37 p. 81-89.

ParvulescuV. & Su, B.L. (2000). Metallosilicate mesoporous catalysts prepared by incorporation of transition metals in the MCM-41 molecular sieves and their catalytic activity in selective oxidation of aromatics (styrene and benzene). Stud Surf Sci Catal 143. Vol. 143, p. 575–584

Pathak, C & Srivastava, V.K., (2012). Silica Reduction Technology for Fly Ash Zeolite Synthesis. Int. J. Pure Appl. Sci. Techno, 9(1), p. 47-51.

Pearce, J.R., Mortier, W.J., Uytterhoeven, J.B. & Lunsford, J.H. (1981). Crystallographic study of the distribution of cations in Y-type zeolites containing Fe^{II} and Fe^{III}. J. Chem. Soc, Faraday Transactions 1: Physical Chemistry in Condensed Phases, Vol. 77, Issue 4, p. 937-946.

Perego C. & Ingallina, P. (2002). Recent Advances in the industrial alkylation of aromatics: New catalysts and new processes. Cat. Tod. 73, p. 3–22.

Perego, C. & Villa, P. (1997). Catalyst preparation methods, Cat. Tod. 34, pages 281-305.

Perego, C., Amarillia, S., Millinia, R., Bellussia, G., Girottib, G. & Terzonib, G. (1996). Experimental and computational study of Beta, ZSM - 12, Y, Mordenite and ERB - 1 in cumene synthesis. Micro. Mater. 6, p. 395 – 404.

Pillay, A. & Peisach, M., (1990). Zeolite analysis PIXE, XRF or Neutron activation. J. Radioanal. Nucl. Chem 153(2) p. 75 – 84.

Pineda, A., Balu, A.M., Campelo, J.M., Luque, R., Antonio Angel Romero, A.A. & Serrano-Ruiz, J.C. (2012). High alkylation activities of ball-milled synthesized low-load supported iron oxide nanoparticles on mesoporous aluminosilicates. Cat. Tod. 187, p. 65– 69.

Pinna, F., (1998). Supported metal catalysts preparation, Cat. Tod. 41, p 129 – 137.

Polat, E., Karaka, M., Demir, H. & Onus, A.N., (2004). Use of natural zeolite (Clinoptilolite) in agriculture. J. Fruit Ornam. Plant Res. Vol. 12, Special ed.

Pollard, M.A. & Heron, C. (2008) Archaeological chemistry, 2nd edition. Royal Society of Chemistry, U.K, p. 29.

Prasetyoko, D., Ramli, Z., Endud, S., Hamdan, H. & Sulikowski, B., (2006). Conversion of rice husk ash to zeolite beta. Waste Manag. 26, p. 1173–1179.

Prasetyoko, D., Ramli, Z., Endud, S., Hamdan, H. & Sulikowski, B., (2010). Synthesis of Zeolite Beta directly from rice husk ash: Effect of reaction composition on crystallinity of Zeolite Beta. Indo. J Chem, 6(1), p. 11-15.

Price, G.L. (2007) Solid-State Ion-Exchange of Zeolites, *in* Catalyst Preparation: Science and Engineering. Regalbuto, J., (ed). Taylor and Francis Group, United States of America, p. 284.

Punshon, T., Seaman, J.C. & Sajwan, K.S. (2003) the production and use of coal fly combustion products, *in* Chemistry of trace elements in fly ash. Sajwan, K.S., Alva, A.K. and Keefer, R.F. (eds) Kluwer Academic New York, p. 1 – 6.

Querol Carceller, X., Moreno, N., Alastuey, A., Juan Mainar, R., Andrés Gimeno, J. M., López-Soler, Á., & Valero, A. (2007). Synthesis of high ion exchange zeolites from coal fly ash. Geologica Acta, 5(1) p. 49.

Querol X., Moreno N., Umana J.C., Alastuey A., Hernadez E., Lopez-Soler A. & Plana F. (2002) Synthesis of zeolites from coal fly ash: An overview. Int. J. Coal Geol, 50, p. 413-423.

Querol X., Moreno N., Umana J.C., Juan R., Hernandez S., Fernandez-Pereira C., Ayora C., Jassen M, Garcia-Martinez G.J., Solano L.A. & Amoros D. (2002) Application of zeolitic materials synthesised from fly ash to the decontamination of waste water and flue gas. J. Chem. Technol. Biotechnol, 77 p. 292-298.

Querol, X., Plana, F., Alastuey, A. & López-Soler, A. (1997). Synthesis of Na-Zeolites from Fly Ash. Fuel. 76 (8) p. 793-799.

Rac, B., Nagy, M., Palinko, I. & Molnar, A. (2007). Application of sulfonic acid functionalized MCM-41 materials-selectivity changes in various probe reactions. App. Catal. A: General 316, p. 152–159.

Rafalowski, M. (2003) Fly Ash Facts for Highway Enginners: Technical Report FHWA-IF-03-019, American Coal Ash Association, Virginia.

Rao, P.R.H.P., Ueyamaa, K. & Matsukata, M., (1998). Crystallization of high silica BEA by dry gel conversion. App. Catal. A: General 166 p. 97-103.

Rebeiro R.F., Rodrigues A.E., Rollmann D.C. & Naccache C. (1984) Zeolite: Science and Technology, Nato ASI Series (Applied Sciences – No. 80)

Reimer, L., (1998). Scanning electron microscopy: Physics of image formation and microanalysis, 2nd Edition. Springer, Heidelberg, p. 2-10.

Richardson, J.T. (1989) Principles of catalyst development. Plenum Press, New York, p. 6 – 7.

Riegel, R.E. & Kent, J.A., (2003). Riegel's Handbook of Industrial Chemistry, 10th Edition, Kluwer Academic, New York, p. 1131.

Ríos R, C. A., Oviedo V, J. A., Henao M, J. A. & Macías L, M. A., (2012). A NaY zeolite synthesized from Colombian industrial coal by-products: Potential catalytic applications. Cat. Tod. Vol. 190, Issue 1, p. 61–67.

Ríos, C. A., Williams, C. D. & Roberts, C. L., (2009). A comparative study of two methods for the synthesis of fly ash-based sodium and potassium type zeolites. Fuel, 88(8) p. 1403-1416.

Rocha, J., Klinowski, J. & Adams, J. M., (1991). Synthesis of zeolite Na-A from metakaolinite revisited. J. Chem. Soc., Faraday Transactions, 87(18), p. 3091-3097.

Rosenwald, R. H. (1949) Alkylation of phenols. *U.S. Patent No. 2,470,902*. Washington, DC.

Ross, J.R.H., (2012) Heterogeneous Catalysis: Fundamentals and Applications, Elsevier, Netherlands, p. 233.

Rueping, M. and Nachtsheim, B.J. (2010) A review of the new developments in the Friedel-Craftts alkylation- from green chemistry to asymmetric catalysis. Beilstein J. Chem., 6 no. 6.

Saer, L.K.A. (2001) Properties and use of coal fly ash: A valuable industrial by-product. Thomas Telford Publishing, London, p. 1-4.

Samir, D. (2009) Understanding the global environment, Dorling Kindersley pvt. ltd. India, p. 385.

Savage, N., Diallo, M., Duncan, J., Street, A. & Sustich, R. (2009). Nanotechnology for clean water. William Andrew Inc, New York, p. 199 – 200.

Savidha, R. & Pandurangan, A. (2004) Vapour phase isopropylation of phenol over zinc- and iron-containing Al-MCM-41 molecular sieves. App. Catal. A: General, Vol. 262, No. 1, p. 1-11.

Scheetz, B. E. & Earle, R. (1998) Utilisation of fly ash. Curr Opin Solid State Mater Sci 3, p. 510-520.

Schmidt, W. and Weidenthaler, C. (2001). A novel synthesis route for high surface area spinels using ion exchanged zeolites as precursors. Micro & Meso Mater. Vol. 48, Issues 1–3, p. 89 -94.

Schwuger, M. J. (1996). Detergents in the environment. Taylor & Francis, ISBN 0-8247-9396-X.

Selvaraj, M., Jeon, S.H., Han, J., Sinha, P.K. & Lee, T.G. (2005). A novel route to produce 4-t-butyltoluene by t-butylation of toluene with t-butylalcohol over mesoporous Al-MCM-41 molecular sieves. App. Catal. A: General 286, p. 44–51.

Sharadqah, S.I., & Al-Dwairi, R.A., (2010). Control of odorants emissions from poultry manure using Jordanian natural zeolites., Vol. 4, No. 4, p. 378-388.

Shigemoto, N., Hayashi, H. & Miyaura, K. (1993) Selective formation of NaX zeolite from coal fly ash by fusion with sodium hydroxide prior to hydrothermal reaction. Jordan J. Civ. Eng. Mater. Sci. 28, p 4781-4786.

Shimizu, K., Niimi, K. & Satsuma, A. (2008). Polyvalent-metal salts of heteropolyacid as catalyst for Friedel-Crafts alkylation reactions. App. Catal. A: General 349, p. 1–5

Shuvaeva, M. A., Nuzhdin, A.L. Bayukov, O.A., Martyanov, O.N. & Bukhtiyarova, G.A. (2011) Synthesis and characterization of silica supported iron-containing catalyst for the Friedel-Crafts benzylation of benzene,*in* Proceedings of the 2nd European conference of Control, and Proceedings of the 2nd European conference on Mechanical Engineering,WSEAS, Spain, p. 126-131.

Singh, R. & Dutta, P.K., (2003). MFI: A case study of zeolite, *in* Handbook of Zeolite Science and Technology. Auerabach, S.M., Carrado, K.A. & Dutta, P.K. (eds). Marcel Dekker Inc., New York., p. 31.

Sirotin, S.V., Moskovskaya, I.F. & Romanovsky, B.V. (2011). Synthetic strategy for Fe-MCM-41 catalyst: a key factor for homogeneous or heterogeneous phenol oxidation. Catal. Sci. Technol. 1, p. 971–980

Smith, M.B. & March, J., (2007). March's advanced organic chemistry: Reactions, mechanisms and structure, 6th edition, John Wiley & Sons, Inc, New Jersey, p. 712.

Smith, M.B., (1946). Organic synthesis. Academic Press, United States of America, p. 1996-2000.

Snyder, R. (1981) The Alkyl Benzenes, Committee on Alkyl Benzene derivatives, Assembly of Life Sciences (US), National Academy Press, p. 1.

Solt, H., Lonyi, F., Miha´lyi, R.M., Valyon, J., Gutierrez, L.B. & Miro, E.E., (2008) A Mechanistic Study of the Solid-State Reactions of H-Mordenite with Indium(0) and Indium(III)oxide. J. Phys.l Chem. C, 112, p.19423–19430

Somerset V., Petrik L. & Iwuoha E., (2008). Alkaline hydrothermal conversion of fly ash precipitates into zeolites 3: The removal of mercury and lead ions from wastewater, J. Environ. Manag. 87 (1), p. 125-131.

Speight, J.G. (2013). The chemistry and technology of coal, 3rd edition. CRC Press, Taylor and Francis group, Florida, p. 440-460.

Stamires, D.N., (1973). Properties of the zeolite, faujasite, substitutional series: A review with new data. Clays Clay Miner, Vol. 21, p. 379-389.

Strohmaier, K.G. (2010). Synthesis approaches, *in* Zeolites and catalysis: Synthesis, reactions and applications. Čejka, J., Corma, A. & Zones, S (eds). Wiley-VCH, Weinheim, p. 50 -86.

Suarez-Ruiz I. & Crelling J.C. (2008) Applied coal petrology: The role of petrology in coal utilization, Academic Press, London, p. 116.

Subotic, B. & Bronic, J., (2005). Theoretical and Practical Aspects of Zeolite Crystal Growth, *in* Handbook of zeolite science and technology, Auerabach, S.M., Carrado, K.A. & Dutta, P.K., (eds). Taylor & Francis, p. 195.

Sun, X. & Zhao, S. (2006). [bmim]CV[FeC13] ionic liquid as catalyst for alkylation of benzene with 1-octadecene. Chin. J. Chem. Eng., 14(3) p. 289–293.

Sutarno S. & Arryanto Y. (2007) Synthesis of faujasite from fly ash and its applications for the hydrocracking of petroleum distillates. Bull. Chem. React. Eng. Catal. 2. p. 45-51.

Szostak, R. (1989) Molecular Sieves – Principles of Synthesis and Identification, Van Nostrand Reinhold, New York, 1st Edition, p. 97.

Taylor, S. F., Sá, J. & Hardacre, C. (2011) Friedel–Crafts alkylation of aromatics with benzyl alcohol over gold-modified silica. ChemCatChem, 3(1) p. 119-121.

Thitsartarna, W., Gularib, E., & Wongkasemjita, S. (2007) Synthesis of Fe-MCM-41 from silatrane and $FeCl_3$ via sol–gel process and its epoxidation acivity. Appl. Organomet. Chem., 22, p. 97–103.

Tian, Z., Qin, Z., Wang, G., Dong, M. & Wang, J., (2008). Alkylation of benzene with propene over HBeta zeolites near supercritical conditions. J. Supercrit. Fluids. Vol. 44, Issue 3, p. 325–330.

Tsuda, T., Lu, B.W., Sasaki, H., Oumi, Y., Itabashi, K., Teranishi, T., & Sano, T. (2004) Direct synthesis of high-silica mordenite and its thermal stability. *in* Recent advances in the science and technology of zeolite and related materials. (eds) Van Steen, E. Callanan, L.H. & Claeys, M. Elsevier B.V. Amsterdam p. 224.

Udayakumar, S., Pandurangan, A. & Sinha, P.K. (2004) Para-selective ethylation of phenol with diethyl carbonate over mesoporous Al-MCM-41 molecular sieves. App. Catal. A: General 272, p. 267–279.

Urquieta-González, E.A., Martins, L., Peguin, R.P.S. & Batista, M.S. (2002) Identification of extra-framework species on Fe/ZSM-5 and Cu/ZSM-5 catalysts typical microporous molecular sieves with zeolitic structure. Mater. Res., Vol. 5, No. 3, p. 321-327.

Uzio, D. (2001) Textural characterisation of catalysts, *in* Physico-Chemical Analysis of Industrial Catalysts: A Practical Guide to Characterization. (ed) John Lynch. Technip, Paris, p. 26.

Vadapalli V.R.K, Gitari W.M., Ellendt A., Petrik L.F. & Balfour G, 2010, Synthesis of zeolite-P from coal fly ash derivative and its utilisation in mine-water remediation. S. Afr. J. Sci 106(5/6) p. 1 – 7.

Van Bekkum, H. & Kloetstra, R.K. (1998). New organic chemical conversions over MCM-41-type Materials. In Studies in surface science and catalysis: Mesoporous Molecular Sieves. Elsevier Science, Amsterdam, p. 176.

Van Steen, E., Callanan, L.H. & Claeys, M. (2005) Recent advances in the science and technology of zeolites and related materials. Elsevier B.V. Amsterdam, p. 1359.

Wagner, P. & Davis, M.E. (2000) Introduction to zeolite science, *in* Photofunctional zeolite: Synthesis, characterization, photocatalytic reactions, light harvesting. Anpo, M., (ed). NOVA Science Publishers Inc, New York, p. 33.

Wajima, T. & Ikegami, Y., (2009). Synthesis of crystalline Zeolite-13X from waste porcelain using alkali fusion. Ceram Int, 35(7), p. 2983-2986.

Wang, H. P., Lin, K. S., Huang, Y. J., Li, M. C. & Tsaur, L. K., (1998). Synthesis of Zeolite ZSM-48 from Rice Husk Ash. J. Hazard. Mater., 58(1-3), p. 147-152.

Wang, Y., Guo, Y., Yang, Z., Cai, H., & Xavier, Q., (2003). Synthesis of zeolites using fly ash and their application in removing heavy metals from waters. Sci.China Ser.D-Earth Sci., 46(9), p. 967-976.

Wang, Y., Song, Y., Huo, W., Jia, M., Jing, X., Yang, P., Yang, Z., Liub, G. & Zhang, W. (2012) Vapor phase ortho-selective alkylation of phenol with methanol over silica–manganese mixed oxide catalysts. Chem. Eng. J. 181– 182, p. 630– 635.

Weckhuysen, B.M. & Wacks, I.E. (2001) Catalysis by supported metal oxides, *in* Handbook of surfaces and interfaces of materials: Surface and interface phenomena.(ed) Nalwa, H.S. Academic Press, San Diego, p. 619 – 630.

Weitkamp, J. (2000) Zeolites and Catalysis. Solid State Ionics 131, p.175-188.

Weitkamp, J. & Puppe, L. (1999). Catalysis and zeolites: Fundamentals and applications. Springer, German.

Wheatley, P.S., Allan, P.K., Teat, S.J., Ashbrook, S.E. & Morris, R.E. (2010) Task specific ionic liquids for the ionothermal synthesis of siliceous zeolites. Chem. Sci., 1, p. 483 – 487.

Williams, C. & Gagan, M., (2002) The Molecular World: Chemical Kinetics and Mechanism. Mortimer, M., and Taylor, P., (eds). Royal Society of Chemistry, Cambridge, p. 235.

Wilson, S.T. (2001). Templating in molecular sieve synthesis. *in* Verified Synthesis of Zeolitic Materials, 2nd Revised Edition. Robson, H. (ed). Elsiever Science, Netherlands p. 28-29.

Woolfson, M.M. (1997) An introduction to X-ray crystallography, 2nd edition. Cambridge University Press, United Kingdom, p. 32.

Xia, M., Long, M., Yang, Y., Chen, C., Cai, W. & Zhou, B., (2011). A highly active bimetallic oxides catalyst supported on Al-containing MCM-41 for fenton oxidation of phenol solution. App. Catal. B: Environ., Vol. 110, p. 118-125.

Xie, F. M., Luo, G. H., Xu, X., & Chen, H. (2012). Alkylation of Benzene with 2-Chloropropane to Prepare Cumene with Chloroaluminate Ionic Liquids as Catalyst. The Chin. J. Proc. Eng., 1, 018.

Xu, R., Pang, W., Yu, J., Huo, Q. & Chen, J., (2007) Chemistry of zeolites and related porous materials: Synthesis and structure. John Wiley and Sons, Singapore, p. 632-635.

Yan X, & Xu, Y., (2010) Chemical vapour deposition: An integrated engineering design for advanced materials, Springer, London, p. 1.

Yang, S.T., Kim, J. & Ahn, W,J. (2010) CO_2 adsorption over ion-exchanged zeolite beta with alkali and alkaline earth metal ions. Micro & Mesop Mater.. Vol. 135, Issues 1–3, p. 90–94.

Yarimbiyik, A.E. (2007) Simulation and measurement of nanometer-scale resistivity of copper films for interconnect applications. ProQuest LLC, USA, p. 33 – 36.

Yeh, C.Y., (2008). Process for benzene alkylation and transalkylation of polyalkylated aromatics over improved Zeolite Beta catalyst. Lummus Technology Inc., New Jersey. US patent CA2589119.

Yoon, S.B., Fang, B., Kim, M., Kim J.H. & Yu, J-S. (2009) Nanostructured supported catalysts for low-temperature fuel cells, *in* Nanostructured Materials, Wilde G. (ed) Elsevier, Amsterdam p. 198.

Yuzaki, K., Yarimizu, T., Ito, S. & Kunimori, K. (1997) Catalytic decomposition of N_2O over supported rhodium catalysts: high activities of Rh/USYand Rh/$Al2O_3$ and the effect of Rh precursors. Catal. Letters 47, p. 173 – 175.

Zecca, M., Centomo, P. & Corain. B. (2008) Metal nanoclusters supported on cross-linked functional polymers: A class of emerging metal catalysts, *in* Metal Nanoclusters in Catalysis and Materials Science: The Issue of Size Control, Corain, B., Schmid, G. & Toshima, N. (eds). Elsevier, Amsterdam, p. 214.

Zhang, B., Ji, Y., Wang, Z., Liua, Y., Sun, H., Yang, W. & Wu, P. (2012) Liquid-phase alkylation of benzene with ethylene over postsynthesized MCM-56 analogues. App. Catal. A: General 443– 444, p. 103– 110.

Zhang, M., Zhang, H., Xu, D., Han, L., Niu, D., Tian, B. & Wu, W., (2011) Removal of Ammonium from Aqueous Solutions Using Zeolite Synthesized from Fly Ash by a Fusion Method. Desalination, 271(1), p. 111-121.

Zhao, H., Xu, Y. & Liu, J., (2011). Selective catalytic reduction of nitric oxide with Fe-Mn-Ce metal oxide-based catalysts. Advanced Materials Research, Vol. 304, p. 31-35.

Zhu, B., Letellier, F., Blanchard, J., Fajerwerg, K., Louis, C., Guillaumme, D., Uzio, D. and Breysse, M., (2006). Preparation of Pt^0/MCM-41: Effect of drying on MCM-41 structure and Pt^0 dispersion. Stud Surf Sci Cata, Vol. 162, 149-156.